UNIVERSIDAD COMPLUTENSE DE MADRID
FACULTAD DE CIENCIAS FÍSICAS

TESIS DOCTORAL

Campos Vectoriales y Ondas Gravitacionales en Cosmología

Vector Fields and Gravitational Waves in Cosmology

MEMORIA PARA OPTAR AL GRADO DE DOCTOR

PRESENTADA POR

Alfredo Delgado Miravet

Director

Antonio López Maroto

Madrid

UNIVERSIDAD COMPLUTENSE DE MADRID
FACULTAD DE CIENCIAS FÍSICAS

TESIS DOCTORAL

Campos Vectoriales y Ondas Gravitacionales en Cosmología
Vector Fields and Gravitational Waves in Cosmology

MEMORIA PARA OPTAR AL GRADO DE DOCTOR

PRESENTADA POR

Alfredo Delgado Miravet

DIRECTOR

Antonio López Maroto

UNIVERSIDAD COMPLUTENSE DE MADRID

FACULTAD DE CIENCIAS FÍSICAS

UNIVERSIDAD
COMPLUTENSE
MADRID

TESIS DOCTORAL

Campos Vectoriales y Ondas Gravitacionales en Cosmología
Vector Fields and Gravitational Waves in Cosmology

MEMORIA PARA OPTAR AL GRADO DE DOCTOR

PROGRAMA DE DOCTORADO EN FÍSICA

Alfredo Delgado Miravet

Director: Antonio López Maroto

Contents

Resumen

El modelo cosmológico estándar es la mejor descripción del Universo que tenemos hoy en día, y una de las aplicaciones más exitosas de la Relatividad General de Einstein. Aunque basta para explicar la expansión y la historia del Universo, aún alberga algunos misterios por resolver, como la naturaleza del sector oscuro o el problema de la asimetría bariónica, que sugieren modelos y procesos más allá de lo que se entiende por física estándar. En los últimos años, se han considerado extensiones al modelo estándar que típicamente involucran nuevos grados de libertad escalares para abordar estos problemas. En esta tesis, consideramos modelos más allá del paradigma escalar, que involucran campos vectoriales y tensoriales, los cuales han ganado popularidad por separado en las últimas décadas. Examinamos tres formas diferentes en las que puede surgir nueva fenomenología:

- *Logrando la bariogénesis con modos tensoriales*. Observamos que el mecanismo de leptogénesis gravitacional puede implementarse sin invocar nuevos acoplos axiales en el sector del inflatón. Mostramos que, en la métrica perturbada de Robertson-Walker que emerge tras la inflación, la propia métrica del espaciotiempo rompe la simetría de paridad y genera una densidad de Pontryagin no nula que puede producir una asimetría materia-antimateria. Analizamos la asimetría producida en diferentes escenarios inflacionarios y de recalentamiento. Mostramos que la asimetría generada puede ser localmente comparable a las observaciones en ciertos casos, aunque el tamaño de las regiones de materia-antimateria es típicamente mucho menor que el radio de Hubble actual.

- *Considerando candidatos alternativos vectoriales para el sector oscuro*. Estudiamos el efecto de modelos vectoriales para el sector oscuro sobre la propagación de ondas gravitacionales, en particular, para la materia oscura y la radiación oscura. Observamos que las oscilaciones coherentes del campo vectorial inducen una supresión anisótropa de la amplitud de las ondas gravitacionales en comparación con la predicción cosmológica estándar. La supresión es insignificante para las ondas gravitacionales generadas astrofísicamente, pero podría ser considerable para las ondas gravitacionales primordiales. Discutimos la posibilidad de detectar este efecto en el espectro de potencias tensorial con futuros detectores de polarización en modo B del fondo cósmico de microondas. Además, para la radiación oscura, la presencia del campo vectorial induce una polarización neta en el fondo de ondas gravitacionales y, para ciertas configuraciones del campo vectorial, una conversión de polarización lineal a circular.

- *Generando campos magnéticos mediante ruptura de invariancia bajo difeomor-*

fismos. Estudiamos la dinámica de campos gauge abelianos invariantes bajo difeomorfismos transversos (TDiff) en contextos cosmológicos. Mostramos que en la aproximación de óptica geométrica, al igual que para las teorías invariantes bajo difeomorfismos, los correspondientes bosones gauge sin masa se propagan a lo largo de geodésicas nulas y el número de partículas se conserva. Además, los vectores de polarización son ortogonales a la dirección de propagación y la polarización física (proyección transversal) se transporta paralelamente a lo largo de las geodésicas. También consideramos espinores de Dirac invariantes TDiff, estudiamos el acoplo a los campos gauge y analizamos las condiciones para evitar violaciones del Principio de Equivalencia de Einstein. Además, se analizan las contribuciones al tensor energía-momento del campo gauge. Encontramos que, en general, la ruptura de la invariancia bajo difeomorfismos hace que las partes eléctrica y magnética del campo vectorial graviten de forma diferente. En el régimen sub-Hubble, recuperamos el comportamiento estándar de la densidad de energía, similar a la radiación. Sin embargo, en el régimen super-Hubble, el comportamiento es totalmente diferente al caso Diff, abriendo así un amplio abanico de posibilidades para la construcción de modelos cosmológicos. En particular, se discuten los posibles efectos sobre la evolución de los campos magnéticos primordiales a gran escala.

Abstract

The cosmological standard model is the best description of the Universe we have got today, and one of the most successful applications of Einstein's General Relativity. Although it suffices to explain the expansion and history of the Universe, it still harbours some mysteries that are yet to be solved, such as the nature of the dark sector or the baryon asymmetry problem, which hint at models and processes beyond what is understood as standard physics. Over the last years, extensions to the Standard Model have been considered, which typically involve new scalar degrees of freedom and attempt to solve these problems. In this thesis, we consider models beyond the scalar paradigm involving vector and tensor fields, which have separately risen in popularity over the last decades. We inspect three different ways in which new phenomenology can arise:

- *Achieving baryogenesis with tensor modes*. We make the observation that the gravitational leptogenesis mechanism can be implemented without invoking new axial couplings in the inflaton sector. We show that, in the perturbed Robertson-Walker background emerging after inflation, the spacetime metric itself breaks parity symmetry and generates a nonvanishing Pontryagin density which can produce a matter-antimatter asymmetry. We analyse the produced asymmetry in different inflationary and reheating scenarios. We show that the generated asymmetry can be locally comparable to observations in certain cases, although the size of the matter-antimatter regions is typically much smaller than the present Hubble radius.

- *Considering alternative vector candidates for the dark sector*. We study the effects of vector models for the dark sector on gravitational-wave propagation, in particular, for dark matter and dark radiation. We find that the coherent oscillations of the vector field induce an anisotropic suppression of the gravitational wave amplitude as compared to the standard cosmology prediction. The suppression is negligible for astrophysically generated gravitational waves but could be sizable for primordial gravity waves. We discuss the possibility of detecting such an effect on the tensor power spectrum with future cosmic microwave background B-mode polarisation detectors. In addition, for dark radiation, the presence of the background vector fields induces a net polarisation of the gravitational wave background and, for certain configurations of the vector field, a linear to circular polarisation conversion.

- *Generating magnetic fields by breaking invariance under diffeomorphisms*. We study the dynamics of Abelian gauge fields invariant under transverse diffeo-

morphisms (TDiff) in cosmological contexts. We show that in the geometric optics approximation, very much as for Diff-invariant theories, the corresponding massless gauge bosons propagate along null geodesics and particle number is conserved. In addition, the polarisation vectors are orthogonal to the propagation direction and the physical (transverse projection) polarisation is parallel transported along the geodesics. We also consider TDiff-invariant Dirac spinors, study the coupling to the gauge fields and analyse the conditions in order to avoid violations of Einstein's Equivalence Principle. The contributions to the energy-momentum tensor of the gauge field are also analysed. We find that, in general, the breaking of Diff invariance makes the electric and magnetic parts of the vector field gravitate in a different way. In the sub-Hubble regime we recover the standard radiation-like behaviour of the energy density. However, in the super-Hubble regime, the behaviour is totally different to the Diff case, thus opening up a wide range of possibilities for cosmological model building. In particular, possible effects on the evolution of large-scale primordial magnetic fields are discussed.

List of publications

[1] A. D. Miravet and A. L. Maroto. "Imprint of ultralight vector fields on gravitational wave propagation". *Phys. Rev. D* 103.12 (2021). DOI: 10.1103/PhysRevD.103.123546. arXiv: 2012.07505.

[2] A. D. Miravet and A. L. Maroto. "Vector dark radiation and gravitational-wave polarization". *JCAP* 09 (2022). DOI: 10.1088/1475-7516/2022/09/014. arXiv: 2203.07125.

[3] A. L. Maroto and A. D. Miravet. "Gravitational leptogenesis from metric perturbations". *Phys. Rev. D* 107.4 (2023). DOI: 10.1103/PhysRevD.107.043538. arXiv: 2207.00465.

[4] A. L. Maroto and A. D. Miravet. "TDiff invariant gauge fields in cosmology". *Accepted for publication in Phys. Rev. D* (2024). arXiv: 2402.18368.

[5] A. L. Maroto and A. D. Miravet. "TDiff-fuelled magnetic fields" (in prep.).

Prelude

Cosmology is the branch of physics that studies the Universe at large scales, as a *whole*, attempting to answer questions about how it originated, what it looked like at very early times, how it has evolved, what it is made of, and how its constituents are distributed, among many other interesting questions. It is a recently developed discipline, with its theoretical formulation starting at the dawn of Einstein's General Relativity (GR) in the early 20th century, and observational precision cosmology having started just about thirty years ago. The 1990s saw a revolution in observational cosmology: While some inferences about the Universe's content were made through galaxy observations and Big Bang nucleosynthesis (BBN) analysis, the field rapidly advanced with precise observations of the cosmic microwave background (CMB) and remote Type Ia supernovae (SNIa). The Universe was then confirmed to be homogeneous and isotropic to a high degree of precision by CMB observations, with tiny fluctuations that were eventually found to be the blueprint of structure formation, which is driven by a non-baryonic pressureless component that we call dark matter (DM). Supernova observations, on the other hand, revealed that the Universe is under an accelerated expansion, driven by an unknown component with negative pressure, which we now call dark energy (DE).

These two mysterious ingredients, cold dark matter (CDM) and dark energy in the form of a cosmological constant Λ, are precisely what the standard Lambda-cold dark matter (ΛCDM) cosmological model is named after. ΛCDM is a phenomenological description of the Universe that, with only a handful of parameters, describes best what we know about the Universe we live in. According to the most recent observational data, the so-called dark sector comprises about 95% of the energy budget of the Universe, with the remaining fraction attributed to standard matter and radiation as we know them on Earth. Despite dominating the present Universe, the nature of the dark sector remains unknown, so exploring candidates for this sector and understanding their imprint on cosmic probes has been one of the main interests for theoretical cosmologists over the last decades. Models based on scalar fields, such as fuzzy dark matter or quintessence, are among the most popular yet simple candidates for the dark sector, which have found success in describing the phenomenology caused by dark matter and dark energy. More recently, models based on vector fields have been growing in popularity over the last few years. Besides having been proved as valid candidates, fulfilling the requirements posed by observations, their non-scalar nature provides a rich phenomenology absent in other models, making them worth exploring. Vector fields constitute one of the two pillars which this Thesis is centred around.

Going a step further in spin, we have got gravitational waves (GWs), propagating

ripples of the spacetime fabric that are described as a massless spin-2 field and that constitute the other pillar of this Thesis. GWs are also the protagonist of arguably the last revolution in cosmic observables, which started in 2014 with the first detection of GWs by interferometer LIGO, about a hundred years after their prediction by Einstein, who thought at the time that they would be too small to be ever observed. A decade later, almost one hundred astrophysical events have been reported since the first observation, with the numbers expected to quickly grow in the coming years. GWs of cosmological origin could be soon detected through B-mode CMB observations. This could potentially clear up some unknowns regarding inflation and the early stages of the radiation-dominated (RD) Universe, which are inaccessible to electromagnetic observations due to the opacity of the primordial plasma.

The main body of this Thesis is structured in two parts. Part I offers a cursory overview of the standard cosmological model, focusing on the topics that are most relevant to our work. While the experienced reader might already be aware of everything laid out in this module, it is still worth taking a glimpse, as it also allows us to introduce the more advanced topics we cover in Part II. More specifically, Chapter 1 delves into the primary observational probes which ΛCDM is based upon, from local experiments on distances and matter distribution to observations of the cosmic microwave background. In Chapter 2, we establish the mathematical formulation of standard cosmology. We introduce the dynamics of an expanding universe and the fluid and thermodynamic description of its components at background level, which we supplement with a quick outlook of metric perturbations. In Chapter 3, we drift off a little from minimal standard cosmology to introduce some hot topics in the early Universe, before Big Bang nucleosynthesis. Here we discuss inflation, arguably the most favoured theory for the primitive Universe, as well as how to link it with standard cosmology and the baryon asymmetry problem. The last Chapter in this Part, Chapter 4, is devoted to gravitational waves. We outline its current observational status and prospects, and then we discuss GWs in a cosmological context, where we analyse their propagation within the standard Universe and characterise stochastic GW backgrounds.

Part II contains the bulk of our work. It is structured in three different chapters that examine different aspects related to vector and tensor fields in a cosmological context. In fact, the idea behind each Chapter follows a different philosophy on how to discover new phenomenology.

- *Achieving baryogenesis with tensor modes* is the focus of Chapter 5. Here, we explore gravitational leptogenesis as a mechanism for generating a matter-antimatter imbalance even without invoking new couplings or altering a minimal inflationary scenario. We show that in the perturbed RW background arising after a slow-roll inflationary epoch, the scalar and tensor (gravitational-wave) power spectra can break parity and generate lepton number through the gravitational lepton anomaly. We analyse the produced asymmetry for different

reheating (RH) scenarios and discuss its effect in the late Universe. This Chapter is based on Ref. [3].

- In Chapter 6, we *consider alternative vector candidates* for the dark sector. In particular, we study the imprint of Abelian vector models constituting a dark matter or dark radiation component on gravitational-wave propagation. The non-scalar character of these models introduces an anisotropic stress that affects the propagation of GWs through an expanding universe. In particular, they induce a multipolar suppression of the GW background, which is modulated about the direction of the vector field, and in the case of vector dark radiation, a net polarisation of the stochastic background. This Chapter is based on Refs. [1; 2].

- Lastly, in Chapter 7, we explore *magnetic field generation in a vector model with broken diffeomorphism invariance*. We consider breaking of diffeomorphism (Diff) invariance down to transverse diffeomorphism (TDiff) invariance for an Abelian gauge (vector) field. We find that in the geometric optics approximation, which corresponds to the sub-Hubble regime for an expanding universe, the phenomenology is analogue to that of the Diff case, making it compatible with GR tests. In the super-Hubble regime, however, the dynamics are different, and in particular, the breaking of conformal invariance induced by Diff breaking for a free electromagnetic field can be exploited to obtain sizeable primaeval magnetic fields in a minimal inflationary scenario. This Chapter is based on Refs. [4; 5].

The text closes with Part III, where we draw the main concluding remarks of our work. It also features five Appendices, which are intended as a supplement to the main work. In Appendix A, we include the customary overview of our notation and conventions, as well as a list of frequently used acronyms. Appendix B contains a collection of useful formulae about special functions we have used in our work. Appendix C contains definitions concerning differential geometry, as well as a list of tensor components for some spacetimes. Appendix D lays out the formalism necessary to work with spinor fields in curved spacetime, which is necessary for Sec. 7.2. The last one, Appendix E, contains an alternate derivation of the TDiff-invariant Lorentz force to that exposed in Sec. 7.2.

I

Standard cosmology overview

1 Observational foundations

Our knowledge about the Universe, past and present, can only come from what we are able to observe, which establishes the basic pillars on which cosmology is built around and which we describe in this Chapter. In Sec. 1.1, we describe the distance ladder and how we can infer the expansion history of the Universe by observing remote objects, and in particular, the recent accelerated expansion caused by a dark energy component. In Sec. 1.2, we introduce the cosmic microwave background as one of the most important cosmological probes. In Sec. 1.3, we discuss dark matter, the key ingredient in structure formation. Sec. 1.4 is dedicated to Big Bang nucleosynthesis, which originated the light element abundances in the Universe. Finally, in Sec. 1.5, we consider intergalactic magnetic fields (IGMFs) and the current observational constraints on them.

1.1 The distance ladder

Looking at the sky is one of the oldest observing methods in human history, and as such, Astronomy has been a discipline since Before the Common Era. Cosmology, being about farther distances, has not been able to develop until about a hundred years ago, when more powerful instruments and techniques were available to detect remote objects.

Pioneering works by Georges Lemaître [Lem27] and Edwin Hubble [Hub29] found a correlation between redshift

$$z = \frac{\lambda_0}{\lambda_i} - 1, \tag{1.1}$$

with λ_0, λ_i the observed and emitted wavelengths respectively, and the luminosity distance d_L to extragalactic objects, resulting in what is known today as Hubble's law

$$z = H_0 d_L, \qquad (z \ll 1). \tag{1.2}$$

Although the values obtained for the Hubble constant H_0 were far from accurate, this correlation meant that the farther an object was, the faster it was receding, indicating an expansion of the Universe. The value of the Hubble constant is usually given in terms of an adimensional reduced Hubble constant h, which is defined as

$$H_0 = 100h\,\mathrm{km\,s^{-1}Mpc^{-1}}. \tag{1.3}$$

Unlike redshift, distance to remote objects is not directly measurable. At large distances, *standard candles* come into play, which are objects whose intrinsic luminosity

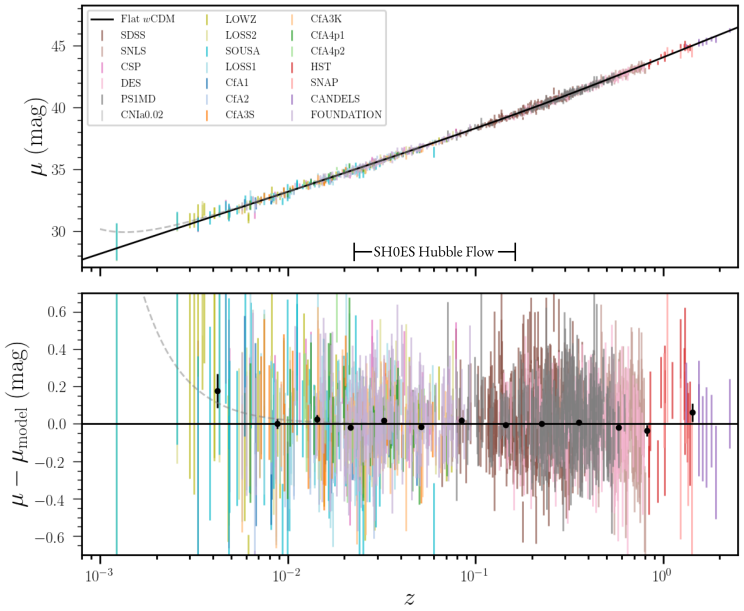

Figure 1.1: Hubble diagram of the Pantheon+ analysis, plotted as distance modulus μ vs. redshift z, for the SNIa as well as the best fit. The interval used by the SH0ES collaboration is also indicated. The bottom panel shows the residuals relative to the best fit. Credit: [Bro+22].

is related to some other measurable variable. Two important examples of standard candles are Cepheids, pulsating stars whose luminosity can be related to the period of the variation of its luminosity, and Type Ia Supernovae, whose peak luminosity and luminosity curve throughout the days after the explosion can be standardised.

Cepheids were widely used in the first measurements of H_0, as being both abundant and fairly bright, they could calibrated by measuring the periods of a bunch of them in the Small Magellanic Cloud [LP12]. Standard candles are then used to calibrate more remote standard candles, going farther in each step in what is known as the distance ladder.

Type Ia Supernovae are the culmination of this ladder, very rare albeit very luminous events, which can outshine entire galaxies and which have been used to measure distances up to redshift $z \sim 2.3$. Precisely, it was thanks to SNIa that, in the late 1990s, two works [Rie+98; Per+99] found the first strong evidence for the accelerated expansion of the Universe. They used measurements of a few tens of SNIa up to $z \sim 0.8$ to determine the next order in the Hubble law

$$H_0 d_L = z + \frac{1}{2}(1 - q_0)z^2 + \ldots, \tag{1.4}$$

where q_0 is the deceleration parameter

$$q_0 = -\left.\frac{\ddot{a}}{aH_0^2}\right|_{\text{today}}, \tag{1.5}$$

and a is the scale factor, which we define in Chapter 2. The deceleration parameter had been defined historically with a minus sign so that it would be positive, as the Universe was expected to be decelerating, but these works found that $q_0 < 0$ at $\sim 3\sigma$ level. This meant that ordinary matter (or even dark matter) could not be the dominant component of the Universe. In a model with non-relativistic matter abundance Ω_M and newly postulated dark energy abundance Ω_Λ

$$q_0 = \Omega_M - \frac{\Omega_\Lambda}{2}, \tag{1.6}$$

meaning that this strange new component, with negative pressure $p_\Lambda = -\rho_\Lambda$ and responsible for the accelerated expansion of the universe, had to be at least twice as abundant as matter. Here, the abundance of each species Ω_i is defined as

$$\Omega_i = \frac{\rho_{0,i}}{\rho_c}, \tag{1.7}$$

with $\rho_{0,i}$ the energy density of the species today and $\rho_c = 3H_0^2/8\pi G$ the critical energy density today.

Subsequent works improved both in the systematics and in the number of supernovae, the most recent being the combined efforts of Pantheon+ [Bro+22] and the SH0ES team [Rie+22] with data from over 1500 distinct SNIa, finding values of $H_0 = 73.5 \pm 1.1\,\mathrm{km\,s^{-1}\,Mpc^{-1}}$ and $\Omega_M = 0.334 \pm 0.018$. Fig. 1.1 shows the Pantheon+ current version of Hubble's diagram.

1.2 Cosmic microwave background

The cosmic microwave background is an electromagnetic background corresponding to the photons that last scattered when they decoupled from matter at $z_{\text{dec}} \sim 1100$, and thus have travelled freely all the way to the present. It was accidentally discovered by Penzias and Wilson in 1964 [PW65] when they detected a background noise in the microwave range coming from every direction in the sky while tinkering with an microwave antenna. While the measurements were performed in only one frequency, they reported an excess temperature of 3.5 K, which is somewhat close to the actual value.

The first space-based experiment focused on observing the CMB arrived in the 1980s with the Soviet detector RELIKT-1 [SS84], which successfully measured a dipole in the CMB. Later reanalysis also hinted at anisotropies in the form of a quadrupole [Str+92]. The follow-up project was discontinued, and CMB observations would not

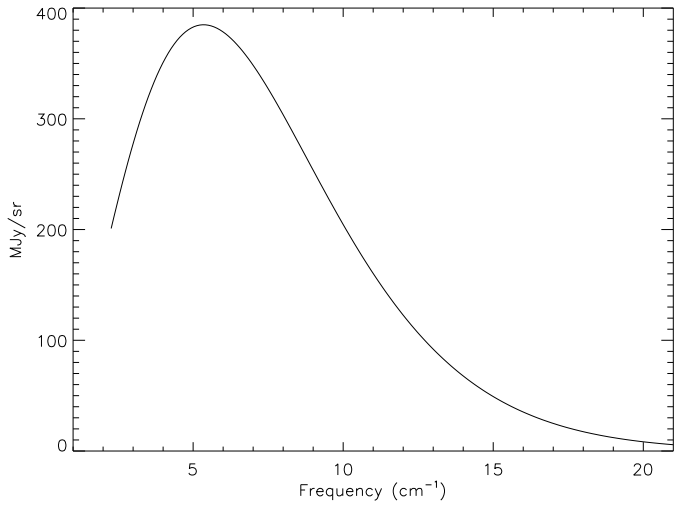

Figure 1.2: The CMB radiation and its fit as a black body, as measured by instrument FIRAS of satellite COBE. The error bars are thinner than the width of the line. Credit: [Fix+96].

be carried out until one decade later by NASA's so-called first-generation experiment Cosmic Background Explorer (COBE) [Bog+92].

COBE's experiments FIRAS [Bog+92] and DMR [Ben+96], designed to measure the CMB spectrum and anisotropies in the CMB respectively, reported an isotropic spectrum that matched a black-body emission of temperature $T_0 = 2.728 \pm 0.004$ K, with is plotted in Fig. 1.2. Deviations from this isotropy were in the form of a dipole at level $\mathcal{O}(10^{-3})$, caused by a Doppler effect with respect to the CMB rest frame, and higher-multipole anisotropies at level $\mathcal{O}(10^{-5})$. These three layers of the CMB are depicted in Fig. 1.3.

The success of COBE's observations was followed up by two subsequent experiments, WMAP and Planck, which would go on to expand the knowledge provided by the CMB.

Planck [Agh+20a] was the most recent space-based mission dedicated to observing the anisotropies of the CMB. It observed the sky for four years, from its launch in 2009 until 2013, in nine frequency bands between 30 and 857 GHz. The Planck mission was aimed at measuring the temperature fluctuation power spectrum with unprecedented resolution and accuracy, as well as gathering data on the polarisation and lensing power spectra. Fig. 1.4 shows the temperature fluctuations observed by Planck, after foreground subtraction and masking of the galactic plane, which immediately reveals

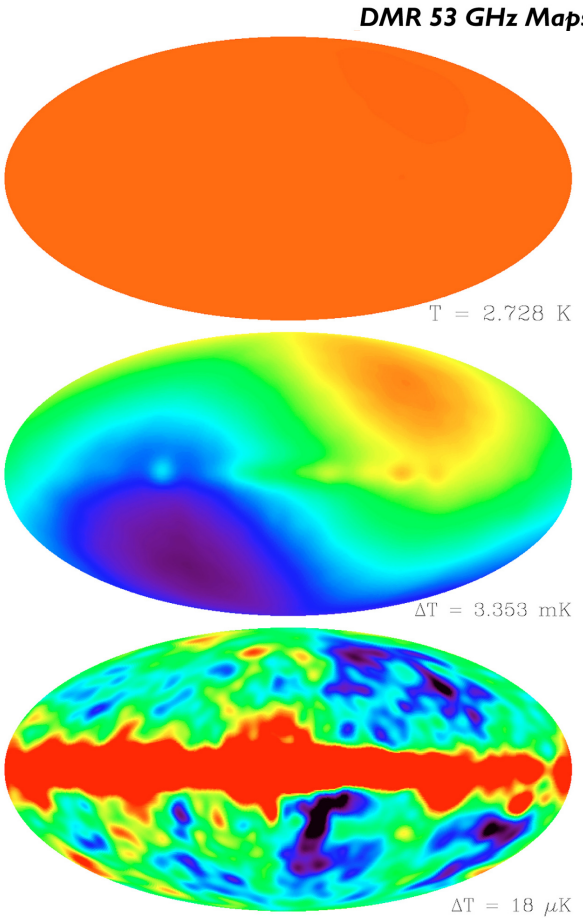

Figure 1.3: Maps on 53 GHz, based on 4-year data from instrument DMR of satellite COBE. The top figure shows the isotropic CMB background. The middle figure shows the dipole with respect to the CMB rest frame after the subtraction of the monopole. The bottom figure shows the residual anisotropies (as well as the Milky Way in the galactic plane) after subtraction of the two elements above. Credit: NASA / COBE Science Team.

a substantial improvement over COBE's sky (Fig. 1.3).

Another key goal of Planck was to use the improved power spectra to provide a robust estimation of cosmological parameters based on a high-redshift observable affected by the evolution of the Universe such as the CMB. These results would serve the purpose of confirming (or invalidating) the already well-established ΛCDM model, whose parameters had already been determined mostly by local experiments, such as SNIa observations (discussed in Section 1.1) or matter distribution analysis (Section 1.3). After its release, Planck's estimation of cosmological parameters would become the most precise estimate of cosmological parameters to date, which are widely used

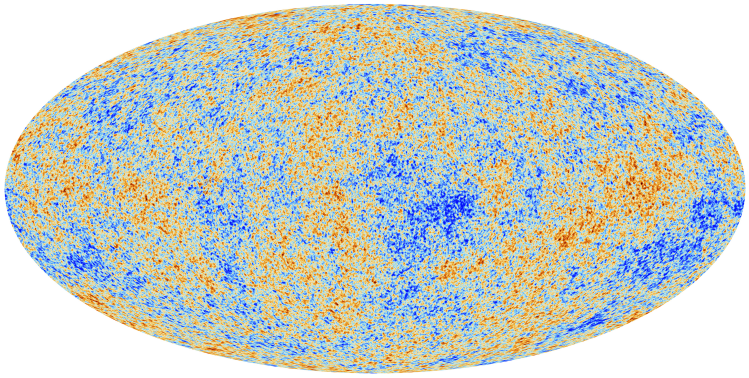

Figure 1.4: The temperature fluctuations in the sky as seen by Planck, after subtraction of the monopole and the dipole. The galactic plane, as well as other regions with substantial emission, have been masked and thus are not visible. Credit: [Agh+20a].

by the community today.

The analysis and fit of the CMB anisotropies are best performed by computing the two-point angular correlation function of the observables (intensity and polarisation). The temperature map $T(\hat{\mathbf{n}})$ is first decomposed into spherical harmonics, thus obtaining the coefficients

$$a^T_{\ell m} = \int \mathrm{d}\hat{\mathbf{n}} Y^*_{\ell m}(\hat{\mathbf{n}}) T(\hat{\mathbf{n}}), \tag{1.8}$$

and then the two-point function is obtained by computing the statistical average over the full sky, which can only depend on ℓ under the isotropy assumption

$$\langle a^{T*}_{\ell m} a^T_{\ell' m'} \rangle = C^{TT}_\ell \delta_{\ell\ell'} \delta_{mm'}. \tag{1.9}$$

Similar multipole expansions can be carried for polarisation and lensing observations, which are detailed in [Agh+20a], and coefficients C^{XY}_ℓ can be computed with X, Y being any of T (temperature), E, B (polarisation in terms of Stokes parameters Q and U respectively) or ϕ (lensing potential). It is then convenient to define the quantity

$$\mathcal{D}^{XY}_\ell = \frac{\ell(\ell+1)}{2\pi} C^{XY}_\ell, \tag{1.10}$$

commonly referred to as the angular power spectrum, which is plotted for the non-zero spectra in Fig. 1.5. In the case of the auto-correlation, $\mathcal{D}^{XX}_\ell$ provides an estimate of the multipole ℓ contribution to the total variance, showing best what scales are more relevant in the spectrum.

The CMB is then able to supply an estimate of cosmological parameters under a minimal ΛCDM model, which chiefly assumes that

1. General Relativity is the correct description of gravitation.

2. The Universe has been expanding and cooling down since early times.

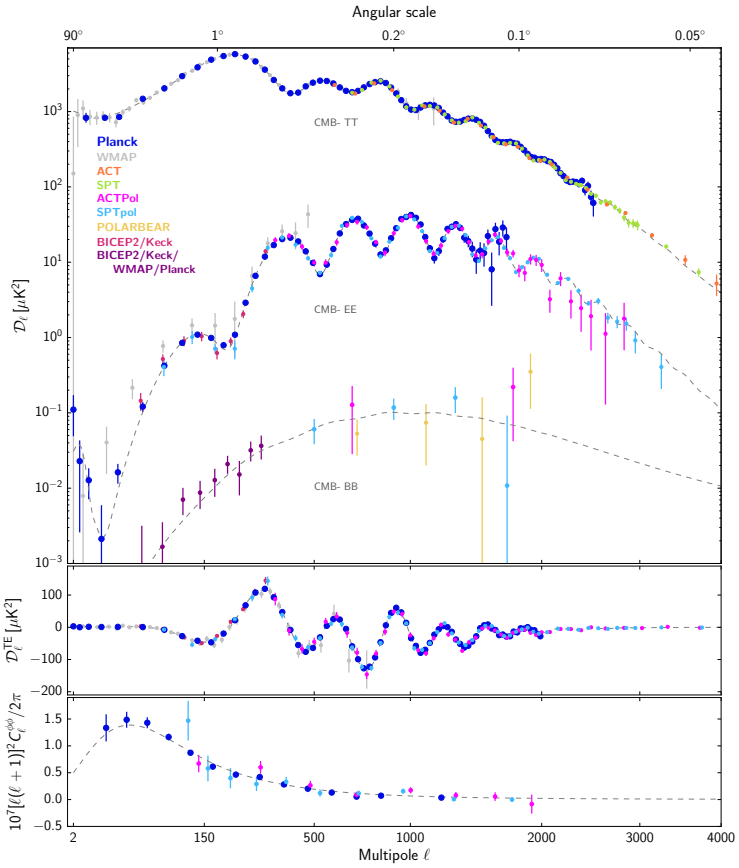

Figure 1.5: Planck's TT, EE, BB, TE and lensing angular power spectra, with data from other Collaborations added. Credit: [Agh+20a].

3. The Universe is extremely homogeneous and isotropic, and its inhomogeneities can be described as scalar Gaussian, adiabatic and nearly scale-invariant perturbations. Tensor perturbations are assumed to be negligible.

4. The Universe is filled with dark energy, with the same equation of state as vacuum energy, non-relativistic dark matter that only interacts gravitationally, ordinary matter as found on Earth and radiation in the form of photons as in the CMB and nearly massless neutrinos. The sum of neutrino masses is assumed to be $\sum m_\nu = 0.06$ eV, in agreement with the normal hierarchy.

5. The Universe's curvature is negligible.

Following these assumptions, a six-parameter ΛCDM can be fitted to the angular power spectra [Agh+20b]. In what follows, we list and describe the six fitted parameters and give the values that best fit the TT, TE, EE and lensing power spectra.

- Baryonic matter abundance $\Omega_B h^2 = 0.02237 \pm 0.00015$.

- Cold dark matter abundance $\Omega_c h^2 = 0.1200 \pm 0.0012$. By comparison with the baryon (regular matter) abundance, this result confirms that the majority of pressureless matter comes in the form of dark matter, which is responsible for structure formation.

- Angular size of the acoustic scale $\theta_* = 1.04092 \pm 0.00031$ (rad), which corresponds to the acoustic oscillations that are visible in the spectra (see Fig. 1.5). The corresponding transverse distance is the comoving sound horizon at recombination, which is the maximum distance that a sound wave could have travelled in the photon-baryon plasma.

- Reionization optical depth $\tau = 0.0544 \pm 0.0073$. Sub-horizon CMB anisotropies are scattered by free electrons after reionization, so the observed amplitude is $A_S e^{-2\tau}$ instead of A_S (see its definition below).

- Scalar power spectrum amplitude $\log\left(10^{10} A_S\right) = 3.044 \pm 0.014$. The scalar perturbation power spectrum is parametrised as $\mathcal{P}_\mathcal{R} = A_S (k/k_*)^{n_S - 1}$, with $k_* = 0.05$ Mpc^{-1} the Planck scalar pivot scale.

- Scalar power spectrum tilt $n_S = 0.9649 \pm 0.0042$. This value confirms a nearly scale-invariant power spectrum $n_S = 1$ while ruling an exactly scale-invariant one at $\sim 8\sigma$ level. Models with little-to-no running of the spectral index around the pivot scales are compatible with Planck's observations [Akr+20]. Inflationary early Universe models are favoured by this scenario (see Sec. 3.1).

From these parameters, other cosmological parameters can be derived, some of which (relevant for our work) we list as follows.

- Hubble constant $H_0 = 67.36 \pm 0.54$. Unlike in local measurements, in which H_0 directly measures the local expansion rate of the Universe, this Hubble parameter estimation is inferred and thus model-dependent. In fact, it is not compatible with the last SNIa (or other local) measurements detailed in Sec. 1.1 up to $\sim 5\sigma$, which is an ongoing problem dubbed the Hubble tension [Di +21].

- Matter abundance $\Omega_M = 0.3153 \pm 0.0073$, which includes the contribution of both ordinary baryonic matter and cold dark matter.

- Dark energy abundance $\Omega_\Lambda = 0.6847 \pm 0.0073$. In agreement with local experiments, a cosmological constant (or something alike) responsible for the accelerated expansion of the universe is the most abundant component of the universe today. Relaxations of the equation of state constraint $p_\Lambda = -\rho_\Lambda$ also yield compatibility with a cosmological constant, although with very large confidence regions.

Some extensions to the minimal cosmological model can also be tested by CMB data, such as having further relativistic species or tensor primordial modes.

- Effective number of relativistic species $N_{\rm eff} = 2.92^{+0.36}_{-0.37}$. The radiation energy density is sometimes given in terms of this parameter

$$\rho_R = \left[1 + N_{\rm eff}\frac{7}{8}\left(\frac{4}{11}\right)^{4/3}\right]\rho_\gamma, \tag{1.11}$$

  with ρ_γ the photon energy density, which is known with almost no error thanks to the precise measurements of the CMB temperature $T_0 = 2.7260 \pm 0.0013$ K [Fix09]. The standard cosmological model predicts $N_{\rm eff} = 3.046$, corresponding to the three families of neutrinos, with a small correction above 3 as they were not completely decoupled from photons at electron-positron annihilation, which yields an abundance of $\Omega_R h^2 = 4.17 \times 10^{-5}$. If one relaxes this assumption, allowing the effective number to vary, the baseline parameters barely change and the constraint above is obtained, which is compatible with having just the standard neutrinos. The error in the estimation is quite large, allowing for extra relativistic species in the description of the components of the Universe, which we will explore in Sec. 6.3. Future Stage-4 CMB experiments will increase the sensitivity up to $\Delta N_{\rm eff} \simeq 0.03$ [Aba+16].

- Tensor-to-scalar ratio r. Tensor perturbations, as predicted by inflation, have not been observed yet. Data gathered by Planck is able to constrain the amplitude of the tensor power spectrum, as gravitational waves contribute to the low-ℓ end of the B-mode polarisation (see Fig. 1.5). The combined efforts of Planck and B-mode observations by the BICEP/Keck Collaboration have been able to set the constraint down to $r_{0.05} < 0.036$ [Ade+21].

- Spatial curvature $\Omega_k = -0.0106 \pm 0.0065$. If one relaxes the assumption of a spatially flat spacetime, Planck's sky apparently favours a closed Universe, although it becomes compatible with no curvature when combining with baryon acoustic oscillation data $\Omega_k = 0.0007 \pm 0.0019$.

Current and future CMB experiments, both ground-based such as POLARBEAR [Suz+16] or BICEP Array [Hui+18] and space-based as LiteBIRD [Haz+19], are focusing primarily on the observation of B-mode polarisation. B-polarisation modes (see [KK16] for a review) are affected both by primordial gravitational waves in the low-multipole ($\ell < 200$) region, as well as gravitational lensing in the high-ℓ end. Observation of tensor modes in the CMB is key to fully unlocking our knowledge of inflation, while gravitational lensing is produced by photons being deflected at low redshift, thus providing information about the Universe in more recent times, after structure formation.

1.3 Dark matter

Dark matter is any form of matter that lacks electromagnetic interaction and constitutes the missing component in the gravitational interactions of some systems at

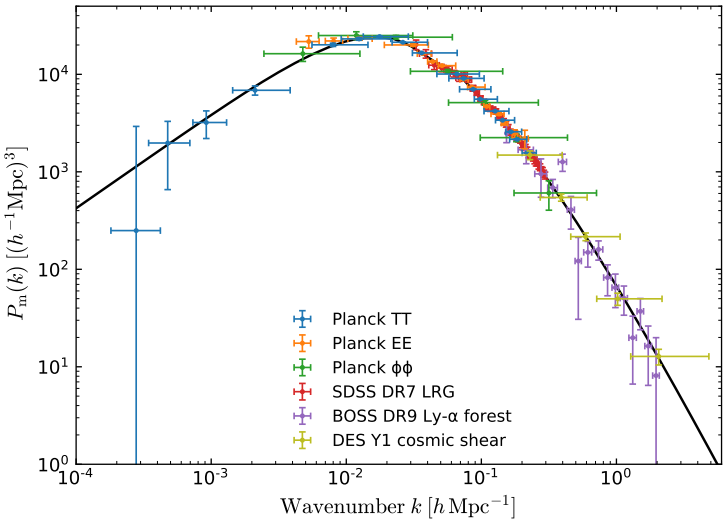

Figure 1.6: Matter power spectrum today, with data from different cosmological probes, as well as the best fit for Planck (solid line), which assumes a cold dark matter model. Credit: [CMP19].

astrophysical and cosmological scales. While it belongs in standard cosmology, the conceptualisation of dark matter predates modern ΛCDM cosmology. The measurement of the rotation curves for several spiral galaxies revealed that visible matter could not be responsible for all the gravitational interaction that caused the motion of the objects within the galactic disk [RFT80]. In fact, visible matter could account for only a fraction of the interaction, and the analysis revealed there was a massive halo that extended farther than visible matter, as velocities of objects far from the centre remained constant, instead of the expected $v(r) \sim r^{-1/2}$. Consequently, the examined spiral galaxies exhibited an approximately spherical dark matter halo, a phenomenon later identified in the velocity dispersion of various galaxy types and clusters through the virial theorem.

As the most abundant contribution to the matter budget in the universe, dark matter plays a pivotal role in structure formation and, ultimately, in the large-scale structure in the present-day Universe. As the process of structure formation depends on the dark matter behaviour, there has been a historical separation between hot and cold dark matter [CL95]

- A *hot* dark matter (HDM) model consists of collisionless particles with large velocity dispersion, displaying a relativistic behaviour at the moment of structure formation. In this scenario, structure formation occurs by fragmentation of large-scale primordial structures. An example of HDM would be a particle that decouples from the thermal bath when it is still relativistic, such as a neutrino.

- A *cold* dark matter model consists of a pressureless fluid which could be consti-

tuted by non-relativistic particles at the moment of structure formation. With CDM, structure formation occurs hierarchically, with larger structures being formed by gravitational collapse and clustering.

The expansion of the Universe makes structure formation not evolve exponentially with time, which allows us to see the imprint of the primordial perturbation power spectrum into matter distribution today. The most favoured scenario by observations is a Universe with cold dark matter, with the small fluctuations in the primordial Universe, as seen in the CMB, conspiring with the attractive nature of gravitationally interacting matter to collapse from small inhomogeneities to form the web of clusters and voids we observe. The information we have got about the early Universe, together with an accurate model of dark matter, should be compatible with the matter power spectrum we see today.

The matter power spectrum can be measured in different regions by various local experiments that are capable, by different means, of mapping the distribution of matter both across the sky and in different redshifts. Fig. 1.6 shows the matter power spectrum $P_m(k)$ with data from a wide range of different experiments, which we discuss as follows (see [CMP19] for a review and for the details on building the plot in Fig. 1.6).

eBOSS survey of the Sloan Digital Sky Survey (SDSS) [Abo+18] has been able to observe thousands of high-redshift ($z > 2$) quasars. The transmitted flux in the Lyman-alpha forest provides information on the matter power spectrum around the Mpc scale. Cosmic shear correlation functions, measured by the Dark Energy Survey (DES) [Tro+18], also contain information on the matter power spectrum in the Mpc scale.

On intermediate scales, the matter power spectrum can be obtained from observations of galaxy clustering, after using a model of halo bias, for example from a sample of red galaxies by SDSS [Rei+10]. For larger scales, the matter power spectrum can be inferred from the angular power spectra measured by Planck [Agh+20a].

The matter power spectrum, which contains information across several orders of magnitude in scale, favours a model of pressureless cold dark matter in the adiabatic mode for perturbations. Baryons cannot be the only responsible for structure formation, as the matter power spectrum would be dominated by acoustic oscillations as the ones seen in the CMB (Sec. 1.2). HDM and CDM predict similar power spectra on large scales, but HDM features a stronger suppression on smaller scales that is not compatible with observations. On the other hand, the isocurvature mode (for either species) does not suppress smaller scales, so adiabatic perturbations, as predicted by inflation, must be the dominant mode in the description of primordial perturbations.

Although a model of cold dark matter with gravitational interaction only is able to reproduce the large-scale structure of the Universe reasonably well, it presents some discrepancies with observations at sub-galactic scales, which are mostly represented by the following problems [BB17]:

- N-body simulations of dark matter-dominated galaxies predict cuspy halos [Nav+10], with steep slopes $\rho(r) \sim 1/r$ near the centre. These are usually described around a Navarro-Frenk-White (NFW) density profile [NFW97]

$$\rho_{\mathrm{NFW}}(r) = \frac{4\rho_0}{\frac{r}{R}\left(1+\frac{r}{R}\right)^2}. \tag{1.12}$$

  On the other hand, observational rotation curves around these halos are best described by a constant density core (for example, [MRdB01]). This is known as the *core-cusp problem*.

- The *missing satellite problem* is a discrepancy between the number of predicted galaxy satellites of a galaxy like the Milky Way, originating in dark matter subhalos [Spr+08], and the current known census of satellites [Drl+15]. This is either a discrepancy between the number of formed dark matter subhalos or a failure to understand why most of these subhalos have not ended up hosting galaxies.

- Also related to galaxy formation, the *too-big-to-fail problem* corresponds to the fact that the local universe hosts too few massive galaxies, with central densities around $10^{10} M_\odot$, as simulations predict massive subhalos to be too dense to host Milky Way satellites [BBK11]. Halos this massive are believed to be too massive to have failed to form stars, so the lack of this kind of galaxy remains unexplained.

Following these issues, both extensions to the standard ΛCDM model and alternatives to cold dark matter have been explored. Cuspy halos can be erased by including some kind of baryonic feedback from supernova explosions and stellar winds in galaxy formation simulations [MWC08]. Other solutions involve modifying the dark matter paradigm itself, such as the proposals in self-interacting cold dark matter [SS00] or warm dark matter [SD01].

Another proposal is along the lines of wave dark matter models. In recent years, there has been a growing interest in the so-called ultralight dark matter models [Ari+12; Hui+17; Cem+18]. These models, also known as fuzzy dark matter, are based on the existence of bosonic fields with very small masses $m \ll 1$ eV, so that their cosmological number density is so high that the interparticle separation would be smaller than their Compton wavelength. In this case, the appropriate description of the dark matter component would be in terms of classical fields (Bose-Einstein condensates) rather than particles. These models could lead to distinctive predictions for the density profiles of galaxies. Thus, recent simulations of dark matter in the form of a Bose-Einstein condensate have shown the formation of a soliton core profile on scales below the de Broglie wavelength surrounded by a halo of excited states [SCB14]. Although ultralight scalars, i.e. spin-zero fields with very small masses ($m \sim 10^{-22}$ eV) such as axion-like particles, have been amongst the most studied proposals, fuzzy dark matter can be extended to higher-spin fields, which we discuss in Sec. 6.2.

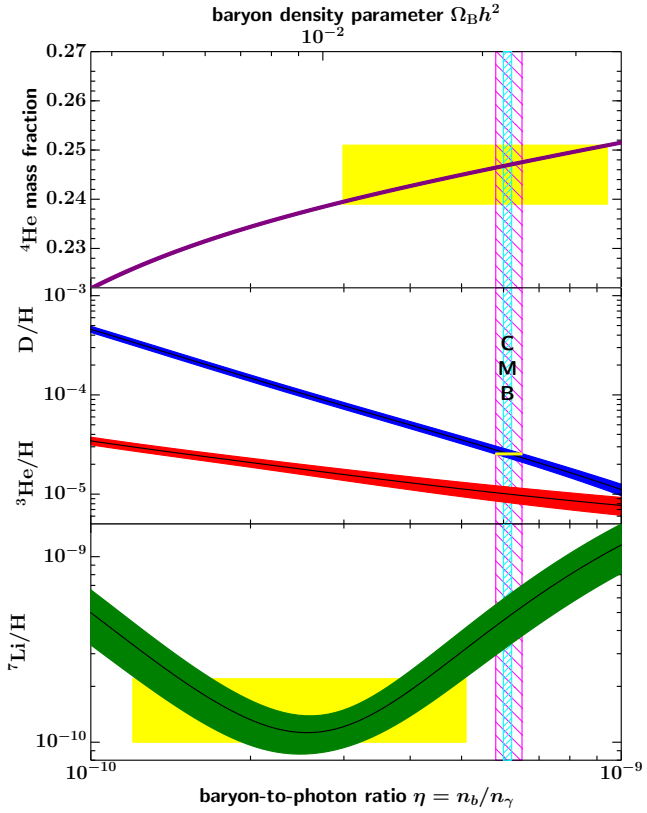

Figure 1.7: Primordial abundances of ^{4}He, D, ^{3}He and ^{7}Li as a function of baryon-to-photon ratio. The bands of the abundances indicate the 2σ confidence region, which mostly comes from uncertainties in the neutron lifetime and nuclear cross-sections. Yellow boxes correspond to the observed abundances. Vertical bands are derived from Planck's estimation on $\Omega_B h^2$. Credit: [Wor+22].

1.4 Big Bang nucleosynthesis

Primordial nucleosynthesis [Gam46; ABG48] is the process during which light nuclei were able to form in the early stages of the universe, back when the temperature was about $T_{\text{nuc}} \sim 0.1$ MeV. At this temperature, the photon energy density has dropped enough so that it is energetically and statistically possible to form deuterium. Besides H, which is protons themselves, Big Bang nucleosynthesis was able to create a good amount of ^{4}He, providing most neutrons in the Universe with a stable nucleus, as well as smaller amounts of D, ^{3}He and ^{7}Li.

Although stars can also generate nuclei from hydrogen in the late stages of stellar evolution, a mechanism dubbed stellar nucleosynthesis, the amounts of D and ^{4}He cannot be explained by any astrophysical process, which makes nucleosynthesis the earliest cosmological probe we have got to date.

The parameter that controls the element production during BBN is the baryonic asymmetry

$$\eta_B = \frac{n_B - n_{\bar{B}}}{n_\gamma} \simeq \frac{n_B}{n_\gamma}, \tag{1.13}$$

often called the baryon-to-photon ratio due to the absence of antibaryons at later times. The computation of primordial abundances in terms of the baryon abundance dates as back as [WFH67] (see the introduction for a nice review of the early history of BBN), much before the determination of cosmological parameters by distance ladder or CMB experiments. There, assuming a CMB temperature of $T_0 \sim 3$ K, it was estimated that baryon abundance needed to be about $\Omega_B h^2 \sim 0.01$ in order to reproduce observed abundances, especially not to overproduce ^{4}He, a remarkable result for its time. Since this work was before realising the need for the dark sector, the low baryon abundance was determined to imply an open Universe.

Updated versions of the code used in [WFH67] are still used in modern calculations. The details on the computation of the primordial abundances, as well as a recompilation of the experiments used to infer them, are extensively discussed and referenced in [Fie+20].

Nowadays, primordial abundances yield about $\eta_B \sim 6 \times 10^{-10}$, which are in good agreement with CMB estimates of baryon abundance by Planck, as shown in Fig. 1.7. In particular, a mean estimation for η_B by BBN and Planck gives the following value [Fie+20]

$$\eta_B = (6.129 \pm 0.039) \times 10^{-10}. \tag{1.14}$$

We must mention two caveats though: First, primordial ^{3}He measurements up to date are poor. Observed abundances are translated into primordial ones after taking into account all possible generation of astrophysical origin, which has not been achieved reliably for this nucleus, so it is disregarded as a cosmological probe. Secondly, there is a noticeable tension between the ^{7}Li abundance and the rest of abundances, especially following the high agreement between the CMB and D abundance predictions. This has been dubbed "the lithium problem" [Fie11], and has not been solved yet.

BBN depends on two more parameters, the neutron lifetime τ_n and the effective number of relativistic species N_{eff}, which was introduced in Eq. (1.11) and already discussed in Sec. 1.2 in the context of CMB. While the neutron lifetime is regarded as an input parameter, BBN can also offer information about N_{eff}. The abundance generated during nucleosynthesis for each element strongly depends on the weak interaction freeze-out that happens slightly before BBN, and this is determined by the expansion rate at freeze-out. A number of neutrino families larger than $N_\nu = 3$ (equivalently, $N_{\text{eff}} = 3.046$) increases the expansion rate, bringing forward in time the freeze-out and leaving a larger number of neutrons to form nuclei during BBN, which modifies the abundance share between different elements. This affects especially the ^{4}He abundance, which gathers practically all free neutrons going into BBN. As a result, N_{eff} can be set as a free parameter and constrained with primordial abundances, which is found in [Fie+20] to be $N_\nu = 2.878 \pm 0.278$.

1.5 Magnetic fields

Magnetic fields [DN13] are everywhere in our Universe. Wherever we have had the means of measuring them, they are present across stars, galaxies and clusters, at different redshifts, featuring a strength around a few microGauss. The magnetic fields we have observed have been found in an astrophysical context and are believed to have been amplified from a primordial seed, whose origin is unknown to this day. One of the most popular amplification mechanisms is the dynamo amplification [Par55], which has been found to work in the context of galaxy [Sch+10] and star [Sur+10] formation.

Small-scale magnetic fields undergo dissipative magnetohydrodynamic (MHD) processes [BJ04], so the presence of magnetic fields below a certain length scale require a constant generation process, such as the electric currents originated by stellar dynamics. On larger scales, the dissipative characteristic time is larger than the age of the Universe, so they preserve the amplified strength.

Current observational data is not able to constrain the seed magnetic field due to uncertainty in the dynamo mechanism. The seed can be small, as dynamos can enhance the magnetic field strength by a large number of orders of magnitude, but it needs to be present before galaxy formation. There are two main possibilities, it either originated in a process in the early universe, such as inflation [TW88] or a phase transition [Vac91], or it was generated along the gravitational collapse causing structure formation. Standard slow-roll inflation (see Sec. 3.1), in particular, cannot generate primordial magnetic fields due to conformal invariance of the free electromagnetic field. As a result, new couplings or breaking of conformal invariance are required for magnetogenesis within inflation. In Chapter 7, we explore the possibility of breaking conformal invariance by breaking invariance under diffeomorphisms and examine the implications on inflation-generated magnetic fields.

If the magnetic fields in the Universe do have their origin in a seed magnetic field, it should still dwell in the voids of the large-scale structure in its primordial form. Here, the absence of structures and matter prevents the dynamo amplification or the dissipative processes from happening, so in this sense, the observation of intergalactic magnetic fields [Kro94] is an interesting source of information for cosmology. Indeed, the primordial magnetic field power spectrum could expand our knowledge about the process responsible for its existence as well as the dynamo mechanism.

Fig. 1.8 summarises the current bounds on intergalactic magnetic fields. At large scales, the magnetic field strength is constrained to a certain range, with bounds coming from two independent experiments. TeV gamma rays originated in blazars (observed at low redshift $z \sim 0.2$) create electron-positron pairs that cascade into less energetic secondary gamma rays. The absence of GeV gamma rays contributing to the source flux is believed to be due to the presence of magnetic fields, which bend the trajectory of charged particles. In [NV10] it was found, with the aid of data from Fermi/LAT telescope, that this imposes a lower bound on intergalactic magnetic fields of $B \geq 10^{-16}$ G, which is independent of correlation length for sufficiently large scales

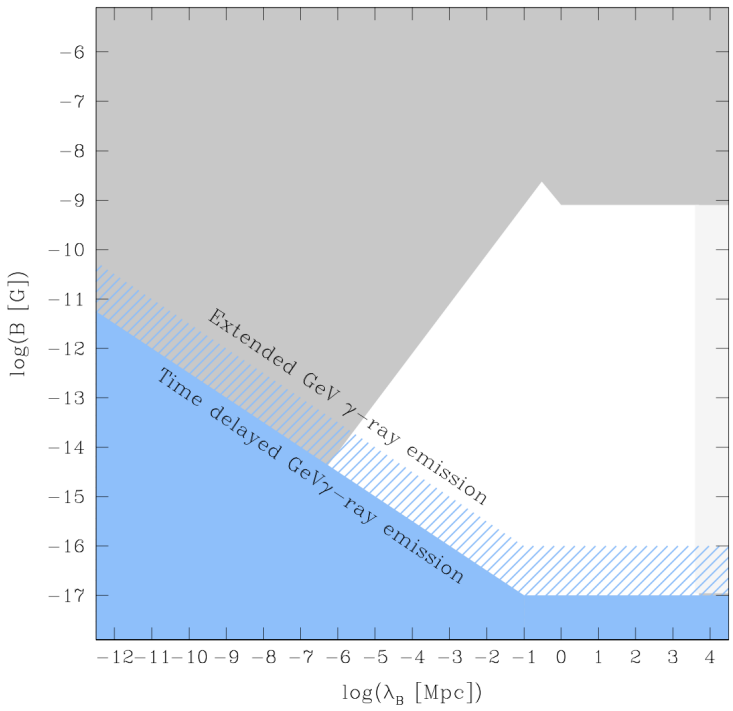

Figure 1.8: Constraints on intergalactic magnetic fields (see the text for more information), plotted as magnetic field intensity B_λ with correlation length λ_B. The allowed region is unshaded. Non-observation of gamma rays yields the constraint in blue. The rest of constraints are provided by CMB observations (upper bound) and MHD turbulence (upper left bound). The lightly shaded region on the right indicates scales larger than the Hubble radius today. Credit: [DN13].

$\lambda_B \geq 1$ Mpc. When considering cascade suppression observed in the time delay of the signal, a more conservative lower bound is found $B \geq 10^{-18}$ G [Der+11]. The upper limit derives from the absence of large-scale anisotropies in the CMB [BFS97], which depends on the tilt of the primordial magnetic field power spectrum [PF11]. The last bound is due to magnetohydrodynamic turbulence, which imposes an upper bound on IGMF injected into the medium by any process [BJ04]. This bound is dependent on scale $B_{\max} \propto \lambda_B$ and corresponds to the upper left bound in Fig. 1.8.

2 ΛCDM overview

In order to describe the history and the dynamics of the Universe, we must find a mathematical formulation within General Relativity, which is regarded as the best description of gravity today, and that is compatible with the observations described in Chapter 1. The description of an expanding Universe is very standard and can be found in many references in the literature. Some of them, which we have found particularly useful when building this Chapter, are [Wei72; KT90; Dod03; Muk05]. We present the basics of metric formalism within GR and notions regarding cosmic distances in Sec. 2.1. In Sec. 2.2, we introduce the perfect fluid description and lay the basic equations of standard cosmology. In Sec. 2.3, thermodynamic quantities and concepts are generalised to an expanding universe. Finally, in Sec. 2.4, we introduce the formalism to describe the small perturbations to the homogeneity of the universe.

2.1 Metric formulation

As we have already established by different probes in Chapter 1, the Universe is homogeneous and isotropic on very large scales. The most general metric for a space-time with these features is the Robertson-Walker (RW) metric, which is given by the following line element

$$\mathrm{d}s^2 = \mathrm{d}t^2 - a^2(t)\left[\frac{\mathrm{d}r^2}{1-kr^2} + r^2(\mathrm{d}\theta^2 + \sin^2\theta\mathrm{d}\phi^2)\right]. \tag{2.1}$$

Here, t is called the cosmological time and $a(t)$ is the scale factor, which accounts for the expansion of the Universe. The scale factor is related to the redshift z (1.1) of an object emitting light at time t_i as

$$1+z = \frac{a(t_0)}{a(t_i)}, \tag{2.2}$$

where t_0 is the present time and we normalise $a(t_0) = 1$.

The parameter k accounts for the curvature of spatial sections. The cases $k = 0$, $k > 0$ and $k < 0$ are referred to as flat, closed or spherical and open or hyperbolic, respectively. In this section, we keep the curvature to give the general equations, but later on we will assume flat spatial sections, which is a scenario favoured by the observations. Note that for $k = 0$, the term in square brackets in (2.1) is simply $\mathrm{d}\mathbf{x}^2$.

The luminosity distance d_L, which is the distance inferred by observing an object with luminosity L and apparent flux l, is defined from the following relation

$$l = \frac{L}{4\pi d_L^2}, \tag{2.3}$$

which after taking into account the effects of the redshift due to the expansion of the universe, can be related to the radial coordinate r of the object as

$$d_L = r(1+z). \tag{2.4}$$

Similarly, the angular distance d_A to an object of proper size D can be inferred from observing its apparent size in the sky $\Delta\theta$

$$\Delta\theta = \frac{D}{d_A}, \tag{2.5}$$

which in terms of coordinates reads

$$d_A = \frac{r}{1+z}. \tag{2.6}$$

It is clear that, for a static universe, $d_A = d_L$ is simply the distance to the object. In an expanding universe, these are just definitions, and in general, the radial coordinate r cannot be identified as the distance to the object. The comoving distance to an object χ can be obtained by integrating along the radial geodesic followed by the light $\mathrm{d}s = 0$ emitted by it at t_1 until the present time, so that

$$\chi = \int_0^r \frac{\mathrm{d}r'}{\sqrt{1-kr'^2}} = \int_{t_1}^{t_0} \frac{\mathrm{d}t}{a(t)}. \tag{2.7}$$

Note that, in the absence of curvature, we can take $r = \chi$ and regard r as the comoving distance as well. Generally, the RW metric can be written in a conformal way by changing coordinates to χ and conformal time $a(\eta)\mathrm{d}\eta = \mathrm{d}t$

$$\mathrm{d}s^2 = a^2(\eta)\left[\mathrm{d}\eta^2 - \mathrm{d}\chi^2 + S_k(\chi)^2(\mathrm{d}\theta^2 + \sin^2\theta\mathrm{d}\phi^2)\right], \tag{2.8}$$

where $S_k(\chi)$ is just r in terms of the comoving distance and has the expression

$$S_k(\chi) = r(\chi) = \frac{1}{\sqrt{k}}\sin\left(\sqrt{k}\chi\right), \tag{2.9}$$

where in the case $k = 0$ the expression must be replaced by its limit.

2.2 Dynamics and fluid description

In order to study the dynamics that describe the evolution of the Universe, we must solve the field equations for the metric, which are Einstein's equations

$$G_{\mu\nu} = 8\pi G T_{\mu\nu}. \tag{2.10}$$

These equations can be obtained via variational principle from an action comprising the Einstein-Hilbert action, i.e. GR's action, and the action for the content of the universe

$$S = S_{\rm EH} + S_m = -\frac{1}{16\pi G}\int \mathrm{d}^4x\,\sqrt{g}R + \int \mathrm{d}^4x\,\sqrt{g}\mathcal{L}_m, \tag{2.11}$$

with the stress-energy tensor generally being derived from the matter action as

$$T^{\mu\nu} = -\frac{2}{\sqrt{g}}\frac{\delta S_m}{\delta g_{\mu\nu}}. \tag{2.12}$$

For the background dynamics, we consider that every component in the universe can be described by means of a perfect fluid with energy density ρ and pressure p. In this case, the stress-energy tensor is given by

$$T_{\mu\nu} = (\rho + p)u_\mu u_\nu - p g_{\mu\nu}, \tag{2.13}$$

with u_μ the four-velocity. In a comoving frame, this simply reduces to

$$T^\mu{}_\nu = \mathrm{diag}(\rho, -p, -p, -p). \tag{2.14}$$

Plugging this stress-energy tensor into Einstein's equations (2.10) with a RW background (2.1), one can obtain Friedmann's equation for homogeneous ρ and p

$$H^2 + \frac{k}{a^2} = \frac{8\pi G}{3}\rho, \tag{2.15}$$

with $H = \dot{a}/a$ the Hubble rate, which describes the expansion rate of the Universe. Here, the overdot indicates derivative with respect to t. The present value of the Hubble parameter $H(t_0) = H_0$ is the Hubble constant, which was introduced in Sec. 1.1. Whenever it might be useful to use conformal time, we denote the conformal Hubble rate as $\mathcal{H} = a'/a = aH$, with the prime indicating derivative with respect to a time coordinate other than t. The other independent Einstein equation is the acceleration equation, which reads

$$\frac{\ddot{a}}{a} = -\frac{4\pi G}{3}(\rho + 3p). \tag{2.16}$$

From these equations, it is immediate to see that an accelerated expansion $\dot{a} > 0$, $\ddot{a} > 0$ is only possible if the dominant component in the Universe satisfies $\rho + 3p < 0$, which cannot be realised by ordinary matter alone.

If there is more than one component that contributes to the stress-energy tensor, ρ and p refer to the total energy density and pressure. An additional constraint, which derives either from these equations or from stress-energy conservation $T^{\mu\nu}{}_{;\nu} = 0$, is the conservation of energy

$$\dot{\rho} + 3H(\rho + p) = 0. \tag{2.17}$$

In background dynamics, it is customary to describe the various components in the Universe in terms of barotropic and constant equations of state $p(\rho) = w\rho$, with

w constant and dependent on the nature of the component. This turns out to be a good approximation in describing the expansion of the Universe, while making the formulation much easier. In this case, Eq. (2.17) can be written as $\frac{\mathrm{d}}{\mathrm{d}t}\left(\rho a^{3(1+w)}\right) = 0$. As a result, the energy density of a component with equation of state w scales as

$$\rho = \rho_0 a^{-3(1+w)}, \tag{2.18}$$

with ρ_0 being the energy density today. Introducing this scaling into Friedmann equation (2.15), one can obtain a relationship between scale factor and time

$$a(t) \propto t^{\frac{2}{3(1+w)}}, \tag{2.19}$$

valid when a fluid with equation of state w dominates. In terms of conformal time

$$a(\eta) \propto \eta^{\frac{2}{1+3w}}. \tag{2.20}$$

It is also convenient to divide each energy density by the critical energy density ρ_c to write the Friedmann equation in terms of the abundances Ω of each species (1.7), with a curvature "abundance" for the sake of completeness

$$\Omega_k = -\frac{k}{H_0^2}. \tag{2.21}$$

At this point, we are ready to be more specific and list every component in our Universe according to the ΛCDM model and observations as discussed in Chapter 1, which we list as follows

- Non-relativistic matter, also called dust, which is pressureless $p = 0$. It is constituted mostly by cold dark matter and about 15% of baryonic, regular matter. The energy density scales as $\rho_M \propto a^{-3}$ and it constitutes about 30% of today's energy budget.

- Radiation, i.e. relativistic particles, with pressure $p = \rho/3$. It is in the form of photons, as seen in the CMB, with a temperature today of $T_0 = 2.7260$ K, as well as three families of neutrinos that were relativistic when decoupled from the primordial plasma at about $T_{\mathrm{dec}} \sim 1$ MeV. The energy density scales as $\rho_R \propto a^{-4}$.

- Dark energy, described as a cosmological constant, with negative pressure $p = -\rho$. It is responsible for the accelerated expansion of the universe. It has constant energy density $\rho_\Lambda = \text{const.}$ and it constitutes about 70% of today's energy budget.

- The curvature term scales as $\propto a^{-2}$. Observations are compatible with flat spatial sections.

One can rescale today's abundances into a less expanded Universe to see that, in very early times, radiation was the dominant component up until the matter-radiation

equality, happening at $z_{\rm eq} \sim 3300$. From that point onwards, matter dominated until very recently, when dark energy started being prominent, at about $z_\Lambda \sim 0.3$.

The Friedmann equation (2.15) can be written in terms of all these components, with their abundances, as

$$H^2 = H_0^2 \left[\Omega_M (1+z)^3 + \Omega_R (1+z)^4 + \Omega_\Lambda + \Omega_k (1+z)^2\right]. \tag{2.22}$$

Evaluating this expression today, one gets the rule of cosmic sum, which is a constraint for the abundances

$$\Omega_M + \Omega_R + \Omega_\Lambda + \Omega_k = 1. \tag{2.23}$$

A useful expression for the comoving distance to an object at redshift z within a certain cosmological model can be obtained by changing variables $\mathrm{d}t = \mathrm{d}a/aH$ in Eq. (2.7), so

$$\chi(z) = \int_0^z \frac{\mathrm{d}z}{H(z)}, \tag{2.24}$$

with $H(z)$ given by Eq. (2.22). Inserting this relation in the expression for the luminosity distance (2.4) and doing an expansion in Taylor series, one can recover Hubble's law up to any desired order in redshift. For a flat Universe with dominant Ω_M and Ω_Λ at low redshift, it reads

$$H_0 d_L = (1+z) H_0 \chi(z) = z + \left(1 - \frac{3}{4}\Omega_M\right) z^2 - \frac{\Omega_M}{8}(1 + 9\Omega_\Lambda) z^3 + \mathcal{O}(z^4), \tag{2.25}$$

from which the deceleration parameter in Eq. (1.6) can be derived.

2.3 Thermodynamics

For an important part of the history of the Universe, particles have been in thermal equilibrium with the photons that we observe in the CMB. In some processes, especially during the earlier stages of the Universe, it is useful to describe the species in terms of thermodynamical quantities.

We know from statistical mechanics that the occupation number of a state with momentum $\mathbf{p}$ is given by the phase space distribution function

$$f(\mathbf{p}) = \frac{1}{e^{(E_\mathbf{p} - \mu)/T} \pm 1}, \tag{2.26}$$

where $E_\mathbf{p} = \sqrt{\mathbf{p}^2 + m^2}$ is the energy of the particle, T the temperature of the thermal bath and μ the chemical potential, which is determined by the characteristics of the chemical equilibrium. The sign + (−) describes a Fermi-Dirac (Bose-Einstein) distribution.

For a particle with g inner degrees of freedom, the number density, energy density and pressure can be obtained by integrating the phase space distribution

$$n = \frac{g}{(2\pi)^3}\int \mathrm{d}^3\mathbf{p}\, f(\mathbf{p}), \tag{2.27a}$$

$$\rho = \frac{g}{(2\pi)^3}\int \mathrm{d}^3\mathbf{p}\, f(\mathbf{p}) E_{\mathbf{p}}, \tag{2.27b}$$

$$p = \frac{g}{(2\pi)^3}\int \mathrm{d}^3\mathbf{p}\, f(\mathbf{p}) \frac{\mathbf{p}^2}{3E_{\mathbf{p}}}. \tag{2.27c}$$

In the ultra-relativistic limit $T \gg m, \mu$, one can obtain compact expressions at leading order for both distributions. In the case of bosons

$$n = \frac{\zeta(3)}{\pi^2} g T^3, \tag{2.28a}$$

$$\rho = \frac{\pi^2}{30} g T^4, \tag{2.28b}$$

where $\zeta(3) \simeq 1.202$ is the Riemann zeta function, while for fermions

$$n = \frac{3}{4}\frac{\zeta(3)}{\pi^2} g T^3, \tag{2.29a}$$

$$\rho = \frac{7}{8}\frac{\pi^2}{30} g T^4, \tag{2.29b}$$

with the pressure $p = \rho/3$ in both cases. In the non-relativistic limit $T \ll m$, both distributions give the same expressions

$$n = g\left(\frac{mT}{2\pi}\right)^{3/2} e^{-(m-\mu)/T}, \tag{2.30a}$$

$$\rho = nm, \tag{2.30b}$$

$$p = nT. \tag{2.30c}$$

Note that, for non-relativistic matter, $\rho \gg p$ immediately follows from $m \gg T$, which is why dust is considered pressureless to a good approximation.

For a thermal bath with a bunch of different particles, the total energy density is dominated by the relativistic species, as the non-relativistic ones are exponentially suppressed. It can be written as

$$\rho_R = \frac{\pi^2}{30} g_*(T) T^4, \tag{2.31}$$

where g_* is the effective number of relativistic degrees of freedom, given by

$$g_*(T) = \sum_{\text{bosons}} g_i \left(\frac{T_i}{T}\right)^4 + \frac{7}{8}\sum_{\text{fermions}} g_i \left(\frac{T_i}{T}\right)^4. \tag{2.32}$$

In this expression, only relativistic species $m \ll T$ must be accounted for, which naturally depends on the temperature. Species with $T_i \neq T$, which have decoupled

from the thermal bath, need to be accounted if they were relativistic when they decoupled. Speaking specifically of the Standard Model (SM) of particles, it reaches its maximum at $g_* = 427/4$ when all particles were relativistic $T \gg m_t$, where $m_t \simeq 173$ MeV is the top quark mass. Its value today is $g_*(T_0) = 3.36$, including photons and neutrinos, with temperature $T_\nu/T = (4/11)^{1/3}$, which decoupled when they were relativistic at $T \sim 1$ MeV. Photons carry a slightly larger temperature as they were heated up during the electron-positron annihilation, which happened around $T \sim m_e \simeq 0.5$ MeV.

For an expanding universe, the first and second laws of thermodynamics can be recast into the conservation of entropy S in a comoving volume V, i.e. $\mathrm{d}S = \mathrm{d}(sV) = 0$, where s is the entropy density, which can be found to be

$$s = \frac{\rho + p - \mu n}{T}. \tag{2.33}$$

Similarly to the energy density, this expression is dominated by the relativistic species in the thermal bath, so we can write

$$s = \frac{2\pi^2}{45} g_{*s}(T) T^3, \tag{2.34}$$

where now g_{*s} is the effective number of relativistic degrees of freedom *for the entropy*, which follows the same guidelines as Eq. (2.32) and is given by

$$g_{*s}(T) = \sum_{\text{bosons}} g_i \left(\frac{T_i}{T}\right)^3 + \frac{7}{8} \sum_{\text{fermions}} g_i \left(\frac{T_i}{T}\right)^3. \tag{2.35}$$

Note that $g_* = g_{*s}$ if there are not any decoupled particles with a different temperature. For the Standard Model, this equality holds until the temperature drops below $T < m_e$, as discussed before, and today it has the value $g_{*s}(T_0) = 43/11 \simeq 3.91$.

The conservation of entropy $S = sa^3 = \text{const.}$ implies the following relation

$$g_{*s}(T) a^3 T^3 = \text{const.}, \tag{2.36}$$

which is useful to relate two different moments with known temperatures. The entropy density is also used to express relic densities: If a certain particle has a conserved particle number N, i.e. its number density $n \propto a^{-3}$, then the quantity n/s is constant with the expansion of the universe. For example, the baryon asymmetry η_B (1.13) has an alternate definition in terms of the entropy density

$$\eta_B^s = \frac{n_B}{s}, \tag{2.37}$$

which is constant if baryon number is conserved. Conversely, from Eqs. (2.28a), (2.34) it follows $s \simeq 1.8 g_{*s} n_\gamma$, so η_B is constant only as long as g_{*s} does not change.

Lastly, let us discuss the concept of *local thermal equilibrium*. The discussion about thermal equilibrium in this section can only be applied if reactions are efficient enough

to follow the expansion of the universe. If they fail to do so, reactions do no longer occur, species fall out of equilibrium and decouple, leaving conserved relic abundances behind. An elaborate analysis of decoupling involves studying the Boltzmann equation applied to the phase space distributions in curved spacetime, which is extensively discussed in many books, including the ones we have cited at the beginning of this Chapter.

Qualitatively, decoupling can be easily understood in terms of the expansion rate H and the interaction rate

$$\Gamma = n\langle\sigma v\rangle, \tag{2.38}$$

where n is the number density of the interacting particle and $\langle\sigma v\rangle$ is the velocity-averaged cross section of the interaction.

- If $\Gamma \gg H$, the interaction is effective enough to follow the expansion of the universe and local thermal equilibrium holds.
- If $\Gamma \ll H$, the interaction falls behind the expansion of the universe and it departs from equilibrium.

An important example of this, which has already been mentioned, is neutrino decoupling. Weak interactions, which have interaction rates $\Gamma \sim G_F^2 T^5$, with $G_F = 10^{-5}\text{GeV}^{-2}$ the Fermi constant, fall behind the expansion of the Universe during the radiation-dominated era $H \sim T^2/M_P$ as temperature decreases with the expansion. The decoupling temperature is often defined as $H(T_{\text{dec}}) = \Gamma(T_{\text{dec}})$, which for neutrinos is $T_{\text{dec}} \sim 1$ MeV.

2.4 The inhomogeneous Universe

The Universe is well described at the background level by a purely homogeneous and isotropic spacetime. However, we know from observations of the CMB (see Section 1.2) that it features primordial inhomogeneities at level $\mathcal{O}(10^{-5})$, so in order to fully describe the phenomenology in the Universe, we need to consider metric perturbations. The formalism we present in this Section was developed and presented with complete detail in [MFB92]. That and [Muk05] are the two main references for what follows.

It is convenient to work on conformal time and write the metric as

$$\mathrm{d}s^2 = a^2(\eta)(\eta_{\mu\nu} + \delta\eta_{\mu\nu})\mathrm{d}x^\mu \mathrm{d}x^\nu, \tag{2.39}$$

where $\delta\eta_{\mu\nu}$ includes all perturbations of the metric. It is customary to perform a *helical decomposition* of the metric perturbations, splitting scalar, vector and tensor behaviours under spatial transformations, which decouple at linear level in the equations of motion. It allows us to write the line element as

$$\mathrm{d}s^2 = a^2(\eta)\Big[(1+2\phi)\mathrm{d}\eta^2 + 2(B_{,i} + S_i)\mathrm{d}\eta\mathrm{d}x^i - \Big((1-2\psi)\delta_{ij} - 2E_{,ij} - 2F_{(i,j)} - h_{ij}^{\mathrm{TT}}\Big)\mathrm{d}x^i\mathrm{d}x^j\Big]. \tag{2.40}$$

- ϕ, B, ψ and E are scalar functions. In practice, scalar perturbations are often analysed in terms of Bardeen's variables

$$\Phi = \phi - \frac{1}{a}\frac{\mathrm{d}}{\mathrm{d}\eta}\left[a(B-E')\right], \qquad \Psi = \psi + \frac{a'}{a}(B-E'), \tag{2.41}$$

  which are gauge-invariant, and equal to ϕ and ψ respectively in the longitudinal gauge $B = E = 0$. The inhomogeneities in the CMB are described in terms of scalar perturbations.

- S_i and F_i are divergence-free vectors $\partial_i S^i = \partial_i F^i = 0$. In an expanding universe, vector perturbations quickly decay and have no impact on cosmic evolution, so they can be disregarded.

- h_{ij}^{TT} is a transverse and traceless (TT) tensor, so it satisfies $\partial_i h_{ij} = 0$, $\delta^{ij} h_{ij} = 0$, where we drop the TT indicators to relax the notation. Tensor perturbations, with two degrees of freedom, can be identified with the propagating degrees of freedom of a massless spin-2 field, which are gravitational waves.

Having perturbed the metric, which enters in the left-hand side of Einstein's equations (2.10), the right-hand side needs to be perturbed as well, which we write as

$$\delta G^{\mu}{}_{\nu} = 8\pi G \delta T^{\mu}{}_{\nu}. \tag{2.42}$$

For a perfect fluid (2.13), the components of the perturbed stress-energy tensor have the following expression

$$\delta T^{0}{}_{0} = \delta\rho, \tag{2.43a}$$

$$\delta T^{0}{}_{i} = \frac{1}{a}(\bar{\rho} + \bar{p})(\delta u_{\parallel i} + \delta u_{\perp i}), \tag{2.43b}$$

$$\delta T^{i}{}_{j} = -\delta p \delta^{i}{}_{j}, \tag{2.43c}$$

where $\bar{\rho}$, $\bar{p}$ refer to the background energy density and pressure, $\delta\rho$, δp are their respective perturbations and we have split the perturbation of the four-velocity into an irrotational part $\delta u_{\parallel i}$ and a divergence-free part $\delta u_{\perp i}$. All of these quantities except $\delta u_{\perp i}$ contribute to the scalar part of the perturbations, including $\delta u_{\parallel i}$, which can be written as the gradient of a scalar function. There is no transverse and traceless part to this tensor, so perfect fluids cannot source gravitational waves, as they do not cause anisotropic stress.

In general, the energy density and pressure are related via some equation of state $p = p(\rho, S)$. Thus, the pressure perturbation can be written as

$$\delta p = c_s^2 \delta\rho + \tau \delta S, \tag{2.44}$$

with $c_s^2 = (\partial p/\partial\rho)_S$ is the squared sound speed and $\tau = (\partial p/\partial S)_\rho$, where the subscripts in these definitions indicate that the partial derivative is taken while keeping that

variable constant, a common notation in thermodynamics. Perturbations with $\delta S = 0$ are dubbed adiabatic perturbations.

For scalar perturbations in the presence of a perfect fluid, Einstein's equations acquire the following form in the longitudinal gauge

$$\nabla^2\Psi - 3\mathcal{H}(\Psi' + \mathcal{H}\Phi) = 4\pi G a^2 \delta\rho, \tag{2.45a}$$

$$(\Psi' + \mathcal{H}\Phi)_{,i} = 4\pi G a^2 (\bar{\rho} + \bar{p})\delta u_{\parallel i}, \tag{2.45b}$$

$$\left[\Psi'' + \mathcal{H}(2\Psi + \Phi)' + (2\mathcal{H}' + \mathcal{H}^2)\Phi + \frac{1}{2}\nabla^2(\Phi - \Psi)\right]\delta_{ij} - \frac{1}{2}(\Phi - \Psi)_{,ij} = 4\pi G a^2 \delta p \delta^i{}_j. \tag{2.45c}$$

The off-diagonal equations in the last expression $i \neq j$ set $\Phi = \Psi$. This allows us to manipulate Eqs. (2.45a)-(2.45c) after introducing (2.44) to find a dynamical equation for Φ

$$\Phi'' + 3(1 + c_s^2)\mathcal{H}\Phi' - c_s^2\nabla^2\Phi + [2\mathcal{H}' + (1 + 3c_s^2)\mathcal{H}^2]\Phi = 4\pi G a^2 \tau \delta S. \tag{2.46}$$

Tensor perturbations, on the other hand, obey the following equations of motion

$$h''_{ij} + 2\mathcal{H}h'_{ij} - \nabla^2 h_{ij} = -16\pi G a^2 \Pi_{ij}, \tag{2.47}$$

where the anisotropic stress Π_{ij} is the transverse-traceless projection of $\delta T^i{}_j$, which vanishes for a perfect fluid. We revisit this equation and investigate the propagation of gravitational waves in Sec. 4.2.

3 Early Universe

The minimal standard model of cosmology is often considered to extend to as early as Big Bang nucleosynthesis. Before the era of recombination, when decoupling occurred and the photons as seen in the CMB were emitted, the Universe was a highly opaque plasma, so electromagnetic observations are not possible. Primordial abundances are the only early observable coming from that opaque Universe that we can reliably study with the knowledge about particle physics as it happens on Earth.

Should we travel further into the past, the description of physics becomes trickier, as processes such as quantum chromodynamics (QCD) confinement, the electroweak (EW) phase transition and others, which we might not be aware of, happen as the temperature of the Universe rises. The only way we can gain insight into this primitive state of the Universe is by analysing the effect of the initial conditions it sets on what we can observe, primarily on the anisotropies of the CMB (Sec. 1.2), but also on IGMF (Sec. 1.5) or stochastic GW backgrounds (Sec. 4.1). Cosmic inflation stands out as the most favoured and agreed upon theory for the earliest Universe, which we overview in Sec. 3.1. In Sec. 3.2, we discuss reheating, which links inflation and standard cosmology. Finally, in Sec. 3.3, we discuss baryogenesis and the issue of the baryon asymmetry generation.

3.1 Inflation

Inflation [Sta80] is an epoch in the early Universe during which it undergoes accelerated expansion, rapidly increasing its size. It was first proposed in [Gut81] as a solution to two problems regarding initial conditions

- The first one is the *flatness problem*, which states that, for the Universe to be as spatially flat as we observe it today, it requires a big fine-tuning of the initial conditions if the radiation-dominated era extends up to Planck energy scales. It still requires a great amount of fine-tuning considering the radiation-dominated era only up to Big Bang nucleosynthesis. A period of accelerated expansion exponentially decreases the curvature, alleviating this issue.

- The second one is the *horizon problem*. This raises a question about the fact that we observe a homogeneous and isotropic Universe even though there are regions in the sky which, if cosmic evolution is as in the cosmological standard model, are causally disconnected. Inflation allows these regions to have been

causally connected before the accelerated expansion happened, which drastically separated them.

There has been a wide variety of proposals to the question of what causes inflation or how it is implemented. The most popular framework, even to this day, was proposed just a few years later than Guth's original work in [Lin83] and it is based on a simple model of a dynamical homogeneous scalar field, dubbed the inflaton, that slowly rolls down a potential. It was shown to be a viable mechanism for a wide variety of initial conditions and shapes of the scalar field potential. It suffices to generate an accelerated expansion and it features a *graceful exit*, i.e. a naturally implemented end to inflation. In what follows, we lay the basics of this *slow-roll inflation*, which can be found in many books in the literature, for example [LL00].

3.1.1 Slow-roll inflation

Let us consider the action of a homogeneous scalar field in a RW background, which reads

$$S[\phi] = \int \mathrm{d}^4x \sqrt{g}\left(\frac{1}{2}g^{\mu\nu}\partial_\mu\phi\partial_\nu\phi - V(\phi)\right). \tag{3.1}$$

The equation of motion can be obtained by varying this action with respect to ϕ, which yields

$$\ddot{\phi} + 3H\dot{\phi} + V'(\phi) = 0. \tag{3.2}$$

The stress-energy tensor, as defined in (2.12), acquires a diagonal form as with a perfect fluid (2.14), so we can identify the energy density and pressure

$$\rho_\phi = \frac{1}{2}\dot{\phi}^2 + V(\phi), \tag{3.3}$$

$$p_\phi = \frac{1}{2}\dot{\phi}^2 - V(\phi). \tag{3.4}$$

Here we see that a scalar field can generate an accelerated expansion by slowly rolling down its potential, in which case the kinetic energy is much smaller than the potential $\dot{\phi}^2 \ll V$. Under this condition, the effective equation of state it acquires is $w_\phi \simeq -1$, mimicking a cosmological constant.

While the slow-roll regime is applicable, the first term in the equation of motion (3.2) can be neglected and it simplifies to

$$3H\dot{\phi} \simeq -V'(\phi), \tag{3.5}$$

while the expansion of the Universe is controlled by Friedmann's equation (2.15)

$$H^2 = \frac{8\pi G}{3}V(\phi), \tag{3.6}$$

so the Hubble rate remains nearly constant during slow-roll and $a(t) \propto e^{Ht}$.

The slow-roll regime works as long as the inflaton does not roll too quickly $\dot{\phi}^2 \ll V$ or accelerate too quickly $\ddot{\phi} \ll H\dot{\phi} \sim V'(\phi)$, so that the approximations we have made so far do hold. This is controlled by the slow-roll parameters

$$\epsilon = \frac{1}{16\pi G}\left(\frac{V'}{V}\right)^2 \simeq -\frac{\dot{H}}{H^2}, \tag{3.7}$$

$$\delta = \frac{1}{8\pi G}\frac{V''}{V}, \tag{3.8}$$

which we demand to be small $\epsilon, |\delta| \ll 1$. The end of inflation is usually defined as the moment when one of these two parameters reaches unity, when the slow-roll approximation no longer holds and the Universe's accelerated expansion halts. Note that the equation of state during inflation can be written in terms of the slow-roll parameters as $w = -1 + 2\epsilon/3$ up to first order. Since $\epsilon > 0$ by definition, slow-roll inflation never crosses the phantom threshold.

A way of gauging time within inflation is the number of e-folds before the end of inflation

$$N(t) = \log\frac{a_f}{a(t)} = \int_t^{t_{\rm end}} \mathrm{d}t' H(t') \simeq 8\pi G \int_{\phi_{\rm end}}^{\phi(t)} \mathrm{d}\hat{\phi}\frac{V(\hat{\phi})}{V'(\hat{\phi})} \tag{3.9}$$

While the exact number depends on the details of the model, we need $40 \sim 50$ e-folds to solve the flatness and horizon problems in a typical realisation of inflation.

3.1.2 Origin of metric perturbations

Besides being able to solve the horizon problems, cosmic inflation has established itself as the theory for the early Universe following its ability to reproduce the small anisotropies we see in the CMB and the inhomogeneities in the matter distribution. It was first realised in [MC81] that the quantum fluctuations of the metric during a de Sitter phase produced a nearly scale-invariant red-tilted power spectrum of metric perturbations. The complete formalism on the perturbations produced by the inflaton was developed in [MFB92], which we already reviewed in Sec. 2.4.

In what follows, we describe the main results of quantising a slow-roll inflation model: The inflaton, which is expanded as a background homogeneous solution plus a perturbative part

$$\phi(\eta, \mathbf{x}) = \bar{\phi}(\eta) + \delta\phi(\eta, \mathbf{x}), \tag{3.10}$$

acts as a source of metric perturbations, entering the right-hand side of (2.42). The perturbed inflaton must then be quantised, and its quantum fluctuations excite the vacuum and produce a Gaussian power spectrum of metric perturbations. For the scalar perturbation Φ in Fourier space, the variance can be expressed as

$$\langle \Phi_{\mathbf{k}} \Phi_{\mathbf{k}'} \rangle = |\Phi_k|^2 \delta^{(3)}(\mathbf{k} - \mathbf{k}'), \tag{3.11}$$

and the power spectrum is defined in terms of the curvature perturbation $\mathcal{R}_{\mathbf{k}}$, which for super-Hubble scales has the virtue of being constant and is related to the scalar

perturbation as

$$\Phi_{\mathbf{k}} = -\frac{3+3w}{5+3w}\mathcal{R}_{\mathbf{k}}, \tag{3.12}$$

where w is the equation of state of the dominating fluid, so the scalar power spectrum is

$$\mathcal{P}_{\mathcal{R}} = \frac{k^3}{2\pi^2}|\mathcal{R}_k|^2. \tag{3.13}$$

Metric perturbations are excited when they dwell inside the Hubble horizon, and after leaving the horizon, they freeze and undergo decoherence, becoming classical perturbations. This primordial power spectrum is often parametrised in terms of an amplitude A_S and a spectral tilt n_S

$$\mathcal{P}_{\mathcal{R}}(k) = A_S\left(\frac{k}{k_*}\right)^{n_S-1}, \tag{3.14}$$

where k_* is a pivot scale. In slow-roll inflation generated by a single scalar field, perturbations are adiabatic, and the parameters that characterise them can be linked to the slow-roll parameters [LL92], as they are sufficient to gauge the size of the perturbations at horizon crossing $k \sim aH$

$$n_S - 1 = -6\epsilon + 2\delta, \tag{3.15}$$

$$A_S = \frac{8}{3\epsilon}\frac{V}{M_P^4}, \tag{3.16}$$

where these quantities must be evaluated at horizon crossing for the pivot scale. Note that, as long as slow-roll holds, the generated spectrum is nearly scale-invariant $|n_S - 1| \ll 1$.

Similarly, a tensor power spectrum is also excited, which is given by

$$\mathcal{P}_T(k) = \frac{k^3}{2\pi^2}|h_k|^2 = 16\pi G\left(\frac{H}{2\pi}\right)^2\Big|_{k=aH}. \tag{3.17}$$

If parametrised similarly to the scalar power spectrum

$$\mathcal{P}_T = A_T\left(\frac{k}{k_*}\right)^{n_T} \tag{3.18}$$

the tensor tilt is

$$n_T = -2\epsilon, \tag{3.19}$$

and the tensor amplitude is usually recast into the tensor-to-scalar ratio

$$r(k_*) = \frac{\mathcal{P}_T(k_*)}{\mathcal{P}_{\mathcal{R}}(k_*)} = 16\epsilon. \tag{3.20}$$

Note that a consistency relation between tensor tilt and tensor-to-scalar ratio holds $r = -8n_T$.

3.2 Reheating

Reheating is the transitory period between the accelerated expansion in inflation and standard cosmology, with a radiation-dominated Universe filled with the particles of the Standard Model. The characteristics of reheating are mostly determined by the inflaton model, how its potential is outside the slow-roll regime and the possible couplings it might have to Standard-Model particles.

Unlike inflation, reheating, even though it involves particles in the Standard Model and is closer to us in time, yields little-to-no impact on large-scale structure observables, so it remains virtually unknown. Recently, it was noted in [FT19] that primordial GW observations in high-frequency bands, together with the radiation limits on BBN, could be a source of information about the reheating equation of state, although no observations have been made in this direction yet.

Due to this lack of knowledge about the reheating phase, in works where only the spacetime dynamics need to be determined and the details of the particle phenomenology are less relevant (such as the one presented in Chapter 5), it is often described in terms of a perfect fluid with effective equation of state w. This, together with the Hubble rate at the end of inflation H_I and the reheating temperature $T_{\rm RH}$, which is defined as the temperature at which the Universe fully thermalises thus ending reheating, are sufficient to describe the dynamics. In this section, we describe reheating in terms of these parameters and determine how it links inflation and standard cosmology.

The inflaton dominates the energy density at the end of inflation, so the Hubble rate is directly related to it via the Friedmann equation (2.15)

$$H_I^2 = \frac{8\pi G}{3}\rho_I. \tag{3.21}$$

This energy density, which still dominates during reheating but now with equation of state w, can be linked to the energy density at the end of reheating by scaling with the energy conservation (2.18) as

$$\rho_I = \rho_{\rm RH}\left(\frac{a_{\rm RH}}{a_I}\right)^{3(1+w)}, \tag{3.22}$$

where a_I and $a_{\rm RH}$ are the scale factors at the end of inflation and reheating, respectively. Taking into account the time evolution of the scale factor in terms of conformal time (2.20) during reheating $a \propto \eta^{2/(1+3w)}$, we can write

$$\frac{a_{\rm RH}}{a_I} = \left(\frac{\eta_{\rm RH}}{\eta_I}\right)^{\frac{2}{1+3w}}. \tag{3.23}$$

By considering that all the energy budget goes into creating the relativistic species of the Standard Model, we can use (2.31) to write the energy density at the end of reheating

$$\rho_{\rm RH} = \frac{\pi^2}{30} g_*(T_{\rm RH}) T_{\rm RH}^4, \tag{3.24}$$

where typically the reheating temperature is large enough to include all species in the Standard Model when counting degrees of freedom for $g_*(T_{\rm RH})$. Finally, entropy conservation (2.36) can be used to write $a_{\rm RH}$ in terms of the reheating temperature

$$a_{\rm RH} = \left(\frac{g_{*s}(T_0)}{g_{*s}(T_{\rm RH})}\right)^{1/3} \frac{T_0}{T_{\rm RH}}. \tag{3.25}$$

Putting these results together, we can obtain expressions for the duration of reheating

$$\frac{\eta_{\rm RH}}{\eta_I} = \left(\frac{45 H_I^2 M_P^2}{4\pi^3 g_*(T_{\rm RH}) T_{\rm RH}^4}\right)^{\frac{1+3w}{6(1+w)}}, \tag{3.26}$$

as well as for the comoving size of the Hubble horizon at the end of inflation $k_I = a_I H_I$

$$k_I = \left(\frac{4\pi^3 g_*(T_{\rm RH})}{45}\right)^{\frac{1}{3+3w}} \left(\frac{g_{*s}(T_{\rm RH})}{g_{*s,0}}\right)^{\frac{1}{3}} \left(\frac{T_{\rm RH}}{M_P}\right)^{\frac{1-3w}{3+3w}} \left(\frac{H_I}{M_P}\right)^{\frac{1+3w}{3+3w}} T_0. \tag{3.27}$$

3.3 Baryogenesis

Matter is ubiquitous, not only on Earth, but in the Universe as a whole. The absence of *antimatter*, which at sufficiently high temperatures in the early stages of cosmic evolution translates into a net excess of matter over antimatter, is one of the long-standing problems in cosmology. This matter-antimatter asymmetry is quantified in terms of the baryonic asymmetry η_B defined in Eq. (1.13) and that we discussed as a key parameter for BBN in Sec. 1.4.

Disregarding this imbalance as a possible initial condition, especially if we accept inflation as an early stage of cosmology, which would drastically dilute the asymmetry, we need baryogenesis, i.e., a process that generates net baryon number after inflation but before primordial nucleosynthesis. In [Sak67], Sakharov identified the three conditions needed for a process to be a valid baryogenesis mechanism, which are 1) violation of baryon number, 2) violation of C-symmetry and CP-symmetry and 3) departure from thermal equilibrium. The sphaleron, a topological solution of the electroweak theory that operates above the electroweak scale, is the only process within the Standard Model capable of producing baryogenesis [KRS85]. Sphalerons violate baryon and lepton number conservation [tHoo76] in a way that $B-L$ is preserved, but are not able to produce the observed asymmetry within the Standard Model (see electroweak baryogenesis below).

Baryogenesis has been a field with many proposals beyond the Standard Model (see [BB21] for a recent review). Some of the most relevant ones have been

- Some *Grand Unification Theories* (GUTs) naturally feature processes that mix quarks and leptons and thus might violate baryon and lepton number conservation, such as leptoquarks, bosons that mediate interactions between baryons and leptons and carry both numbers. GUTs were especially considered during

the early stages of baryogenesis research, and the first viable proposals were discussed in this framework [DS78].

- *Electroweak baryogenesis* is the name that receives the baryon number generation during the electroweak phase transition [FS93; CKN93]. For EW baryogenesis to work, the electroweak phase transition is required to be first order in order to generate a departure from equilibrium and not to wipe out the generated asymmetry. Such a strongly first-order phase transition is not possible without modifications to the Standard Model, especially to the Higgs sector, which is responsible for the phase transition.

- *Leptogenesis* is a categorisation that refers to models that implement first some mechanism that violates lepton number, which is later converted into baryon number through electroweak sphaleron processes. The original implementation of this mechanism [FY86] relied on the introduction of right-handed Majorana neutrinos in the Standard Model, whose mass term breaks lepton symmetry. For right-handed neutrinos in thermal equilibrium, this mechanism requires a reheating temperature $T_{\rm RH}$ above the right-handed neutrino mass m_R which should satisfy $m_R \gtrsim 10^9$ GeV [BDP05; Kam+20]. For non-thermally produced neutrinos these constraints could be relaxed [Asa+99; PU04; CMO22]. *Gravitational leptogenesis* [APS06] is a particular leptogenesis proposal that relies on the chiral gravitational lepton anomaly to generate the lepton imbalance. In Chapter 5, we talk about this realisation of leptogenesis and analyse its viability within a minimal inflationary scenario.

4 Gravitational waves

Gravitational waves are a cornerstone of Einstein's general theory of relativity [Ein18], which are propagating waves of the spacetime curvature with no Newtonian equivalent. This Chapter aims to motivate its introduction in a cosmological context as one of the observational pillars of the future in cosmology. In Sec. 4.1, we discuss the present state and forecast of GW observations. In Sec. 4.2, we analyse the propagation of GWs in an expanding universe. Finally, we introduce the formalism to study stochastic GW backgrounds in Sec. 4.3.

4.1 Observational status

A new era in observational astrophysics and cosmology opened up in 2015 when LIGO [Aas+15], a set of two four-kilometre Michelson laser interferometers, detected a gravitational-wave signal for the first time, named GW150914 [Abb+16] after the date of the event. This signal originated in the last stages of inward spiralling and merger of two solar-mass black holes (BHs), and it perfectly matched the predictions of General Relativity.

Over the last decade, joint efforts of LIGO and two more interferometers, VIRGO [Ace+15] since the second observation run and more recently KAGRA [Aku+19], which joined for the ongoing fourth observation run, have been able to resolve dozens of gravitational waves. While most observations are compatible with BH-BH mergers, mergers of two neutron stars (NS) [Abb+17a] and BH-NS mergers [Abb+21] have also been observed. Some observations, such as GW190814 [Abb+20], also feature compact objects in the mass gap between the heaviest known NS and the lightest known BH, whose nature remains unknown.

The first detected NS-NS merger GW170814 [Abb+17a] was also the first observation made by three interferometers, the two from LIGO and the VIRGO one. The addition of a third detector allowed to measure the polarisation of the wave for the first time, and it also improved the localisation in the sky, reducing the 90% credible area from 1160 deg^2 down to 60 deg^2. Such an improvement created the possibility of tracking the mergers in search for electromagnetic counterparts, and in fact, the gamma-ray burst GRB170817A was found in the same region of the sky as the GW source just two seconds later [Abb+17b]. The time delay between the two signals allowed to put a limit on an anomalous GW velocity c_T, which GR predicts to be the

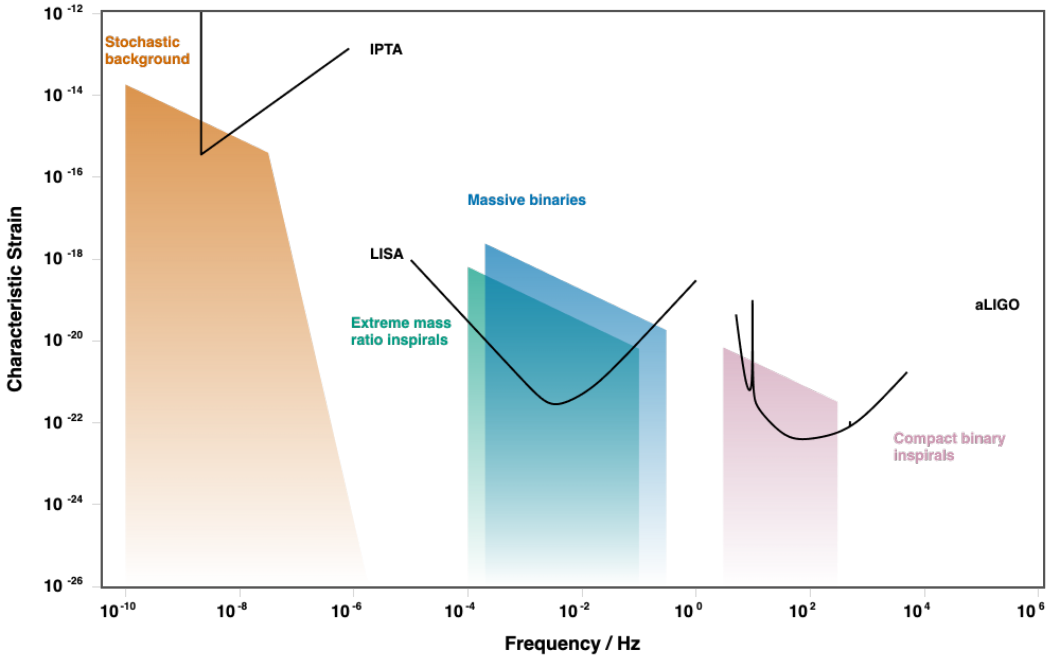

Figure 4.1: GW strains expected for different sources, sorted as a function of frequency. The design sensitivity curves of various operating and forecast detectors are also plotted. Three clear frequency bands can be identified: Solar-mass compact object mergers belong in the high-frequency band, which is explored by ground-based interferometers. An intermediate-frequency band of GWs is generated by mergers involving massive black holes, which will be investigated by space-based interferometers. Stochastic GW backgrounds belong in the low-frequency band and can be directly observed by pulsar timing arrays. Credit: [MCB15].

speed of light

$$\delta c = \frac{|c_T - c|}{c}, \tag{4.1}$$

at $\delta c \lesssim \mathcal{O}(10^{-15})$ in the GW detector operating band (10 Hz-10 kHz). Such a strong constraint ruled out many models beyond General Relativity, which featured different GW phase velocities or massive gravitons.

Solar-mass compact object mergers are not the only possible source of GWs in the Universe. In Fig. 4.1, we plot the expected GW strain over the frequency spectrum for different types of sources. Mergers involving massive objects, such as massive binaries or extreme mass ratio inspirals, are expected to be observed in lower frequencies by planned space-based GW detectors, such as LISA [Ama+17] or TianQin [Luo+16]. Space-based detectors are also Michelson interferometers but feature much longer arms, thus allowing for observation of lower-frequency GWs, which are planned to start operating in the 2030s.

On the frequency lower end, there are the gravitational-wave stochastic backgrounds. These, contrary to the resolved single events described in the previous cases, are unresolved cumulative signals that are described statistically. Two differentiated types of stochastic backgrounds have been predicted, often dubbed astrophysical and cosmological. On the one hand, the astrophysical background is a cumulative signal that originates in a cosmic population of unresolved supermassive binaries happening in a hierarchical structure formation scenario [Ses+04]. The presence of this kind of background can be tracked down by observing the time of arrival from millisecond pulsars in pulsar-timing arrays (PTAs). Recently, analysis of the 12.5-year observation by the NANOGrav collaboration [Arz+20] have found statistical evidence for such an isotropic background, although with some discrepancies with GR predictions.

On the other hand, cosmological backgrounds are originated by events prior to structure formation, such as phase transitions [CDS10] or an inflationary phase, as we discussed in Sec. 3.1. We revisit the inflationary tensor power spectrum in more detail in Sec. 4.3. A stochastic background generated by slow-roll inflation, in particular, although it spans all frequencies, is not feasible to be detected directly by current or forthcoming interferometers due to its small strength [Las+16]. The future detection of primordial GW could take place not directly but through the measurement of the low-multipole ($\ell < 200$) region of the CMB polarisation B-mode angular power spectrum, on which we commented at the end of Sec. 1.2. Ongoing and future experiments with a strong focus on B-mode observations are forecast to measure the CMB B-mode polarisation in the coming years, with enough precision to detect the imprint of a tensor power spectrum with tensor-to-scalar ratio as small as $r = 10^{-3}$.

The gravitational waves that conform the primordial GW background, having travelled all the way through from the end of inflation, are very sensitive to any modification of the matter-energy content of the universe in any cosmological era which could affect its propagation. In particular, and unlike perfect fluids or scalar fields, the presence of a coherent vector field that could play any role in the dark sector, could induce a non-zero contribution to the tensor anisotropic stress, altering its propagation. We investigate this possibility in Chapter 6. In what follows, we describe its standard propagation, within ΛCDM.

4.2 Gravitational-wave propagation

In this section, we investigate the propagation of gravitational waves in an expanding universe. The equation of motion was derived in the framework of tensor metric perturbations in Sec. 2.4, which is (2.47). Let us focus first on propagation in vacuum, with no anisotropic stress

$$h''_{ij} + 2\mathcal{H}h'_{ij} - \nabla^2 h_{ij} = 0. \tag{4.2}$$

The tensor perturbation h_{ij} is transverse and traceless, and symmetric as it is part of the metric tensor. After Fourier-transforming the tensor metric perturbation, if

we work in a frame $\{\mathbf{u}_1, \mathbf{u}_2, \mathbf{u}_3\}$ so that $\mathbf{u}_3 = \hat{\mathbf{k}}$ is the propagation direction of the GW with wavevector $\mathbf{k}$, then this tensor can be written as

$$h_{ij} = \begin{pmatrix} h_+ & h_\times & 0 \\ h_\times & -h_+ & 0 \\ 0 & 0 & 0 \end{pmatrix}, \tag{4.3}$$

where $\{+, \times\}$ (named plus and cross polarisation respectively) refer to the linear polarisation basis. These can be easily related to the right-left circular polarisation basis via

$$h_{\substack{R \\ L}} = \frac{h_+ \mp i h_\times}{\sqrt{2}}. \tag{4.4}$$

In either basis, Eq. (4.2) yields the well-known GW propagation equation in vacuum

$$h_\lambda'' + 2\mathcal{H} h_\lambda' + k^2 h_\lambda = 0, \tag{4.5}$$

where $k = |\mathbf{k}|$ and $\lambda = \{+, \times\}$ is one of the polarisations.

The evolution of an arbitrary GW mode can be qualitatively understood by changing functions to $v_\lambda = a h_\lambda$, which leaves the propagation equation as follows

$$v_\lambda'' + \left(k^2 - \frac{a''}{a}\right) v_\lambda = 0. \tag{4.6}$$

In a typical cosmological epoch, $a(\eta) \propto \eta^\alpha$, so $a''/a \propto 1/\eta^2 \sim \mathcal{H}^2$. Thus, inside the Hubble horizon $k \gg \mathcal{H}$, the last term in (4.6) can be neglected and v_λ allows for an oscillatory solution with constant amplitude. As a result, the GW mode h_λ oscillates with its amplitude damped as $1/a$.

Outside the Hubble horizon $k \ll \mathcal{H}$, the k^2 term in Eq. (4.5) can be neglected, and h_λ admits a solution in terms of a constant mode and a damping mode, the former of which dominates in the long term. To a good approximation, we can thus consider that super-Hubble waves remain at a constant value regardless of the background expansion, as it is always possible to find a solution $h_\lambda' = 0$. In fact, in the super-Hubble regime, the equation can be re-written as $(a^2 h_\lambda')' = 0$, so the non-constant mode $h_\lambda' \propto a^{-2}$ is a decaying mode in a normal cosmological scenario.

The exact propagation in ΛCDM can only be derived by first solving the Friedmann equation (2.22) for $a(\eta)$, taking into account all abundances, and then solving the GW propagation equation. This can only be done numerically. An example of the evolution for different wavelengths is shown in Fig. 4.2, where the qualitative behaviour discussed above is well depicted. However, it is still interesting to analyse the phenomenology in the different epochs of cosmic evolution, which we present as follows.

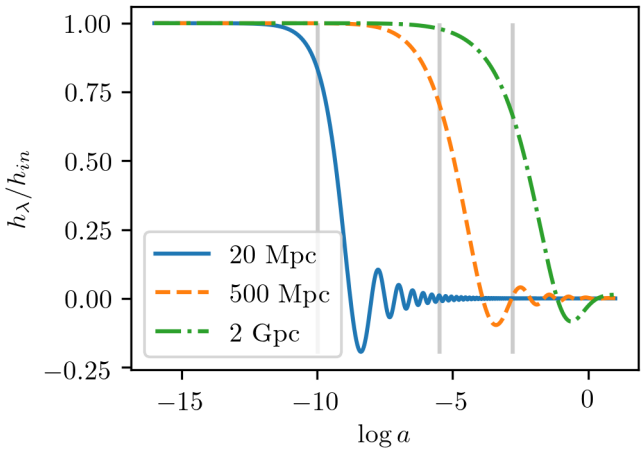

Figure 4.2: Time evolution of GWs in ΛCDM, normalised by their primordial value, with three different reduced wavelengths k^{-1} as indicated in the legend. The vertical lines indicate when each GW enters the Hubble horizon, i.e. $k = \mathcal{H}$, and coincide with the moment the damped oscillation starts.

4.2.1 Matter-dominated era

When dust dominates, the scale factor can be written as $a(\eta) = a_M \eta^2$, which leaves the propagation equation (4.5) as

$$h_\lambda'' + \frac{4}{\eta} h_\lambda' + k^2 h_\lambda = 0. \tag{4.7}$$

This equation admits solutions in terms of the spherical Bessel functions of order $\ell = 1$ (see Appendix B), which can be written in terms of trigonometric functions

$$h_\lambda(\eta) = \frac{C_1}{(k\eta)^2}\left(\frac{\sin k\eta}{k\eta} - \cos k\eta\right) + \frac{C_2}{(k\eta)^2}\left(\frac{\cos k\eta}{k\eta} + \sin k\eta\right). \tag{4.8}$$

In the super-Hubble limit, the mode with C_2 is a decaying mode, so we discard it, while the other one reaches an asymptotic value of $C_1/3$. Setting a constant value $h_{\rm in}$ outside the horizon, a general solution in the MD era can be readily obtained

$$h_\lambda(\eta) = \frac{3h_{\rm in}}{(k\eta)^2}\left(\frac{\sin k\eta}{k\eta} - \cos k\eta\right), \tag{4.9}$$

which indeed decays as $h_\lambda \propto 1/\eta^2 \propto 1/a$ inside the horizon.

4.2.2 Radiation-dominated era

When relativistic species dominate, before the matter-radiation equality, the scale factor can be written as $a(\eta) = a_R \eta$. In this case, we can make $a''/a = 0$ exactly, so Eq.

(4.6) can be solved in terms of trigonometric functions for v_λ. Thus, the GW modes acquire the following form

$$h_\lambda(\eta) = C_1 \frac{\sin k\eta}{k\eta} + C_2 \frac{\cos k\eta}{k\eta}. \tag{4.10}$$

In the super-Hubble regime, the mode multiplying C_2 is decaying, so we discard it. Again, setting a constant value $h_{\rm in}$ outside the horizon, the solution is

$$h_\lambda(\eta) = h_{\rm in} \frac{\sin k\eta}{k\eta}. \tag{4.11}$$

Lastly, let us mention a phenomenon that modifies GW propagation and that is especially relevant during the RD era. Free streaming of relativistic particles is the only process within the Standard Model known to cause anisotropic stress, which enters the right-hand side of Eq. (2.47). Photon free streaming, happening after the recombination era $z_{\rm rec} \simeq 1100$, occurs when matter is already dominating the expansion of the universe, so the effect it causes is very small. *Neutrino free streaming*, on the other hand, occurs after neutrinos decouple from the primordial plasma at $T_{\rm dec} \simeq 1$ MeV, when the universe is still in the radiation-dominated era. It was first noted in [Wei04], and it modifies Eq. (4.5) as follows

$$h_\lambda'' + 2\mathcal{H}h_\lambda' + k^2 h_\lambda = -24 f_\nu \mathcal{H}^2 \int_{\eta_{\rm dec}}^{\eta} {\rm d}\eta' \frac{j_2[k(\eta-\eta')]}{k^2(\eta-\eta')^2} h_\lambda'(\eta'), \tag{4.12}$$

where $\eta_{\rm dec}$ is the time of neutrino decoupling, $f_\nu = \rho_\nu/\rho$ is the neutrino fraction of energy density and j_2 is a spherical Bessel function (see Appendix B.1). During RD era after neutrino decoupling, $f_\nu = \rho_\nu/\rho_\gamma \simeq 0.4$ for three neutrino families.

The effect of neutrino free streaming is most felt by modes that entered the horizon after neutrino decoupling, in order to have $h_\lambda' \neq 0$, but before the matter-dominated era, when the neutrino fraction $f_\nu \to 0$. Numerical analysis yields that modes satisfying these conditions have an almost identical solution in the super-Hubble regime, while deep inside the horizon they follow Eq. (4.11) with a diminished amplitude $h_{\rm in} \to 0.8 h_{\rm in}$.

4.3 Tensor power spectra and Stokes parameters

The tensor perturbations predicted by inflation, as well as by other unresolvable astrophysical sources, can be described in terms of a stochastic Gaussian background of GWs. One can define the tensor power spectrum $P_T(\mathbf{k},\eta)$ in the usual way

$$\sum_{\lambda,\lambda'} \langle h_\lambda(\eta,\mathbf{k}) h_{\lambda'}^*(\eta,\mathbf{k}')\rangle = \delta^{(3)}(\mathbf{k}-\mathbf{k}') P_T(\mathbf{k},\eta), \tag{4.13}$$

where $\langle \ldots \rangle$ represents an ensemble average. Similarly, power spectra for both linear polarisations can also be defined, as well as a correlator between them

$$\langle h_+(\eta,\mathbf{k}) h_+^*(\eta,\mathbf{k}')\rangle = \delta^{(3)}(\mathbf{k}-\mathbf{k}') P_+(\mathbf{k},\eta), \tag{4.14a}$$

$$\langle h_\times(\eta,\mathbf{k})h_\times^*(\eta,\mathbf{k}')\rangle = \delta^{(3)}(\mathbf{k}-\mathbf{k}')P_\times(\mathbf{k},\eta), \tag{4.14b}$$

$$\langle h_+(\eta,\mathbf{k})h_\times^*(\eta,\mathbf{k}')\rangle = \delta^{(3)}(\mathbf{k}-\mathbf{k}')P_{+\times}(\mathbf{k},\eta). \tag{4.14c}$$

If linear polarisations are uncorrelated, i.e. $\langle h_+ h_\times^*\rangle = \langle h_\times h_+^*\rangle = 0$, then the total power spectrum is just the sum of the partial power spectra $P_T = P_+ + P_\times$, whereas the difference $P_+ - P_\times$ yields the net linear polarisation of the GW background. If correlation does exist, its real part is associated with linear polarisation as well, whereas its imaginary part indicates parity violation.

In order to quantify these degrees of polarisation, it is possible to define the Stokes parameters for the GWs [ST08; GM17] I, Q, U and V, which are analogous to their more common electromagnetic counterparts. These can be expressed in terms of the plus and cross power spectra and the plus-cross correlator (4.14) as

$$I = P_+ + P_\times = P_T, \tag{4.15a}$$

$$Q = P_+ - P_\times, \tag{4.15b}$$

$$U = -2\,\mathrm{Re}\,P_{+\times}, \tag{4.15c}$$

$$V = -2\,\mathrm{Im}\,P_{+\times}. \tag{4.15d}$$

I is the total power spectrum, Q accounts for linear polarisation in the plus-cross basis, U measures linear polarisation in a basis that differs in a rotation from the former, and V gauges the circular polarisation. Non-zero Q or U parameters indicate an anisotropic GW configuration, whereas a non-zero V parameter means a parity-violating configuration.

The primordial GW background generated during inflation is typically described as a Gaussian, isotropic and unpolarised stochastic ensemble (even though each particular realisation does not need to be so individually), in which case the equality

$$P_{+,\mathrm{in}} = P_{\times,\mathrm{in}} = \frac{1}{2}P_{T,\mathrm{in}} \tag{4.16}$$

arises naturally, with "in" referring to primordial quantities. The primordial tensor power spectrum per logarithmic interval in k, denoted $\mathcal{P}_{T,\mathrm{in}}$, was defined in Eq. (3.17) and is related to P_T as

$$\mathcal{P}_{T,\mathrm{in}}(k) = \frac{k^3}{2\pi^2}P_{T,\mathrm{in}}(k). \tag{4.17}$$

This is often parametrised as in Eq. (3.18), and the tensor amplitude A_T is usually written in terms of the comoving curvature power spectrum amplitude A_S (3.14) and the tensor-to-scalar ratio r (3.20).

The power spectrum within standard cosmology can then be obtained at a later time through the transfer function $T(k,\eta)$, which relates the value of a specific GW mode at a specific time with its primordial value

$$h_\lambda(k,\eta) = T(k,\eta)h_\lambda(k,\eta_{\mathrm{in}}). \tag{4.18}$$

The transfer function for modes that enter the Hubble horizon during MD and RD eras can be directly read from Eqs. (4.9) and (4.11) respectively. In every case, $T \to 1$ when modes have not entered the Hubble horizon yet $k\eta \ll 1$, and they decay $T \ll 1$ deep inside the horizon $k\eta \gg 1$.

Since power spectra are quadratic in h, they relate via the squared modulus of the transfer function, one has

$$P_T(k,\eta) = |T(k,\eta)|^2 P_{T,\mathrm{in}}(k), \tag{4.19}$$

and similarly for the power spectrum per log interval $\mathcal{P}_T(k,\eta)$. Notice that in standard cosmology, the transfer function does not depend on the propagation direction nor the polarisation of the GW, as can be seen from the equation of propagation (4.5). As a result, if the GW background is primordially isotropic or unpolarised, these will be ever-present features of this background at any future time.

Another interesting quantity to compute, which is related to the tensor power spectrum and is widely used to express the sensitivity of GW detectors, is the GW abundance today per log frequency interval [Mag07]. It is usually defined as follows

$$\Omega_{\mathrm{GW}} = \frac{1}{\rho_c}\frac{\mathrm{d}\rho_{\mathrm{GW}}}{\mathrm{d}\log k}, \tag{4.20}$$

where the gravitational wave density today is given by

$$\rho_{\mathrm{GW}} = \frac{\langle h'_{ij} h'_{ij} \rangle}{32\pi G}. \tag{4.21}$$

The GW abundance can be related to the tensor power spectrum today as

$$\Omega_{\mathrm{GW}} = \frac{k^2}{12H_0^2}\mathcal{P}_T(k,\eta_0), \tag{4.22}$$

which can ultimately be written in terms of the primordial power spectrum (4.17) thanks to the transfer function (4.19).

4.3.1 Modified propagation

Even though the primordial background is unpolarised, there is also the possibility that, in the framework of a theory beyond the standard cosmology, the modified GW propagation equations differ for both polarisations, resulting in a richer power spectrum in later stages of cosmic evolution. Let us introduce the formalism necessary to characterise this different propagation. The deviation from ΛCDM can then be encoded in four *ratio functions* $R_{\lambda\lambda'}$, which are defined as the ratio of the GW amplitudes beyond (labelled *new*) and within the cosmological standard model (labelled *SM*)

$$\begin{pmatrix} h_+^{\mathrm{new}} \\ h_\times^{\mathrm{new}} \end{pmatrix} = \begin{pmatrix} R_+ & R_{+\times} \\ R_{\times+} & R_\times \end{pmatrix} \begin{pmatrix} h_+^{\mathrm{SM}} \\ h_\times^{\mathrm{SM}} \end{pmatrix}, \tag{4.23}$$

where we define $R_\lambda \equiv R_{\lambda\lambda}$. Note that non-zero $R_{\lambda\lambda'}$ with $\lambda \neq \lambda'$ are only possible when both polarisations mix, since one has to act as a source of the other. Besides cosmological parameters, these ratio functions can have additional dependencies such as the direction of observation or new parameters of the model.

These ratio functions play the role of a transfer function, only linking two different cosmological models instead of two times. Therefore, in order to relate power spectra emerging from standard and modified propagations, we need to consider the corresponding squared modulus of ratio functions as one does with transfer functions in (4.19).

Let us consider a theory for which both linear polarisations mix, a phenomenon that can affect all Stokes parameters. With the idea that ratio functions mimic transfer functions, we can write the Stokes parameters (4.15) for the new theory in terms of the standard cosmology tensor power spectrum (4.19) $P_T^{\rm SM}$ and the ratio functions as $S = \mathcal{S} P_T^{\rm SM}$, where S is any of the four Stokes parameters and $\mathcal{S}$ the associated reduced Stokes parameter. These have the following expressions

$$\mathcal{I} = \frac{1}{2}(|R_+|^2 + |R_\times|^2 + |R_{+\times}|^2 + |R_{\times+}|^2), \tag{4.24a}$$

$$\mathcal{Q} = \frac{1}{2}(|R_+|^2 - |R_\times|^2 + |R_{+\times}|^2 - |R_{\times+}|^2), \tag{4.24b}$$

$$\mathcal{U} = -\mathrm{Re}(R_+ R_{\times+}^* + R_\times R_{+\times}^*), \tag{4.24c}$$

$$\mathcal{V} = -\mathrm{Im}(R_+ R_{\times+}^* - R_\times R_{+\times}^*). \tag{4.24d}$$

It is clear from these equations that an anisotropic configuration of the GW background can be achieved either by having a different propagation for each polarisation $R_+ \neq R_\times$ or a correlation between them $R_{\lambda\lambda'} \neq 0$. Parity violation requires this correlation to be complex.

II

Beyond the standard picture

5 Gravitational leptogenesis from metric perturbations

Leptogenesis is one of the most popular mechanisms in order to achieve baryogenesis. It involves generating lepton asymmetry with some sort of mechanism operating in the early Universe, which is later translated into the baryon sector via the sphaleron process. We discussed this more extensively in Sec. 3.3.

In [APS06], an alternative mechanism for leptogenesis was proposed which is not based on the introduction of heavy Majorana leptons, but on the chiral gravitational anomaly. In the electroweak sector, lepton number is conserved at the classical level, but at quantum level it can be violated via an anomalous Ward identity given a non-trivial topology of the gauge field. One way of achieving this violation is precisely the sphaleron, which violates lepton and baryon number simultaneously and is sourced by the electroweak gauge field itself [Dob+97]

$$\nabla_\mu j^\mu_L = \nabla_\mu j^\mu_B = \frac{1}{(4\pi)^2}\left(\frac{g^2}{2} W\tilde{W} + g'^2 B\tilde{B}\sum(y_L^2 - y_R^2)\right), \tag{5.1}$$

where j_L and j_B are the lepton and baryon currents respectively, W and B are the $\mathrm{SU}_L(2)$ and $\mathrm{U}_Y(1)$ electroweak fields and the sum in hypercharge $\sum(y_L^2 - y_R^2)$ spans all fermions, either quarks or leptons, and has the same value in the Standard Model in either case. This lepton number violation can also be achieved thanks to the gravitational field, which acts as a source of this lepton number violation [AW84]. In the presence of a gravitational field, the chiral coupling due to the imbalance of left and right-handed species in the neutrino families, which is not featured in the baryonic sector, induces an additional term when computing the anomalous lepton current, which can be written as [AW84]

$$\nabla_\mu j^\mu_L = \frac{N_{R-L}}{24(4\pi)^2} R\tilde{R}, \tag{5.2}$$

where N_{R-L} is the difference between the number of right-handed and left-handed lepton species. As a matter of fact, it has been shown that neutrino masses, either Dirac or Majorana, do not affect the predictions of the gravitational leptogenesis [ALS18].

The necessary ingredient in this case for the generation of a net lepton number is the existence of a primordial chiral gravitational wave background which contributes to the Pontryagin density $R\tilde{R}$. As commented in Sec. 4.3, standard inflation models do not generate a chiral background of gravitational waves. In order to generate such a chiral background, extended inflationary models involving axial couplings of the

inflaton field have been considered. Thus for example, a gravitational Chern-Simon coupling of a pseudo-scalar inflaton field was originally proposed in [APS06], although some consistency issues were discussed in [AM05; LQR05]. Other possibilities include a Chern-Simons interaction between the pseudo-scalar inflaton and a $U(1)$ gauge field [PP17] and non-abelian gauge fields coupled to an axionic inflaton [MNS18; CD18]. Alternative ways of generating a parity-violating GW background have been considered in [KK19; AAG18; Bar21].

The aim of this Chapter is to make the observation that the gravitational leptogenesis mechanism can be implemented without invoking new axial couplings in the inflaton sector. Indeed, the perturbed Robertson-Walker background emerging after inflation already breaks parity thus generating a non-vansihing Pontryagin density. Notice that although the probability distribution functions for the production of left and right-handed gravity waves are the same in ordinary inflation models, our universe is a particular realisation of the Gaussian process in which the actual amplitude of left and right-handed gravitational wave excitations can be different. We thus conclude that the minimal Standard Model with left-handed neutrinos together with an ordinary inflationary model driven by a scalar inflaton field already contains all the ingredients to generate a lepton asymmetry after inflation.

This Chapter is structured as follows: In Sec. 5.1, we introduce the formalism for gravitational leptogenesis in a RW background. We particularise this formalism to a reheating phase in Sec. 5.2 and obtain the resulting lepton asymmetry for a matter-dominated reheating and a general reheating. In Sec. 5.3, we discuss the characteristic size of the variance in lepton number, and finally, we examine the implications for the late Universe in Sec. 5.4.

5.1 Gravitational leptogenesis

Let us then consider a spatially flat RW spacetime with scalar and tensor perturbations in the longitudinal gauge. We will ignore vector perturbations as they are not typically produced during inflation. The line element in conformal time can be obtained from Eq. (2.40) and reads

$$\mathrm{d}s^2 = a^2(\eta)\left[(1+2\Phi)\mathrm{d}\eta^2 - ((1-2\Psi)\delta_{ij} - h_{ij})\mathrm{d}x^i\,\mathrm{d}x^j\right]. \tag{5.3}$$

The Pontryagin density that sources the leptonic current in (5.2) can be written in terms of the electric and magnetic parts of the Weyl tensor (see Appendix C for their definitions) as [dRio+20]

$$R\tilde{R} = \frac{1}{2}\varepsilon^{\mu\nu}{}_{\rho\sigma}R_{\mu\nu\alpha\beta}R^{\rho\sigma\alpha\beta} = 16E_{\mu\nu}B^{\mu\nu}, \tag{5.4}$$

The unperturbed part of the metric (5.3) does not contribute to either the electric or magnetic parts of the Weyl tensor. On the other hand, all scalar, vector and tensor components contribute to the electric part, whereas only vector and tensor ones add to

the magnetic part. For the metric (5.3), the non-vanishing components of these two tensors are

$$E_{ij} = \frac{1}{6}\delta_{ij}\nabla^2(\Phi+\Psi) - \frac{1}{2}(\Phi+\Psi)_{,ij} - \frac{1}{4}(h''_{ij} + \nabla^2 h_{ij}), \tag{5.5a}$$

$$B_{ij} = \frac{1}{4}(\epsilon^{ikl}h'_{jk,l} + \epsilon^{jkl}h'_{ik,l}). \tag{5.5b}$$

This means that the leading contribution to $R\tilde{R}$ is second order in metric perturbations, and it features a scalar-tensor contribution and a tensor-tensor contribution. The Pontryagin density is then found to be

$$R\tilde{R} = -\frac{2}{a^4}\epsilon^{jkl}h'_{ik,l}[2(\Phi+\Psi)_{,ij} + h''_{ij} + \nabla^2 h_{ij}]. \tag{5.6}$$

In the comoving frame, we can write $j^\mu_L = (n_L/a, \mathbf{0})$ to leading order in perturbations, where n_L is the physical lepton number density. Inserting these expressions into (5.2) we obtain the leptonic number density after integrating in time

$$n_L = \frac{N_{R-L}}{24(4\pi)^2 a^3}\int \mathrm{d}\eta\, a^4 R\tilde{R}, \tag{5.7}$$

where in the Standard Model of particles $N_{R-L} = -3$.

Let us now expand the scalar and tensor perturbations in terms of creation and annihilation operators

$$\Phi(\eta,\mathbf{x}) = \int \frac{\mathrm{d}^3 p}{(2\pi)^{3/2}}\left(\Phi(p,\eta)b_{\mathbf{p}}\, e^{i\mathbf{p}\cdot\mathbf{x}} + \Phi^*(p,\eta)b^\dagger_{\mathbf{p}}\, e^{-i\mathbf{p}\cdot\mathbf{x}}\right) \tag{5.8}$$

and

$$h_{ij}(\eta,\mathbf{x}) = \int \frac{\mathrm{d}^3 k}{(2\pi)^{3/2}}\sum_{\lambda=+,-}\left(h_\lambda(k,\eta)e^\lambda_{ij}(\hat{\mathbf{k}})a_{\mathbf{k},\lambda}\, e^{i\mathbf{k}\cdot\mathbf{x}} + h^*_\lambda(k,\eta)e^{\lambda\,*}_{ij}(\hat{\mathbf{k}})a^\dagger_{\mathbf{k},\lambda}\, e^{-i\mathbf{k}\cdot\mathbf{x}}\right), \tag{5.9}$$

where $\lambda = \pm$ correspond to the ± 2 helicity modes. The corresponding polarisation tensors can be written as

$$e^\lambda_{ij}(\hat{\mathbf{k}}) = \varepsilon^{\lambda *}_i(\hat{\mathbf{k}})\varepsilon^{\lambda *}_j(\hat{\mathbf{k}}), \tag{5.10}$$

with $\boldsymbol{\varepsilon}^\lambda(\hat{\mathbf{k}})$ the helicity ± 1 polarisation vectors, which satisfy

$$\mathbf{k}\cdot\boldsymbol{\varepsilon}^\lambda(\hat{\mathbf{k}}) = 0, \tag{5.11a}$$

$$\mathbf{k}\times\boldsymbol{\varepsilon}^\lambda(\hat{\mathbf{k}}) = -i\lambda k\boldsymbol{\varepsilon}^\lambda(\hat{\mathbf{k}}), \tag{5.11b}$$

$$\boldsymbol{\varepsilon}^\lambda(\hat{\mathbf{k}})^*\cdot\boldsymbol{\varepsilon}^{\lambda'}(\hat{\mathbf{k}}) = \delta_{\lambda\lambda'}. \tag{5.11c}$$

Also, notice that in the absence of chiral couplings $h_+ = h_- = h$. The creation and annihilation operators obey the usual commutation relations

$$[a_{\mathbf{k},\lambda}, a^\dagger_{\mathbf{k}',\lambda'}] = \delta^{(3)}(\mathbf{k}-\mathbf{k}')\delta_{\lambda\lambda'}, \tag{5.12a}$$

$$[b_{\mathbf{p}}, b^\dagger_{\mathbf{p}'}] = \delta^{(3)}(\mathbf{p}-\mathbf{p}'). \tag{5.12b}$$

It is straightforward to see that the expectation value of the scalar-tensor contribution to the lepton number in the Bunch-Davies vacuum vanishes. Indeed, we can schematically write $\langle n_L \rangle \sim \langle \Phi h' \rangle = \langle \Phi \rangle \langle h' \rangle = 0$. Therefore, the leading contribution to the expectation value would be the tensor-tensor one, which has been already explored in previous works [APS06; PP17; Kam+20]. Direct computation provides the following expression

$$\langle R\tilde{R} \rangle = -2 \int \frac{\mathrm{d}^3 k}{(2\pi)^3} k \sum_\lambda \lambda e^\lambda_{ij}(\hat{\mathbf{k}}) e^{\lambda *}_{ij}(\hat{\mathbf{k}}) h'_\lambda (h^{*\prime\prime}_\lambda - k^2 h^*_\lambda). \tag{5.13}$$

As already pointed out in the aforementioned works, this contribution vanishes in the absence of parity breaking in the gravitational-wave power spectrum. In this case, $h_\lambda = h$ and

$$\sum_\lambda \lambda e^\lambda_{ij}(\hat{\mathbf{k}}) e^{\lambda *}_{ij}(\hat{\mathbf{k}}) = \sum_\lambda \lambda = 0. \tag{5.14}$$

As a result, gravitational leptogenesis has only been taken into account as a valid mechanism when considering inflationary scenarios with axial couplings, such as natural inflation [PP17] or a gravitational Chern-Simons coupling [Kam+20].

However, the variance of the lepton number density is in general non-vanishing, even in the absence of axial couplings. Since in terms of operators $R\tilde{R} \sim \Phi h + hh$, we can schematically write

$$\langle n_L^2 \rangle \sim \langle (R\tilde{R})^2 \rangle \sim \langle \Phi\Phi \rangle \langle hh \rangle + \langle hhhh \rangle, \tag{5.15}$$

where the first term is proportional to the scalar power spectrum times the tensor power spectrum, whereas the second one can be reduced to products of two tensor power spectra if the spectrum is Gaussian. Precisely, the root mean square $n_L^{\mathrm{rms}} = \langle n_L^2 \rangle^{1/2}$ provides an estimate of the produced lepton density in a typical realisation of the random process.

Since the tensor-to-scalar ratio of the primordial power spectra $r < 0.1$, as we discussed in Sec. 1.2, we expect the scalar-tensor contribution to dominate over the tensor-tensor one, so we can consider only the first term in (5.15). Thus, the variance can be obtained by computing

$$\langle n_L^2 \rangle = \left(\frac{1}{32\pi^2 a^3} \right)^2 \epsilon_{jkl} \epsilon_{nrs} \left\langle \int \mathrm{d}\eta (\Phi + \Psi)_{,ij} h'_{ik,l} \int \mathrm{d}\eta' (\Phi + \Psi)_{,mn} h'_{mr,s} \right\rangle. \tag{5.16}$$

By inserting the expansions (5.8) and (5.9) into the variance and formally taking the expectation value, one can obtain the following expression

$$\langle n_L^2 \rangle = \left(\frac{1}{16\pi^2 a^3} \right)^2 \int \frac{\mathrm{d}^3\mathbf{k}\, \mathrm{d}^3\mathbf{p}}{(2\pi)^6} k^2 \sum_\lambda p_i p_j e^\lambda_{ij}(\hat{\mathbf{k}}) p_k p_l e^{\lambda *}_{kl}(\hat{\mathbf{k}}) \int \mathrm{d}\eta\, \Phi(\mathbf{p},\eta) h'_\lambda(\mathbf{k},\eta) \int \mathrm{d}\eta'\, \Phi^*(\mathbf{p},\eta') h^{*\prime}_\lambda(\mathbf{k},\eta'), \tag{5.17}$$

where we have simplified the cross products with the aid of Eq. (5.11b) and we have considered absence of anisotropic stress, which yields $\Phi = \Psi$. In a typical scenario,

the modes of scalar and tensor perturbations do not depend on the direction of the wavevector, only on its modulus. In that case, the only terms with angular dependence are the products of momenta and polarisation vectors, namely

$$p_i p_j e^{\lambda}_{ij}(\hat{\mathbf{k}}) p_k p_l e^{\lambda *}_{kl}(\hat{\mathbf{k}}) = |\mathbf{p}\cdot\boldsymbol{\varepsilon}^{\lambda}(\hat{\mathbf{k}})|^4. \tag{5.18}$$

By considering that $\mathbf{k}$ is aligned with the z axis, a general momentum $\mathbf{p}$ in spherical coordinates and any of the possibilities for the polarisation vector, it can be shown that this combination is independent of polarisation and that

$$|\mathbf{p}\cdot\boldsymbol{\varepsilon}^{\lambda}(\hat{\mathbf{k}})|^2 = \frac{p^2}{2}\sin^2\theta, \tag{5.19}$$

which makes the angular integration very simple

$$\int \mathrm{d}^2\Omega_{\mathbf{k}}\,\mathrm{d}^2\Omega_{\mathbf{p}}\,|\mathbf{p}\cdot\boldsymbol{\varepsilon}^{\lambda}(\hat{\mathbf{k}})|^4 = 8\pi^2\int_{-1}^{1}\mathrm{d}\cos\theta\left(\frac{p^2}{2}\sin^2\theta\right)^2 = \frac{32\pi^2}{15}p^4. \tag{5.20}$$

With this result, and in the absence of chiral couplings, the whole expression in (5.17) is independent of λ, so the sum over polarisations can be performed trivially. Putting everything together, the variance can be written in a compact manner as

$$\langle n_L^2\rangle = \frac{1}{3840\pi^8 a^6}\int \mathrm{d}k\,\mathrm{d}p\,k^4 p^6\left|\int \mathrm{d}\eta\,\Phi(p,\eta)h'(k,\eta)\right|^2. \tag{5.21}$$

5.2 Leptogenesis during reheating

For the sake of concreteness, we will assume that the net lepton number density at the end of inflation is negligible, so we will consider the leptogenesis produced throughout the stage of reheating by the inflationary primordial metric perturbations. For simplicity, we consider that the energy content during reheating is described by means of an effective fluid with a barotropic equation of state $p = w\rho$, with w constant, which we formulated in Sec. 3.2. We will also parametrise the primordial power spectra as

$$\mathcal{P}_S(p) = \frac{p^3}{2\pi^2}|\Phi_p|^2 = A_\Phi\left(\frac{p}{k_*}\right)^{n_S-1} \tag{5.22}$$

for the scalar perturbations, which can ultimately be related to the curvature power spectrum $\mathcal{P}_\mathcal{R}$ defined in Eq. (3.14) through (3.12), and

$$\mathcal{P}_T(k) = \frac{k^3}{2\pi^2}|h_k|^2 = A_T\left(\frac{k}{k_*}\right)^{n_T} \tag{5.23}$$

for the tensor perturbations, as in Eq. (3.18). When needed, we will use the values obtained by the Planck collaboration to characterise the perturbation power spectra, which we laid out in Sec. 1.2, and assume a scale-invariant tensor power spectrum $n_T = 0$, which is a good approximation for inflation-generated spectra.

The primordial power spectra generated during inflation have a natural ultraviolet (UV) cutoff at the scale $k_I = a_I H_I$, corresponding to the size of the comoving Hubble horizon at the end of inflation, as modes with $k > k_I$ have never left the horizon and could not become classical metric perturbations. Imposing this upper limit in the momentum integrals in (5.21), we can change variables in order to extract all quantities with dimensions from the integrals. Then, the total lepton number variance generated during reheating is

$$\langle n_L^2 \rangle_{\rm RH} = \frac{1}{960\pi^4}\left(\frac{k_I}{a_{\rm RH}}\right)^6 \mathcal{P}_S(k_I)\mathcal{P}_T(k_I) I(\eta_{\rm RH}) \tag{5.24}$$

where

$$I(\eta) \quad = \quad \int_0^1 {\rm d}x \int_0^1 {\rm d}y\, x^{n_T+1} y^{n_S+2} \left| \int_{\eta_I}^{\eta} {\rm d}\hat{\eta}\, \tilde{\Phi}(k_I y, \hat{\eta}) \tilde{h}'(k_I x, \hat{\eta}) \right|^2 \tag{5.25}$$

is a numerical factor determined by the evolution of the perturbations during reheating. Here, $\tilde{\Phi}(k,\eta) = \Phi(p,\eta)/\Phi(p,\eta_I)$ is the scalar perturbation normalised to its value at the end of inflation, and similarly for the tensor mode. Notice that the x and y integrals are dominated by the upper integration limits for usual values for the tilts, which correspond to modes with $k \simeq p \simeq k_I$.

As we discussed in Sec. 3.2, all quantities involving reheating are determined by choosing three free parameters: the Hubble rate at the end of inflation H_I, the reheating temperature $T_{\rm RH}$ and the reheating equation of state w. The production of lepton number is also fully determined by these three quantities. By changing variables $\tau = \hat{\eta}/\eta_I$ into (5.25), one can obtain

$$I(\eta_{\rm RH}) = \int_0^1 {\rm d}x \int_0^1 {\rm d}y\, x^{n_T+1} y^{n_S+2} \left| \int_1^{\eta_{\rm RH}/\eta_I} {\rm d}\tau\, \tilde{\Phi}(k_I y, \eta_I \tau) \frac{\partial}{\partial \tau} \tilde{h}(k_I x, \eta_I \tau) \right|^2 . \tag{5.26}$$

In order to compute the value of this integral, we need to solve the evolution of the metric perturbation modes for each momentum in the integration range, given by Eqs. (2.46) and (2.47), and then compute the time and momentum integrals. This involves solving second-order ordinary differential equations and then integrating the resulting functions, which in general is not possible to do analytically. In order to fully understand the behaviour of the mechanism, we start by solving a case with expressions simple enough to give an analytical estimate, which is a reheating with $w = 0$, a typical scenario for reheating after slow-roll inflation, and then consider the more general reheating scenario.

5.2.1 Reheating with $w = 0$

In a reheating with $w = c_s^2 = 0$, the adiabatic metric perturbations obey the following equations of motion in the absence of anisotropic stress

$$\Phi_p'' + 3\mathcal{H}\Phi_p' + (2\mathcal{H}' + \mathcal{H}^2)\Phi_p = 0, \tag{5.27a}$$

$$h_k'' + 2\mathcal{H}h_k' + k^2 h_k = 0. \tag{5.27b}$$

In a matter-dominated (MD) phase, the scale factor evolves as $a(\eta) \propto \eta^2$, so the Hubble parameter is $\mathcal{H} = 2/\eta$. This makes the term proportional to Φ_p in (5.27a) vanish, so we find the solution

$$\Phi(p,\eta) = C_{1p} + \frac{C_{2p}}{\eta^5}. \tag{5.28}$$

We will neglect the second term, as it is a suppressed mode that rapidly vanishes, so we can consider $\Phi = \text{const.}$ throughout its whole reheating evolution. Note that, although its evolution does not depend on wavenumber p, the initial conditions might do. For the tensor modes, the solution is given by Eq. (4.9).

The integration constants in both solutions can be obtained by matching these solutions at the start of reheating (end of inflation η_I) with the values given by the primordial power spectra (5.22), (5.23), at very early times and outside the Hubble horizon, and imposing vanishing derivative. In terms of the normalised functions $\tilde{\Phi}$ and $\tilde{h}$, these are

$$\tilde{\Phi}(p,\eta) = 1, \tag{5.29a}$$

$$\tilde{h}(k,\eta) = \frac{1}{k^3\eta^3}\left[(k^3\eta_I^2\eta - 3k(\eta-\eta_I))\cos[k(\eta-\eta_I)] + (3 + 3k^2\eta\eta_I - k^2\eta_I^2)\sin[k(\eta-\eta_I)]\right]. \tag{5.29b}$$

As we would expect, the tensor modes approach a constant in the super-Hubble regime $k\eta \ll 1$, whereas after entering the Hubble horizon they oscillate with damped amplitude. Since the scalar perturbation is constant, the time integral in Eq. (5.25) can be easily done

$$\int_{\eta_I}^{\eta_{\rm RH}} \mathrm{d}\hat{\eta}\, \tilde{\Phi}(k_I y,\hat{\eta})\tilde{h}'(k_I x,\hat{\eta}) = \tilde{h}(k_I x,\eta_{\rm RH}) - 1, \tag{5.30}$$

as $h(k_I x,\eta_I) = 1$. The numerical factor then is

$$I(\eta_{\rm RH}) = \frac{1}{3+n_S}\int_0^1 \mathrm{d}x\, x^{n_T+1}[\tilde{h}(k_I x,\eta_{\rm RH}) - 1]^2, \tag{5.31}$$

where the case $n_S = -3$ needs to be treated separately.

Despite its compact form, the long expression for $\tilde{h}$ does not allow obtaining a result by direct computation. However, we can make an approximation for Eq. (5.30) in order to obtain an analytical expression: If the mode is still super-Hubble at the end of reheating, then $\tilde{h}(k,\eta_{\rm RH}) = 1$ and the integral vanishes, as $h' \simeq 0$ over the whole integral span. If, on the other hand, the mode is deep into the Hubble horizon at the end of reheating, then its amplitude has already decayed enough so that $\tilde{h}(k,\eta_{\rm RH}) \ll 1$. Taking into account these limits, we write

$$\tilde{h}(k,\eta_{\rm RH}) - 1 = -\theta(k\eta_{\rm RH} - 1), \tag{5.32}$$

which is an accurate approximation everywhere except around $k\eta_{\rm RH} \simeq 1$, where the transition would be smoother. However, since the momentum integrals in Eq. (5.25) are dominated by the upper limit, this barely introduces error. With this approximation, we have

$$I(\eta_{\rm RH}) = \frac{1}{(3+n_S)(2+n_T)}\left[1-\left(\frac{1}{k_I\eta_{\rm RH}}\right)^{n_T+2}\right], \tag{5.33}$$

where the case $n_T = -2$ needs to be obtained separately.

We can now compute the lepton number to entropy ratio at the end of reheating by dividing by the entropy density (2.34), which yields

$$\frac{n_L^{\rm rms}}{s} = \frac{3\sqrt{15}}{16\pi^4}\frac{k_I^3}{g_{*s,0}T_0^3}\left[\frac{\mathcal{P}_S(k_I)\mathcal{P}_T(k_I)}{(3+n_S)(2+n_T)}\right]^{1/2}\left[1-\left(\frac{1}{k_I\eta_{\rm RH}}\right)^{n_T+2}\right]^{1/2} \tag{5.34}$$

It is interesting to compare this ratio with the baryon asymmetry (1.13) after the partial conversion of leptonic asymmetry via sphalerons [KRS85], which is

$$\frac{n_L^{\rm rms}}{s} = \frac{79}{28}\left|\frac{n_B}{s}\right| = 2.45\times 10^{-10}. \tag{5.35}$$

Inserting the expression for k_I (3.27) and omitting numerical factors, this requirement imposes the following relation

$$\left(\frac{T_{\rm RH}}{M_P}\right)\left(\frac{H_I}{M_P}\right)[\mathcal{P}_S(k_I)\mathcal{P}_T(k_I)]^{1/2} \sim 10^{-10}. \tag{5.36}$$

At CMB scales, the maximum values for the power spectra allowed by the current limits on the tensor-to-scalar ratio are $\mathcal{P}_S\mathcal{P}_T \sim \mathcal{P}_\mathcal{R}\mathcal{P}_T \sim 10^{-20}$. Translating these values to inflationary scales, this relation would require both the inflationary sector and the reheating to happen around Planck scales, which is not allowed. Thus, a $w = 0$ reheating typically produces a local asymmetry which is several orders of magnitude smaller than the observed baryon asymmetry. The only possibility to have a sizeable asymmetry for $w = 0$ would then be to have blue-tilted power spectra that enhance the perturbations at the k_I scale. In the case of the tensor power spectrum, this could conflict with current Big Bang nucleosynthesis bounds on relativistic species (see the discussion in Sec. 1.4), as the GW energy density contributes to the radiation budget.

5.2.2 General reheating

In a general reheating with equation of state w, perturbations obey the following equations of motion

$$\Phi_p'' + 3(1+w)\mathcal{H}\Phi_p' + [wp^2 + 2\mathcal{H}' + (1+3w)\mathcal{H}^2]\Phi_p = 0, \tag{5.37a}$$

$$h_k'' + 2\mathcal{H}h_k' + k^2 h_k = 0, \tag{5.37b}$$

while the Hubble parameter is

$$\mathcal{H} = \frac{a'}{a} = \frac{2}{(1+3w)\eta}. \tag{5.38}$$

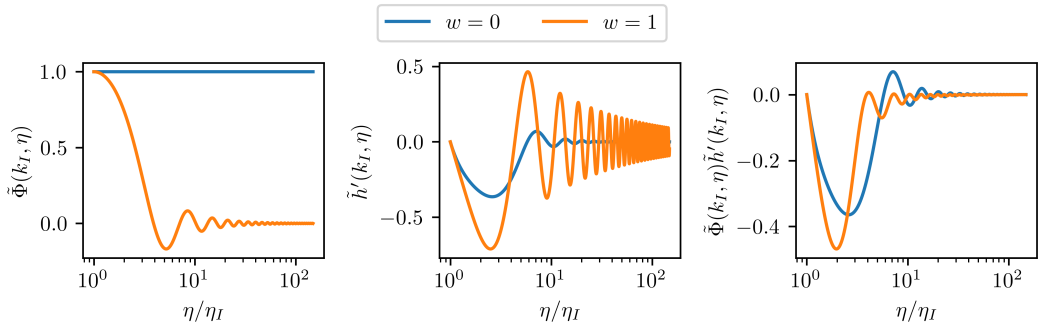

Figure 5.1: Time evolution of the perturbations $\tilde{\Phi}(k_I,\eta)$ (left), $\tilde{h}'(k_I,\eta)$ (centre) and their product (right), which is the integrand of the time integral in Eq. (5.25), for reheating equations of state $w = 0, 1$ and wavenumber $k = p = k_I$.

Similarly to the matter-dominated case, we can obtain general solutions (5.37) in terms of Bessel functions

$$\Phi(p,\eta) = (p\eta)^{-r}[C_{1p}J_r(\sqrt{w}p\eta) + C_{2p}Y_r(\sqrt{w}p\eta)], \tag{5.39a}$$

$$h(k,\eta) = (k\eta)^{s}[D_{1k}J_s(k\eta) + D_{2k}Y_s(k\eta)], \tag{5.39b}$$

with $J_{r,s}$ and $Y_{r,s}$ Bessel functions of order $r = (5+3w)/(2+6w)$ and $s = (3w-3)/(2+6w)$ respectively and $C_{1,2}$, $D_{1,2}$ constants that might depend on p and k. By looking at the asymptotic behaviour of Bessel functions, we can see that scalar and tensor modes remain constant outside the horizon ($k\eta \ll 1$), while well inside the horizon they oscillate with decreasing amplitude, except for $w = 0$, where $\Phi = \text{const.}$ even inside the horizon, as we analysed in Sec 5.2.1.

In Fig. 5.1 we show the behaviour of the perturbations together with the product appearing in the integrand of (5.25) for different values of w for the dominant modes. We can see that contributions to the time integral in (5.25) occur only when tensor modes enter the Hubble horizon, since in the super-Hubble regime $h' \simeq 0$.

Generally, and unlike in the case $w = 0$, it is not possible to solve the integrals in Eq. (5.25) as a function of w, and in most cases not even after giving w a specific value. We thus need to solve the equations of motion for the modes (5.37) numerically for each momentum in the integration range, and then calculate the time and momentum integrals. By doing so, and integrating up to different times, we plot the time evolution of function $I(\eta)$ in Fig. 5.2, which provides the time dependence of the lepton production. The different behaviour for each equation of state, and hence the different interference between scalar and tensor modes, translates into a different time evolution of $I(\eta)$. We can also see that leptogenesis takes place in a few Hubble times, therefore, far from the instantaneous reheating limit, i.e. $\eta_{\rm RH} \gg \eta_I$, $I(\eta)$ reaches an asymptotic value, which depends only on w. In addition, also far from the instantaneous reheating limit, we find that in general $I(\eta_{\rm RH}) = \mathcal{O}(10^{-1})$. Thus, from (5.24), we see that, apart

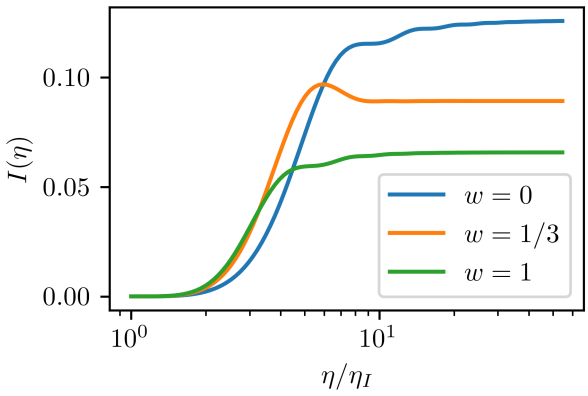

Figure 5.2: Time evolution of $I(\eta)$ in (5.25) for three different reheating equations of state. For inflationary and reheating scales so that $\eta_{\rm RH}/\eta_I \gg 1$, the integral evaluates to its asymptotic value and, as a result, it depends only on w.

from the power spectra which are (almost) scale-invariant, the relevant quantity in determining the size of $n_L^{\rm rms}/s$ is the factor $(k_I/a_{\rm RH})^3$. As a matter of fact, we can extract the dependence on H_I and $T_{\rm RH}$ from such a factor

$$\frac{k_I}{a_{\rm RH}} = \frac{a_I H_I}{a_{\rm RH}} \propto H_I \left(\frac{H_I^2}{T_{\rm RH}}\right)^{-\frac{1}{3(1+w)}} \tag{5.40}$$

and obtain

$$\left.\frac{n_L^{\rm rms}}{s}\right|_{\rm RH} \propto \sqrt{A_S A_T}\left(\frac{H_I}{M_P}\right)^{\frac{1+3w}{1+w}}\left(\frac{T_{\rm RH}}{M_P}\right)^{\frac{1-3w}{1+w}} \tag{5.41}$$

for $n_s \simeq 1$, meaning that leptogenesis is enhanced for high inflation scales and, in the case of stiff reheating scenarios with $w > 1/3$, for low reheating temperatures.

In the left panel of Fig. 5.3, we plot $n_L^{\rm rms}/s$ in the $(T_{\rm RH}, H_I)$ parameter space for a stiff equation of state $w = 1$ during reheating. We see that the asymmetry in (5.35) can be locally generated for inflationary scales above $H_I = 10^{12}$ GeV and reheating temperatures larger than the electroweak threshold. The dashed area on the bottom right corner indicates inconsistent reheating, as it is not possible with the given parameters, and it is bounded by the instantaneous reheating scenario $\eta_{\rm RH}/\eta_I = 1$, which from Eq. (3.26) imposes

$$H_I = \left(\frac{4\pi^3 g_*}{45}\right)^{1/2} \frac{T_{\rm RH}^2}{M_P}. \tag{5.42}$$

In the right panel of Fig. 5.3 we plot the values of $n_L^{\rm rms}/s$ in the $(T_{\rm RH}, w)$ parameter space for an inflation scale corresponding to $H_I = 10^{13}$ GeV, which for a typical slow-roll tensor spectrum amplitude (3.17)

$$A_T = \frac{16}{\pi}\left(\frac{H_I}{M_P}\right)^2 \tag{5.43}$$

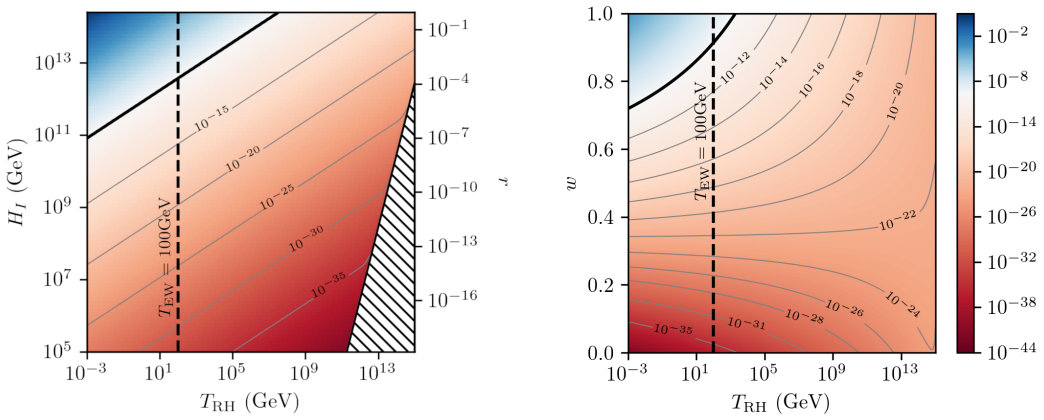

Figure 5.3: Values of $n_L^{\rm rms}/s$ for power spectra with Planck 2018 scalar amplitude and scale-invariant tensor power spectrum $A_T = 16/\pi(H_I/M_P)^2$ with fixed equation of state $w = 1$ (left) and fixed inflation scale $H_I = 10^{13}$ GeV (right). We only consider temperatures $T_{\rm RH} > 1$ MeV in order to ensure the existence of a BBN period. The vertical dashed line shows the threshold of the electroweak scale, which is the minimum temperature for the sphaleron process to be effective. The solid black line shows the parameters that yield the value (5.35), which scales as in (5.41). The dashed area on the bottom right corner of the left panel is excluded since reheating is not possible in such a parameter range, with the boundary corresponding to instantaneous reheating (5.42). The contour lines (in grey) in the left panel deviate from (5.41) close to the limit of instantaneous reheating.

corresponds to a tensor-to-scalar ratio of $r \simeq 10^{-3}$. We can see that large baryon asymmetries can be generated for stiff equations of state and reheating temperatures near the electroweak scale. For a radiation behaviour $w = 1/3$, we find that, as expected, the production is not sensitive to the reheating temperature. Here we can also verify the results obtained in the previous section with $w = 0$ which, as we had anticipated, are not efficient at producing lepton number for scale-invariant power spectra. Comparing these results with those obtained in [APS06] with the axial coupling, we find that for the instantaneous reheating case and the parameters used in that work, we get $n_L^{rms}/s \sim 10^{-20}$ which is slightly above their results.

The vertical dashed line appearing on both panels in Fig. 5.3 corresponds to the electroweak scale $T_{\rm EW} \sim 100$ GeV. This temperature is a threshold for the gravitational leptogenesis mechanism to work. The conversion from lepton to baryon number is produced via electroweak sphalerons, a topological solution of the electroweak theory that can no longer operate if the electroweak transition has already occurred, so the conversion mechanism is barely efficient below energies of 1 TeV. As a result, inflationary scenarios with low reheating temperatures are not valid in this framework.

5.3 Size of matter-antimatter regions

The variance of the lepton number density obtained in (5.24) only provides the typical amplitude of local fluctuations. In order to determine the size of the matter-antimatter regions it is necessary to calculate the correlation function

$$\xi(\mathbf{r}) = \langle n_L(\mathbf{x}+\mathbf{r}) n_L(\mathbf{x}) \rangle \tag{5.44}$$

The computation is very similar to that preceding Eq. (5.17), except for the additional dependence in $\mathbf{r}$, which naturally appears as an exponential

$$\xi(\mathbf{r}) = \left(\frac{1}{16\pi^2 a^3}\right)^2 \int \frac{\mathrm{d}^3\mathbf{p}\,\mathrm{d}^3\mathbf{k}}{(2\pi)^6} k^2 |\mathbf{p}\cdot\boldsymbol{\varepsilon}^\lambda(\hat{\mathbf{k}})|^4 e^{i(\mathbf{p}+\mathbf{k})\mathbf{r}} \left| \int \mathrm{d}\eta\, \Phi(p,\eta) h'_\lambda(k,\eta) \right|^2 . \tag{5.45}$$

The angular integration cannot be computed for a general equation of state, but if we consider $w = 0$ and scale-invariant scalar and tensor power spectra, it is possible to obtain analytical expressions, thanks to the fact that $\Phi = \text{const}$. Thus, changing variables $\mathbf{p} = \mathbf{q} - \mathbf{k}$, we can write

$$\xi(r) = \frac{A_\Phi A_T}{2048\pi^4 a^6} \int_{k_0}^{k_I} \mathrm{d}k \int \mathrm{d}q\, k q^6 \int_{-1}^{1} \mathrm{d}y\, e^{iqry} \int_{-1}^{1} \mathrm{d}x \frac{(1-x^2)^2}{(q^2+k^2-2kqx)^{3/2}}, \tag{5.46}$$

where k_0 and k_I denote the infrared and ultraviolet cutoffs of the production. In this case, $k_0 = 1/\eta_{\mathrm{RH}}$ in order to have sub-Hubble tensor perturbations, and k_I is the natural cut-off corresponding to the size of the Hubble horizon at the end of inflation. The angular integrals yield the following results

$$\int_{-1}^{1} \mathrm{d}y\, e^{iqry} = \frac{2\sin qr}{qr}, \tag{5.47}$$

$$\int_{-1}^{1} \mathrm{d}x \frac{(1-x^2)^2}{(q^2+k^2-2kqx)^{3/2}} = \begin{cases} \frac{16}{105k^5}(7k^2-3q^2), & k > q, \\ \frac{16}{105q^5}(7q^2-3k^2), & k < q. \end{cases} \tag{5.48}$$

The following limits can be obtained

$$\xi(r) = \begin{cases} \dfrac{41 A_\Phi A_T}{483840\pi^4} \left(\dfrac{k_I}{a}\right)^6, & k_I r \ll 1 \\ -\dfrac{11 A_\Phi A_T}{26880\pi^4} \left(\dfrac{k_I}{a}\right)^6 \dfrac{\cos(k_I r)}{k_I^2 r^2}, & k_I r \gg 1 \end{cases} \tag{5.49}$$

The correlation function is constant at very short scales, meaning that regions separated by a distance $l < 1/k_I$ are similarly correlated, and then it decays with length while oscillating. The comoving coherence length associated to the lepton number variance is therefore $l_{\mathrm{coh}} \simeq 1/k_I$, as it determines the size over which an oscillation is completed, which is much smaller than the observable universe. In fact, the quantity

$$\xi_R = \int_{r<R} \mathrm{d}^3\mathbf{r}\, \xi(\mathbf{r}) \tag{5.50}$$

is related to the root mean squared fluctuation at a certain scale R, and it can be seen that it peaks around $R \sim 1/k_I$.

Although these results are specific to scale-invariant power spectra in a matter-dominated reheating, we have analysed several other cases numerically, with different red and blue-tilted power spectra and for equations of state in the range $0 \leq w \leq 1$, and in every case we found the coherence length to be of the order of k_I.

Variance in gravitational leptogenesis generates patches of size about $l_{\rm coh}$ with similar amounts of matter over antimatter or vice versa, which hints at a scale-dependent lepton number power spectrum. We thus expect that these small matter-antimatter regions will annihilate each other on subhorizon scales, providing an average asymmetry over a comoving scale r_0 given by the weighted variance [KT90]

$$\langle n_L^2 \rangle_{r_0} = \left\langle \frac{1}{V_W^2} \left(\int \mathrm{d}^3\mathbf{r}\, n_L(\mathbf{x}+\mathbf{r}) W(\mathbf{r}) \right)^2 \right\rangle, \tag{5.51}$$

where $W(\mathbf{r})$ is a window function of characteristic size r_0 and $V_W = \int \mathrm{d}^3\mathbf{r}\, W(\mathbf{r})$ its volume. By inserting the expression for the lepton number (5.7) and expanding the perturbations we can obtain

$$\langle n_L^2 \rangle_{r_0} = \left(\frac{1}{16\pi^2 a^3} \right) \int \frac{\mathrm{d}^3\mathbf{p}\, \mathrm{d}^3\mathbf{k}}{(2\pi)^3} k^2 \sum_\lambda |\mathbf{p}\cdot\boldsymbol{\varepsilon}^\lambda(\hat{\mathbf{k}})|^4 \frac{|\hat{W}(\mathbf{k}+\mathbf{p})|^2}{V_W^2} e^{i(\mathbf{p}+\mathbf{k})\mathbf{r}} \left| \int \mathrm{d}\eta\, \Phi(p,\eta) h'_\lambda(k,\eta) \right|^2, \tag{5.52}$$

where

$$\hat{W}(\mathbf{k}) = \int \frac{\mathrm{d}^3\mathbf{r}}{(2\pi)^{3/2}} e^{-i\mathbf{k}\mathbf{r}} W(\mathbf{r}) \tag{5.53}$$

is the Fourier transform of the window function. Differently to the previous calculations, the angular integration cannot be computed straight away, as the convolution of the two window functions has resulted in the factor $|\hat{W}(\mathbf{k}+\mathbf{p})|$, which is angular-dependent. This holds even if the window function depends on modulus only $W(\mathbf{r}) = W(r)$, in which case $\hat{W}(\mathbf{k}) = \hat{W}(k)$, as the modulus $k+p$ is angle-dependent. We cannot change variables to $\mathbf{q} = \mathbf{k}+\mathbf{p}$ either, because doing so would introduce angular dependence in one of the power spectra. Therefore, we need to make a choice of window function in order to continue. We pick a Gaussian window function

$$W(r) = e^{-r^2/2r_0^2}, \quad \frac{|\hat{W}(\mathbf{k})|^2}{V_W^2} = \frac{1}{(2\pi)^3} e^{-k^2 r_0^2}. \tag{5.54}$$

Now we can perform the angular integration in $x = \cos\theta$, with θ the angle between $\mathbf{k}$ and $\mathbf{p}$, as

$$\langle n_L^2 \rangle_{r_0} = \frac{1}{4096\pi^8 a^6} \int \mathrm{d}k\, \mathrm{d}p\, k^4 p^6 e^{-(k^2+p^2)r_0^2} \left| \int \mathrm{d}\eta\, \Phi(p,\eta) h'_\lambda(k,\eta) \right|^2 \int_{-1}^{1} \mathrm{d}x (1-x^2)^2 e^{-2kpr_0^2 x}. \tag{5.55}$$

The angular integral yields

$$\int_{-1}^{1} \mathrm{d}x (1-x^2)^2 e^{-2kpr_0^2 x} = \frac{1}{2(kpr_0^2)^5}[(3+4k^2p^2r_0^4)\sinh\left(2kpr_0^2\right) - 6kpr_0^2\cosh\left(kpr_0^2\right)], \tag{5.56}$$

so the weighed variance can be computed as

$$\langle n_L^2 \rangle_{r_0} = \frac{1}{8192\pi^8 a^6 r_0^{10}} \int \mathrm{d}k\, \mathrm{d}p\, [(3+4k^2p^2r_0^4)\sinh\left(2kpr_0^2\right) - 6kpr_0^2\cosh\left(kpr_0^2\right)] \times e^{-(k^2+p^2)r_0^2} \frac{p}{k} \left| \int \mathrm{d}\eta\, \Phi(p,\eta) h'_\lambda(k,\eta) \right|^2 . \tag{5.57}$$

Next, we normalise the metric perturbations by their primordial values in order to extract the power spectra (5.22), (5.23). By considering scale-invariant power spectra, we can write

$$\langle n_L^2 \rangle_{r_0} = \frac{A_\Phi A_T}{2048\pi^4 a^6 r_0^{10}} \int \mathrm{d}k\, \mathrm{d}p\, [(3+4k^2p^2r_0^4)\sinh\left(2kpr_0^2\right) - 6kpr_0^2\cosh\left(kpr_0^2\right)] \times \frac{e^{-(k^2+p^2)r_0^2}}{p^2k^4} \left| \int \mathrm{d}\eta\, \tilde{\Phi}(p,\eta) \tilde{h}'_\lambda(k,\eta) \right|^2 . \tag{5.58}$$

The calculation now requires picking a specific reheating scenario, in order to solve the equations of motion for the metric perturbations and compute the time integral. However, we can make the following approximation: Metric perturbations are either constant or evolving as a damped oscillation. As the metric perturbations are normalised by their primordial values, the time integrand can reach values $\mathcal{O}(1)$ at most. In addition, $h' = 0$ outside the Hubble horizon, and when it enters the horizon, it decays in a few Hubble times, suppressing the integrand regardless of the value of the scalar perturbation, so we can consider the integral to be around $\mathcal{O}(1)$. This is only true if the tensor perturbation enters the Hubble horizon at some point during the evolution, which imposes an infrared cut-off at k_{RH} if we are considering only the production during reheating. There would be the natural UV cut-off at k_I as well, corresponding to the size of the Hubble horizon at the end of inflation, but the upper limits are taken care of by the Gaussian exponentials. Thus, we symbolically write

$$\left| \int \mathrm{d}\eta\, \tilde{\Phi}(p,\eta) \tilde{h}'_\lambda(k,\eta) \right|^2 \sim \mathcal{O}(1)\theta(k - k_{\mathrm{RH}}). \tag{5.59}$$

Note that this approximation is almost exact in the case $w = 0$, except for small corrections around $k = k_{\mathrm{RH}}$, as discussed in Sec. 5.2.1. The approximation allows us to do the momentum integrals and obtain

$$\langle n_L^2 \rangle_{r_0} = \frac{A_\Phi A_T}{2048\pi^4 (a r_0)^6} \frac{1}{(k_{\mathrm{RH}} r_0)^3} \left[2k_{\mathrm{RH}} r_0 e^{-k_{\mathrm{RH}}^2 r_0^2} + \sqrt{\pi}(2k_{\mathrm{RH}}^2 r_0^2 - 1)\mathrm{erf}(k_{\mathrm{RH}} r_0) \right]. \tag{5.60}$$

Typically, the size r_0 which we are interested in weighing the variance over will be the size of the Hubble horizon at a later time. This size is much greater than the size

of the Hubble horizon at the end of reheating for an expanding universe, which can be determined from the reheating temperature as

$$k_{\rm RH} = a_{\rm RH} T_{\rm RH} = 2.1 \times 10^{26} {\rm Mpc}^{-1} \left(\frac{T_{\rm RH}}{M_P} \right). \tag{5.61}$$

As a result, $k_{\rm RH} r_0 \gg 1$ for all relevant scales and reheating scenarios, and the dominant term is

$$\langle n_L^2 \rangle_{r_0} = \frac{A_\Phi A_T}{1024 \pi^{7/2} (a r_0)^6} \frac{1}{k_{\rm RH} r_0}. \tag{5.62}$$

Compared to the local variance in (5.24), this quantity is suppressed as

$$\langle n_L^2 \rangle_{r_0} \simeq \frac{1}{(k_I r_0)^6} \frac{1}{k_{\rm RH} r_0} \langle n_L^2 \rangle, \tag{5.63}$$

exhibiting a clear blue-tilted behaviour. Again, although this analytical result is valid for scale-invariant power spectra, we have been able to check numerically that the suppression (5.63) holds for different tilts. Contrary to the correlation function, this check could be done analytically, as the momentum integrals in Eq. (5.58) can be computed even for general tilts in terms of hypergeometric special functions. However, the resulting expressions are fairly long and complicated to work with, so we have opted for a numerical analysis instead.

Thus, on regions of order $r_0 = H_0^{-1}$, the expected lepton asymmetry will be several orders of magnitude smaller than observations, even for the most enhanced scenarios of stiff equations of state, low reheating temperatures and high inflation scales. Although far from explaining the baryon asymmetry numbers, it is still a mechanism that generates a certain net amount of lepton number (and baryon number, after the sphalerons play their role) and its implications in the late universe should be analysed, which we do in the following section.

5.4 Phenomenology in the late Universe

Let us examine the implications of this gravitational leptogenesis mechanism for standard cosmology. Firstly, the lepton number asymmetry generated during reheating can be converted into baryon asymmetry only if $T_{\rm RH}$ is above the electroweak scale. Around and above this temperature, QCD confinement has not occurred yet, so the baryon number is in the form of quarks, which are relativistic. Quarks interact in this pre-confinement plasma with a mean free path Γ_q^{-1} which can be estimated as

$$\Gamma_q = n_q \langle \sigma v \rangle \sim T, \tag{5.64}$$

causing diffusion of the baryon number. Here, we have taken into account that the quarks are relativistic and in equilibrium with the thermal plasma, and have estimated $\langle \sigma v \rangle \sim \alpha_s / T^2$. As a result, perturbations in the baryon asymmetry are suppressed on

scales below the corresponding (comoving) Silk length which can be estimated at the moment of confinement as follows [KT90]

$$r_S^2(T_{\rm QCD}) = \int_0^{a_{\rm QCD}} {\rm d}a\, \frac{\Gamma_q^{-1}(a)}{a^3 H(a)} = \frac{a_{\rm QCD}}{H_0 T_0 \sqrt{\Omega_R}} \simeq (10^{-16}\ {\rm Mpc})^2, \tag{5.65}$$

with $a_{\rm QCD} \simeq T_0/T_{\rm QCD}$ the scale factor at the confinement temperature $T_{\rm QCD} \simeq 300$ MeV.

After confinement, quarks can no longer exist as free particles and form bound states, namely protons and neutrons. These particles are now non-relativistic and still interact with photons, which makes the baryon diffusion scale drop significantly, so the comoving size of the matter-antimatter patches freezes after confinement. We can calculate the weighted variance of the baryon asymmetry at the Silk scale $r_0 = r_S$ from (5.51). Note that, after inserting (5.24) into (5.63), the dependence on the inflation scale cancels out (except for the nearly scale-invariant power spectra), so the Silk scale becomes the only relevant one. We obtain

$$\left.\frac{\langle n_B^2\rangle^{1/2}}{s}\right|_{r_S} \simeq 10^{-36}\left(\frac{H_0}{k_0}\right)^{1/2} \tag{5.66}$$

for an infrared cutoff k_0.

Thus, we have the following behaviour for the *rms* baryon asymmetry fluctuations at a given r_0 scale

$$\left.\frac{n_B^{\rm rms}}{s}\right|_{r_0} \simeq \begin{cases} 10^{-36}\left(\dfrac{H_0}{k_0}\right)^{1/2}, & r_0 < r_S \\ 10^{-36}\left(\dfrac{H_0}{k_0}\right)^{1/2}\left(\dfrac{r_S}{r_0}\right)^{7/2}, & r_0 > r_S \end{cases} \tag{5.67}$$

i.e. for regions smaller than the Silk scale at QCD confinement, diffusion suppresses baryon fluctuations, generating patches of homogeneous lepton number density of typical size r_S, and the abundance must be obtained through the weighted variance over the Silk length, which does not depend on the inflationary parameters. For larger patches $r_0 > r_S$, the averaged abundance is damped as shown in Eq. (5.63).

6 Vector fields and gravitational-wave propagation

The description of the dark sector typically includes new degrees of freedom in the form of scalar fields. Models containing additional vector fields have also been proposed in different cosmological contexts in recent years. From the pioneering works on inflation driven by vector fields [For89] to the more recent ones based on non-abelian gauge fields (see [MSS13] and references therein), the vector inflation models have shown a rich phenomenology including the possible generation of primordial vector modes or statistical anisotropies in the CMB power spectrum [ACW07; WKS10]. Vector fields have also been proposed as candidates for dark energy, either from potential terms [Arm04; BH07] or from purely kinetic actions [BM08; BM09], and as ultralight dark matter candidates [NS11].

This Chapter is devoted to studying the effects of cosmological vector fields on GW propagation. We start by laying the state of the art about vectors in a cosmological context in Sec. 6.1. In Sec. 6.2, we introduce ultralight vector fields (ULVFs) as a dark matter candidate and analyse their impact on GW propagation, which we replicate in Sec. 6.3 for a vector dark radiation model. Finally, in Sec. 6.4, we draw the implications on GW of having an Abelian vector field with a generic potential.

6.1 Vectors in cosmology

Vector field models are usually characterised by an action featuring a kinetic and a potential term for the homogeneous vector field

$$S = \int \mathrm{d}^4x\,\sqrt{g}\left(-\frac{1}{4}F_{\mu\nu}F^{\mu\nu} - V(A^2)\right), \tag{6.1}$$

with $F_{\mu\nu} = \partial_\mu A_\nu - \partial_\nu A_\mu$ the field strength and $A^2 = A_\mu A^\mu$. The equations of motion read as follows

$$F^{\mu\nu}{}_{;\nu} + 2V'(A^2)A^\mu = 0, \tag{6.2}$$

and the stress-energy tensor (2.12) is

$$T^\alpha{}_\beta = \left(\frac{1}{4}F_{\mu\nu}F^{\mu\nu} + V(A^2)\right)\delta^\alpha{}_\beta - F^{\alpha\mu}F_{\beta\mu} - 2V'(A^2)A^\alpha A_\beta. \tag{6.3}$$

In principle, a cosmological model including a vector field would introduce anisotropies in the stress-energy tensor, and the description of the Universe in terms of an isotropic spacetime would no longer hold. However, it was proven in [Cem+12] that a

coherently oscillating homogeneous vector field will render an isotropic stress-energy tensor on average, mimicking a perfect fluid, provided that the oscillations are faster than the universe expansion rate. Indeed, the anisotropies in this scenario are suppressed by a factor $\mathcal{H}/\omega$, where ω is the oscillation frequency of the field. This isotropy theorem was generalised in subsequent works to non-Abelian fields [CMN13] and higher-spin fields [CMN14].

Let us write the equation of motion (6.2) in components for a flat RW background in conformal time (C.18). Setting $\mu = 0$ yields

$$V'(A^2)A^0 = 0. \tag{6.4}$$

While a stable solution $V'(A^2) = 0$ is possible, this would set the vector field motionless at an extrema of the potential (typically a minimum), so the isotropy theorem cannot be applied. Instead, we focus on solutions with $A_0 = 0$, so the vector field $A_\mu(\eta) = (0, \mathbf{A})$ is purely space-like $A^2 = -a^{-2}\mathbf{A}^2$. With $\mu = i$, we have

$$A_i'' - 2a^2 V'(A^2)A_i = 0. \tag{6.5}$$

The components of the stress-energy tensor are

$$\rho = T^0{}_0 = \frac{1}{2a^4}A_i'A_i' + V(A^2), \tag{6.6a}$$

$$p_i = -T^i{}_i = \frac{1}{a^4}\left(\frac{1}{2}A_j'A_j' - A_i'A_i'\right) - V(A^2) - \frac{2}{a^2}V'(A^2)A_iA_i \quad \text{(no sum over } i\text{)}, \tag{6.6b}$$

$$T^i{}_0 = 0, \tag{6.6c}$$

$$T^i{}_j = \frac{1}{a^4}A_i'A_j' + \frac{2}{a^2}V'(A^2)A_iA_j, \quad (i \neq j). \tag{6.6d}$$

It was shown in [Cem+12] that, by averaging the equations of motion over rapid oscillations, the following relation can be obtained

$$\left\langle \frac{A_i'A_j'}{a^4} \right\rangle = -\left\langle \frac{2V'(A^2)A_iA_j}{a^2} \right\rangle, \tag{6.7}$$

which makes the off-diagonal part of $\langle T^\mu{}_\nu \rangle$ vanish. Thus, a coherently fast-oscillating vector field renders an isotropic stress-energy tensor, where the averaged pressures are all the same

$$\langle p_i \rangle = \left\langle \frac{A_j'A_j'}{2a^4} \right\rangle - \langle V(A^2) \rangle, \tag{6.8}$$

mimicking a perfect fluid indeed. The average equation of state will depend on the type of potential term driving the oscillations. In particular, a simple polynomial potential $V(A^2) = \lambda(A_\mu A^\mu)^n$ will lead to an average equation of state

$$w = \frac{\langle p \rangle}{\langle \rho \rangle} = \frac{n-1}{n+1}, \tag{6.9}$$

which agrees with the case of coherently oscillating scalar fields.

Following this result, models of dark matter or dark radiation can be built based on quadratic or quartic potentials, respectively. Even though the anisotropic stress vanishes in the fast-oscillation regime at background level, this is not necessarily true at the level of perturbations, as it was already shown in [CMN17]. Precisely, having an anisotropic stress modifies the propagation equation of gravitational waves (2.47). In the following sections, we study the anisotropic stress generated by a vector dark matter and a vector dark radiation models, and how that generates an imprint on gravitational-wave propagation.

6.2 Ultralight vector field

The possibility of constructing models of ultralight dark matter from coherently oscillating massive vector fields has been growing in popularity recently as a proposal for dark matter. Ultralight vector fields [CMN17; Agr+20; Co+19; Bas+19; DHN19; NIS20] are a natural spin-1 extension of scalar fuzzy dark matter, and are constituted by spin-1 bosons with very small masses ($m \ll 1$ eV) and very weak interactions. This kind of model exhibits a completely new phenomenology compared to the more standard ultralight dark matter models based on scalar fields. The effect of ULVF on the scalar sector of cosmological metric perturbations has already been analysed in [CMN17], and it produces the desired effect of suppressing structure formation on scales smaller than its comoving de Broglie wavelength $\lambda_{dB} = (\mathcal{H}ma)^{-1/2}$. The typical galactic size in our Universe is associated with a field of mass $m \sim 10^{-22}$ eV, meaning that lighter fields have an astrophysical-sized de Broglie wavelength, and thus could not conform the totality of the dark matter in the Universe. The presence of the background vector field also induces a mixing between scalar, vector and tensor modes which allows the generation of gravitational waves from the usual density perturbations.

Aside from its dynamics, its production has also been studied in different contexts, such as inflation [GMR16; NNW20] or by misalignment mechanisms [NS11]. However, it has been shown that even though the standard misalignment mechanism works for a wide mass range, it requires large, highly tuned non-minimal couplings to the scalar curvature [Ari+12]. In addition, these couplings lead to perturbative unitarity violation at low energies in longitudinal photon-graviton scattering, and also to a negative kinetic term of the longitudinal mode for a certain range of momenta, thus threatening the vacuum stability. These issues have been discussed in previous works but none of them have succeeded in ensuring the viability of the mechanism [AHJ20]. As a result, alternative mechanisms which include couplings to axion fields have been proposed in [Agr+20; Co+19; Bas+19; DHN19].

Regarding the detection of ULVF DM, the possible indirect detection through the generation of induced atomic transitions was considered in [ÁC19], the use of optomechanical accelerometers as resonant detectors was explored in [Man+21]. The

generation of gravitational waves associated with density perturbations was studied in [CMN17]. It was found that the generated signal would be too small to be detected by gravitational-wave interferometers and could only have an effect on the CMB. More recently, possible effects on pulsar timing signals have been considered in [LU18; NIS20].

The aim of this Section is precisely to analyse the effects of ultralight vector fields on GW propagation. With that purpose, we consider a model based on a homogeneous massive abelian vector field. We analyse the parameter space in which the field behaves as ULVF dark matter and its dynamics and equation of state in past epochs. Then, we study its effects on GW propagation and calculate the range of modes and parameters for which the impact is larger with respect to standard ΛCDM, analysing the modified tensor power spectrum.

6.2.1 Ultralight vector field dynamics

Let us consider a massive abelian vector field in a RW background. The corresponding action is obtained by choosing a mass-like potential for the action (6.1), which reads

$$S = \int \mathrm{d}x \sqrt{g}\left(-\frac{1}{4}F_{\mu\nu}F^{\mu\nu} + \frac{1}{2}m^2 A_\mu A^\mu\right). \tag{6.10}$$

The minus sign in the potential is due to stability requirements, since the vector field is purely spacelike, as we discussed in Sec. 6.1.

The equations of motion for the vector field are obtained by inserting the potential in (6.2)

$$F^{\mu\nu}{}_{;\nu} - m^2 A^\mu = 0. \tag{6.11}$$

We consider a homogeneous vector field, thus dependent solely on conformal time η, whose spatial components we choose, for simplicity, to point in a fixed direction (linear polarisation). After conveniently orienting the spatial axes, it can be written as

$$A_\mu(\eta) = (A_0(\eta), 0, 0, A_z(\eta)). \tag{6.12}$$

Fixing $\mu = 0$ in (6.11) gives

$$m^2 A_0 = 0, \tag{6.13}$$

so the temporal component is required to vanish for a massive field, as expected, whereas the spatial part of the equation yields

$$A_z'' + m^2 a^2 A_z = 0. \tag{6.14}$$

We can study now the behaviour of A_z at different stages of the cosmological evolution. It can be seen that for $ma \gg \mathcal{H}$ the field oscillates rapidly around the potential minimum. Thus, introducing a Wentzel-Kramers-Brillouin (WKB) ansatz

$$A_z(\eta) = F_k(\eta)\cos\int^\eta \omega(\eta')\,\mathrm{d}\eta', \tag{6.15}$$

where $F_k(\eta)$ is a slowly varying function, and substituting back in (6.14) up to next-to-leading adiabatic order, we get

$$A_z(\eta) = A_{z,0} a^{-1/2}(\eta) \cos \int^{\eta} m a(\eta') \mathrm{d}\eta' , \tag{6.16}$$

where $A_{z,0}$ is a normalisation constant.

Now, in order to study the effect of this vector field on the RW background, we need to compute the stress-energy tensor for this theory, which can be obtained from (6.3)

$$T^{\mu}{}_{\nu} = \left(\frac{1}{4} F_{\rho\sigma} F^{\rho\sigma} - \frac{1}{2} m^2 A_\rho A^\rho \right) \delta^{\mu}{}_{\nu} - F^{\mu\rho} F_{\nu\rho} + m^2 A^\mu A_\nu . \tag{6.17}$$

We can write down the Friedmann equation with the stress-energy tensor given by this theory

$$\mathcal{H}^2 = \left(\frac{a'}{a} \right)^2 = \frac{8\pi G}{3} \rho_A a^2 , \tag{6.18}$$

with

$$\rho_A = T^0{}_0 = \frac{A_z'^2}{2a^4} + \frac{m^2}{2a^2} A_z^2 . \tag{6.19}$$

If, instead, we want to consider this ULVF within the framework of ΛCDM, we must simply add this energy density to the total energy density of all the other species when writing the Friedmann equation.

By substituting the WKB solution (6.16) into Eq. (6.19), we can see that $\rho_A \propto a^{-3}$ with no oscillation at leading order, which means that, in the regime in which the WKB condition $ma \gg \mathcal{H}$ is valid, the vector field behaves as non-relativistic matter, so that it could be part of the unexplained dark matter component. Consequently, we must ensure this behaviour throughout the whole matter-dominated epoch. Fig. 6.1 displays the redshift at which the field starts to oscillate as a function of its mass and thus starts behaving as matter. In order not to spoil the beginning of the matter-dominated era, we see that $m \gtrsim 10^{-27}$ eV.

At earlier times, when the WKB condition is not satisfied, if one imposes that the time derivative of the field is zero at early epochs, it remains constant at its initial value $A_{z,0}$, so that the energy density scales as $\rho_A \propto a^{-2}$. This holds until $ma \simeq \mathcal{H}$ is reached, when the vector field begins to oscillate as described before and behaves as matter. In Fig. 6.2, we show the numerical evaluation of the vector field energy density. Wee see that the energy density now scales as a^{-3} with small oscillations around this scaling.

6.2.2 Effect on GW propagation

The presence of a vector field introduces anisotropic stress at perturbation level, even if perturbations of the vector field are not considered. This anisotropic stress will affect the GW propagation, which can be studied through the perturbed Einstein

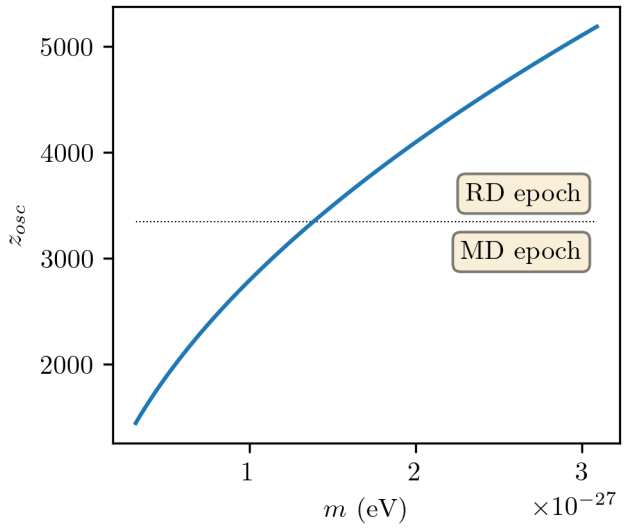

Figure 6.1: Starting point of vector field oscillation expressed in redshift as a function of its mass, computed with a ΛCDM background. The horizontal line corresponds to the matter-radiation equality redshift $z_{eq} \simeq 3350$, which separates RD and MD epochs. Consistency with ΛCDM requires this moment to occur in the RD epoch, yielding a lower bound for the ULVF mass.

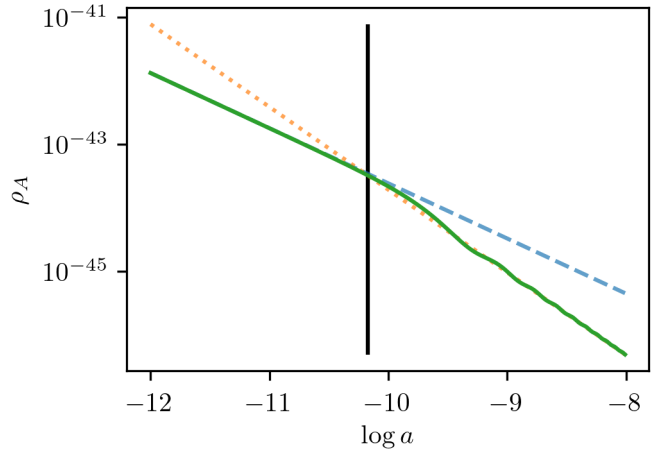

Figure 6.2: ULVF energy density (in arbitrary units) as a function of the scale factor, for $m = 10^{-26}$ eV in a ΛCDM background. Dashed and dotted lines represent a^{-2} and a^{-3} (matter-like) scalings respectively. The vertical line corresponds to $ma = \mathcal{H}$, after which the energy density oscillates around $\rho_A \propto a^{-3}$ as a consequence of the field oscillation.

equation (2.47). The anisotropic stress Π_{ij} can be obtained by projecting the perturbed stress-energy tensor onto its TT part

$$\Pi_{ij} = \Lambda_{ij,lm}\delta T^{l}{}_{m}, \tag{6.20}$$

where

$$\Lambda_{ij,lm} = P_{il}P_{jm} - \frac{1}{2}P_{ij}P_{lm} \tag{6.21}$$

is the TT projector and

$$P_{ij} = \delta_{ij} - \hat{k}_i\hat{k}_j, \tag{6.22}$$

with $\hat{\mathbf{k}}$ the unit vector in the GW propagation direction.

After perturbing the metric in the stress-energy tensor (6.17), one gets

$$\delta T^{i}{}_{j} = -\frac{1}{a^4}h_{ik}A'_jA'_k + \frac{m^2}{a^2}h_{ik}A_jA_k + \text{terms including } \delta^{i}{}_{j}, \tag{6.23}$$

where the TT projection of δ^i_j vanishes, so that

$$\begin{aligned}\Pi_{ij} = &-\frac{1}{a^4}\left[h_{ik}A'_jA'_k - \hat{k}_j\hat{k}_m h_{ik}A'_mA'_k - \frac{1}{2}(\delta_{ij}-\hat{k}_i\hat{k}_j)h_{lk}A'_lA'_k\right]\\ &+\frac{m^2}{a^2}\left[h_{ik}A_jA_k - \hat{k}_j\hat{k}_m h_{ik}A_mA_k - \frac{1}{2}(\delta_{ij}-\hat{k}_i\hat{k}_j)h_{lk}A_lA_k\right].\end{aligned} \tag{6.24}$$

Notice that because of the presence of the background vector field, it would be possible to have anisotropic stress at the linear level in perturbations coming from scalar and vector modes that would source gravitational waves [CMN17], as the anisotropic stress could feature terms such as $\delta T^{i}{}_{j} \sim \Phi A^i A_j$. However, in this work, we will only concentrate on the effect on propagation so we will ignore the new source terms coming from scalar and vector perturbations and consider only the terms that are linear in tensor perturbations.

We calculate the components of the anisotropic stress in the orthonormal basis [CMN17] defined by the vectors

$$\{\hat{\mathbf{u}}_1, \hat{\mathbf{u}}_2, \hat{\mathbf{u}}_3\} = \{\hat{\mathbf{u}}_{pk}, \cos\theta\hat{\mathbf{u}}_p - \sin\theta\hat{\mathbf{u}}_a, \sin\theta\hat{\mathbf{u}}_p + \cos\theta\hat{\mathbf{u}}_a\}, \tag{6.25}$$

where $\hat{\mathbf{u}}_a$ is the unit vector that points in the direction of the vector field, which remains constant during its evolution, so that $\mathbf{A} = |\mathbf{A}|\hat{\mathbf{u}}_a$, $\hat{\mathbf{u}}_3 = \hat{\mathbf{k}}$, $\cos\theta = \hat{\mathbf{k}}\cdot\hat{\mathbf{u}}_a$ and

$$\hat{\mathbf{u}}_{pk} = \frac{\hat{\mathbf{k}}\times\hat{\mathbf{u}}_a}{\sin\theta}, \qquad \hat{\mathbf{u}}_p = \frac{\hat{\mathbf{k}} - \cos\theta\hat{\mathbf{u}}_a}{\sin\theta}. \tag{6.26}$$

Since $\hat{\mathbf{u}}_3$ is the direction of GW propagation, we can use the expression (4.3) for h_{ij}. The non-vanishing components of the projected stress-energy tensor are listed as follows

$$\Pi_{11} = -\Pi_{22} = \frac{\sin^2\theta}{2a^4}\left(-\mathbf{A}'^2 + m^2a^2\mathbf{A}^2\right)h_+, \tag{6.27a}$$

$$\Pi_{12} = \frac{\sin^2\theta}{2a^4}\left(-\mathbf{A}'^2 + m^2a^2\mathbf{A}^2\right)h_\times. \tag{6.27b}$$

Thus, in this basis, we easily get the following expression from the Einstein equation (2.47)

$$h_\lambda'' + 2\mathcal{H}h_\lambda' + \left[k^2 - 8\pi G \sin^2\theta \left(\frac{\mathbf{A}'^2}{2a^2} - \frac{m^2}{2}\mathbf{A}^2\right)\right] h_\lambda = 0, \tag{6.28}$$

with $\lambda = +, \times$.

If the vector field is not oscillating (i.e. it remains constant) when the GW mode enters the Hubble horizon, the only effect we effectively get is a shift in the momentum k and thus a slight displacement of the instant when the mode enters the horizon. As the effective momentum acquires a slightly larger value, which is modulated by the angle θ, the mode enters the horizon slightly before it usually does, with the most affected GWs being the ones that propagate perpendicular to the vector field.

On the other hand, more interesting effects, such as changes in the GW amplitude, are expected to happen to modes that enter the horizon when the vector field is already oscillating, in particular to all modes that become sub-Hubble during the matter-dominated epoch.

Let us write the vector field abundance today (1.7), when the WKB approximation (6.16) must be valid, as

$$\Omega_A = \frac{\rho_{A,0}}{\rho_c} = \frac{4\pi G}{3}\frac{m^2 A_{z,0}^2}{H_0^2}. \tag{6.29}$$

Note that, as this field behaves as matter today, we must have $\Omega_A < \Omega_M$ necessarily. If we introduce this as well as the WKB expression for the vector field in (6.28) and we perform a change of variable $h_\lambda = v_\lambda/a$, we get the following equation:

$$v_\lambda'' + \left[k^2 - \frac{a''}{a} + \frac{3\Omega_A H_0^2 \sin^2\theta}{a}\cos\left(2\int^\eta ma(\eta')\,\mathrm{d}\eta'\right)\right] v_\lambda = 0. \tag{6.30}$$

Thus, modifications in the GW propagation could appear given the following requirements:

- The vector field must be oscillating at some point of the cosmological evolution: $ma \gg \mathcal{H}$, which is ensured as long as we keep the matter-radiation equality unaffected, as discussed before.
- The vector field term must be greater or at least of the order of the k^2 and the damping terms, i.e. $3\Omega_A H_0^2 \sin^2\theta/a \gtrsim k^2, a''/a$.
- If the vector field term oscillates very quickly, it could be averaged out, resulting in no effect. Thus, the frequency ma cannot be much larger than the GW oscillation frequency, and since the former is monotonically increasing, the effect is going to be more noticeable if the vector field has oscillated for a short time when the GW mode enters the horizon.

Taking all of this into account, the most affected modes are going to be those around $k^2 = H_0^2/a_*$, with a_* defined as the scale factor at which the vector field starts

behaving as matter, which can be approximately determined by $ma_* = \mathcal{H}(a_*)$. The complicated structure of the differential equation does not allow much further analysis, and all calculations and results must be obtained numerically, which is discussed in the following section.

Another major point is the fact that this new contribution makes the GW phase velocity c_T slightly different from the speed of light c. The relative difference between these two δc, defined in Eq. (4.1), is bounded by observations at $\delta c \lesssim \mathcal{O}(10^{-15})$ in the operating range of ground-based detectors $f = 10$ Hz ~ 10 kHz, as we already discussed in Sec. 4.1. The modified dispersion relation that appears in the propagation equation (6.28) can be seen either as an anomalous velocity for the tensor modes $c_T \neq 1$ or an effective mass of the graviton $m_g \neq 0$ [EZ18] and, after realising that the modification is much smaller than unity, it yields a deviation of

$$\delta c = \frac{4\pi G \sin^2\theta}{k^2}\left|\frac{\mathbf{A}'^2}{2a^2} - \frac{m^2}{2}\mathbf{A}^2\right|. \tag{6.31}$$

Taking into account that the term in absolute value is $\sim \rho_A$, this results in a much smaller deviation, at about $\delta c \lesssim \mathcal{O}(10^{-38})$ for the mentioned frequencies and the constraints on Ω_A.

The effect of the vector field on GW propagation is parametrised through the ratio functions, defined in Eq. (4.23), which will depend on all parameters of our model. For our ULVF model, linear polarisations do not mix and obey the same equation of motion, so $R_+ = R_\times = R$ and $R_{+\times} = R_{\times+} = 0$. It is important to bear in mind that, for sufficiently long times, the effect of the vector field is negligible, so gravitational waves recover their usual sub-Hubble or super-Hubble behaviour. At this point, the ratio between the two solutions remains constant and can be computed at the most convenient time. Unless the contrary is stated, we will always refer to this long-time ratio function.

Since the ratio function depends on the angle θ, the evolved tensor power spectrum also does. Typically, the power spectrum as defined in Eq. (3.18) is trivially integrated over solid angle, but the anisotropy of our model in the vector-GW angle makes this integration non-trivial. Let us define

$$\mathcal{P}_T(k,\eta) = \frac{1}{2}\int_{-1}^{1} \mathrm{d}\cos\theta\, \mathcal{P}_T(k,\eta,\theta), \tag{6.32}$$

where the 1/2 factor is introduced to keep the normalisation consistent. With this definition and taking into account the discussion about ratio functions in Sec. 4.3.1, we can link this angle-dependent power spectrum to the primordial one as

$$\mathcal{P}_T(k,z,\theta) = \frac{1}{2}|T(k,z)|^2 |R(k,m,\theta,\Omega_A)|^2 \mathcal{P}_{T,in}(k). \tag{6.33}$$

In terms of usual observables, i.e. the scalar power spectrum (3.14) and the tensor-to-scalar ratio (3.20), whose observational values were discussed in Sec. 1.2, we can

finally write down

$$\mathcal{P}_T(k,z,\theta) = \frac{1}{2} r(k_*) A_S(k_*) \left(\frac{k}{k_*}\right)^{n_T} |T(k,z)|^2 |R(k,m,\theta,\Omega_A)|^2. \tag{6.34}$$

Therefore, the only calculation that we must perform within our model in order to determine the tensor power spectrum $\mathcal{P}_T$ is the computation of the ratio function for a set of given input parameters. This involves solving the evolution of GWs (6.28) twice per parameter set, once in standard cosmology, switching off the action of the vector field, and once with the vector field. The GW propagation can be solved analytically only in a handful of scenarios, typically when only one species dominates the energy budget of the universe, so we cannot obtain analytical expressions even for standard cosmology. We must then proceed numerically, and since exploring a large region of the parameter space involves a big computational effort, we must develop a methodology able to solve the propagation as fast as possible, which we detail as follows.

6.2.3 Numerical model and results

Conformal time η does not appear explicitly in any of the equations, so we can get rid of it to work in terms of the scale factor $a(\eta)$, which is more convenient. However, as the scale factor spans several orders of magnitude, we will work with the $x = \log a(\eta)$ variable in order to improve calculation performance. Eqs. (6.14) and (6.28), to solve in terms of x, are listed as follows:

$$\partial_x^2 A_z + \frac{\partial_x \mathcal{H}}{\mathcal{H}} \partial_x A_z + \frac{m^2 e^{2x}}{\mathcal{H}^2} A_z = 0, \tag{6.35a}$$

$$\partial_x^2 h_\lambda + \left(2 + \frac{\partial_x \mathcal{H}}{\mathcal{H}}\right) \partial_x h_\lambda + \frac{1}{\mathcal{H}^2} \left[k^2 - 4\pi G \sin^2\theta \left(e^{-2x} \mathcal{H}^2 (\partial_x A_z)^2 - m^2 A_z^2\right)\right] h_\lambda = 0.$$

The inconvenience of eliminating conformal time is that now the Hubble parameter $\mathcal{H}$ appears in the equations. Its expression *including* the vector field energy density can be written by modifying (2.22) as

$$\mathcal{H}^2 = H_0^2 e^{2x} \left[(\Omega_M - \Omega_A) e^{-3x} + \Omega_R e^{-4x} + \Omega_\Lambda + \frac{4\pi G}{3 H_0^2 e^{2x}} \left(\frac{\mathcal{H}^2 (\partial_x A)^2}{e^{2x}} + m^2 A^2\right)\right], \tag{6.36}$$

where the last term in the square brackets must equal Ω_A when evaluated today ($x = 0$). The matter abundance today consisting of the ultralight vector field is subtracted from the total matter Ω_M, yielding the term $(\Omega_M - \Omega_A) a^{-3}$ which includes the CDM and baryon contributions. Thus, when evaluated today, the factors including Ω_A cancel out. Notice that depending on the Ω_A value, the share of ULVF dark matter vs. CDM varies.

The way of solving this system would be to solve (6.36) for $\mathcal{H}$. Then, plugging the result into (6.35a), we solve the differential equation in order to get the solution for the vector field. Finally, having the solution for the vector field, we solve the

GW propagation (6.35b). This procedure, however, has several inconveniences. The main one is using the expression for $\mathcal{H}$ that contains A and its derivative explicitly, as it enlarges considerably the equation for the vector field. In addition, having a denominator that can be close to zero results in numerical inaccuracies. On the other hand, large masses for the vector field translate into thousands of oscillations before arriving at the present moment $x = 0$, which can take long computing times even if the ΛCDM Hubble parameter (2.22) is used. Lastly, we would like Ω_A to be an input parameter of our model, but since it is a quantity calculated at $x = 0$ rather than an initial value, this requirement would turn our equations into a boundary value problem over a large interval, in which the primordial value of the vector field should be fine-tuned to yield the desired Ω_A, with a shooting method for example, making the process fairly slow. In practice, it is not possible to numerically solve this system as a boundary value problem in many cases, as the integration of a large number of oscillations for both the vector field and the GW is impracticable.

Instead, we can argue that the effect of the vector field on the background does not have a large impact on its own evolution. This is sensible as the vector energy density scales initially as a^{-2} and then behaves as matter in a radiation-dominated epoch, making it subdominant throughout this period. After a few oscillations of the field, the WKB approximation is valid and its presence can be accounted for by treating it as standard matter. Thus, the equation for the vector field (6.35a) is integrated using the standard ΛCDM Hubble parameter

$$\mathcal{H}^2_{\Lambda\text{CDM}} = H_0^2 e^{2x}\left(\Omega_M e^{-3x} + \Omega_R e^{-4x} + \Omega_\Lambda\right), \tag{6.37}$$

with initial conditions $A_z(x_{\text{in}}) = A_{\text{in}}$, $A_z'(x_{\text{in}}) = 0$, until the scale factor grows by a factor e^2 after the field started oscillating. At this point, it oscillates sufficiently fast as to use the WKB solution (6.16), so we match both solutions at the first minimum after this point, which is easy to track numerically, where the vector field satisfies $A_z(x_{\text{min}})/A_{\text{in}} = A_{\text{min}}$. With that, we can write

$$A_z(x) = A_{\text{in}} A_{\text{min}} e^{-(x-x_{\text{min}})/2} \cos\left(\int_{x_{\text{min}}}^{x} \frac{m e^x}{\mathcal{H}_{\Lambda\text{CDM}}}\,\mathrm{d}x\right), \tag{6.38}$$

valid for $x > x_{\text{min}}$.

With this solution, we can calculate the abundance today (6.29) and get the primordial value A_{in} in terms of Ω_A

$$A_{\text{in}} = \left(\frac{3\Omega_A H_0^2}{4\pi G m^2 e^{x_{\text{min}}} A_{\text{min}}}\right)^{1/2}, \tag{6.39}$$

thus fixing the boundary problem issue. Fig. 6.3 shows a comparison between an exact solution and the solution we will be using, thus leading to small errors, as the relative error is less than 1% and oscillates about the exact values, so the effect practically integrates out in the GW propagation equation. Being able to use the WKB

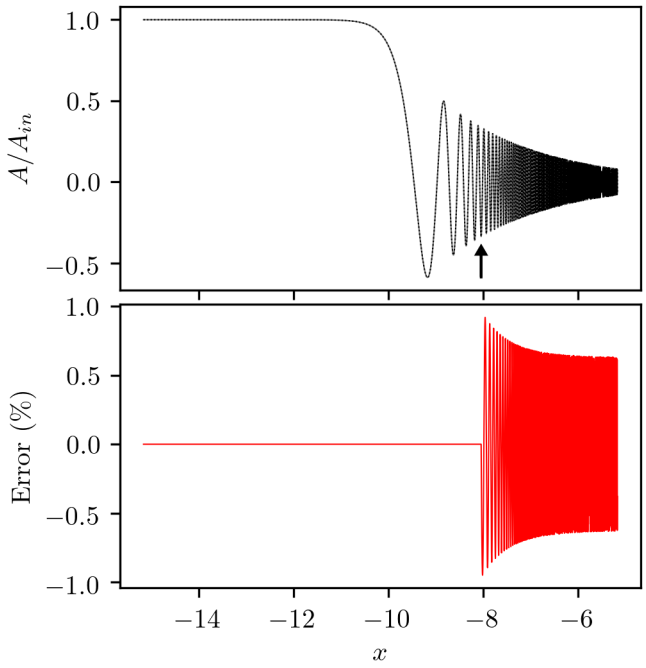

Figure 6.3: Comparison between the exact solution and our two-part model, employing the WKB approximation, for $m = 10^{-26}$ eV. The upper panel shows the exact solution (solid line) and the approximate one (dotted line), displaying a very small difference, as well as an arrow that indicates the minimum from which the WKB solution is used. The lower panel shows the relative error, compared to the oscillation amplitude, which remains below 1%. The oscillatory behaviour indicates that the error is mostly due to a small phase difference between both solutions.

approximation allows us to compute results much faster, as the integration of the large number of oscillations before reaching the present time would have taken much computation time, and now we can evaluate an analytical expression instead, which is much cheaper.

This two-part solution for the vector field can be plugged into the complete Hubble parameter (6.36), where, in the combination $A' = \mathcal{H}\partial_x A$, we must use (6.37) in order to have a consistent solution, as this is the Hubble parameter that we have used to solve A. Finally, we solve the GW evolution (6.35b). The starting integration point $x_{\rm in}$ must be early enough so that the field is still constant and the GW mode is super-Hubble with $\mathcal{H}(x_{\rm in}) \gg \{e^{x_{\rm in}} m, k\}$.

The GW propagation equation (6.35b) must be solved twice, once for a ΛCDM background ($\Omega_A = 0$) and then again for our model with a certain set of parameters. Fig. 6.4 shows a couple of examples of GW propagation with and without the vector field. The main effect, which is fairly visible in those figures, is that the GW amplitude

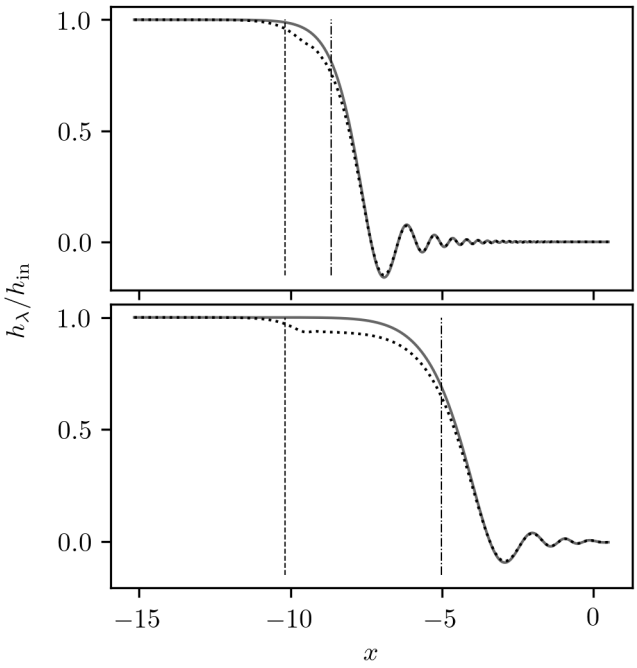

Figure 6.4: GW evolution for a ΛCDM background and our model, in solid and dotted lines respectively, and wavenumbers of $k = 10^{-31}$ eV (above) and $k = 10^{-32}$ eV (below). The rest of the parameters are fixed to $m = 10^{-26}$ eV, $\Omega_A = 0.25$, $\theta = \pi/3$. Vertical lines correspond to the ULVF oscillation beginning $ma = \mathcal{H}$ (dashed) and the GW entering the Hubble horizon $k = \mathcal{H}$ (dash-dotted).

experiences a smooth diminution the moment the ULVF starts behaving as matter as long as this event occurs whilst the GW mode is super-Hubble. If it occurs when the GW is already deep inside the Hubble horizon, little to no effect is noticed. This amplitude shift remains practically the same after the wave enters the horizon, which is what gives the ratio function its value.

With both solutions at hand, the transfer function (4.18) can be obtained from the ΛCDM one by directly dividing the value of the GW today by its primordial value. The ratio function is computed through the comparison of both solutions for sufficiently long times, as discussed in Section 6.2.2. An example for different masses can be seen in Fig. 6.5, showing that there is a specific region where the effects are more noticeable, which corresponds to wavenumbers around $k = H_0/\sqrt{a_*}$. As a_* depends solely on the ULVF mass, the k value for which the ratio function reaches its absolute minimum depends only on the mass as well, meaning that the variation of the angle θ or Ω_A produces a shift in the vertical axis, but not in the horizontal one. In particular, the deviation from ΛCDM is bigger the larger Ω_A is and the closer to $\pi/2$ the angle θ is, as can be seen in Figs. 6.6 and 6.7 respectively. One last point to note is that

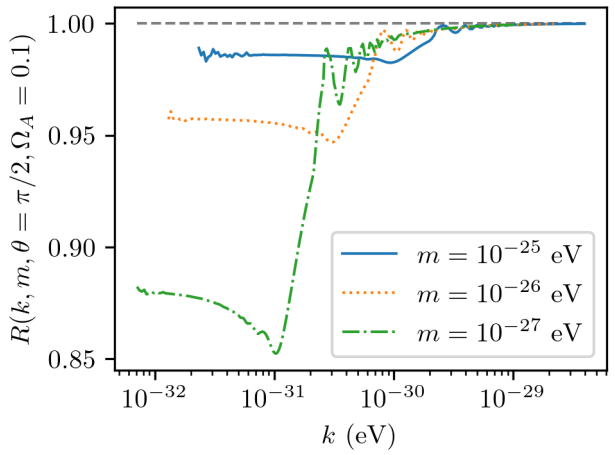

Figure 6.5: Ratio function for different ULVF masses, with fixed $\theta = \pi/2$ and $\Omega_A = 0.1$. The deviation from ΛCDM $R = 1$ is larger the smaller the mass is. There is a global minimum at k_{min}, different for each mass, where the deviation is maximum. For $k \ll k_{\text{min}}$, the ratio tends to a constant value smaller than 1 (with little deviations in the figure due to numerical inaccuracy), whereas for $k \gg k_{\text{min}}$ it tends to unity.

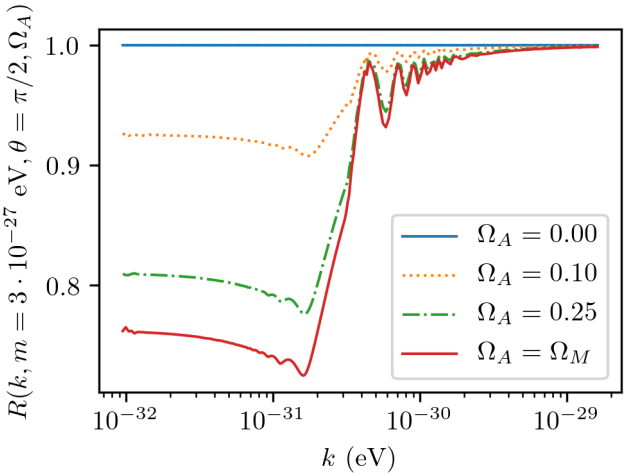

Figure 6.6: Ratio function for different ULVF abundances, with fixed $m = 3 \cdot 10^{-27}$ eV and $\theta = \pi/2$. The deviation from ΛCDM is larger the greater the abundance, which has a natural bound at Ω_M. The wavenumber of maximum deviation (global minimum) does not depend on Ω_A, as opposed to mass (see Fig. 6.5). The choice $\Omega_A = 0$ is exactly ΛCDM $R = 1$, as expected.

setting $\Omega_A = 0$ in our model corresponds exactly with ΛCDM, thus resulting in a ratio function with value unity, but setting $\theta = 0$ does not. This is because, even though $\theta = 0$

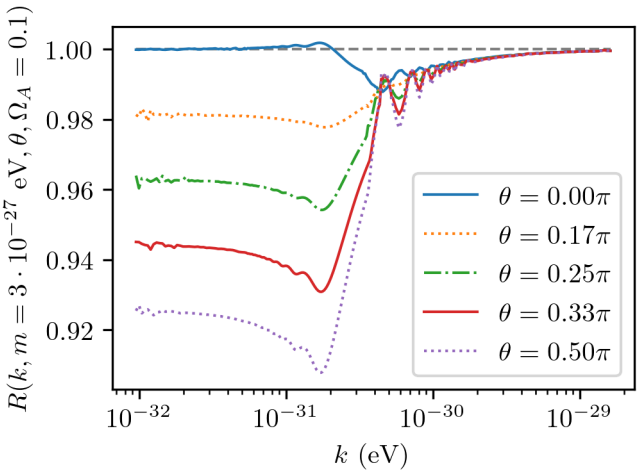

Figure 6.7: Ratio function for different vector field-wavevector angles θ, with fixed $m = 3 \cdot 10^{-27}$ eV and $\Omega_A = 0.1$. The deviation from ΛCDM is larger the closer to $\pi/2$ θ is. Angles in the range $\pi/2 < \theta \leq \pi$ yield results that can be obtained from this picture, as the dependence in the propagation equation (6.28) is $\sin^2\theta$. Note that the wavenumber of maximum deviation does not depend on θ (obviating the extreme choice $\theta = 0$) and that the case $\theta = 0$ is not exactly ΛCDM despite having no extra term in the propagation equation, as the ULVF still affects the background evolution.

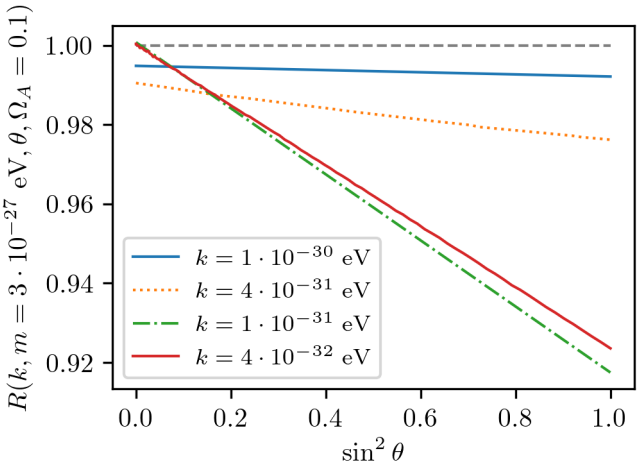

Figure 6.8: Ratio function as a function of $\sin^2\theta$, with fixed $m = 3 \cdot 10^{-27}$ eV and $\Omega_A = 0.1$, for various wavenumber values. The dashed grey line corresponds to ΛCDM. The almost linear dependence suggests an approximately quadrupolar angular modulation of the GW power spectrum.

eliminates the additional term in (6.35b), there is still a slight effect in the background accounted in $\mathcal{H}$, so we get $R \neq 1$ even though there is no direct coupling between GWs and the ULVF in the propagation equation. Note that, for the masses we are considering, the ultralight vector field cannot conform the totality of the dark matter, as discussed in the introduction of Sec. 6.2.

For a given ULVF mass and any non-zero abundance and angle, the qualitative behaviour of the ratio function can be understood as follows: The modes that enter the Hubble horizon around the time the vector field starts oscillating $k^2 = H_0^2/a_*$ are the most suppressed ones as we had already anticipated, so the ratio function acquires its minimum value here. For longer-wavelength modes, the vector starts oscillating much before the wave enters the horizon, which induces a shift in the GW amplitude, which can be seen in the lower panel of Fig. 6.4. This amplitude difference is then kept in the sub-Hubble regime. If the two events are very far apart, the shift is eventually the same for every k, as can be seen in the low-k asymptotic behaviour of Fig. 6.5. For shorter-wavelength modes, the GW is already deep in the Hubble horizon when the vector field starts oscillating and no effect is appreciated, so $R \to 1$.

The ratio function exhibits non-trivial k and θ dependencies as shown in Figs. 6.5 and 6.8, which could make it possible to detect the presence of ULVF dark matter in certain mass ranges. Forthcoming CMB experiments are expected to detect primordial gravitational waves with sensitivity as small as $\sigma(r) \sim 10^{-3}$ through CMB B-mode observations (see the discussion at the end of Sec. 1.2). Therefore, some effects in the B-mode power spectrum resulting from the ULVF presence are expected, on the one hand, as an angular modulation of the tensor power spectrum in that multipole range. As shown in Fig. 6.8, this modulation would be approximately quadrupolar. Both effects would be more important for masses near the lower limit of $m \sim 10^{-27}$ eV, as can be seen in Fig. 6.5. Notice also that astrophysically-generated GWs typically have larger frequencies, where the ratio function tends to unity and therefore no effect in propagation is expected.

We plot in Fig. 6.9 the tensor power spectrum at decoupling time for various sets of parameters, in which we can see that the ULVF presence suppresses the power spectrum with respect to ΛCDM for small masses. The effect is more evident at low k (multipoles $\ell < 100$), where the ratio function is not unity for these small masses.

6.3 Vector dark radiation

Another possibility to build around a coherently oscillating vector field is a dark radiation component. Dark radiation is the possible radiation component existing in the Universe in addition to the standard radiation content corresponding to photons and three families of neutrinos. The abundance of dark radiation is usually parametrized through the effective number of neutrino species $N_{\rm eff}$ defined in (1.11). The Standard Model prediction is $N_{\rm eff}^{\rm SM} = 3.046$ so that the abundance of dark radiation is

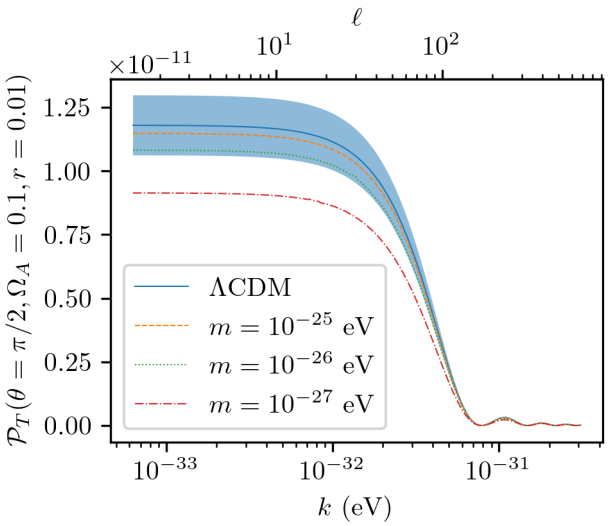

Figure 6.9: Tensor power spectrum at decoupling time for different ULVF masses, $\theta = \pi/2$, ULVF abundance of $\Omega_A = 0.1$, primordial tensor-to-scalar ratio $r = 0.01$ and no tensor spectral tilt $n_T = 0$. The rest of the parameters in Eq. (6.34), corresponding to the scalar sector of the primordial power spectrum correspond to the Planck cosmology (Sec. 1.2). The upper abscissa axis represents the approximate multipole moment ℓ corresponding to the wavenumber, taking into account its angular size at the last scattering surface. The blue band represents the values compatible with ΛCDM according to the design tensor-to-scalar precision of LiteBIRD $\sigma(r) = 10^{-3}$. Smaller masses (as well as bigger ULVF abundances) are more likely to be detected as deviations from ΛCDM.

parametrized by

$$\Delta N_{\rm eff} = N_{\rm eff} - 3.046. \tag{6.40}$$

The current limits on this parameter derive from CMB observations and BBN (see Secs. 1.2 and 1.4 respectively for more details), which bound the possible amount of dark radiation at $\Delta N_{\rm eff} \lesssim 0.3$. In terms of abundance today, this is about $\Omega_{\rm DR} \lesssim 10^{-6}$.

Dark radiation increases the expansion rate of the universe in the radiation era, thus reducing the size of the sound horizon at recombination. This can be compensated by an increase in the Hubble parameter today H_0 so that the CMB temperature power spectrum remains unchanged [BCH20]. Thus, dark radiation has been proposed as a possible way to alleviate the H_0 tension between local universe and CMB observations [Rie+19]. The effect of dark radiation on inflation-produced gravity waves has been studied in [JMN12].

Dark radiation is usually described by means of new relativistic particles weakly interacting with the Standard Model sector. Thus, models based on axion-like particles

have been proposed in [CM13; Mar16], supersymmetric candidates have also been considered related to the cosmological gravitino problem or axino decays [Ich+07; Has12] among others.

In order to construct dark radiation models from cosmological vector fields, we will focus on a conformal vector model [Aso+21] with a quartic self-interaction potential. An important consequence of this modification that we will analyse in this Section is that, unlike the case of massive vector fields, vector dark radiation can induce a net polarisation of the primordial gravitational wave background. This would be a clear smoking gun of this kind of model. Indeed, the primordial background of gravitational waves generated during inflation is expected to be unpolarised in standard cosmology. Nonetheless, it is possible to generate circularly polarised primordial gravitational waves in extended versions of inflation, for example with Chern-Simons gauge or gravitational couplings of the inflaton [LWK99; Sor11]. Primordial helical turbulence produced in first-order phase transition has been also proposed as a mechanism for the generation of gravitational wave circular polarisation [KGR05]. After inflation, polarisation of the gravitational wave backgrounds, both astrophysical and cosmological, can be induced by interaction with matter structures [CDF19], though the amount of polarisation produced by this mechanism is relatively small. Prospects for the detection of gravitational wave polarisation with current and future detectors have been explored in [KS16; Dom+20; SK22].

6.3.1 Vector dark radiation dynamics

In this section, we consider a simple model for dark radiation based upon a vector field A_μ with a quartic potential, which we introduce in the action (6.1)

$$S = \int \mathrm{d}^4x\sqrt{-g}\left(-\frac{1}{4}F_{\mu\nu}F^{\mu\nu} - \frac{\lambda}{4}(A^2)^2\right), \tag{6.41}$$

where λ is a dimensionless parameter that determines the strength of the self-interaction.

The equations of motion for the vector field are obtained by varying the action and read

$$F^{\mu\nu}{}_{;\nu} + \lambda A^\mu A^2 = 0. \tag{6.42}$$

Again, we consider a flat RW background metric and a homogeneous vector field $A_\mu(\eta)$, which depends solely on conformal time η. Setting $\mu = 0$ in (6.42), we get

$$\lambda A_0 A^2 = 0. \tag{6.43}$$

We are not interested in the lightlike solution $A^2 = 0$, since the vector field would simply grow linearly in time and a fast oscillation around the potential minimum is necessary to ensure that anisotropic pressures average out, as discussed in Sec. 6.1.

This necessarily sets $A_0 = 0$ for a self-interacting field. Therefore, the equation with $\mu = i$ reads

$$A_i'' + \lambda \mathbf{A}^2 A_i = 0, \tag{6.44}$$

with $\mathbf{A}^2 = \delta^{ij} A_i A_j$ the squared modulus of the spatial part of the vector field. This equation of motion allows for several configurations of the vector field, of which we shall analyse two particular cases: Linear and circular polarisation.

Linear polarisation

In the case of a linearly polarised vector field, which follows the same idea as the previous section (6.12), it evolves along a fixed direction which can be identified with the z-axis after a convenient orientation of the axes

$$A_\mu(\eta) = (0, 0, 0, A_z(\eta)). \tag{6.45}$$

Working out the spatial equations of motion (6.44) in components, we get

$$A_z'' + \lambda A_z^3 = 0. \tag{6.46}$$

which agrees with the corresponding equation in flat space-time thanks to the conformal invariance of the action (6.41). An analytic solution in terms of Jacobi elliptic functions can be readily obtained [Fin+00]. In Appendix B.2, we collect some useful properties of these functions. Assuming an initial value $A(\eta_{\rm in}) = A_{\rm in}$ with zero derivative and setting $\eta_{\rm in} = 0$ for simplicity, the solution is given by

$$A_z(\eta) = A_{\rm in}\, \mathrm{cn}\left(\sqrt{\lambda} A_{\rm in} \eta; 1/2\right), \tag{6.47}$$

where $\mathrm{cn}(x; m)$ is the elliptic cosine function with square modulus m. This function is periodic on its first argument, with period $4K(m)$, where $K(m)$ is the complete elliptic integral of the first kind, and in particular $K(1/2) \simeq 1.854$. Thus, the field has got a naturally associated comoving frequency, given by

$$\omega = \sqrt{\lambda} A_{\rm in}. \tag{6.48}$$

Such frequency can be compared with the expansion rate of the Universe, given by the comoving Hubble parameter $\mathcal{H} = a'/a$, so that if the condition $\omega \gg \mathcal{H}$ is satisfied, the average energy-momentum tensor becomes isotropic.

The stress-energy tensor obtained from the action (6.41) reads

$$T^\mu{}_\nu = \frac{1}{4}\left[F_{\rho\sigma}F^{\rho\sigma} + \lambda (A^2)^2\right]\delta^\mu{}_\nu - F^{\mu\rho}F_{\nu\rho} - \lambda A^\mu A_\nu A^2. \tag{6.49}$$

The energy density can then be calculated by plugging the analytical solution (6.47) into the stress-energy tensor

$$\rho_A = T^0{}_0 = \frac{1}{2a^4}\left(A_z'^2 + \frac{\lambda}{2} A_z^4\right) = \frac{\lambda A_{\rm in}^4}{4a^4}, \tag{6.50}$$

which as expected for a conformal theory scales exactly as radiation, i.e., $\rho_A \propto a^{-4}$. It is immediate then to obtain today's abundance

$$\Omega_A = \frac{\rho_{A,0}}{\rho_c} = \frac{2\pi G}{3H_0^2}\lambda A_{\rm in}^4. \tag{6.51}$$

The model is completely characterized at the background level by two parameters (ω, Ω_A), i.e. the oscillation frequency and the dark radiation abundance. The current observational constraints on such parameters come, on one hand, from the limits on the effective number of neutrino species discussed at the beginning of Sec. 6.3. Thus,

$$\Omega_A \leq \frac{\Delta N_{\rm eff}}{N_{\rm eff}^{\rm SM} + \frac{8}{7}\left(\frac{11}{4}\right)^{4/3}} \Omega_R^{\rm SM} \simeq 0.04\Omega_R \simeq 3\cdot 10^{-6}. \tag{6.52}$$

On the other hand, constraints on the frequency ω come from the requirement of isotropy. Since the vector points in the direction of the z axis, the pressures $p_i = -T^i{}_i$ can be different

$$p_x = p_y = \frac{\rho_A}{3}\left[3 - 6\,{\rm cn}^4(\omega\eta; 1/2)\right], \tag{6.53a}$$

$$p_z = \frac{\rho_A}{3}\left[12\,{\rm cn}^4(\omega\eta; 1/2) - 3\right]. \tag{6.53b}$$

The pressures are oscillating around the isotropic configuration of $p_x = p_y = p_z = \rho_A/3$ with a larger amplitude in the z direction. Notice that the average of the term involving the elliptic function is $\langle {\rm cn}^4\rangle = 1/3$. In the regime of fast oscillations $\omega \gg \mathcal{H}$, the effect of the pressure oscillations on the background metric is suppressed by $\mathcal{H}/\omega$. Therefore, for sufficiently large frequencies, the energy-momentum tensor can be replaced by the average isotropic tensor. It is also worth noting that the average pressure

$$\bar{p} = \frac{1}{3}\sum_i p_i = \frac{\rho_A}{3} \tag{6.54}$$

does not oscillate and renders the expected equation of state $w = 1/3$.

Since $\mathcal{H}$ is monotonically decreasing in radiation and matter-dominated epochs, once the field has entered the fast-oscillation regime, it will not leave it throughout its whole evolution afterwards. In particular, if it oscillates quickly at the end of reheating, when the radiation temperature is $T_{\rm RH}$, i.e. provided

$$\omega \gg \mathcal{H}(T_{\rm RH}) = 265\ {\rm Hz}\left(\frac{T_{\rm RH}}{10^{10}\ {\rm GeV}}\right). \tag{6.55}$$

then the field will be in the fast oscillation regime at all times afterwards.

Even if the frequency is below this value, the field would meet the fast oscillation regime at a later time. In order to ensure a standard isotropic evolution from the time of BBN and recover the observed abundances of light elements in the Universe, the corresponding condition reads

$$\omega \gg \mathcal{H}(T_{\rm nuc}) = 1.4\cdot 10^{-11}\ {\rm Hz}\left(\frac{T_{\rm nuc}}{\rm MeV}\right), \tag{6.56}$$

with the nucleosynthesis temperature being around $T_{\rm nuc} \sim 0.1$ MeV. In any case, if the anisotropies generated by the vector field, which can be roughly estimated as Ω_A/Ω_R, are smaller than the typical amplitude of anisotropies of the CMB, i.e. $\mathcal{O}(10^{-5})$ one should not worry about the fast-oscillation condition.

Circular polarisation

The linearly polarised solution constrains the oscillation of the field to a single direction, but that does not need to be the case. Another simple solution to the equation of motion (6.44) can be obtained by fixing the modulus of the field to be comovingly constant, i.e. $\mathbf{A}^2 = \alpha^2$, with α a real constant. Under this condition, the equations of motion read

$$A_i'' + \lambda\alpha^2 A_i = 0, \tag{6.57}$$

which has a solution in terms of trigonometric functions, so that the vector field revolves in a circular motion, with frequency

$$\omega = \sqrt{\lambda}\alpha. \tag{6.58}$$

If we choose the z-direction to be perpendicular to the rotation plane, and the vector field to initially point towards the x-direction, the particular solution can be written as

$$\mathbf{A}(\eta) = \alpha(\cos\omega\eta, \sin\omega\eta, 0). \tag{6.59}$$

Notice that this solution is compatible with the initial ansatz $\mathbf{A}^2 = \alpha^2$.

The stress-energy tensor is still given by (6.49), though both energy density and pressures are different due to the different solutions. On the one hand, the energy density is homogeneous and given by

$$\rho_A = \frac{3\lambda\alpha^4}{4a^4}, \tag{6.60}$$

so that today's abundance is

$$\Omega_A = \frac{2\pi G\lambda\alpha^4}{H_0^2}, \tag{6.61}$$

which together with the frequency ω can be used as the two parameters that characterise our model. On the other hand, the pressures $p_i = -T^i{}_i$ are given by

$$p_x = \frac{\rho_A}{3}\left[1 + 4\cos\big(2\omega\eta\big)\right], \tag{6.62a}$$

$$p_y = \frac{\rho_A}{3}\left[1 - 4\cos\big(2\omega\eta\big)\right], \tag{6.62b}$$

$$p_z = \frac{\rho_A}{3}, \tag{6.62c}$$

and the non-vanishing anisotropic pressures are

$$T^x{}_y = T^y{}_x = -\frac{\rho_A}{3}\sin\big(2\omega\eta\big). \tag{6.63}$$

As in the linearly polarised case, the pressures oscillate around the homogeneous configuration of a radiation component, given by $p_i = \rho/3$ and vanishing anisotropic pressures. It is also easy to check that the average pressure does not oscillate. In the fast-oscillation regime $\omega \gg \mathcal{H}$ these deviations average out, so the discussion in the previous section regarding the value of the frequency ω and the isotropy of the Universe can also be applied here.

6.3.2 Effect on GW propagation

In order to analyse the effects of the background vector field on GW propagation, we need to consider the perturbed TT Einstein's equation Eq. (2.47). In this case, the stress-energy tensor (6.49) up to first order in metric perturbations reads

$$\delta T^i{}_j = -\frac{1}{a^4} h_{ik} A'_j A'_k + \frac{\lambda}{a^4}(A_i A_j h_{lm} + A_j A_k h_{ik}\delta_{lm}) A_l A_m + \text{terms involving } \delta^i{}_j, \tag{6.64}$$

and its TT projection (6.20) is

$$\begin{aligned}\Pi_{ij} = &-\frac{1}{a^4}\left[h_{il}A'_jA'_l + \hat{k}_j\hat{k}_m h_{il}A'_mA'_l - \frac{1}{2}(\delta_{ij}-\hat{k}_i\hat{k}_j)h_{lm}A'_lA'_m\right]\\ &+\frac{\lambda \mathbf{A}^2}{a^4}\left[h_{il}A_jA_l + \hat{k}_j\hat{k}_m h_{il}A_mA_l - \frac{1}{2}(\delta_{ij}-\hat{k}_i\hat{k}_j)h_{lm}A_lA_m\right]\\ &+\frac{\lambda h_{kn}A_kA_n}{a^4}\left[A_iA_j - \hat{k}_i\hat{k}_lA_jA_l - \hat{k}_j\hat{k}_lA_iA_l\right.\\ &\qquad\left.+\frac{1}{2}(\delta_{ij}+\hat{k}_i\hat{k}_j)\hat{k}_l\hat{k}_mA_lA_m - \frac{1}{2}(\delta_{ij}-\hat{k}_i\hat{k}_j)\mathbf{A}^2\right].\end{aligned} \tag{6.65}$$

From this point onwards, we need to look at the two configurations described above separately, as they are going to introduce different terms in the GW propagation equation.

Linearly polarised vector field

Firstly, let us look at the linearly polarised vector field. Thanks to the axial symmetry around the direction of observation, we choose a basis in which GWs travel along the z-axis and the vector field is contained in the yz-plane, which allows us to use the basis defined in Eq. (6.25) and the expression in (4.3) for the tensor perturbation. In this basis, the non-vanishing components are given by

$$\Pi_{11} = -\Pi_{22} = \frac{\sin^2\theta}{2a^4}\left[-\mathbf{A}'^2 + \lambda\mathbf{A}^4(1+\sin^2\theta)\right]h_+, \tag{6.66a}$$

$$\Pi_{12} = \frac{\sin^2\theta}{a^4}\left(-\mathbf{A}'^2 + \lambda\mathbf{A}^4\right)h_\times. \tag{6.66b}$$

so we arrive at the modified equations of propagation for GWs, which read

$$h''_\lambda + 2\mathcal{H}h'_\lambda + \left[k^2 - \frac{8\pi G\sin^2\theta}{a^2}\left(\mathbf{A}'^2 - \lambda\mathbf{A}^4 L_\lambda\right)\right]h_\lambda = 0, \tag{6.67}$$

where θ is the angle between the direction of propagation and the vector field i.e. $\cos\theta = \hat{\mathbf{k}}\cdot\hat{\mathbf{A}}$ and

$$L_\lambda = \begin{cases} 1+\sin^2\theta, & \lambda = + \\ 1, & \lambda = \times \end{cases} \tag{6.68}$$

is a term that depends on the linear polarisation mode. Here we see that the generation of a net GW linear polarisation is related to the anisotropy of the background vector field, since both equations differ as long as $\theta \neq 0$ even in the fast-oscillation regime of the field, which yields an isotropic stress-energy tensor at background level. Having different equations for both linear polarisations also implies a correlation between circular polarisations due to propagation, since their equations are no longer separable, but no net circular polarisation is generated. Thus for the primordial stochastic background, we expect an anisotropic modification of intensity and linear polarisation power spectra.

If we write the equations in terms of the analytic solution for the field obtained in Section 6.3.1, we get the following expressions

$$h_+'' + 2\mathcal{H}h_+' + \left[k^2 + \frac{6H_0^2\Omega_A\sin^2\theta}{a^2}\left((3+2\sin^2\theta)\,\mathrm{cn}^4(\omega\eta;1/2)-1\right)\right]h_+ = 0, \tag{6.69a}$$

$$h_\times'' + 2\mathcal{H}h_\times' + \left[k^2 + \frac{6H_0^2\Omega_A\sin^2\theta}{a^2}\left(3\,\mathrm{cn}^4(\omega\eta;1/2)-1\right)\right]h_\times = 0. \tag{6.69b}$$

The amplitude of the new terms is proportional to the dark radiation abundance Ω_A, as happened with a ULVF model. In particular, one can expect a non-negligible effect so long as $6H_0^2\Omega_A/a^2 \gg \{a''/a,\, k^2\}$ is satisfied at some point of the propagation. As a matter of fact, since in the radiation-dominated epoch $a''/a \propto 1/a$, the new term can grow quickly as we go back in time and eventually become dominating in the early universe as can be seen in Fig. 6.10.

It is also worth noting that the vector field contribution is slightly larger in the plus equation and contains an additional $\sin^4\theta$ anisotropic modulation compared to the cross equation, so any effect resulting from the vector field will be enhanced for this polarisation. If the new term is subdominant, the mode will behave the standard way as described in Section 4.2.

Regarding the GW phase velocity modification (4.1), in this case, it is different for each polarisation and is given by

$$\delta c_\lambda = \frac{4\pi G\sin^2\theta}{k^2}\left|\mathbf{A}'^2 - \lambda\mathbf{A}^4 L_\lambda\right|. \tag{6.70}$$

Taking into account the constraints of this model, the deviation is $\delta c \leq \mathcal{O}(10^{-44})$ in the LIGO frequency operating range, even smaller than with the ULVF, the difference being that the upper bound on Ω_A is now smaller. The difference in velocity between polarisations produces a Shapiro delay as well as residuals for pulsars [Sha64], although the effects are too small to be measured with current or near-future detectors.

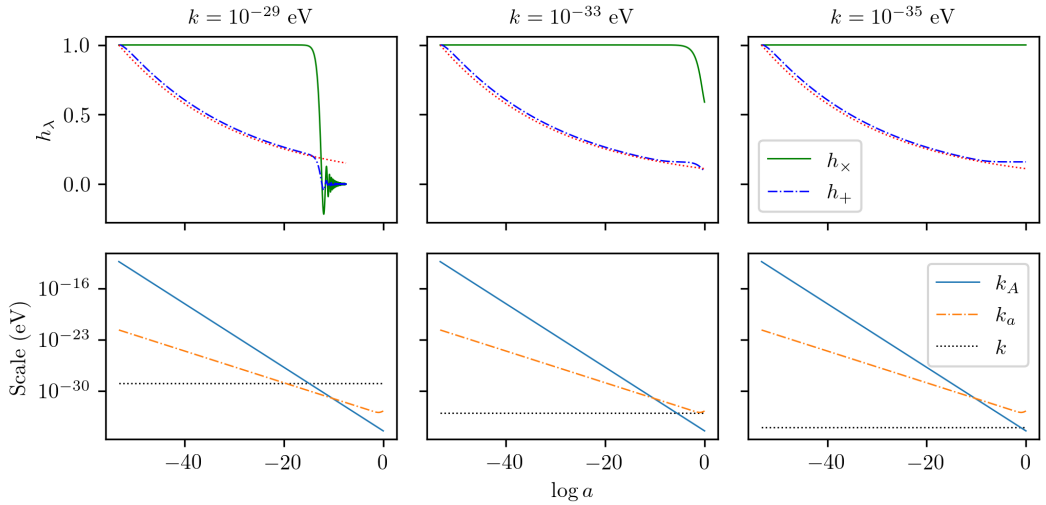

Figure 6.10: GW evolution for $\Omega_A = \Omega_R/100$, $\omega = 2500$ Hz, $\theta = \pi/2$ and three different wavenumbers, one in each column. The fast-oscillation regime applies throughout the entire evolution, so the results are valid for any frequency ω that satisfies so. The top row shows the evolution of the plus (dash-dotted) and cross (solid) modes, the latter being just the standard evolution in ΛCDM, as well as the analytical solution for plus modes in a radiation-dominated epoch (dotted), given by Eq. (6.73). The modes are normalised by their primordial values. The bottom row shows the scales of the different terms in the propagation equation corresponding to the evolution above them, with $k_a = \sqrt{|a''/a|}$ the damping term scale and $k_A = \sqrt{6\Omega_A} H_0 |\sin\theta|/a$ the vector field term scale.

On the other hand, depending on the vector field oscillation frequency ω, we can consider two regimes. In the slow-oscillation regime $\omega \ll \mathcal{H}$ both polarisations are affected, with the oscillating term being larger for the plus polarisation. An analytical solution of the differential equation is not possible in this case.

If instead, the oscillation of the field is fast enough ($\omega \gg \mathcal{H}$), the elliptic function can be averaged leading to the following effective equations:

$$h_\lambda'' + 2\mathcal{H}h_\lambda' + \left[k^2 + \frac{4H_0^2\Omega_A \sin^4\theta}{a^2}\delta_{\lambda,+}\right] h_\lambda = 0, \tag{6.71}$$

where $\delta_{\lambda,+}$ is the Kronecker delta. So in the fast-oscillation regime, the behaviour of the cross polarisation reduces to the standard propagation equation in ΛCDM, whereas the plus polarisation is still affected. It is also worth noting that these equations are independent of ω, so changing the frequency of the field has no effect as long as the fast oscillation condition is satisfied. This much simpler equation allows for an analytic solution when the vector field term dominates. Thus, in a radiation-dominated era, in

which $a(\eta) = a_R \eta$, with $a_R \simeq H_0 \sqrt{\Omega_R}$, the mode evolution reduces to

$$h_+'' + \frac{2}{\eta} h_+' + \frac{4H_0^2 \Omega_A \sin^4\theta}{a_R^2 \eta^2} h_+ = 0, \tag{6.72}$$

which has the following solution

$$h_+(\eta) = C_1 \eta^{-\frac{1}{2}(1-\sqrt{1-4\xi})} + C_2 \eta^{-\frac{1}{2}(1+\sqrt{1-4\xi})}, \tag{6.73}$$

where C_1, C_2 are integration constants and

$$\xi = \frac{4H_0^2 \Omega_A \sin^4\theta}{a_R^2} \simeq 4 \sin^4\theta \frac{\Omega_A}{\Omega_R} \ll 1. \tag{6.74}$$

Thus, for fast-oscillating vector fields in the radiation-dominated era, super-Hubble GW plus modes undergo a slight damping with $h_+ \propto a^{-\xi}$ in contrast with the constant behaviour of such modes in ΛCDM. Oscillation would be possible as long as $\xi > 1/4$, but the upper bound on Ω_A implies that $\xi < 0.16$, which forbids it. A similar analysis can be done for a matter-dominated epoch, in which the plus polarisation features a constant mode that dominates the long-time behaviour.

Fig. 6.10 shows the numerical evolution of three different modes alongside the radiation-dominated solution in the fast-oscillation regime. We can see the qualitative behaviour of the GW modes when each of the three terms in the propagation equation dominates:

1. If the term a''/a dominates, the mode is a purely super-Hubble mode so that it remains at a constant value.

2. If the wavenumber term k dominates, the mode is a purely sub-Hubble mode, which oscillates with its amplitude damped as $1/a$.

3. If the vector field term dominates *and* the fast-oscillation regime applies, the cross mode remains unaffected so it evolves according to whichever of the other two terms is dominating. The plus mode decays as $a^{-\xi}, \xi > 0$ according to Eq. (6.73). A net GW polarisation is thus generated during this stage.

The change in the total power spectrum and the generated non-zero linear polarisation power spectrum can be described by means of the Stokes parameters $\mathcal{I}$ and $\mathcal{Q}$, as defined in Eq. (4.24). $\mathcal{U} = \mathcal{V} = 0$ since the linear polarisations do not mix in the chosen basis ($R_{+\times} = R_{\times+} = 0$).

In our model, the power spectra are anisotropic, exhibiting a dependence on the polar angle θ, so we shall perform a multipole decomposition of both non-zero reduced Stokes parameters as

$$\mathcal{S}(k, \theta, \eta) = \sum_\ell \sqrt{\frac{2\ell+1}{2}} \mathcal{S}_\ell(k, \eta) P_\ell(\cos\theta), \tag{6.75}$$

where P_ℓ are the Legendre polynomials (see Appendix B.3) and the normalisation is chosen so that $||\mathcal{S}||^2 = \sum_\ell \mathcal{S}_\ell^2$, where the norm takes the standard form

$$||\mathcal{S}||^2 = \int_{-1}^{1} \mathrm{d}\cos\theta\, \mathcal{S}^2(\theta). \tag{6.76}$$

Both $\mathcal{I}_\ell$ and $\mathcal{Q}_\ell$ vanish for odd ℓ since the GW propagation equation is invariant under the transformation $\theta \to \theta' = \pi - \theta$. On top of that, the modulation of the new term in the GW propagation equation is proportional to $\sin^2\theta$ and $\sin^4\theta$, so since the power spectra contain the square of the GW amplitudes, we expect a significant contribution coming from multipoles up to $\ell = 8$.

Finally, let us define the *degree of polarisation* $\mathcal{D}$, which measures how polarised the GW background is. For that purpose, we shall take into account that the Stokes parameters satisfy $I^2 \geq Q^2 + U^2 + V^2$, with the equality holding when there is total polarisation. Thus, an appropriate way to define the degree of polarisation is

$$\mathcal{D}^2 = \frac{\mathcal{Q}^2 + \mathcal{U}^2 + \mathcal{V}^2}{||\mathcal{I}||^2}, \tag{6.77}$$

which can be decomposed into multipoles as well. In this case, it is given simply by

$$\mathcal{D}_\ell = \frac{\mathcal{Q}_\ell}{\sqrt{\sum_l \mathcal{I}_\ell^2}}, \tag{6.78}$$

which gives a measure of how much linear polarisation there is in each multipole. If the GW background is completely polarised, i.e. only one of the two polarisations occurs, then $\sum_\ell \mathcal{D}_\ell^2 = 1$, and if that configuration happens to be allocated in a particular multipole $\ell = n$ alone, then $\mathcal{D}_n = 1$, with all the other components vanishing.

Fig. 6.11 shows a particular example of this multipole decomposition for the different Stokes parameters evaluated today. We see the suppression of power in the monopole $\mathcal{I}_0$ at large scales with respect to ΛCDM, similarly to that found for vector dark matter, and the generation of a quadrupole and hexadecapole contributions which are absent in ΛCDM, whereas higher multipoles are negligible. On the other hand, we also see a large degree of polarisation with a monopole distribution and also non-negligible polarisation with quadrupolar and hexadecapolar distribution patterns. We can clearly see that a larger amount of net polarisation happens for modes with smaller wavenumbers k, along with a diminution of the total power spectrum, both originated by the decay of the plus modes. Such an effect is due to the fact that modes with larger wavenumbers enter the Hubble horizon earlier in their evolution, so that they undergo the decay caused by the vector field for a shorter time. An extreme yet clear indicator of this is that modes with $k \gtrsim 10^{-11}$ eV have always been inside the Hubble horizon (for the chosen reheating scale $T_{\rm RH} = 10^{10}$ GeV), and as a result no difference from standard cosmology is observed for them, so that $R_+ = R_\times = 1$ (equivalently, $\mathcal{I} = 1, \mathcal{Q} = 0$). On the other side, we have those modes with wavelengths larger than

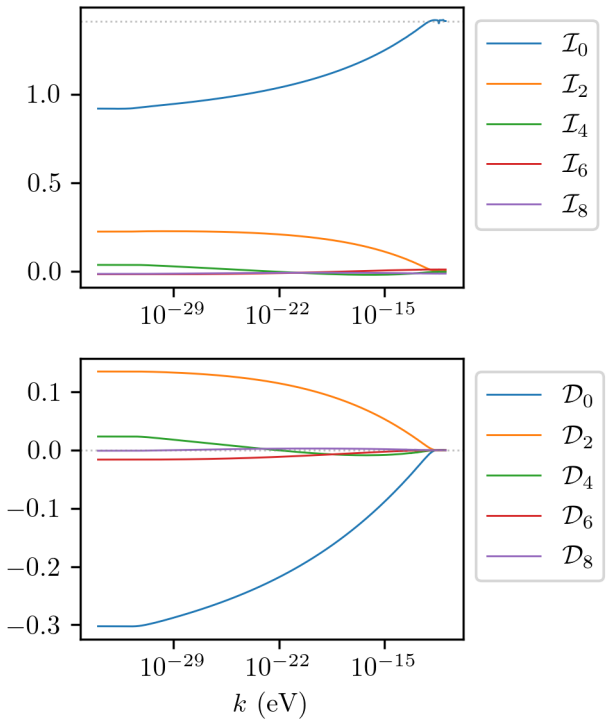

Figure 6.11: Multipole expansion up to $\ell = 8$ of intensity and degree of polarisation today, for $\Omega_A = \Omega_R/100$ and $\omega = 2500$ Hz. The grey dotted line in the $\mathcal{I}_\ell$ plot is the value $\mathcal{I}_0 = \sqrt{2}$, which corresponds to the case of no polarisation and no deviation from standard cosmology $R_+ = R_\times = 1$.

today's Hubble radius $k < H_0 \simeq 10^{-33}$ eV so they have always been super-Hubble and have evolved in the same way irrespective of k, giving rise to the flat plateau observed in the low-k region of the figure.

If the frequency of the vector field is not large enough to be always in the fast oscillation regime, the GW modes are affected by the slow oscillation of the vector field. Since $\omega\eta \ll 1$, the elliptic cosine in Eq. (6.69) is approximately constant with value $\mathrm{cn} \simeq 1$. As a result, and as long as the modes are super-Hubble, they undergo a damping which is similar to that of the plus mode in the fast-oscillation regime, but steeper, as the vector field term is now slightly larger (even larger for the plus polarisation). When the vector field enters the fast-oscillation regime, the cross polarisation mode freezes and follows a standard propagation, whereas the plus mode keeps damping, with a less steep slope, until it enters the Hubble horizon. This can be seen in Fig. 6.12, which shows that the monopole $\mathcal{I}_0$ is more suppressed for smaller frequencies, as both polarisations are damped for longer. All curves have the same behaviour for wavenumbers $k \gg \omega$, i.e. for modes that enter the Hubble radius during the slow-oscillation phase of the vector field. This particular example aims just to illustrate the

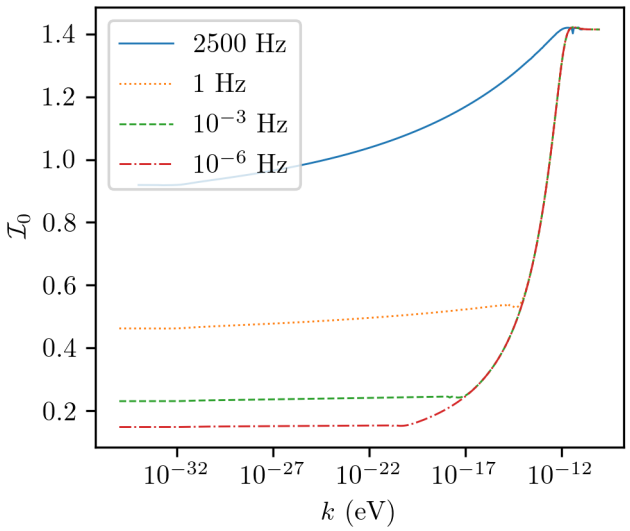

Figure 6.12: Monopole of the total power spectrum today $\mathcal{I}_0$ as a function of wavenumber, for $\Omega_A = \Omega_R/100$ and four different frequencies ω of the field. Smaller frequencies yield a larger suppression of the power spectrum, as a result of the field oscillating slowly for longer.

effect of a slow oscillation, since the anisotropy magnitude, about $\Omega_A/\Omega_R = 1/100$, is higher than the typical cosmological perturbations, and thus an accurate study would require a description in terms of a Bianchi I spacetime background.

Circularly polarised vector field

We repeat now the same analysis with the circularly polarised vector field. We now label the GW propagation direction as "3" instead of "z" so as to avoid confusion with the (x,y,z) system of coordinates defined by the vector field. Thus, the GW propagates along the 3-axis and, thanks to axial symmetry, we choose the normal to the vector field rotation plane $\hat{\mathbf{n}}$ to be in the 23-plane. In addition, we choose the vector field to be initially oriented towards the 1-direction, so that A_x as defined in Eq. (6.59) coincides with A_1 in this coordinate system. This layout is shown in Fig. 6.13. The GW propagation equations are now given by

$$h_+'' + 2\mathcal{H}h_+' + k^2 h_+ + \frac{2\Omega_A H_0^2}{a^2}[(F+B)h_+ + Mh_\times] = 0, \tag{6.79a}$$

$$h_\times'' + 2\mathcal{H}h_\times' + k^2 h_\times + \frac{2\Omega_A H_0^2}{a^2}[(F-B)h_\times + Mh_+] = 0, \tag{6.79b}$$

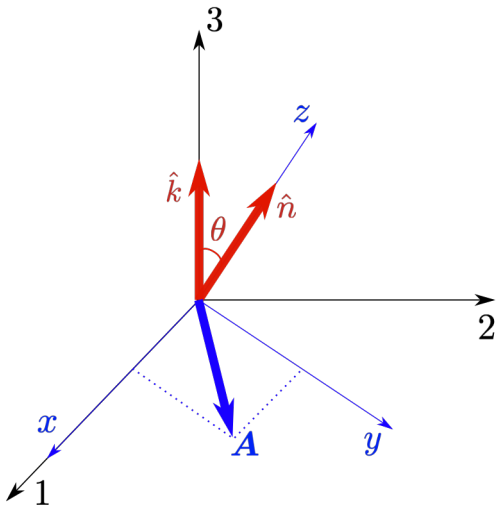

Figure 6.13: Coordinate systems arrangements for the circularly polarised vector field. The GW coordinate system is labelled (1,2,3) so that the GW travels along the 3-direction, defined by the wavenumber $\hat{\mathbf{k}}$. The vector field coordinate system is labelled (x,y,z), with the field rotating in the xy-plane, defined by its normal $\hat{\mathbf{n}}$, which forms an angle θ with the propagation direction. The GW plane is chosen so that directions 1 and x match.

where

$$F = \frac{\lambda(A_1^2+A_2^2)(A_1^2+A_2^2+2\alpha^2)-2(A_1'^2+A_2'^2)}{\lambda\alpha^4}$$
$$= \cos^4\omega\eta+\cos^4\theta\sin^4\omega\eta+2\sin^2\theta\cos 2\omega\eta+\frac{1}{2}\cos^2\theta\sin^2 2\omega\eta, \tag{6.80a}$$
$$B = \frac{\mathrm{Re}[(A_1+iA_2)^4]}{\alpha^4} = \cos^4\omega\eta+\cos^4\theta\sin^4\omega\eta-\frac{3}{2}\cos^2\theta\sin^2 2\omega\eta, \tag{6.80b}$$
$$M = \frac{\mathrm{Im}[(A_1+iA_2)^4]}{\alpha^4} = 2\cos\theta\sin 2\omega\eta(\cos^2\omega\eta-\cos^2\theta\sin^2\omega\eta), \tag{6.80c}$$

and $\cos\theta = \hat{\mathbf{k}}\cdot\hat{\mathbf{n}}$. These equations exhibit some similarities with the linearly polarised case: The new terms are proportional to the abundance Ω_A and dominate in the early universe for modes with sufficiently small k due to the a^{-2} scaling, in which case they are expected to affect GWs in the early stages of their evolution. The equations are also different for each polarisation, which produces a net polarisation of the GW background. On top of that they are coupled, with each mode acting as a source of the other, which enhances the polarisation generation, but this mixing is purely real, so

parity is still preserved.

When $\omega\eta \gg 1$, a fast-oscillation regime applies, in which the oscillations of the vector field can be averaged for the integration of the GW propagation, resulting in

$$\langle F\rangle = \frac{3}{8}\left(1+\cos^4\theta\right) + \frac{1}{4}\cos^2\theta, \tag{6.81a}$$

$$\langle B\rangle = \frac{3}{8}\left(1+\cos^4\theta\right) - \frac{3}{4}\cos^2\theta, \tag{6.81b}$$

$$\langle M\rangle = 0. \tag{6.81c}$$

In this regime, the polarisations do not mix anymore, so if there is any mixing between both polarisations it needs to happen when the vector field is revolving slowly. As with the linearly polarised vector field, it is also possible to obtain the analytical solution for super-Hubble modes in the radiation-dominated era, which is given by (6.73) for both polarisations with

$$\xi_{\substack{+\\ \times}} = \frac{2H_0^2\Omega_A\langle F\pm B\rangle}{a_R^2} \simeq 2\langle F\pm B\rangle\frac{\Omega_A}{\Omega_R}. \tag{6.82}$$

Since the long-time behaviour of the modes is $h_\lambda \propto a^{-\xi_\lambda}$, and $\xi_+ > \xi_\times$, super-Hubble plus-polarised modes are more suppressed than cross-polarised ones, especially around $\theta = \pi/2$ where the difference is maximum.

Let us look at the Stokes parameters now. Circular polarisation of GWs still does not occur, therefore $\mathcal{V} = 0$, but as opposed to the previous section, now both linear polarisations do mix, which implies $\mathcal{U} \neq 0$. Fig. 6.14 shows all three non-zero Stokes parameters as a function of wavenumber for the same abundance and frequency as in Fig. 6.11. Once again, $\mathcal{I}$ and $\mathcal{Q}$ receive contributions from even multipoles only. This is because the equations of propagation are different in a term proportional to B, which is even in $0 \leq \theta \leq \pi$. However, the anisotropy created by the mixing of both polarisations, which is governed by M, is odd in this same interval, so $\mathcal{U}$ receives a contribution from odd multipoles only.

Despite this new source of anisotropy, the generation of net linear polarisation is still dominated by the difference in the term that involves $F \pm B$ in Eq. (6.79), rather than the source term, since $\mathcal{Q} \gg \mathcal{U}$. The sourcing is only possible when the vector dark radiation is not oscillating rapidly, which cannot happen for a long period without breaking background isotropy. Similarly to the previous case, modes with larger wavelengths are more suppressed and exhibit a larger degree of linear polarisation. Comparatively, the total power spectrum suffers a greater diminution, since the circularly polarised vector field causes both GW polarisations to decay, instead of just one of them. As a result, the difference in propagation between polarisations is smaller, which causes the net polarisation to be smaller as well.

The only region in k where $\mathcal{U}$, and therefore the mixing, become important corresponds to modes that initially (at the end of reheating in this case) were sub-Hubble, i.e. $k \gtrsim \mathcal{H}_{\rm RH}$. In that case, the polarisations do not undergo a different super-Hubble

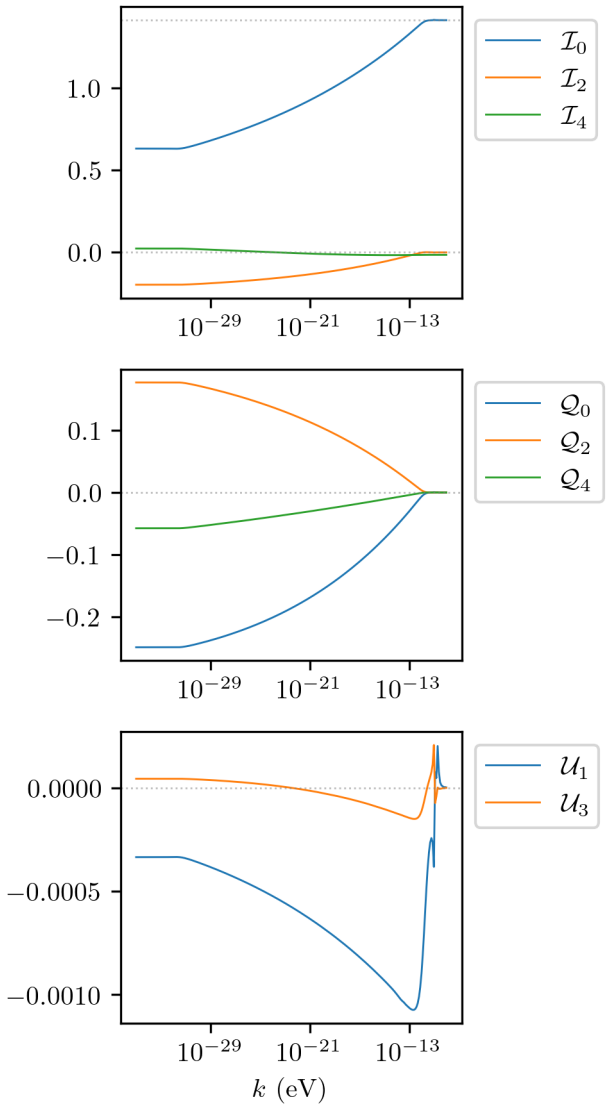

Figure 6.14: Multipole expansion of the reduced Stokes parameters today for the circularly polarised vector field, with $\Omega_A = \Omega_R/100$ and $\omega = 2500$ Hz. $\mathcal{I}$ and $\mathcal{Q}$ have even multipoles, whereas $\mathcal{U}$ has odd ones. The linear polarisation is dominated by $\mathcal{Q} \gg \mathcal{U}$ except in the high-k region, where the total spectrum remains unchanged $\mathcal{I}_0 = \sqrt{2}$ but polarisation still appears (see Fig. 6.15).

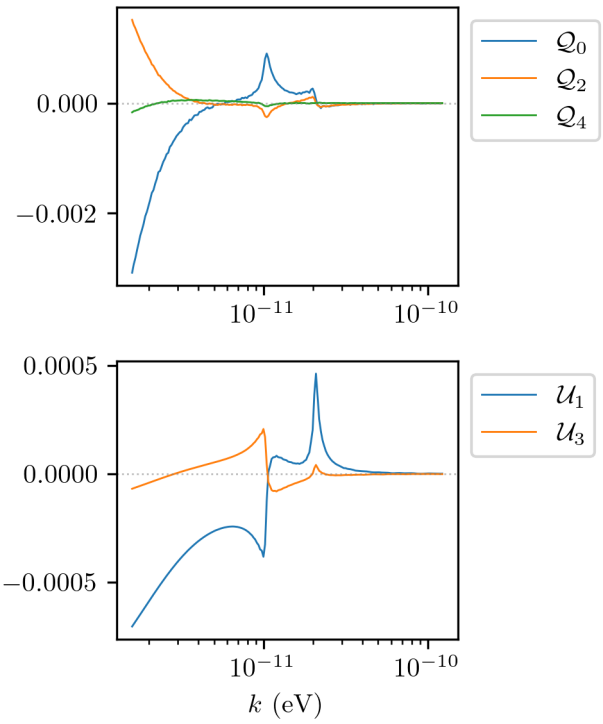

Figure 6.15: Stokes parameters $\mathcal{Q}$ and $\mathcal{U}$ today in the high-wavenumber region, smaller than the size of Hubble horizon at reheating, with $\mathcal{H}_{\rm RH} \simeq 10^{-12}$ Hz. In this region, both Stokes parameters accountable for linear polarisation are about the same size. The fundamental and first overtone of $k = \omega \simeq 10^{-11}$ eV are seen as resonances. For larger k, both parameters go to zero, as net linear polarisation is no longer generated.

damping phase, so $\mathcal{Q}$ is suppressed, and at the same time, k is not large enough to completely dominate the evolution, which would make both polarisations evolve the same way.

Fig. 6.15 shows a zoom of this high-wavenumber region. Besides the already mentioned suppression of $\mathcal{Q}$ at the scale of the Hubble horizon, two resonances at $k = \omega \simeq 10^{-11}$ eV and its first overtone are also apparent. For bigger wavenumbers, the k term completely dominates the propagation and no sign of polarisation is observed. Note that this discussion is valid for GWs of cosmological origin. Even though high-frequency GWs coming from astrophysical events (such as compact binaries or pulsars) lie around this region in wavelength, this effect and resonances would not be present, as they originate when the mode is well inside the Hubble horizon.

For the sake of completeness, we plot in Fig. 6.16 the monopole of the total power spectrum for different frequencies of the vector field, which exhibit the same behaviour as the ones discussed in Fig. 6.12.

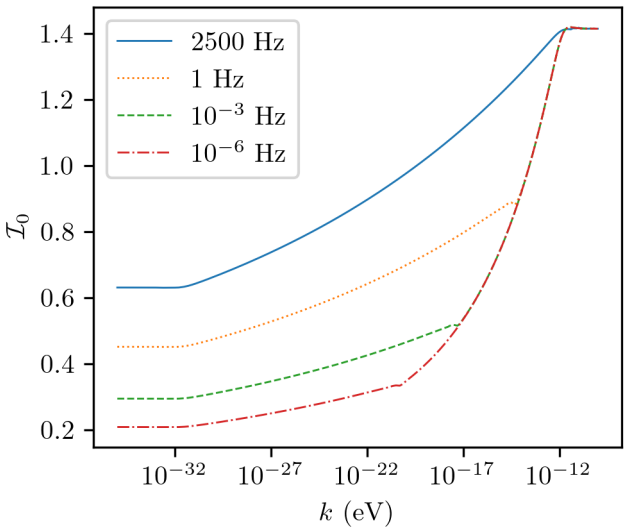

Figure 6.16: Monopole of the total power spectrum $\mathcal{I}_0$ today as a function of wavenumber, for $\Omega_A = \Omega_R/100$ and four different frequencies ω of the circularly polarised field. The behaviour is similar to that of the linearly polarised vector field, with smaller vector field frequencies causing a larger suppression.

6.3.3 Polarised primordial background

Up to this point, we have studied the effect of the dark radiation vector field on the propagation of GWs originating from an unpolarised stochastic background. Although that is the standard assumption, there is also the possibility of having a primordial background with some degree of polarisation. In order to explore this scenario, let us consider the extreme example of a background which is initially totally linearly polarised with $h_\times = 0$. This in particular implies according to (4.4) that $h_L = h_R$, i.e., for every right-handed tensor mode, there is a left-handed one with the same direction, amplitude and phase [GM17].

In terms of analysing the propagation of the modes, the only difference is that there is no × polarisation at origin nor a significant amount of + modes sourced by × modes, which makes $R_{+\times} = R_\times = 0$. For the linearly polarised vector field, since tensor polarisations do not mix, it just means that the total power spectrum is reduced by half and becomes completely polarised, as only one of the two polarisations contributes.

For the circularly polarised vector field, GW polarisations are mixed, therefore the analysis is slightly different. The total power spectrum and the net linear polarisation are still dominated by the fact that cross polarisation is missing at origin. In terms of the reduced Stokes parameters (4.24) $\mathcal{I} \simeq \mathcal{Q}$, since $|R_+| \gg |R_{\times+}|$ as the sourced mode is considerably smaller than the source. In this case, $\mathcal{I}$ is roughly halved compared to its value with the unpolarised primordial background.

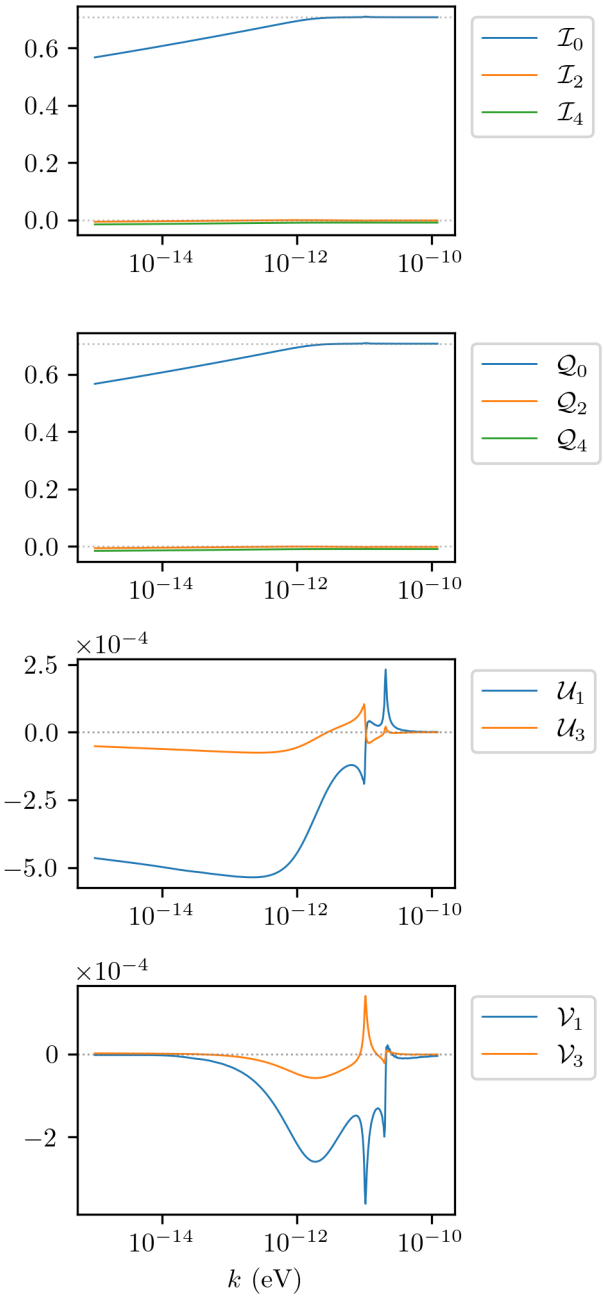

Figure 6.17: Multipole expansion of the reduced Stokes parameters today when the primordial background is initially totally linearly polarised. Such a scenario allows for non-zero net circular polarisation $\mathcal{V}$ generation in the high-wavenumber region, which also presents resonances at $k = \omega \simeq 10^{-11}$ eV and its first overtone due to the polarisation mixing.

The novelty is that this situation also opens up the possibility of creating net circular polarisation. This requires the product $R_+ R^*_{\times +}$ to have a non-vanishing imaginary part, i.e., that h_+ and $h_\times$ do not share the same phase. That happens just for modes which initially have $k \simeq \mathcal{H}$, which we have already discussed in the previous section. In this regime, the $h_\times$ mode, which is absent initially, needs to be produced before effectively entering the Hubble horizon, which is what creates this phase delay between both polarisations and ultimately a circularly polarised realisation. We plot in Fig. 6.17 all reduced Stokes parameters for this high-k region. As stated before, $\mathcal{I}$ acquires half the values as in the unpolarised background, and $\mathcal{Q}$ is roughly equal to it. The other linear polarisation $\mathcal{U}$, now much smaller than $\mathcal{Q}$, is also halved, as the contribution sourced by the $h_\times$ mode is not present, while still exhibiting two resonances, the fundamental one being at $k = \omega$. The new addition, the circular polarisation parameter $\mathcal{V}$, is about the same order of magnitude as $\mathcal{U}$, and since it is also generated by polarisation mixing, it also has got the resonances and only odd-multipole contributions. As expected, the net circular polarisation goes to zero as k is so big that it completely dominates the evolution, and also as we go to very small k, where the difference in phase between polarisations disappears.

6.4 GW propagation for a general vector potential

Lastly, let us examine the GW propagation as affected by an abelian vector field in a flat RW background with a general potential, whose action is given by (6.1). As discussed in Sec. 6.1, we need $A_0 = 0$ in order to ensure background isotropy, while the spatial component dynamics are determined by Eq. (6.5).

Now we need to make an assumption about the field to allow for further analysis. A circularly polarised-like solution, i.e. the vector field revolving within a particular plane, cannot be readily studied for an arbitrary potential. The geometry of the motion will be more complicated in general, describing non-periodic or open trajectories that are unknown unless a particular potential is chosen, so we restrict ourselves to a linearly polarised ansatz (6.45). The solution for the only remaining component can be found after specifying the shape of the potential. This solution will describe oscillations around the minimum of the potential and, as we have seen in every studied case, should have a naturally arising frequency that defines slow and fast-oscillation regimes. The isotropy of the associated stress-energy tensor can only be guaranteed in the latter.

For tensor perturbations, we follow the same procedure as in previous sections. The perturbed stress-energy tensor can be written

$$\delta T^i{}_j = -\frac{1}{a^4} h_{ik} A'_j A'_k - \frac{2}{a^4} V'(A^2) h_{ik} A_j A_k \\ - \frac{2}{a^4} V''(A^2) A_i A_j h_{lm} A_l A_m + \text{ terms involving } \delta^i{}_j, \quad (6.83)$$

which, after taking its TT projection, allows us to arrive at the modified propagation

equations for GWs:

$$h_+'' + 2\mathcal{H}h_+' + \left[k^2 - \frac{8\pi G \sin^2\theta}{a^2}\left(\mathbf{A}'^2 + 2a^2V'(A^2)\mathbf{A}^2 + 2V''(A^2)\mathbf{A}^4\sin^2\theta\right)\right]h_+ = 0, \quad (6.84a)$$

$$h_\times'' + 2\mathcal{H}h_\times' + \left[k^2 - \frac{8\pi G \sin^2\theta}{a^2}\left(\mathbf{A}'^2 + 2a^2V'(A^2)\mathbf{A}^2\right)\right]h_\times = 0. \quad (6.84b)$$

In these equations, θ is again the angle between the direction of propagation of the GW mode and the direction of the vector field, and $\mathbf{A}^2 = \delta^{ij}A_iA_j = A_z^2$, so that $\mathbf{A}^2 = -a^2A^2$. The propagation for both polarisations is manifestly different provided that $V''(A^2) \neq 0$, which is true for any potential with the exception of constant or mass-like quadratic potentials and as in the quartic case, this implies the generation of a net linear polarisation. Note that linear polarisations do not mix regardless of the potential, because since the vector field always points in the same direction, it is possible to align its transversal part with one of the two polarisations, and the net linear polarisation occurs in that basis.

For a generic polarisation of the vector field, we also expect for a general potential with $V''(A^2) \neq 0$ a similar phenomenology to that studied for a circularly polarised vector in the quartic case, with generation of Q and U polarisation modes.

7 TDiff-invariant gauge field theory

Einstein's General Relativity is the best description of gravity we have got today. It has performed exceptionally well in multiple tests ranging from the Solar System orbits to gravitational lensing and has been able to describe purely gravitational phenomena such as black holes and gravitational waves. It also serves as a theoretical framework for the standard ΛCDM cosmology. GR relies on invariance under general coordinate transformations, i.e., invariance under diffeomorphisms (Diff) and Einstein's equivalence principle [Wil14], which is equivalent to the weak equivalence principle (WEP), local Lorentz invariance (LLI) and local position invariance (LPI). GR comes with its shortcomings though: Its lack of description of quantum gravity and the unknown fundamental nature of the dark sector of Cosmology have motivated the search for alternatives to GR. Generally, these modifications of GR consist of additional degrees of freedom, implemented in multiple ways, that alter the behaviour of gravity in a certain regime, typically at very long or very short distances.

Over the last decade, there has been a growing interest in theories that break Diff-invariance down to invariance under transverse diffeomorphisms (TDiff), a subgroup restricted to volume-preserving general transformations. Early works include [Alv+06; AFL08], in which a stability analysis of TDiff-invariant theories is performed at classical and one-loop levels. Here it was found that by enhancing the symmetry group with local Weyl invariance (dubbed WTDiff), the additional scalar degree of freedom is removed, thus propagating the same degrees of freedom as GR and preventing possible ghost instabilities. Unimodular gravity (see [CGG22] for a nice review), the most popular TDiff-invariant theory for gravity and which was first explored by Einstein back in 1919 [Ein19], falls into this category and features the metric determinant treated as a non-dynamical scalar, so only the traceless part of Einstein's equations contribute to the dynamics. In Unimodular Gravity, the cosmological constant becomes an integration constant [Unr89], which is an interesting feature that has been extensively explored.

TDiff models beyond unimodular gravity have also been considered in [Pir06; Alv+06]. In these models, the metric determinant is a dynamical field and the corresponding spectrum includes a scalar graviton in addition to the standard massless spin-2 graviton. Also, the cosmological evolution in TDiff-invariant theories propagating a scalar graviton mode was recently investigated in [BM24].

Breaking down to TDiff was also considered in the coupling to matter in the case of scalar fields in [AF07; AFL09] and possible violations of the Einstein Equivalence

Principle were found. However, in [Mar23], it was shown that, in the geometric optics approximation, when breaking down to TDiff invariance by a global factor in the matter action, the three types of masses (inertial, active and passive) agree with those of standard Diff invariant theories thus avoiding the mentioned conflicts. In addition, it was found that in cosmological contexts on super-Hubble scales, these models exhibit a completely different behaviour of the energy-momentum tensor which makes them very useful tools for the description of the dark sector. Thus in particular in [AdCM24] a unified model of the dark sector with a single TDiff scalar field and the same number of free parameters as ΛCDM was presented. TDiff-invariant scalar fields in arbitrary backgrounds have been considered in [JMM24b]. There it was shown that in the kinetic regime, these models behave as perfect adiabatic fluids and the corresponding speed of sound can be explicitly obtained. The covariantised version of the model has been explored in [JMM24a].

Following the novelties in scalar field dynamics found in [Mar23], in this Chapter we focus on extending the formalism to TDiff-invariant spin-1 Abelian fields in a cosmological context. In particular, breaking Diff invariance in the electromagnetic sector also breaks conformal invariance, which is one of the viable ways of generating sizeable primaeval intergalactic magnetic fields during the inflation stage of the Universe, as we discussed back in Sec. 1.5. The Chapter is organised as follows: In Sec. 7.1 we lay the basics of a TDiff-invariant Abelian gauge field and showcase the differences with respect to standard electromagnetism. We show that in the geometric optics approximation, dynamics are equivalent to Diff-invariant electromagnetism, analyse the particular case of coupling to a TDiff-invariant Dirac field and perform the covariant quantisation of the vector field. In Sec. 7.3, we analyse the dynamics in the context of an expanding universe and study the sub-Hubble and super-Hubble regimes for electric and magnetic fields. Finally, in Sec. 7.4, we examine the viability of inflation-generated TDiff-invariant magnetic fields as a candidate for primordial magnetic fields.

7.1 TDiff-invariant gauge field theory

Let us consider the most general action for an Abelian vector field $A_\mu(x)$ which is gauge invariant and invariant under transverse diffeomorphisms, to lowest order in field and metric derivatives and without parity violating terms, [BSZ11]

$$S_A = -\frac{1}{4}\int \mathrm{d}^4x\, f(g) F_{\mu\nu}F^{\mu\nu}, \tag{7.1}$$

with $f(g)$ an arbitrary function of the metric determinant $g = |\det g_{\mu\nu}|$. The condition $f(g) > 0$ ensures the action is free from ghosts or gradient instabilities [BSZ11; Rub14].

This action is invariant under the group of transverse diffeomorphisms, which is a subgroup of full diffeomorphisms. In terms of infinitesimal coordinate transformations,

TDiff transformations are implemented by

$$x^\mu \to \tilde{x}^\mu = x^\mu + \xi^\mu, \quad \partial_\mu \xi^\mu = 0, \tag{7.2}$$

so there is one less gauge degree of freedom. Restricting the symmetry group in this way allows us to write the action for any type of field (to lowest order in metric derivatives) with a general $f(g)$. Indeed, the variation of a general action

$$S = \int \mathrm{d}^4x\, f(g)\mathcal{L} \tag{7.3}$$

with $\mathcal{L}$ scalar function of the fields and their derivatives and the metric under diffeomorphisms can be shown to be [Mar23]

$$\delta S = \int \mathrm{d}^4x\, \partial_\mu \xi^\mu [f(g) - 2g f'(g)]\mathcal{L}, \tag{7.4}$$

where the prime in $f'(g)$ denotes derivative with respect to its argument. This variation vanishes by either setting $f(g) = \sqrt{g}$, which grants invariance under the full group of diffeomorphisms, or by restricting ourselves to TDiff transformations $\partial_\mu \xi^\mu = 0$. The Diff-invariant case can always be recovered by taking the limit $f(g) \to \sqrt{g}$. Notice that under TDiff transformations, scalar densities (such as g) behave as pure scalars.

Note that we break Diff invariance down to TDiff invariance only in this sector, while preserving full Diff-invariant actions in every other sector, in particular, in the Einstein-Hilbert action, so that the total action for the TDiff vector field coupled to gravity would be

$$S = S_{EH} + S_A = -\frac{1}{16\pi G}\int d^4x\sqrt{g}R - \frac{1}{4}\int \mathrm{d}^4x\, f(g) F_{\mu\nu}F^{\mu\nu}, \tag{7.5}$$

7.1.1 Dynamics

Let us examine the dynamics of the TDiff-invariant vector field. We can obtain the equations of motion for the vector field by varying the action (7.5) with respect to it

$$\partial_\mu [f(g)F^{\mu\nu}] = 0. \tag{7.6}$$

Variations of the total action (7.5) with respect to the metric tensor yields the corresponding Einstein equation

$$R^{\mu\nu} - \frac{1}{2}g^{\mu\nu}R = 8\pi G T^{\mu\nu} \tag{7.7}$$

where the stress-energy tensor, appearing on the right-hand side of the equation is obtained from the usual definition (2.12). For the action (7.1), it is given by

$$T^\alpha{}_\beta = \frac{f(g)}{\sqrt{g}}\left(\frac{1}{2}f_1 F_{\mu\nu}F^{\mu\nu}\delta^\alpha{}_\beta - F^{\alpha\mu}F_{\beta\mu}\right), \tag{7.8}$$

where we define

$$f_n = \left(\frac{\mathrm{d}}{\mathrm{d}\log g}\right)^n \log f(g), \tag{7.9}$$

with log the natural logarithm, and in particular, up to second-order derivatives,

$$f_1 = g\frac{f'}{f}, \tag{7.10}$$

$$f_2 = f_1 - f_1^2 + g^2\frac{f''}{f}, \tag{7.11}$$

so that in the Diff case $f(g) = \sqrt{g}$ we have $f_1 = 1/2$ and $f_n = 0$ for $n > 1$. Because of the breaking of Diff invariance, the stress-energy tensor defined in (7.8) is not necessarily conserved under solutions of the field equations of motion, i.e. $\nabla_\mu T^{\mu\nu} \neq 0$ and does not reduce to the canonical one in flat spacetime (see [AF07; AFL09] for a discussion). However, since Diff invariance is not broken in the gravity sector, Bianchi identities $\nabla_\mu G^{\mu\nu} = 0$ ensure $\nabla_\mu T^{\mu\nu} = 0$, i.e. the energy-momentum is conserved on the solutions of Einstein's equations. Speaking in practical terms, the conservation of the stress-energy tensor will impose constraints between the different functions in the metric tensor, which cannot be fixed *a priori* with a coordinate transformation due to having one less gauge degree of freedom in TDiff models.

7.1.2 Geometric optics approximation

The breaking of diffeomorphism invariance could have important implications for the consistency of the theory [AFL09; Mar23]. The presence of the spacetime-dependent function $f(g)$ could violate the Equivalence Principle since it is not guaranteed that vector field particles follow geodesics of the space-time geometry. In order to analyse this problem, and following the same approach as done in [AFL09; Mar23] for scalar fields, we will consider the geometric optics approximation [MTW73; Mar23]. Geometric optics works as long as the typical variation length of the field, i.e. the wavelength λ, is much shorter than any other relevant length L, such as the length at which the amplitude of the field varies or the typical variation length of the space-time. The geometric optics approximation is commonly used for the electromagnetic sector, for which the following three principles are realised:

1. Light rays are null geodesics.
2. The polarisation vector is parallel-propagated along the rays and is perpendicular to the rays.
3. The amplitude is governed by an adiabatic invariant, which can be understood as the conservation of the photon number.

In what follows, we explore if our model obeys the same principles. In this approximation, a mode of the vector potential can be written as a product of an exponential,

which is rapidly changing, and a slowly evolving complex amplitude that is expanded perturbatively in powers of λ/L

$$A_\mu(x) = \mathrm{Re}\left[(V_\mu + W_\mu\epsilon + \ldots)e^{i\theta(x)/\epsilon}\right], \tag{7.12}$$

where $\theta(x)$ is a real function, ϵ is a dummy power-counting parameter and the wavevector is $k_\mu = \partial_\mu\theta$. Note that the amplitude functions V_μ, W_μ... are allowed to depend both on position and on k_μ. Terms of order $\mathcal{O}(1/\epsilon^n)$, $n > 0$ are valid in the geometric optics approximation, whereas terms of order $\mathcal{O}(1)$, $\mathcal{O}(\epsilon)$, etc. are said to belong to post-geometric optics, where the conditions stated above do no longer hold. As a result, only the functions V_μ and θ have no post-geometric optics corrections.

With all of this established, let us delve into the equations of motion. Firstly, the action (7.1) is invariant under a gauge transformation of the field

$$A_\mu(x) \to A'_\mu(x) = A_\mu(x) + \partial_\mu\phi(x), \tag{7.13}$$

with $\phi(x)$ a smooth function, as it leaves the field strength tensor unchanged. This allows us to use the Lorentz gauge condition, which can be written as

$$\nabla_\mu A^\mu = \left[\frac{i}{\epsilon}k_\mu(V^\mu + W^\mu\epsilon + \ldots) + (V^\mu + W^\mu\epsilon + \ldots)_{;\mu}\right]e^{i\theta/\epsilon} = 0. \tag{7.14}$$

At leading order $\mathcal{O}(1/\epsilon)$, this yields

$$k_\mu V^\mu = 0, \tag{7.15}$$

which means that the amplitude of the field (or the polarisation vector) is perpendicular to the direction of propagation. The next order

$$V^\mu{}_{;\mu} + ik_\mu W^\mu = 0, \tag{7.16}$$

already belongs to the post-geometric regime $\mathcal{O}(1)$, and in fact shows a deviation from this perpendicularity for the second term in the expansion of the amplitude.

The equation of motion for the vector field (7.6) at leading order $\mathcal{O}(1/\epsilon^2)$ yields

$$k_\mu V^\mu k^\nu - k_\mu k^\mu V^\nu = 0, \tag{7.17}$$

which after applying the gauge condition (7.15) gives us the null condition of the rays

$$k_\mu k^\mu = 0. \tag{7.18}$$

From this equation, we can write

$$(k_\mu k^\mu)_{;\alpha} = 0, \tag{7.19}$$

and since k_μ is the gradient of a scalar, we can commute covariant derivatives $k_{\mu;\nu} = k_{\nu;\mu}$ to find

$$k^\mu k_{\mu;\alpha} = k^\mu k_{\alpha;\mu} = 0, \tag{7.20}$$

which is nothing but the geodesic equation. Thus, we confirm that very much as in standard Diff-invariant electromagnetism, in TDiff theories, massless gauge bosons propagate along geodesics of space-time in the geometric optics approximation.

The next-to-leading order equation of motion gives us the following expression

$$\partial_\mu\left(\frac{f}{\sqrt{g}}\right)(k^\mu V^\nu - k^\nu V^\mu) + \frac{f}{\sqrt{g}}\left[(k^\mu V^\nu)_{;\mu} - (k^\nu V^\mu)_{;\mu} + k_\mu V^{\nu;\mu} - k_\mu V^{\mu;\nu} + ik_\mu(k^\mu W^\nu - k^\nu W^\mu)\right] = 0. \quad (7.21)$$

After using the gauge condition (7.15) and the previous order equation (7.18), this expression can be simplified to

$$\frac{\sqrt{g}}{f}\partial_\mu\left(\frac{f}{\sqrt{g}}\right)(k^\mu V^\nu - k^\nu V^\mu) + V^\nu k^\mu{}_{;\mu} + 2k^\mu V^\nu{}_{;\mu} = 0, \quad (7.22)$$

where we have also used the commutation of covariant derivatives $k_{\mu;\nu} = k_{\nu;\mu}$.

By decomposing the amplitude into a (real) magnitude V and a (complex) polarisation vector v^μ, i.e. $V^\mu = Vv^\mu$ with $v^\mu v^*_\mu = -1$ and $V^\mu V^*_\mu = -V^2$, this expression allows us to obtain the equation for the propagation of the magnitude and polarisation. Thus, if we contract this equation with V^*_ν (and add the corresponding complex conjugate) we can further simplify the expression and find a conserved current

$$\nabla_\mu\left(\frac{f}{\sqrt{g}}V^2 k^\mu\right) = 0. \quad (7.23)$$

Thus, very much as in the Diff invariant case, we can write an adiabatic invariant which can be identified with the conserved particle number. Notice however that the conserved current is modified by a $f(g)/\sqrt{g}$ factor which is a typical feature of TDiff-invariant theories, and it was already found in the scalar case in [Mar23]. This is simply due to the fact that the action is changed by a factor $f/\sqrt{g}$, which also appears naturally in the derivation of Noether currents.

Finally, introducing the decomposition in mangnitude and polarisation in (7.22) and using (7.23) we get the propagation equation for the polarisation vector

$$k^\mu v^\nu{}_{;\mu} = \frac{1}{2}\frac{\sqrt{g}}{f}\partial_\mu\left(\frac{f}{\sqrt{g}}\right)k^\nu v^\mu. \quad (7.24)$$

We see that, unlike the Diff-invariant case, in which the polarisation vector is parallel transported along the geodesic ($k^\mu v^\nu{}_{;\mu} = 0$), in the TDiff case, the polarisation vector changes. However, the change takes place along the (unphysical) longitudinal k^μ direction so that the conditions $k_\mu v^\mu = 0$ and $v^\mu v^*_\mu = -1$ will be satisfied along the entire ray. In particular, for any vector field l_μ which is parallel transported along the geodesic ($k^\mu l_{\nu;\mu} = 0$) and is orthogonal to k_μ, ($k_\mu l^\mu = 0$), the projected polarisation remains constant along the geodesic since

$$k^\mu(v^\nu l_\nu)_{;\mu} = (k^\mu v^\nu{}_{;\mu})l_\nu + k^\mu l_{\nu;\mu}v^\nu = \frac{1}{2}\frac{\sqrt{g}}{f}\partial_\mu\left(\frac{f}{\sqrt{g}}\right)k^\nu v^\mu l_\nu = 0 \quad (7.25)$$

In conclusion, in TDiff theories and in the geometric optics approximation, massless vector bosons propagate along null geodesics, the polarisation vectors are orthogonal to the propagation direction, particle number is conserved and the physical (transverse projection) polarisation is parallel transported along the geodesic.

7.1.3 Covariant quantisation

We will consider the quantisation of the gauge field by extending the usual covariant quantisation approach [Pfe02; BM10; IZ12] to the TDiff case. It is well known that the Lorentz gauge condition $\nabla_\mu A^\mu = 0$ cannot be imposed consistently at the operator level but only by restricting the physical Hilbert space of the theory by means of the so-called Gupta-Bleuler condition. This formalism requires to modify the action for the vector field as

$$S_A = \int \mathrm{d}^4x\, f(g)\left(-\frac{1}{4}F_{\mu\nu}F^{\mu\nu} - \frac{\xi}{2}(\nabla_\mu A^\mu)^2\right), \tag{7.26}$$

where ξ is an arbitrary parameter. The corresponding equations of motion in vacuum now read

$$\nabla_\mu\left[\frac{f(g)}{\sqrt{g}}F^{\mu\nu}\right] + \xi\nabla^\nu\left[\frac{f(g)}{\sqrt{g}}\nabla_\mu A^\mu\right] = 0 \tag{7.27}$$

We need to find a complete set of modes that solve the equation of motion derived from the complete action, so we proceed as usual, performing an expansion of the vector field in modes, in terms of creation and annihilation operators

$$A_\mu(x) = \int \frac{\mathrm{d}^3\mathbf{k}}{(2\pi)^{3/2}}\sum_\lambda\left[a_{\mathbf{k}\lambda}A_{\mu,k\lambda}(x) + a^\dagger_{\mathbf{k}\lambda}A^*_{\mu,k\lambda}(x)\right], \tag{7.28}$$

where the sum in polarisations spans four polarisations $\lambda = 0,1,2,3$, only two of which are physical, and the field satisfies the Gupta-Bleuler condition

$$\nabla^\mu A^{(+)}_\mu|\psi\rangle = 0, \tag{7.29}$$

where $|\psi\rangle$ is a physical state and $A^{(+)}_\mu$ is the positive frequency part of the field operator. This condition ensures that on physical states $\langle\psi|\nabla^\mu A_\mu|\psi\rangle = 0$.

The modes of the vector field are chosen to be orthonormal with respect to the inner product, which is defined the usual way [BM10]:

$$(A_{k\lambda}, A_{k'\lambda'}) = i\int_\Sigma \mathrm{d}\Sigma_\mu\left[A^*_{\nu,k\lambda}\Pi^{\mu\nu}_{k'\lambda'} - \Pi^{*\mu\nu}_{k\lambda}A_{\nu,k'\lambda'}\right] = -(2\pi)^3\eta_{\lambda\lambda'}\delta^{(3)}(\mathbf{k}-\mathbf{k}'), \tag{7.30}$$

where $\mathrm{d}\Sigma_\mu = n_\mu\,\mathrm{d}\Sigma = n_\mu\sqrt{g_\Sigma}\,\mathrm{d}^3x$ is the volume element on the spatial Cauchy hypersurface Σ, with n_μ a unit vector normal to the hypersurface Σ, g_Σ the (absolute value of the) determinant of the metric induced on Σ and $\eta_{\lambda\lambda'} = \mathrm{diag}(1,-1,-1,-1)$. In particular, if n_μ is purely timelike, then $n_\mu = ((g^{00})^{-1/2}, \mathbf{0})$, and if the metric tensor is diagonal, then $n_\mu = (\sqrt{g_{00}}, \mathbf{0})$ and $\mathrm{d}\Sigma_\mu = \sqrt{g}(\mathrm{d}^3\mathbf{x}, \mathbf{0})$.

The generalised conjugate momentum $\Pi^{\mu\nu}$ is defined as

$$\delta S_A = \frac{1}{2}\int \mathrm{d}^4x\,\sqrt{g}\,\Pi^{\mu\nu}\delta(\partial_\mu A_\nu), \tag{7.31}$$

which for our action, including the Gupta-Bleuler term (7.26), takes the following form

$$\Pi^{\mu\nu} = -\frac{f(g)}{\sqrt{g}}\left(F^{\mu\nu} + \xi g^{\mu\nu}\nabla_\alpha A^\alpha\right) \tag{7.32}$$

The inner product (7.30) does not depend on the particular choice of hypersurface Σ, as the current

$$j^\mu = A^*_{1\nu}\Pi_2^{\mu\nu} - \Pi_1^{*\mu\nu}A_{2\nu} \tag{7.33}$$

is conserved $\nabla_\mu j^\mu = 0$ under the equations of motion, with $A_{1\nu}$ and $A_{2\nu}$ solutions of the free equations of motion (7.27) and $\Pi_1^{\mu\nu}$ and $\Pi_2^{\mu\nu}$ the corresponding momenta. By defining the momentum projected onto the normal direction n_μ to the spatial hypersurface Σ

$$\pi^\mu = n_\lambda \Pi^{\lambda\mu}, \tag{7.34}$$

we can now use the equal-time commutation relations

$$\left[A_\mu(\tau,\mathbf{x}), A_\nu(\tau,\mathbf{x}')\right] = 0, \tag{7.35a}$$
$$\left[\pi^\mu(\tau,\mathbf{x}), \pi^\nu(\tau,\mathbf{x}')\right] = 0, \tag{7.35b}$$
$$\left[A_\mu(\tau,\mathbf{x}), \pi^\nu(\tau,\mathbf{x}')\right] = i\frac{\delta_\mu{}^\nu}{\sqrt{g_\Sigma}}\delta^{(3)}(\mathbf{x}-\mathbf{x}') \tag{7.35c}$$

to obtain the commutation relations between creation and annihilation operators.

Inserting the expansion of the vector field (7.28) into the first commutation relation (7.35a), we have

$$\left[A_\mu(\tau,\mathbf{x}), A_\nu(\tau,\mathbf{x}')\right] = \int \frac{\mathrm{d}^3\mathbf{k}\,\mathrm{d}^3\mathbf{k}'}{(2\pi)^3}\sum_{\lambda\lambda'}\Big([a_{\mathbf{k}\lambda}, a_{\mathbf{k}'\lambda'}]A_{\mu,k\lambda}A_{\nu,k'\lambda'} + [a^\dagger_{\mathbf{k}\lambda}, a^\dagger_{\mathbf{k}'\lambda'}]A^*_{\mu,k\lambda}A^*_{\nu,k'\lambda'} + [a_{\mathbf{k}\lambda}, a^\dagger_{\mathbf{k}'\lambda'}]\left(A_{\mu,k\lambda}A^*_{\nu,k'\lambda'} - A^*_{\mu,k'\lambda'}A_{\nu,k\lambda}\right)\Big) = 0. \tag{7.36}$$

This, and the same can be obtained through (7.35b), necessarily implies

$$[a_{\mathbf{k}\lambda}, a_{\mathbf{k}'\lambda'}] = [a^\dagger_{\mathbf{k}\lambda}, a^\dagger_{\mathbf{k}'\lambda'}] = 0, \tag{7.37}$$

as well as $[a_{\mathbf{k}\lambda}, a^\dagger_{\mathbf{k}'\lambda'}] = f(\mathbf{k},\lambda)\delta^{(3)}(\mathbf{k}-\mathbf{k}')\delta_{\lambda\lambda'}$, so that the term multiplying this commutator can vanish after using both deltas to eliminate a sum and an integral. The expression for $f(\mathbf{k},\lambda)$ can be obtained from (7.35c), which reads

$$\int \frac{\mathrm{d}^3\mathbf{k}\,\mathrm{d}^3\mathbf{k}'}{(2\pi)^3} n_\lambda \sum_{\lambda\lambda'}[a_{\mathbf{k}\lambda}, a^\dagger_{\mathbf{k}'\lambda'}]\left(A_{\mu,k\lambda}\Pi^{*\lambda\nu}_{k'\lambda'} - \Pi^{\lambda\nu}_{k\lambda}A^*_{\mu,k'\lambda'}\right) = i\frac{\delta_\mu{}^\nu}{\sqrt{g_\Sigma}}\delta^{(3)}(\mathbf{x}-\mathbf{x}'). \tag{7.38}$$

We now multiply by $\sqrt{g_\Sigma}$, integrate over space and contract the free indices to find

$$\int \frac{\mathrm{d}^3\mathbf{k}\,\mathrm{d}^3\mathbf{k}'}{(2\pi)^3}\sum_{\lambda\lambda'}[a_{\mathbf{k}\lambda},a^\dagger_{\mathbf{k}'\lambda'}]\int \mathrm{d}^3x\,\sqrt{g_\Sigma}n_\lambda\left(A_{\mu,k\lambda}\Pi^{*\lambda\mu}_{k'\lambda'}-\Pi^{\lambda\mu}_{k\lambda}A^*_{\mu,k'\lambda'}\right)=4i. \tag{7.39}$$

Finally, by using the normalisation condition (7.30) to replace the spatial integral, the commutator needs to be

$$[a_{\mathbf{k}\lambda},a^\dagger_{\mathbf{k}'\lambda'}]=-\eta_{\lambda\lambda'}\delta^{(3)}(\mathbf{k}-\mathbf{k}'),\text{ with }\lambda,\lambda'=0,1,2,3 \tag{7.40}$$

Geometric optics limit

Let us now use the inner product we have just defined to find the normalisation of the vector field modes in the geometric optics approximation. In order not to overcrowd the equations, allow us to write the modes of the field (7.12) now as

$$A_{\mu,k\lambda}(x)=U_{\mu,k\lambda}(x)e^{i\theta_{\mathbf{k}\lambda}(x)}, \tag{7.41}$$

where we have dropped the dummy expansion parameter and gathered the whole amplitude into a single object. In terms of the field strength, the scalar product can be written as

$$(A_{k\lambda},A_{k'\lambda'})=-i\int \mathrm{d}^3\mathbf{x}\sqrt{g_\Sigma}n_\mu\frac{f}{\sqrt{g}}\Big[A^*_{\nu,k\lambda}F^{\mu\nu}_{k'\lambda'}-F^{*\mu\nu}_{k\lambda}A_{\nu,k'\lambda'} +\xi g^{\mu\nu}(A^*_{\nu,k\lambda}\nabla_\alpha A^\alpha_{k'\lambda'}-\nabla_\alpha A^{*\alpha}_{k\lambda}A_{\nu,k'\lambda'})\Big]. \tag{7.42}$$

The field strength in terms of the modes is

$$F^{\mu\nu}_{k\lambda}=g^{\mu\rho}g^{\nu\sigma}(ik_\rho U_{\sigma,k\lambda}-ik_\sigma U_{\rho,k\lambda}+\partial_\rho U_{\sigma,k\lambda}+\partial_\sigma U_{\rho,k\lambda})e^{i\theta_{\mathbf{k}\lambda}}. \tag{7.43}$$

At leading order, terms involving derivatives of the amplitude $\partial_\mu U_\nu$ do not contribute. Expanding the inner product (7.42), with $k'\lambda'=k\lambda$, we get the following expression at leading order

$$(A_{k\lambda},A_{k\lambda})=2\sqrt{g_\Sigma}\frac{f}{\sqrt{g}}(2\pi)^3\delta^{(3)}(\mathbf{0})n_\mu\left[k^\mu U^*_{\sigma,k\lambda}U^\sigma_{k\lambda}+(\xi-1)\mathrm{Re}(k^\sigma U^\mu_{k\lambda}U^*_{\sigma,k\lambda})\right]. \tag{7.44}$$

In the Feynman gauge $\xi=1$, the last term vanishes, and we can impose (7.30) to obtain the normalisation of the vector field

$$U^*_{\rho,k\lambda}U^\rho_{k\lambda}=\frac{-\eta_{\lambda\lambda}}{2fn_\mu k^\mu}\sqrt{\frac{g}{g_\Sigma}}\quad\text{(no sum over }\lambda\text{)}. \tag{7.45}$$

As a result, the vector field at leading order in geometric optics can be finally written as

$$A_{\mu,k\lambda}(x)=\left(\frac{g}{g_\Sigma}\right)^{1/4}\frac{1}{\sqrt{2f|n_\mu k^\mu|}}u_{\mu,k\lambda}e^{i\theta(x)}, \tag{7.46}$$

with $u_{\mu,k\lambda}$ a polarisation vector that satisfies $k_\mu u^\mu_{k\lambda}=0$ and $u^*_{\mu,k\lambda}u^\mu_{k\lambda}=\eta_{\lambda\lambda}$ (no sum over λ).

7.2 Coupling to an external current

So far we have considered the free gauge field, without any kind of coupling to an external source, which does not need to be the case. For this reason, let us consider a general coupling to an external current j^μ

$$S = -\int \mathrm{d}^4x \left(f(g)\frac{1}{4}F_{\mu\nu}F^{\mu\nu} + f_D(g) j^\mu A_\mu \right), \tag{7.47}$$

with $f_D(g)$ an arbitrary function of the metric determinant and j^μ an external Diff vector current that we assume does not depend on the vector field A_μ. Imposing gauge invariance of the full action requires the external current to satisfy the conservation equation given by

$$\nabla_\mu \left(\frac{f_D(g)}{\sqrt{g}} j^\mu \right) = 0. \tag{7.48}$$

Thus we see that, as we have already seen in Section 7.1.2, conserved currents are modified by a factor $f_D(g)/\sqrt{g}$ when breaking Diff invariance down to TDiff invariance.

The equation of motion for the vector field is then modified to

$$\nabla_\mu \left[\frac{f(g)}{\sqrt{g}} F^{\mu\nu} \right] = \frac{f_D(g)}{\sqrt{g}} j^\nu. \tag{7.49}$$

which can be rewritten as

$$\nabla_\mu F^{\mu\nu} + \frac{\sqrt{g}}{f(g)} \partial_\mu \left(\frac{f(g)}{\sqrt{g}} \right) F^{\mu\nu} = \frac{f_D(g)}{f(g)} j^\nu. \tag{7.50}$$

Notice that in the adiabatic approximation in which terms involving metric derivatives are negligible compared to those involving derivatives of the field strength, the equations of motion reduce to

$$\nabla_\mu F^{\mu\nu} \simeq \frac{f_D(g)}{f(g)} j^\nu, \tag{7.51}$$

which agrees with the standard Diff expression for the Maxwell equations but only if $f_D(g) = f(g)$. In general, $f_D(g) \neq f(g)$ could induce a space-time dependence of fermionic charges in contradiction with LPI. In the following, we present the explicit construction of the conserved current from TDiff invariant Dirac spinors.

7.2.1 TDiff Dirac spinors and the Lorentz force

Let us now consider the particular case of a Dirac field Ψ that couples to the gauge field, which will allow us to obtain the Lorentz force law by analysing its semiclassical limit. The Dirac action can be written in an explicitly self-adjoint way [BD84] as

$$S_D[\Psi] = \int \mathrm{d}^4x\, f_D(g) \left[\frac{i}{2} (\bar{\Psi}\gamma^\mu D_\mu \Psi - D_\mu \bar{\Psi}\gamma^\mu \Psi) - m\bar{\Psi}\Psi \right], \tag{7.52}$$

where $\bar{\Psi} = \Psi^\dagger \gamma^0$ (this γ^0 is the usual gamma matrix used in flat spacetime) is the Dirac adjoint and the covariant derivatives are

$$D_\mu \Psi = \mathfrak{D}_\mu \Psi + iqA_\mu \Psi, \tag{7.53a}$$
$$D_\mu \bar{\Psi} = \mathfrak{D}_\mu \bar{\Psi} - iqA_\mu \bar{\Psi}, \tag{7.53b}$$

where $\mathfrak{D}$ implements the spin-connection covariant derivatives. The formulation related to covariant derivatives and how to mathematically deal with fermions in curved spacetime is laid out in Appendix D.

We can easily identify the current that couples to the electromagnetic field as

$$j^\mu = q\bar{\Psi}\gamma^\mu \Psi. \tag{7.54}$$

As shown before, if the gauge function $f(g)$ agrees with the fermion function $f_D(g) = f(g)$, the Dirac current sources the gauge field exactly as in the Diff-invariant case, so we make this choice from now onwards.

Let us now tackle the derivation of the TDiff version of Dirac's equation in curved spacetime from the action. We start by integrating by parts the term with $D_\mu \bar{\Psi}$, as one usually does in flat spacetime. After expanding it, it has the following form

$$S_{\bar{\Psi}} = -\frac{i}{2}\int \mathrm{d}^4x\, f(g)(D_\mu \bar{\Psi})\gamma^\mu \Psi = -\frac{i}{2}\int \mathrm{d}^4x\, f(g)(\partial_\mu \bar{\Psi} - \bar{\Psi}\Gamma_\mu - iqA_\mu \bar{\Psi})\gamma^\mu \Psi. \tag{7.55}$$

We now integrate the first term by parts, expand derivatives and collect the terms in a convenient way to write the following

$$S_{\bar{\Psi}} = \frac{i}{2}\int \mathrm{d}^4x \left(f\bar{\Psi}\gamma^\mu D_\mu \Psi + \bar{\Psi}\left(\partial_\mu(f\gamma^\mu) - f[\gamma^\mu, \Gamma_\mu]\right)\Psi\right). \tag{7.56}$$

The second term can be simplified by using the result in Eq. (D.14)

$$\partial_\mu(f\gamma^\mu) - f[\gamma^\mu, \Gamma_\mu] = \gamma^\mu \partial_\mu f - f\Gamma^\mu_{\mu\lambda}\gamma^\lambda = \sqrt{g}\gamma^\mu \partial_\mu\left(\frac{f}{\sqrt{g}}\right), \tag{7.57}$$

where we have also used the identity (C.6). This term obviously vanishes in the Diff-invariant case $f(g) = \sqrt{g}$ but does not otherwise, so the action, written in its most common form, acquires an additional term

$$S_D = \int \mathrm{d}^4x\, f\bar{\Psi}\left[i\gamma^\mu D_\mu + \frac{i}{2}\frac{\sqrt{g}}{f}\gamma^\mu \partial_\mu\left(\frac{f}{\sqrt{g}}\right) - m\right]\Psi. \tag{7.58}$$

The Dirac equation is easily obtained by performing variations of this action with respect to $\bar{\Psi}$

$$\left[i\gamma^\mu D_\mu + \frac{i}{2}\frac{\sqrt{g}}{f}\gamma^\mu \partial_\mu\left(\frac{f}{\sqrt{g}}\right) - m\right]\Psi = 0. \tag{7.59}$$

The equation of motion for the Dirac conjugate can be obtained by integrating by parts the other term in the action, or equivalently, by taking the adjoint of this equation of motion. Using Eq. (D.8), it is immediate to take the conjugate and write

$$iD_\mu\bar{\Psi}\gamma^\mu + \frac{i}{2}\frac{\sqrt{g}}{f}\partial_\mu\left(\frac{f}{\sqrt{g}}\right)\bar{\Psi}\gamma^\mu + m\bar{\Psi} = 0. \tag{7.60}$$

The new term contains derivatives of the metric, which do not affect the dynamics at leading order of the adiabatic expansion. In other words, our Dirac equation is equivalent to the usual one in the geometric optics approximation, which we will see in what follows.

Before doing so, one can easily check that the Dirac action is invariant under global U(1) transformations of the spinor field $\Psi \to e^{i\alpha}\Psi$, which as expected implies that the Noether current

$$j^\mu_N = \frac{f(g)}{\sqrt{g}}\bar{\Psi}\gamma^\mu\Psi, \tag{7.61}$$

is a vector under TDiff transformations that satisfies

$$\nabla_\mu\left[\frac{f(g)}{\sqrt{g}}\bar{\Psi}\gamma^\mu\Psi\right] = \mathscr{D}_\mu\left[\frac{f(g)}{\sqrt{g}}\bar{\Psi}\gamma^\mu\Psi\right] = 0, \tag{7.62}$$

where in the first step we have used that the term in square brackets is a scalar with respect to the covariant derivative $\mathfrak{D}$. Here, $\mathscr{D}$ is the total covariant derivative, which is introduced in Appendix D. Using Leibniz's rule, the equations of motion and changing $\mathscr{D}_\mu\Psi = \mathfrak{D}_\mu\Psi$ when necessary, it is immediate to check the conservation of this current.

Let us examine the Dirac equation in the geometric optics approximation. We write the Dirac field as a rapidly oscillating exponential times a slowly varying amplitude

$$\Psi(x) = \left(\psi_0 + \psi_1\epsilon + \dots\right)e^{i\theta(x)/\epsilon}, \tag{7.63}$$

where ϵ is a dummy power-counting parameter. We also define $k_\mu = \partial_\mu\theta(x)$, so that the amplitudes depend both on this momentum and spatial position $\psi_n = \psi_n(x, \partial\theta)$.

Following an analogy with a semi-classical analysis [OK23], where the parameter ϵ would play the role of $\hbar$, every term originating from the purely kinetic part of the action must carry an additional ϵ. Thus, we write

$$\left[i\gamma^\mu(\epsilon\mathfrak{D}_\mu + iqA_\mu) + \frac{i\epsilon}{2}\frac{\sqrt{g}}{f}\gamma^\mu\partial_\mu\left(\frac{f}{\sqrt{g}}\right) - m\right]\Psi = 0. \tag{7.64}$$

and similarly for its Dirac conjugate. Now it is immediate to realise that the new term, coming from breaking down to TDiff invariance, does not contribute at leading order, as one would expect. The equations of motion (7.64) and conservation equation (7.62) at leading order $\mathcal{O}(\epsilon^0)$ are given by

$$(\gamma^\mu p_\mu + m)\psi_0 = 0, \tag{7.65a}$$

$$\bar{\psi}_0(\gamma^\mu p_\mu + m) = 0, \tag{7.65b}$$

$$\partial_\mu(f\bar{\psi}_0\gamma^\mu\psi_0) = 0, \tag{7.65c}$$

with $p_\mu = k_\mu + qA_\mu$. With the aid of the equations of motion, we can write the current as

$$\bar{\psi}_0 \gamma^\mu \psi_0 = -\frac{1}{m} p^\mu \bar{\psi}_0 \psi_0, \tag{7.66}$$

where we have used the anti-commutation relations of the gamma matrices as well. With this, the conservation equation can be written

$$\nabla_\mu \left(\frac{f}{\sqrt{g}} \bar{\psi}_0 \psi_0 p^\mu \right) = 0, \tag{7.67}$$

which features the usual $f/\sqrt{g}$ factor that goes along currents. On the other hand, by multiplying both equations of motion together, we can write

$$\bar{\psi}_0 \left[(p_\mu \gamma^\mu)^2 + 2m p_\mu \gamma^\mu + m^2 \right] \psi_0 = 0. \tag{7.68}$$

Using the equations of motion and the fact that $(p_\mu \gamma^\mu)^2 = p_\mu p^\mu$, we obtain

$$p_\mu p^\mu = m^2, \tag{7.69}$$

which is the usual dispersion relation for a particle under the effect of an electromagnetic field. Let us note that, since k_μ is the gradient of a scalar, then $\nabla_\mu k_\nu = \nabla_\nu k_\mu$, so

$$\nabla_\mu p_\nu - \nabla_\nu p_\mu = q(\nabla_\mu A_\nu - \nabla_\nu A_\mu) = q F_{\mu\nu}. \tag{7.70}$$

This allows us to differentiate the dispersion relation and obtain

$$p^\mu \nabla_\mu p_\nu = q\, p^\mu F_{\mu\nu}, \tag{7.71}$$

which is the standard Lorentz-Dirac equation. In this equation, we observe that the Lorentz force in the TDiff case is unchanged with respect to the Diff expression provided $f_D(g) = f(g)$. In Appendix E, we present an alternative derivation of the TDiff-invariant Lorentz force law, in which the starting point is the action of a massive point-particle coupled to the electromagnetic field.

7.3 TDiff vector fields in cosmological backgrounds

Let us turn our attention to a cosmological scenario by examining the dynamics of vector fields in a homogeneous and isotropic expanding universe. The line element is given by the flat RW metric

$$\mathrm{d}s^2 = b^2(\tau)\,\mathrm{d}\tau^2 - a^2(\tau)\,\mathrm{d}\mathbf{x}^2, \tag{7.72}$$

where $b(\tau)$, $a(\tau)$ are the lapse function and scale factor, respectively. Note that due to not having Diff invariance, we cannot start by changing the time coordinate to the usual cosmological time $\mathrm{d}t = b(\tau)\mathrm{d}\tau$ [Mar23].

7.3.1 Homogeneous fields

Let us start by considering the simple case of homogeneous vector fields $A_\mu(\tau) = (A_0(\tau), \mathbf{A}(\tau))$. The equations of motion (7.6) are given in this case by

$$\mathbf{A}'' + \left[(6f_1 - 2)\frac{a'}{a} + (2f_1 - 2)\frac{b'}{b}\right]\mathbf{A}' = 0, \tag{7.73}$$

with $A_0(\tau)$ unconstrained, as it does not appear in the field strength tensor, so it can be determined via gauge fixing. In this Chapter, everywhere except on the function $f(g)$, the primes represent derivatives with respect to the time coordinate $' = \mathrm{d}/\mathrm{d}\tau$. In principle, this equation cannot be integrated unless we can solve Einstein's equations for $a(\tau)$ and $b(\tau)$, even if we assume a specific $f(g)$.

The stress-energy tensor components for this configuration (the energy density ρ and pressure in each direction p_i) are given by

$$\rho = T^0{}_0 = \frac{f(g)}{\sqrt{g}}(1 - f_1)\frac{|\mathbf{A}'|^2}{a^2 b^2}, \tag{7.74a}$$

$$-p_i = T^i{}_i = \frac{f(g)}{\sqrt{g}}\frac{1}{a^2 b^2}\left(A_i'^2 - f_1|\mathbf{A}'|^2\right) \quad \text{(no sum over } i\text{)}, \tag{7.74b}$$

with the off-diagonal elements $T^0{}_i = T^i{}_0 = T^i{}_j (i \neq j) = 0$. Due to the nature of the vector field, we have a configuration with anisotropic pressures, which in general do not need to be equal. However, we can compute a mean equation of state as

$$\bar{w} = \frac{\bar{p}}{\rho} = \frac{\frac{1}{3}\sum_i p_i}{\rho} = \frac{f_1 - \frac{1}{3}}{1 - f_1}, \tag{7.75}$$

which in the Diff case $f_1 = 1/2$ equals $\bar{w} = 1/3$, as expected for a free vector field, which behaves as radiation.

One of the main differences of TDiff-invariant field theories compared to their Diff-invariant counterpart is that the stress-energy conservation equations are not automatically fulfilled under solutions to the field's equations of motion. Although the stress-energy tensor is conserved on solutions of the Einstein equations, the non-linearity and complexity of Einstein's equations make it more practical to use conservation equations in order to obtain constraints involving the metric components and their derivatives. This allows us to determine some functions in the metric that we have not been able to fix previously, due to having one less gauge degree of freedom as a result of having a reduced symmetry group. In particular, this is the case of the lapse function $b(\tau)$ in the TDiff-invariant RW metric, as time dilations are not TDiff.

Let us examine now the conservation equations. Explicitly, for the spacetime (7.72), they are given by

$$\partial_\mu T^\mu{}_0 + 3\frac{a'}{a}T^0{}_0 - \frac{a'}{a}T^i{}_i = 0, \tag{7.76a}$$

$$\partial_\mu T^\mu{}_i + \left(2\frac{a'}{a} + \frac{b'}{b}\right)T^0{}_i - \frac{aa'}{b^2}T^i{}_0 = 0. \tag{7.76b}$$

In the case of a homogeneous vector field, the second conservation equation is identically zero, whereas the first one yields the following equation

$$(2-2f_1)\mathbf{A}''\cdot\mathbf{A}'+|\mathbf{A}'|^2\left[(-3+11f_1-6f_1^2-6f_2)\frac{a'}{a}+(-3+5f_1-2f_1^2-2f_2)\frac{b'}{b}\right]=0. \quad (7.77)$$

We can eliminate the dependence on the vector field by taking the scalar product of the field equation of motion (7.73) with $\mathbf{A}'$ and substituting it into (7.77), so we have

$$(1-5f_1+6f_1^2-6f_2)\frac{a'}{a}+(1-3f_1+2f_1^2-2f_2)\frac{b'}{b}=0. \quad (7.78)$$

We will refer to this constraint as the "electric condition", since as we show below, it is the constraint that having an electric field imposes onto the spacetime. In particular, it allows to obtain $b(\tau)$ from $a(\tau)$ for a given $f(g)$. Notice that in the Diff case with $f_1=1/2$ and $f_2=0$ the equation is trivially satisfied for any $b(\tau)$. This constraint can be inserted into the equations of motion (7.73), which now become

$$\mathbf{A}''-\frac{8f_2}{1-3f_1+2f_1^2-2f_2}\frac{a'}{a}\mathbf{A}'=0. \quad (7.79)$$

Note that, for a $f(g)$ so that $f_2=0$, such as a power law, the equation of motion is simply $\mathbf{A}''=0$, so the vector potential evolves linearly with time $\mathbf{A}\propto\tau$ and $F_{0i}=\text{const}$. If we think in terms of electric $\mathbf{E}$ and magnetic $\mathbf{B}$ fields, defined as

$$E_i=F_{0i},\quad B_i=\frac{1}{2}\epsilon_{ijk}F_{jk}, \quad (7.80)$$

this particular configuration of a homogeneous vector field corresponds to a constant electric field with vanishing magnetic field, as we had anticipated.

In particular, for a power-law $f(g)=g^\alpha$, the explicit dependence between a and b can be extracted by integrating (7.78), yielding

$$b(\tau)\propto a^{\frac{1-3\alpha}{\alpha-1}}(\tau). \quad (7.81)$$

If we insert this expression into the equation of motion (7.73), the term in square brackets vanishes, as expected since $f_2=0$. Taking into account this time dependence, both the energy density and pressure (7.74) evolve with the scale factor as

$$\rho,p_i\propto a^{-2/(1-\alpha)}, \quad (7.82)$$

which in the Diff invariant case ($\alpha=1/2$) reads $\rho\propto a^{-4}$, as expected for a radiation component.

Homogeneous magnetic field

We work on a configuration with a constant magnetic field now. Taking into account the definition of the magnetic field (7.80), we need a vector potential that takes the following form in order to obtain a homogeneous configuration:

$$A_i = \frac{1}{2}\epsilon_{ijk}x^j B_k, \tag{7.83}$$

with a constant $\mathbf{B}$, because in any other case, a non-homogeneous electric field would arise as well. Since the field strength $F_{ij} = \text{const.}$, with all other components zero, it is easy to see that it satisfies the equations of motion (7.6).

The non-zero components of the stress-energy tensor now are

$$\rho = T^0{}_0 = \frac{f(g)}{\sqrt{g}}\frac{f_1}{a^4}\mathbf{B}^2, \tag{7.84a}$$

$$-p_i = T^i{}_i = \frac{f(g)}{\sqrt{g}}\frac{1}{a^4}[(f_1-1)\mathbf{B}^2 + B_i^2] \quad \text{(no sum over } i\text{)}, \tag{7.84b}$$

$$T^i{}_j = \frac{f(g)}{\sqrt{g}}\frac{1}{a^4}\Big((f_1-1)\mathbf{B}^2\delta^i{}_j + B_iB_j\Big), \tag{7.84c}$$

where we have used that $F_{ij}F_{ij} = 2\mathbf{B}^2$. The average equation of state is

$$\bar{w} = \frac{\bar{p}}{\rho} = \frac{f_1}{3(2-3f_1)}, \tag{7.85}$$

which again yields $\bar{w} = 1/3$ for the Diff-invariant case.

The conservation of the stress-energy tensor together with the field equations of motion impose now the "magnetic condition", namely

$$\frac{a'}{a}\left(2-7f_1+6f_1^2+6f_2\right) + \frac{b'}{b}(-f_1+2f_1^2+2f_2) = 0. \tag{7.86}$$

Notice once more that in the Diff case $f_1 = 1/2$ and $f_2 = 0$ the condition is trivially satisfied. In the particular case of a power-law $f(g) = g^\alpha$, this condition is solved by the following relation between b and a

$$b(\tau) \propto a^{\frac{2-3\alpha}{\alpha}}(\tau). \tag{7.87}$$

Interestingly, both the condition and the relationship between b and a are different from those in the purely electric case (7.78, 7.81), which translates into a different spacetime depending on the vector field configuration that it hosts. Notice however that these conditions approach the same values as $\alpha \to 1/2$.

The energy density and pressures (7.84) now scale as

$$\rho, p_i \propto a^{-(1+2\alpha)/\alpha}, \tag{7.88}$$

with the same radiation-like behaviour $\rho \propto a^{-4}$ in the Diff-invariant case. Notice however that for $\alpha > 1/2$ the magnetic energy density dilutes more slowly than radiation, which could provide a mechanism for amplification of primordial magnetic fields, which is later explored in Sec. 7.4.

Following these different results, we wonder whether it is possible to have both TDiff-invariant electric and magnetic fields in a RW background while satisfying the corresponding conservation equations. In that case, we should be able to find a more general solution to the conservation equation $b(a)$ that interpolates between the two we have already obtained, which we explore as follows.

General homogenous field

Let us look back at the individual electric and magnetic conditions separately for a general $f(g)$. Since the various f_n that appear in these equations are in general a function of the metric determinant g, it is useful to substitute $b = b(g,a)$, for which we use the following expression

$$\frac{b'}{b} = \frac{1}{2}\frac{g'}{g} - 3\frac{a'}{a}. \tag{7.89}$$

Inserting this into the electric condition (7.78), we obtain

$$\frac{a'}{a}(-2+4f_1) + \frac{1}{2}\frac{g'}{g}(1-3f_1+2f_1^2-2f_2) = 0. \tag{7.90}$$

By making $t = \log g$, $F = \log f$ and integrating we get to

$$\log a = \frac{1}{4}\int \mathrm{d}t\, \frac{1-2\dot{F}+2\dot{F}^2-2\ddot{F}}{1-2\dot{F}}, \tag{7.91}$$

where the overdots denote derivatives with respect to t. After performing the integration it becomes the following condition

$$C_E a^4 = \frac{g}{f}(1-2f_1), \tag{7.92}$$

with C_E a constant.

Working similarly, the magnetic condition (7.86) can be written as

$$\frac{a'}{a}(1-2f_1) + \frac{1}{4}\frac{g'}{g}(-f_1+2f_1^2+2f_2) = 0, \tag{7.93}$$

which can be solved to

$$C_B a^4 = f(1-2f_1), \tag{7.94}$$

with C_B a constant.

Again, note how the electric and magnetic conditions are different. It is also easy to realise that these constraints are automatically fulfilled when $f = \sqrt{g}$. They are equivalent to (7.81, 7.87) when introducing $f(g) = g^\alpha$.

In order to examine whether a consistent conservation equation with an electromagnetic configuration can be obtained, we can write, without loss of generality, the following expression for the vector potential

$$A_i(\tau) = \phi_i(\tau) + \frac{1}{2}\epsilon_{ijk}x^j B_k, \tag{7.95}$$

which gives the most general homogeneous configuration, with electric field $E_i(\tau) = \phi_i'(\tau)$ and constant magnetic field B_i. The magnetic field needs to be constant because otherwise a non-homogeneous electric field is present, as discussed in the previous section.

Unfortunately, unlike in the purely electric or magnetic case, the conservation equation cannot be explicitly obtained for a general $f(g)$, so throughout the rest of this section, we assume a power-law $f(g) = g^\alpha$. The time evolution of the electric field can easily be obtained thanks to the equation of motion (7.73), which solves to

$$\mathbf{E}(\tau) = \mathbf{E_0} a^{2-6\alpha}(\tau) b^{2-2\alpha}(\tau), \tag{7.96}$$

where $\mathbf{E_0}$ is the value of the electric field when $a = b = 1$. In this case, the conservation of the stress-energy tensor imposes the following constraint

$$\frac{E_0^2}{B^2}(a^6 b^2)^{1-2\alpha}\left[\frac{a'}{a}(1-5\alpha+6\alpha^2) + \frac{b'}{b}(1-3\alpha+2\alpha^2)\right] + \left[\frac{a'}{a}\left(1-\frac{7}{2}\alpha+3\alpha^2\right) + \frac{b'}{b}\left(-\frac{\alpha}{2}+\alpha^2\right)\right] = 0, \tag{7.97}$$

where $E_0 = |\mathbf{E_0}|$ and $B = |\mathbf{B}|$. Making the substitution $b = b(g,a)$ as in the previous cases, we obtain

$$(1-2\alpha)\frac{a'}{a}\left(2\frac{E_0^2}{B^2}g^{1-2\alpha} - 1\right) = (1-2\alpha)\frac{g'}{g}\left(\frac{1-\alpha}{2}\frac{E_0^2}{B^2}g^{1-2\alpha} - \frac{\alpha}{4}\right). \tag{7.98}$$

Notice that the condition is automatically fulfilled in the Diff case $\alpha = 1/2$ as expected. For $\alpha \neq 1/2$, we can divide this expression by $1-2\alpha$ and it can be easily integrated to obtain the following relation

$$C_{EM} a^4 = g^\alpha - 2g^{1-\alpha}\frac{E_0^2}{B^2}. \tag{7.99}$$

This expression generalises the electric and magnetic conditions for a power-law $f(g)$. As one could have predicted, it depends on the values of the electric and magnetic fields, and it is compatible with the electric (7.78) and magnetic (7.86) conditions in the $E_0 \gg B$ and $E_0 \ll B$ limits, respectively. Note that this relation works only for homogeneous fields, which in practical terms means that we will be able to use it for modes in the super-Hubble regime. Sub-Hubble modes, as we will explore in future sections, fall into the geometric optics approximation and behave as in a Diff-invariant theory.

7.3.2 Inhomogeneous fields

In order to study further configurations, we need to consider a vector field $A_\mu(\tau,\mathbf{x})$ that depends both on time coordinate and spatial position. The equations of motion (7.6) now read, in terms of the field strength

$$\partial_i F_{0i} = 0, \tag{7.100a}$$

$$\partial_0 F_{0i} + \left[(6f_1-2)\frac{a'}{a} + (2f_1-2)\frac{b'}{b}\right] F_{0i} = \frac{b^2}{a^2}\partial_j F_{ji}. \tag{7.100b}$$

These equations cannot be explicitly solved unless we invoke a particular ansatz for either the field strength or the vector field, which we have already done in the previous section.

The stress-energy tensor has the following components:

$$T^0{}_0 = \rho = \frac{f}{\sqrt{g}}\left[\frac{1-f_1}{a^2b^2}F_{0i}F_{0i} + \frac{f_1}{2a^4}F_{ij}F_{ij}\right], \tag{7.101a}$$

$$T^0{}_i = \frac{f}{\sqrt{g}}\frac{1}{a^2b^2}F_{0j}F_{ij}, \tag{7.101b}$$

$$T^i{}_0 = -\frac{f}{\sqrt{g}}\frac{1}{a^4}F_{0j}F_{ij}, \tag{7.101c}$$

$$T^i{}_j = \frac{f}{\sqrt{g}}\left[\frac{1}{2}f_1\left(\frac{1}{a^4}F_{kl}F_{kl} - \frac{2}{a^2b^2}F_{0k}F_{0k}\right)\delta^i{}_j + \frac{1}{a^2b^2}F_{i0}F_{j0} - \frac{1}{a^4}F_{ik}F_{jk}\right], \tag{7.101d}$$

$$T^i{}_i = \mathrm{tr}\left(T^i{}_j\right) = -3\bar{p} = \frac{f}{\sqrt{g}}\left[\frac{1-3f_1}{a^2b^2}F_{0i}F_{0i} + \frac{\frac{3}{2}f_1-1}{a^4}F_{ij}F_{ij}\right]. \tag{7.101e}$$

With these, we can write the conservation equations

$$\begin{aligned}2(1-f_1)F_{0i}\partial_0 F_{0i} + \frac{b^2}{a^2}f_1F_{ij}\partial_0F_{ij} - \frac{b^2}{a^2}\partial_i(F_{0j}F_{ij})\\ + F_{0i}F_{0i}\left[\frac{a'}{a}\left(-3+11f_1-6f_1^2-6f_2\right) + \frac{b'}{b}(-3+5f_1-2f_1^2-2f_2)\right]\\ + \frac{b^2}{a^2}F_{ij}F_{ij}\left[\frac{a'}{a}\left(-3+11f_1-6f_1^2-6f_2\right) + \frac{b'}{b}(-3+5f_1-2f_1^2-2f_2)\right] = 0,\end{aligned} \tag{7.102a}$$

$$\begin{aligned}\partial_0(F_{0j}F_{ij}) + \frac{b^2}{a^2}f_1F_{kl}\partial_iF_{kl} - 2f_1F_{0j}\partial_iF_{0j} + \partial_j(F_{i0}F_{j0}) - \frac{b^2}{a^2}\partial_j(F_{ik}F_{jk})\\ + F_{0j}F_{ij}\left[\frac{a'}{a}(-2+6f_1) - \frac{b'}{b}(-2+2f_1)\right] = 0.\end{aligned} \tag{7.102b}$$

After inserting the equations of motion into the conservation equations, we get

$$(1-2f_1)\frac{b^2}{a^2}F_{0j}\partial_i F_{ij}+\frac{b^2}{a^2}f_1F_{ij}\partial_0F_{ij}-\frac{b^2}{a^2}F_{ij}\partial_iF_{0j}$$
$$+F_{0i}F_{0i}\left[\frac{a'}{a}\left(1-5f_1+6f_1^2-6f_2\right)+\frac{b'}{b}(1-3f_1+2f_1^2-2f_2)\right]$$
$$+\frac{1}{2}\frac{b^2}{a^2}F_{ij}F_{ij}\left[\frac{a'}{a}\left(2-7f_1+6f_1^2+6f_2\right)+\frac{b'}{b}(-f_1+2f_1^2+2f_2)\right]=0, \quad (7.103a)$$

$$F_{0j}\partial_0F_{ij}-2f_1F_{0j}\partial_iF_{0j}+F_{0j}\partial_jF_{0i}+\frac{b^2}{a^2}f_1F_{jk}\partial_iF_{jk}-\frac{b^2}{a^2}F_{jk}\partial_jF_{ik}=0. \quad (7.103b)$$

If we set $f=\sqrt{g}$ in these equations, the terms in square brackets vanish, whereas the rest of the terms cancel out with the aid of the Bianchi identities $\partial_{(i}F_{jk)}=0$, as expected since the conservation of the stress-energy tensor is identical in the Diff-invariant case.

Note that the term in square brackets that multiplies $F_{0i}F_{0i}$ in (7.103a) is what we dubbed the electric condition (7.78). As $F_{0i}F_{0i}=\mathbf{E}^2$, this is the only term that survives when we have a homogeneous electric field. Similarly, $F_{ij}F_{ij}=2\mathbf{B}^2$, so we easily identify the term in square brackets that multiplies this combination as the magnetic condition (7.86).

We can also observe in (7.101a) that the electric and magnetic parts of TDiff fields gravitate differently. Thus, the electric energy density is proportional to $1-f_1$ whereas the magnetic energy density is proportional to f_1, so that they only gravitate in the same proportion in the Diff invariant case.

Maxwell's equations

In this section, we take a look at the equations of motion of a free electromagnetic field (7.100) written in terms of the electric and magnetic fields (7.80). These, including the external current in (7.47) for the sake of completeness, and with $f_D(g)=f(g)$, read as follows

$$\nabla\cdot\mathbf{E}=a^2b^2j^0, \quad (7.104a)$$
$$\frac{b^2}{a^2}\nabla\times\mathbf{B}=\mathbf{E}'+\left[(6f_1-2)\frac{a'}{a}+(2f_1-2)\frac{b'}{b}\right]\mathbf{E}+a^2b^2\mathbf{j}, \quad (7.104b)$$

where $\mathbf{j}$ is the spatial part of j^μ. These correspond to the well-known Gauss's law for the electric field and Ampère's law, respectively, with a slight change due to the Diff-invariance breaking. On top of these, the Bianchi identities are also satisfied by definition of the field strength

$$\partial_\mu F_{\alpha\beta}+\partial_\alpha F_{\beta\mu}+\partial_\beta F_{\mu\alpha}=0. \quad (7.105)$$

By substituting $(\mu,\alpha,\beta)=(0,i,j)$ and contracting with ϵ_{ijk}, we obtain Faraday's law

$$\mathbf{B}'+\nabla\times\mathbf{E}=0, \tag{7.106}$$

whereas doing $(\mu,\alpha,\beta)=(i,j,k)$ and contracting with ϵ_{ijk}, we complete our set of Maxwell equations in vacuum with Gauss's law for the magnetic field

$$\nabla\cdot\mathbf{B}=0. \tag{7.107}$$

For completeness' sake, we also have the conservation equations, which after substituting the equations of motion into them (see Eq. (7.103)) acquire the following form in the absence of currents:

$$\begin{aligned}(1-2f_1)[\mathbf{E}\cdot(\nabla\times\mathbf{B})+\mathbf{B}\cdot(\nabla\times\mathbf{E})]&\\ +\frac{a^2}{b^2}\mathbf{E}^2\left[\frac{a'}{a}\left(1-5f_1+6f_1^2-6f_2\right)+\frac{b'}{b}(1-3f_1+2f_1^2-2f_2)\right]&\\ +\mathbf{B}^2\left[\frac{a'}{a}\left(2-7f_1+6f_1^2+6f_2\right)+\frac{b'}{b}(-f_1+2f_1^2+2f_2)\right]=0,&\end{aligned} \tag{7.108a}$$

$$(1-2f_1)\nabla\left(\mathbf{E}^2-\frac{b^2}{a^2}\mathbf{B}^2\right)=0. \tag{7.108b}$$

Working with the equations in this form is rather complicated, so we might seek to eliminate the electric field from the equations of motion. We can easily do so by taking the curl of Ampère's law (7.104b) and using Faraday's law (7.106) in it, which leads us to an equation of motion for the magnetic field

$$\mathbf{B}''-\frac{b^2}{a^2}\nabla^2\mathbf{B}+\left[(6f_1-2)\frac{a'}{a}+(2f_1-2)\frac{b'}{b}\right]\mathbf{B}'=a^2b^2\nabla\times\mathbf{j}. \tag{7.109}$$

Working in Fourier modes and in the absence of external currents, we can analyse the super-Hubble regime ($\frac{b}{a}k\ll\frac{a'}{a},\frac{b'}{b}$), which features a straight-forward general solution for the magnetic field derivative provided a power-law $f(g)=g^\alpha$

$$\mathbf{B}_k'(\tau)\propto a^{2-6\alpha}(\tau)b^{2-2\alpha}(\tau). \tag{7.110}$$

Note, however, that if we require the electric field to be homogeneous as well, Faraday's law (7.106) necessarily implies $\mathbf{B}_k'=0$, as we already noted in Sec. 7.3.1.

Sub-Hubble regime

In order to analyse the sub-Hubble limit, in the absence of external currents, we cannot neglect the first derivative term in Eq. (7.109) straight away. Working with a power law $f(g)=g^\alpha$, we perform a change of function $\mathbf{B}_k(\tau)=a^{\frac{3}{2}-3\alpha}(\tau)b^{\frac{1}{2}-\alpha}(\tau)\hat{\mathbf{B}}_k(\tau)$

that eliminates the first derivative term. We also perform a change of variable to conformal time η, $\mathrm{d}\tau = \frac{a}{b}\mathrm{d}\eta$, which leaves the equation of motion as follows

$$\hat{\mathbf{B}}_k^{(2)} + \left(k^2 + \frac{1}{4}\left[3(2\alpha-1)(6\alpha-5)\left(\frac{a^{(1)}}{a}\right)^2 + 6(2\alpha-1)\left((2\alpha-1)\frac{a^{(1)}b^{(1)}}{ab} + \frac{a^{(2)}}{a}\right)\right.\right.$$
$$\left.\left. +(4\alpha(2-\alpha)-3)\left(\frac{b^{(1)}}{b}\right)^2 + 2(1-2\alpha)\frac{b^{(2)}}{b}\right]\right)\hat{\mathbf{B}}_k = 0, \quad (7.111)$$

where the superscript in parenthesis $a^{(n)}$ denotes the n-th derivative with respect to conformal time η. In the sub-Hubble limit, the term in square brackets can be ignored and this function admits an easy solution in terms of complex exponentials

$$\hat{\mathbf{B}}_k(\eta) = \mathbf{c}_1 e^{-ik\eta} + \mathbf{c}_1^* e^{ik\eta}, \quad (7.112)$$

where we have imposed that the field is real.

Reverting to the original variables, we have got

$$\mathbf{B}_k(\tau) = g^{(1-2\alpha)/4}\left(\mathbf{c}_1 e^{-ik\eta} + \mathbf{c}_1^* e^{ik\eta}\right), \quad \eta = \int^\tau \mathrm{d}s\,\frac{b(s)}{a(s)}, \quad (7.113)$$

and if we introduce this behaviour into the magnetic part of the energy density (7.101a) (the remaining exponentials can be integrated out thanks to rapid oscillation), we obtain for the average energy density

$$\langle \rho_B \rangle = \frac{f}{\sqrt{g}}\frac{f_1}{2a^4}\langle F_{ij}F_{ij}\rangle = g^{\alpha-1/2}\frac{\alpha}{a^4}\langle \mathbf{B}^2\rangle = \frac{2\alpha|\mathbf{c}_1|^2}{a^4}, \quad (7.114)$$

which scales exactly as in the Diff-invariant case. Thus, sub-Hubble modes behave as if the Diff-invariance had not been broken down to TDiff, a result that we revisit with the geometric optics approximation in what follows.

The same analysis can be performed in terms of the electric field instead of the magnetic field. If we take the curl of Faraday's law (7.106) and insert it into the time derivative of Ampère's law (7.104b), we obtain the following equation of motion for the electric field

$$\mathbf{E}'' - \frac{b^2}{a^2}\nabla^2\mathbf{E} + \left[6f_1\frac{a'}{a} + 2(f_1-2)\frac{b'}{b}\right]\mathbf{E}' + \left[2(3f_1+18f_2-1)\frac{a'^2}{a^2} + 2(3-3f_1+2f_2)\frac{b'^2}{b^2}\right.$$
$$\left. -8(f_1-3f_2)\frac{a'}{a}\frac{b'}{b} + 2(3f_1-1)\frac{a''}{a} + 2(f_1-1)\frac{b''}{b}\right]\mathbf{E} = 0. \quad (7.115)$$

By working in Fourier space, performing a change of function $E_k(\tau) = a^{-3\alpha+\frac{1}{2}}(\tau)$ $b^{-\alpha+\frac{3}{2}}(\tau)\hat{E}_k(\tau)$ and changing variable to conformal time η, the equation of motion has the following expression

$$\hat{\mathbf{E}}_k^{(2)} + \left(k^2 + \frac{1}{4}\left[(1-4\alpha^2)\left(\frac{b^{(1)}}{b}\right)^2 - 3(1-8\alpha+12\alpha^2)\left(\frac{a^{(1)}}{a}\right)^2 - 6(2\alpha-1)^2\frac{a^{(1)}}{a}\frac{b^{(1)}}{b}\right.\right.$$
$$\left.\left. +6(2\alpha-1)\frac{a^{(2)}}{a} + 2(2\alpha-1)\frac{b^{(2)}}{b}\right]\right)\hat{\mathbf{E}}_k = 0. \quad (7.116)$$

Again, we can neglect the whole term in square brackets in the sub-Hubble regime, and obtain a solution for the electric field in terms of complex exponentials

$$\hat{\mathbf{E}}_k(\eta) = \mathbf{c}_2 e^{-ik\eta} + \mathbf{c}_2^* e^{ik\eta}. \tag{7.117}$$

In terms of the original variables, we have got

$$\mathbf{E}_k(\tau) = g^{(1-2\alpha)/4}\frac{b}{a}(\mathbf{c}_2 e^{-ik\eta} + \mathbf{c}_2^* e^{ik\eta}), \quad \eta = \int^\tau \mathrm{d}s\, \frac{b(s)}{a(s)}, \tag{7.118}$$

which implies a typical radiation behaviour for the averaged electric part of the energy density (7.101a)

$$\langle \rho_E \rangle = \frac{f}{\sqrt{g}}\frac{1-f_1}{a^2 b^2}\langle F_{0i}F_{0i}\rangle = g^{\alpha-1/2}\frac{1-\alpha}{a^2 b^2}\langle \mathbf{E}^2\rangle = 2(1-\alpha)\frac{|\mathbf{c}_2|^2}{a^4}. \tag{7.119}$$

which again scales with the expansion as in the Diff case.

One last thing to note about these expressions is that, while the scaling is exactly as in the Diff-invariant case, the electric and magnetic fields have different shares of the total energy density, as they are weighed by factors $1-\alpha$ and α, respectively. However, Faraday's law imposes

$$\mathbf{c}_1 = \hat{\mathbf{k}} \times \mathbf{c}_2 \tag{7.120}$$

on the solutions we have just obtained for the electric and magnetic fields. Since the electric field is transverse, this implies $|\mathbf{c}_1| = |\mathbf{c}_2|$, so when computing the total electromagnetic energy density

$$\langle \rho_{\mathrm{EM}} \rangle = \langle \rho_E \rangle + \langle \rho_B \rangle = 2(1-\alpha)\frac{|\mathbf{c}_2|^2}{a^4} + 2\frac{\alpha|\mathbf{c}_1|^2}{a^4} = \frac{2|\mathbf{c}_1|^2}{a^4}, \tag{7.121}$$

the dependence on α cancels out and it does not depend on the TDiff function at all.

Geometric optics and the Bunch-Davies vacuum

In an expanding universe, the sub-Hubble regime corresponds in practice to the geometric optics approximation. The ansatz for the field is slightly less general, doing a pure plane wave expansion for the spatial part and separating spatial and temporal dependencies in the rapidly oscillating exponential

$$A_{\mu,k\lambda}(x) = U_{\mu,k\lambda}(x) e^{i\mathbf{k}\cdot\mathbf{x} - i\int^\tau \omega_k(\tau')\mathrm{d}\tau'}. \tag{7.122}$$

We can now use every result we obtained in Sec. 7.1.2 by identifying

$$\theta_{\mathbf{k}\lambda}(x) = \mathbf{k}\cdot\mathbf{x} - \int^\tau \omega_k(\tau')\,\mathrm{d}\tau' \tag{7.123}$$

and

$$k_\mu = \partial_\mu \theta = (-\omega_k, \mathbf{k}). \tag{7.124}$$

The Lorentz gauge condition (7.15) now reads

$$a^2\omega_k U_\tau + b^2\mathbf{k}\cdot\mathbf{U} = 0, \tag{7.125}$$

and the equation of motion (7.17) gives us the usual dispersion relation of a massless field

$$\omega_k^2 = \frac{b^2}{a^2}\mathbf{k}^2. \tag{7.126}$$

The normalisation of the amplitude U_μ can be obtained either from the next-to-leading order equation or the inner product normalisation condition. We use the later method, as we already have a final expression in Eq. (7.46). With a RW background, the normal vector has to be $n_\mu = (b, \mathbf{0})$, so we easily obtain

$$A_{\mu,k\lambda}(x) = \sqrt{\frac{b^2}{2f\omega_k}}u_\mu e^{i\mathbf{k}\cdot\mathbf{x} - i\int^\tau \omega_k(\tau')\mathrm{d}\tau'} \tag{7.127}$$

for a positive-frequency mode, with $u_\mu k^\mu = 0$ and $u_\mu^* u^\mu = -1$.

Choosing the positive-frequency modes in (7.28) so that, in the sub-Hubble regime, they are given by Eq. (7.127), we define the Bunch-Davies vacuum $|0\rangle$ as

$$a_{\mathbf{k}\lambda}|0\rangle = 0, \quad \forall \mathbf{k}, \lambda. \tag{7.128}$$

Using these expressions for the modes of the vector field in computing the vacuum expectation value of the energy density (7.101a), one can find $\langle\rho\rangle \propto a^{-4}$. Again, the dynamics in the geometric optics approximation are equivalent to those in a Diff-invariant scenario, so breaking down to TDiff invariance does not disturb the well-settled dynamics on short scales.

7.4 TDiff-enhanced magnetic fields

Breaking Diff invariance in the electromagnetic sector also breaks conformal invariance. This could in principle look like an issue, but it turns out to be a feature that we can exploit to obtain sizeable primaeval magnetic fields, as pointed out in [TW88]. Maxwell's electrodynamics in a Robertson-Walker background is a conformally trivial theory. This means that magnetic fields cannot be generated from quantum fluctuations during inflation, and in addition, any magnetic field dilutes as $\rho_B \propto a^{-4}$ with the expansion of the universe. Conformal invariance violation allows to produce magnetic fields during inflation, and on top of that, they do not necessarily need to evolve as in standard electromagnetism. Therefore, larger values of the magnetic field could be obtained today with a standard inflationary model. The observational constraints of intergalactic magnetic fields were discussed in Sec. 1.5.

7.4.1 Magnetic power spectrum

In what follows, we will obtain the power spectrum of the magnetic field that arises as quantum fluctuations during inflation. The solution of the modes in Eq. (7.127) is valid for the quantisation during the sub-Hubble regime, so it suffices to compute the vacuum expectation value $\langle \rho_B \rangle$. The magnetic power spectrum $\rho_B(k)$ is defined as the energy density per log interval as usual, so that

$$\langle \rho_B \rangle = \int \frac{\mathrm{d}k}{k} \rho_B(k), \tag{7.129}$$

with the total magnetic energy density as the magnetic part in Eq. (7.101a), which in terms of the strength tensor is

$$\rho_B = \frac{f}{\sqrt{g}} \frac{f_1}{2a^4} F_{ij} F_{ij}. \tag{7.130}$$

Using the complete expression for the vector field (7.28), with $A_{\mu,k\lambda}$ given by the geometric optics solution (7.127), the field strength has the following form

$$F_{ij}(x) = \int \frac{\mathrm{d}^3\mathbf{k}}{(2\pi)^{3/2}} \sum_\lambda \left[a_{\mathbf{k}\lambda} (ik_i A_{j,k\lambda} - ik_j A_{i,k\lambda}) + a^\dagger_{\mathbf{k}\lambda} (-ik_i A^*_{j,k\lambda} + ik_j A^*_{i,k\lambda}) \right]. \tag{7.131}$$

When computing the magnetic energy density and taking the vacuum expectation value, only the term with $\langle a_{\mathbf{k}\lambda} a^\dagger_{\mathbf{k}'\lambda'} \rangle = \delta^{(3)}(\mathbf{k} - \mathbf{k}') \delta_{\lambda\lambda'}$ contributes. Doing so, and dropping the $k\lambda$ subindices to alleviate the notation, we have

$$\langle \rho_B \rangle = \int \frac{\mathrm{d}^3 k}{(2\pi)^3} \frac{f}{\sqrt{g}} \frac{f_1}{a^4} \sum_\lambda (k^2 \mathbf{U} \cdot \mathbf{U}^* - |\mathbf{k} \cdot \mathbf{U}|^2). \tag{7.132}$$

We can now use the gauge condition (7.125) and the dispersion relation (7.126) to obtain

$$|\mathbf{k} \cdot \mathbf{U}|^2 = \frac{a^4}{b^4} \omega^2 U_0 U_0^* = \frac{a^2}{b^2} k^2 U_0 U_0^*. \tag{7.133}$$

Introducing this in the previous expression, we have

$$\langle \rho_B \rangle = \int \frac{\mathrm{d}^3 k}{(2\pi)^3} \frac{f}{\sqrt{g}} \frac{f_1}{a^4} \sum_\lambda k^2 \left(\mathbf{U} \cdot \mathbf{U}^* - \frac{a^2}{b^2} U_0 U_0^* \right). \tag{7.134}$$

Note that the term in parenthesis can be identified as $-a^2 U^*_\mu U^\mu$, so using the normalisation of the vector field (7.127), trivially summing over polarisations and integrating the angular part, we obtain

$$\langle \rho_B \rangle = \int \frac{\mathrm{d}k}{k} \frac{f_1}{2\pi^2} \frac{k^4}{a^4}, \tag{7.135}$$

so we finally identify the magnetic power spectrum

$$\rho_B(k) = \frac{f_1}{2\pi^2} \frac{k^4}{a^4}. \tag{7.136}$$

Following the same procedure, one can obtain the following expression for the electric power spectrum

$$\rho_E(k) = \frac{1-f_1}{2\pi^2}\frac{k^4}{a^4}. \tag{7.137}$$

There are several important things to note about these expressions. These energy densities scale as a^{-4}, as we would expect for a free vector field that behaves like radiation. Again, this agrees with the fact that, in the sub-Hubble regime and when the geometric optics approximation is applicable, the phenomenology of a TDiff-invariant field is analogous to its Diff-invariant counterpart. The total energy density (i.e. the sum of the electric and magnetic contributions) is independent of the TDiff aspect of the theory, as the factors f_1 cancel out. However, when considering the electric and magnetic fields separately, the different multiplicative factors in the energy density mean that they gravitate differently even in the geometric optics approximation, except in the Diff-invariant scenario, as we discussed in Sec. 7.3.2.

On a different note, at the moment of horizon crossing $k = aH$, which is the very last moment when the sub-Hubble regime can be applied, the power spectrum $\rho_B(k) \sim H_I^4$, which is nearly scale-invariant in a typical inflationary scenario. The fraction of energy density stored in a mode at horizon crossing is then

$$\frac{\rho_B(k)}{\rho_{\text{tot}}} \sim \left(\frac{H_I}{M_P}\right)^2 \sim \frac{\rho_I}{M_P^4}, \tag{7.138}$$

where ρ_I is the energy density of the inflaton (3.21).

7.4.2 Power spectrum evolution

After the first horizon crossing, which happens during inflation, the mode enters the super-Hubble regime, where the combination $F_{ij}F_{ij}$ becomes constant, as discussed in Sec. 7.3.1, so the energy density (as well as the power spectrum) scales as

$$\rho_B \propto \frac{f}{a^4\sqrt{g}} = \frac{f}{ba^7}. \tag{7.139}$$

In order to study the evolution of the power spectrum we can, for each mode, take its value at the first horizon crossing and then match it with the super-Hubble scaling until the mode reenters the horizon later on. The only thing remaining for this calculation is substituting the lapse function in terms of the scale factor $b = b(a)$, which turns out to be slightly more problematic than what one could expect.

Energy conservation

Let us look back at the conservation of the stress-energy tensor by retaking the conservation condition having both electric and magnetic field (7.99). There are two main caveats in using this expression: On the one hand, this condition takes into account only the super-Hubble part of the spectrum, which typically is receiving energy

from the sub-Hubble part as modes exit the horizon, so even if the later is conserved due to its Diff behaviour, they cannot be analysed separately. On the other hand, it depends on the electric and magnetic field intensities, unlike the purely electric or magnetic conditions, which do not depend on either amplitude, so in principle the complete condition does not allow to obtain a functional form for $b(a)$ independently of the fields. However, we show in the following that, in the regimes we are interested in, it is not necessary to use the complete electromagnetic condition.

For the super-Hubble regime, using the expressions we obtained in Sec. 7.3.1 into Eq. (7.101a), we can write

$$\rho_E = g^{\alpha-1/2}(1-\alpha)\frac{1}{a^2b^2}E_0^2 a^{4-12\alpha}b^{4-4\alpha}, \tag{7.140a}$$

$$\rho_B = g^{\alpha-1/2}\frac{\alpha}{a^4}B^2. \tag{7.140b}$$

Evaluating the ratio at horizon crossing and equating it to the sub-Hubble ratio, we obtain

$$\frac{E_0^2}{B^2} = g_k^{2\alpha-1}, \tag{7.141}$$

with $g_k = g(a_k, b_k)$. Therefore, the electromagnetic energy conservation condition does depend on the mode we are dealing with for $\alpha \neq 1/2$, as it becomes

$$C_{EM}a^4 = g^\alpha\left[1-2\left(\frac{g}{g_k}\right)^{1-2\alpha}\right]. \tag{7.142}$$

For a single mode in the super-Hubble regime, the ratio between electric and magnetic energy densities, using the ratio (7.141), can be written as

$$\left.\frac{\rho_E(k)}{\rho_B(k)}\right|_{\text{super-Hubble}} = \frac{1-\alpha}{\alpha}\left(\frac{g}{g_k}\right)^{1-2\alpha}. \tag{7.143}$$

Here we can see that, for each mode and $\alpha \neq 1/2$, either the electric or magnetic energy density is going to dominate not long after the mode crosses the horizon. In fact, when a mode crosses the horizon, there is already a collection of super-Hubble modes, for which the electric or magnetic energy density already dominates. Therefore, we can safely assume that the super-Hubble contribution to one of the energy densities is going to be much larger than the other one. Thus, we can use the conservation equations as if there were only electric or magnetic field, depending on which one dominates. Since this discussion only applies to a power-law $f(g)$, we need to use the power-law conditions, given by Eq. (7.78) for electric domination and Eq. (7.86) for magnetic domination.

The conditions for either domination are listed below:

$$|\rho_E| \gg |\rho_B| : \begin{cases} g' > 0 & \text{and} \quad \alpha < 1/2 \\ g' < 0 & \text{and} \quad 1/2 < \alpha < 1 \text{ or } \alpha > 1 \end{cases}$$

$$|\rho_B| \gg |\rho_E| : \begin{cases} g' > 0 & \text{and} \quad \alpha > 1/2 \\ g' < 0 & \text{and} \quad 0 < \alpha < 1/2 \text{ or } \alpha < 0 \end{cases}$$

We have taken absolute values as values $\alpha > 1$ ($\alpha < 0$) yield a negative electric (magnetic) energy density, which is not an issue provided that the negative energy density is subdominant. Therefore, the scenarios marked in red must be avoided, as the dominant component has a negative energy density. We discuss each case separately as follows:

- Electric domination: If the electric energy density dominates, the energy conservation yields $b \propto a^{(3\alpha-1)/(1-\alpha)}$, so the metric determinant $g = b^2 a^6 \propto a^{4/(1-\alpha)}$, which satisfies $g' > 0$ if $a' > 0$ (expanding universe) and $\alpha < 1$. Therefore, considering the electric condition only is correct for expanding universes and $\alpha < 1/2$. In this case, the energy densities scale as $\rho_E \propto a^{2/(\alpha-1)}$ and $\rho_B \propto a^{-8-2/(\alpha-1)}$. Note that the sum of the exponents of both scale factors is constant and independent of α, $\rho_E \rho_B \propto a^{-8}$, so the more that the electric field dominates, the more subdominant the magnetic field is.

- Magnetic domination: If the magnetic energy density dominates, the energy conservation yields $b \propto a^{(2-3\alpha)/\alpha}$, so the metric determinant $g = b^2 a^6 \propto a^{4/\alpha}$, which satisfies $g' > 0$ if $a' > 0$ (expanding universe) and $\alpha > 0$. Therefore, considering the magnetic condition only is correct for expanding universes and $\alpha > 1/2$. In this case, the energy densities scale as $\rho_E \propto a^{2/\alpha-8}$ and $\rho_B \propto a^{-2/\alpha}$. Note that, again, the sum of the exponents of both scale factors is constant and independent of α, $\rho_E \rho_B \propto a^{-8}$, so now the more that the magnetic field dominates, the more subdominant the electric field is.

Since we are interested in primaeval magnetic field amplification, in what follows we consider the range of magnetic domination $\alpha > 1/2$, which will allow us to use the magnetic condition for energy conservation.

Conductivity

There is one more detail that might affect the equations of motion of the electromagnetic field which we need to examine. Up to this point, we have only considered the free electromagnetic field in an expanding universe, without any coupling to an external current. This does not need to be the case, as for most of the known thermal history of the Universe there has been a large density of electrically charged particles, which results in a Universe featuring a large conductivity σ_c. In order to account for this fact, we introduce in Maxwell's equations (7.104) a current proportional to the electric field as per Ohm's law, following [TW88]

$$j^\mu - u^\mu u_\nu j^\nu = \sigma_c F^{\mu\nu} u_\nu, \tag{7.144}$$

which reduces to $j^i = b\sigma_c F^{i0}$ for a neutral plasma $u_\mu j^\mu = 0$. This introduces a term in the right-hand side of the magnetic field equation of motion (7.109)

$$\mathbf{B}'' - \frac{b^2}{a^2}\nabla^2\mathbf{B} + \left[(6f_1-2)\frac{a'}{a} + (2f_1-2)\frac{b'}{b}\right]\mathbf{B}' = -b\sigma_c\mathbf{B}'. \tag{7.145}$$

A very high conductivity $\sigma_c \to \infty$ requires the magnetic field to be constant $\mathbf{B}' \to 0$, which makes the magnetic field behave as in the super-Hubble regime. This applies also in the sub-Hubble regime as long as $a\sigma_c \gg k$, which can be identified as the overdamped regime.

Following this, we discuss now the phenomenology originated by conductivity [TW88]. We are interested in magnetic fields of comoving size $\lambda = 2\pi/k \gtrsim 0.1$ Mpc, so we shall estimate whether conductivity dominates before the present moment. As commented before, this discussion matters for sub-Hubble modes only, because both super-Hubble and high-conductivity regimes exhibit the same behaviour. As a result, we can skip the discussion on modes that enter the horizon during reheating, as modes featuring such short wavelengths are irrelevant in the context of cosmological magnetic fields.

Starting at some point during reheating and continuing during the radiation-dominated era, conductivity is very high before electron-positron annihilation at $T_{\rm ann} = m_e = 0.5$MeV, due to the large density of electrically charged particles. After annihilation, only one over 10^{10} electrons per photon survive, so the conductivity drops to $\sigma_c \sim 10^{-10} m_e/e^2 \sim 10^{-9} m_e$. Here, the charge of the electron $e^2 = 4\pi\alpha \simeq 4\pi/137 \sim 1/10$, with $\alpha \simeq 1/137$ the fine structure constant. We compare this value to the wavenumber of modes that enter the horizon in this period

$$\left.\frac{\sigma_c}{k/a}\right|_{\rm sub-Hubble} \gtrsim \frac{\sigma_c}{(k/a)_{\rm ann}} = \frac{\sigma_c}{H_{\rm ann}} \sim \frac{\sigma_c}{T_{\rm ann}^2/M_P} \sim 10^{13} \gg 1, \tag{7.146}$$

so conductivity stays high during the RD era.

During the matter-dominated era, after matter-radiation equality $a > a_{\rm eq} \simeq 1/3400$, conductivity drops again after recombination, as only about 1 in 10^3 electrons do not combine to form neutral hydrogen, so now $\sigma_c \sim 10^{-12} m_e$. Evaluating the ratio

$$\left.\frac{\sigma_c}{k/a}\right|_{\rm sub-Hubble} \gtrsim \frac{\sigma_c}{(k/a)_{\rm eq}} = \frac{\sigma_c a_{\rm eq}}{k_{\rm eq}} \sim 10^{22} \gg 1, \tag{7.147}$$

where $k_{\rm eq} = 0.01{\rm Mpc}^{-1}$ is the mode that enters the horizon at matter-radiation equality. As a result, for the modes we are interested in, it is safe to assume that the Universe has been highly conducting since some point during reheating until the present time.

Power spectrum today

Following Fig. 7.1, let us review the complete evolution of the energy density of a mode $\rho_B(k)$. During inflation, the fluctuations of the magnetic field get excited, which

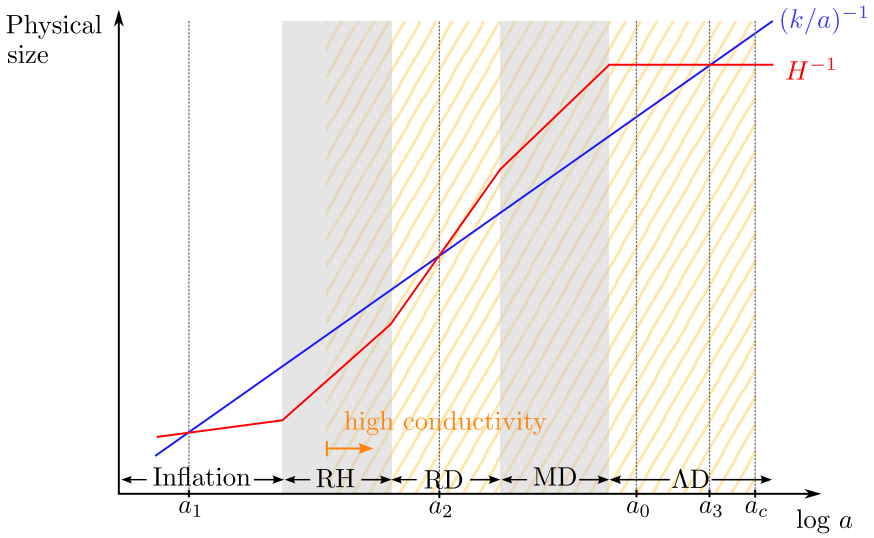

Figure 7.1: Evolution of the Hubble radius (in red) and the wavelength of a mode with comoving wavenumber k (in blue). The striped yellow region corresponds to a high conductivity period, which starts during reheating and ends at scale factor a_c. Scale factors for n-th horizon crossing a_n and today a_0 are also labelled.

acquire the following value at the first horizon crossing $a = a_1 = k/H_I$ in terms of the energy density (7.136)

$$\rho_B(k)\big|_{a=a_1} = \rho_B(k = aH) = \frac{\alpha}{2\pi^2} H_I^4. \tag{7.148}$$

Then, if the magnetic field dominates over the electric field, this energy density evolves as $\rho_B \propto a^{-2/\alpha}$, with $\alpha > 1/2$. This scaling holds if at least one of the following conditions is satisfied:

1. The mode is super-Hubble, which is satisfied until the mode re-enters the horizon at a second crossing at $a = a_2$.

2. The Universe is highly conductive $a\sigma_c \gg k$. Following the previous discussion, the Universe is highly conductive until $a_c \gg 1$.

As a result of the high conductivity, this scaling holds for the whole evolution of the mode since it first left the horizon, so we just need to evaluate it at the moment a we are interested in. Scaling the energy density, we have

$$\rho_B(k) = \frac{\alpha}{2\pi^2} H_I^4 \left(\frac{k}{aH_I}\right)^{2/\alpha}, \tag{7.149}$$

with the particular case $a = a_0 = 1$ for the energy density today. We can also define the magnetic power spectrum as

$$P_B(k) = \frac{2\pi^2}{k^3}\rho_B(k) \propto k^{\frac{2}{\alpha}-3}, \tag{7.150}$$

which displays a tilt

$$n_B = \frac{2}{\alpha} - 3 \tag{7.151}$$

in the range $-1 \leq n_B \leq 1$ for $1/2 \leq \alpha \leq 1$, and also the magnetic field intensity today at a certain scale λ, which follows from (7.136)

$$B_\lambda = \sqrt{\frac{\rho_{B,0}(k)}{\alpha}}\Bigg|_{k=\frac{2\pi}{\lambda}}. \tag{7.152}$$

By substituting the energy density, one can obtain the following expression

$$B_\lambda = \frac{1.3\,\mu\text{G}}{(2.5\times 10^{50})^{(1-\alpha)/\alpha}}\left(\frac{H_I}{10^{13}\text{GeV}}\right)^{(2\alpha-1)/\alpha}\left(\frac{\text{Mpc}}{\lambda}\right)^{1/\alpha}, \tag{7.153}$$

which allows for values of the magnetic field of the order of the μG at galactic scales near $\alpha \simeq 1$. These expressions encapsulate the following features of the magnetic power spectrum:

1. The spectrum can be either red or blue-tilted, with $-1 \leq n_B \leq 1$ for the range $\frac{1}{2} \leq \alpha \leq 1$.

2. The energy density depends on the inflation scale as $\rho_B \propto H_I^{4-2/\alpha}$, so it grows larger for higher scales of inflation. On top of that, the larger α is, the more it grows with the inflation scale. This is depicted in Fig. 7.2.

3. The magnetic field intensity is enhanced for larger α, which is caused by the ratio k/H_I being typically very small. This can be seen also in Fig. 7.2.

In Fig. 7.2, we plot the predicted magnetic field intensity today for a coherence scale of $\lambda = 1$Mpc together with the current large-scale bounds on IGMF, which were discussed in Sec. 1.5. We see that a TDiff-invariant electromagnetic sector can reproduce the expected values for IGMF with a minimal inflationary sector, provided a TDiff parameter $\alpha \gtrsim 0.8$ and a sufficiently energetic inflation.

The lower bound in Fig. 7.2 is given by blazar observations by Fermi/LAT, which are low-redshift events, so we can directly impose the standard bounds into our model. The upper bound, however, comes from limits on CMB anisotropies which have been scaled up to today $\rho_B^{\text{CMB}} = \rho_{B,0}a_{\text{CMB}}^{-4}$. Since the magnetic energy density scales differently in our model $\rho_B^{\text{CMB}} = \rho_{B,0}a_{\text{CMB}}^{-2/\alpha}$, we need to adapt the bound in order to reflect the different dilution between the CMB and the present time. Moreover, these CMB bounds depend on magnetic power spectrum tilt, which is related to our parameter

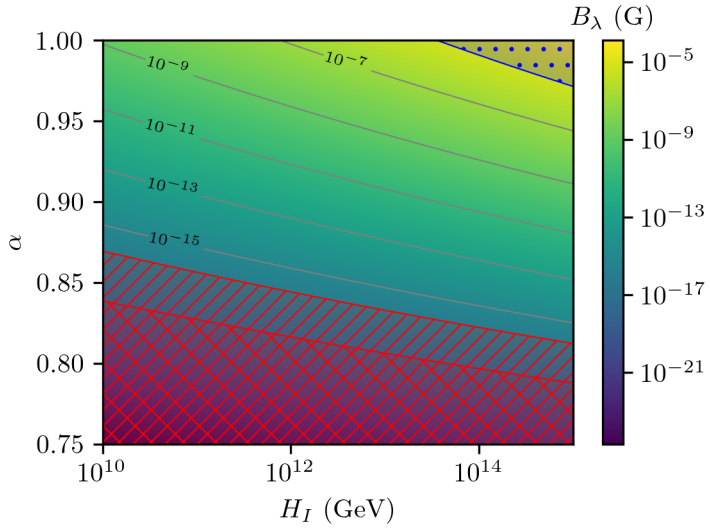

Figure 7.2: Magnetic field intensity B_λ today (in Gauss) for a mode of wavelength $\lambda = 1$Mpc, as a function of the inflation scale H_I and the TDiff function exponent α. The upper right blue dotted region indicates the region excluded by large-scale CMB observations. The bottom red striped region corresponds to values $B_{1\text{Mpc}} \lesssim 10^{-16}$ and $B_{1\text{Mpc}} \lesssim 10^{-18}$ G, excluded by blazar observations, depending on whether the least conservative bound is chosen or not, respectively (see Sec. 1.5 for details). We do not plot all values down to $\alpha = 1/2$ as they are excluded by blazar observations.

α (7.151). In [PF11], the dependence of tilt in the CMB bounds was examined, which showed that blue-tilted power spectra are more restricted. In particular, they found $B_{1\text{Mpc}} \lesssim 1$ nG for $n_B = 1$ and $B_{1\text{Mpc}} \lesssim 6$ nG for $n_B = -1$ at 2σ level, with a somewhat linear regression between the two of them. We have translated these limits when computing the CMB limits in our plot. The maximum value that a TDiff-invariant electromagnetic sector can produce in the $1/2 < \alpha \leq 1$ range and that is compatible with the CMB bound is $B_{1\text{Mpc}} = 2.6\mu$G for $\alpha = 1$, which is of the order of observed galactic magnetic fields.

III

Conclusions and appendices

Concluding remarks

In what follows, we draw the conclusions of the three blocks of this thesis, each of which has allowed us to find new phenomenology beyond the standard cosmological picture:

- GRAVITATIONAL LEPTOGENESIS FROM METRIC PERTURBATIONS. We have analysed the baryon asymmetry produced by gravitational leptogenesis during reheating with a minimal inflationary model, without the need to add new axial couplings. This mechanism operates within standard cosmology and is capable of generating a sizeable asymmetry at a local level for high inflation scales and stiff reheating equations of state. However, when considering the weighed variance over cosmological distances, the magnitude of the asymmetry is much smaller than the observed one. Due to Silk diffusion, the typical size of matter-antimatter regions is about the Silk length at confinement.

  We have considered simple power laws for the scalar and tensor primordial spectra in the whole range of scales with the amplitudes and spectral indices measured from CMB observations. However, as shown in (5.24), the produced lepton density depends on the values of the power spectra at the k_I scale, which can be separated from the scales measured in the CMB by many orders of magnitude. This means that a possible running of the spectral indices could affect the predictions of the model. An interesting possibility would be the presence of features in the scalar power spectrum at small scales. In particular, it has been shown that the presence of (broad) peaks could play an important role in the generation of primordial black holes after inflation [CG15]. Gravitational leptogenesis with features in the scalar power spectrum and scalar-induced gravitational waves was considered in [AR23], showcasing a small enhancement of leptogenesis versus the flat power spectrum.

  The lepton-to-entropy ratio strongly depends on the equation of state during the reheating phase and stiff equations enhance the generated asymmetry. This possibility has been recently discussed in [Kam+20] where kination-dominated reheating scenarios [Spo93] have been considered. An interesting consequence of early phases with a stiff equation of state is the generation of a blue tilt in the transfer function of tensor modes [FT19] which could render the primordial gravitational wave background observable for the sensitivity and frequency range of future detectors such as LISA, Einstein Telescope or Cosmic Explorer. Even when considering the *rms* fluctuation at Silk scale, which eliminates the explicit dependency on the inflation scale, both a kination phase and the presence of fea-

tures in the power spectra introduce a dependency on the particular inflationary scenario.

Even though primordial metric perturbations do not seem to be able to generate the observed homogeneous asymmetry on Hubble scales, the produced baryon asymmetry could in principle act as a source of baryonic isocurvature perturbations. However, according to the obtained results, these perturbations would be very small for observable scales. Finally, let us mention that beyond the linear regime, gravitational lepton generation in chiral astrophysical systems could also provide potential experimental ways to test the leptogenesis mechanism discussed in this work.

- VECTOR FIELDS AND GRAVITATIONAL-WAVE PROPAGATION. We have studied coherent vector fields in an expanding universe, which play the role of matter and radiation components in the dark sector. We have analysed their effect on GW propagation and, in particular, on the primordial GW background generated during inflation. We observe a suppression of the primordial GW background in some frequency bands due to the effect of the vector field, which is mostly relevant while the GW mode is super-Hubble, as the sub-Hubble propagation is identical to standard cosmology. The suppression in GW intensity exhibits an anisotropic pattern determined by the direction of the vector field. The effect on GWs with astrophysical origin is negligible.

  For ultralight vector fields, which are suitable dark matter candidates, the suppression occurs as long as the GW mode enters the Hubble horizon after the ULVF starts behaving as matter, which happens for long-wavelength modes. This suppression is anisotropic and is maximized for GWs propagating orthogonally to the direction of the background vector field. We infer from the tensor power spectrum at decoupling time that the effects of ULVF dark matter could be significant enough to be detectable for masses near the lower bound of $m \sim 10^{-27}$ eV. This mass has an associated de Broglie wavelength of astrophysical size, and as a result, it is not suitable for describing the totality of the dark matter abundance but a part of it. It is also interesting to explore the possibilities to generate the ULVF dark matter abundance by different suitable mechanisms such as misalignment [NS11] whilst avoiding suppression during inflation.

  In the case of vector dark radiation, we have computed the Stokes parameters for the primordial GW background today, assuming it was initially Gaussian, isotropic and unpolarised. In the two studied cases (linearly and circularly polarised vector field), we find that a net linear polarisation is generated, mainly due to the different damping of each of the two linear polarisations, which is observed on even multipoles only. A linearly polarised vector field causes a larger suppression of the polarisation that is more aligned with the direction at which it points, but not a mixing between + and × modes, thus generating

only Q polarisation of the GW. In the case of the rotating vector field, there is also a mixing between + and × modes so that both Q and U polarisations with an anisotropic pattern are generated. Since U is produced by the mixing of + and × polarisations, it contains odd multipoles only. This polarisation generation is especially important at large scales. We have also studied the case of a background which is initially totally polarised with pure linear polarisation. We have found that for a circularly polarised vector field, net GW circular polarisation is produced for modes with wavelengths initially comparable to the size of the Hubble horizon.

The presence of either the ultralight vector field or the vector dark radiation would result in a modification of the low-multipole CMB B-mode signal. The B mode is expected to be measured by the next generation of CMB experiments, as we discussed in Sec. 4.1. With the forecast sensitivity of future CMB experiments, we expect that the effects resulting from ULVF, in the aforementioned cases, and vector dark radiation would be measurable, mainly as an angular modulation of the tensor power spectrum, in the low multipole range. A more detailed study of these effects would require the computation of the complete B-mode power spectrum, which could be obtained by the modification of any of the already existing Boltzmann codes, such as CLASS [BLT11], in order to include the ULVF in the background and metric perturbation equations. With the B-mode power spectrum at hand, one could determine if the deviations from ΛCDM that we have predicted in this work are large enough to be distinguishable in CMB measurements by direct comparison.

Although it is possible to detect the polarisation of a GW stochastic background with interferometers [KS16; Dom+20; SK22], the typical frequency range covered by this type of detector is far away from those in which linear GW polarisation is generated. However, the resonances observed in the Q and U parameters in the dark radiation case appear in the detectable frequency range for certain values of the vector field oscillation frequency, although for typical primordial power spectra, the corresponding amplitude would be negligibly small.

Finally, let us briefly discuss neutrino free streaming, which we introduced in Sec. 4.2. Decoupled neutrinos induce a suppression in the amplitude of GWs ranging from 5% to 20% for the modes that enter the Hubble horizon well after the neutrinos decouple from the photons, which corresponds to scales $k \ll (10^{-4}\mathrm{Mpc})^{-1}$. Although the neutrino-induced damping is degenerate in this wavenumber region with the monopole suppression produced by the vector field, it does not feature an anisotropic suppression nor a polarisation generation of the gravitational wave background and could be observationally disentangled.

- TDIFF-INVARIANT VECTOR FIELD THEORY. In this work, we have studied the dynamics of Abelian gauge fields which break diffeomorphism invariance down to

transverse diffeomorphisms. We have shown that in the geometric optics approximation, very much as for Diff invariant theories, the corresponding massless gauge bosons propagate along null geodesics and particle number is conserved. In addition, the polarisation vectors are orthogonal to the propagation direction and the physical (transverse projection) polarisation is parallel transported along the geodesics. We have also studied the coupling to TDiff invariant Dirac spinors. We conclude that in order to avoid violations of Einstein's Equivalence Principle i.e. either Weak Equivalence Principle violations or violations of Local Position Invariance, the breaking of Diff invariance should be introduced by the same global $f(g)$ function for all the different fields. In this case, we recover the standard expressions for the Maxwell and Lorentz-Dirac equations.

We have also analysed the contributions to the energy-momentum tensor of the gauge fields. We find that, in general, the breaking of Diff invariance makes the electric and magnetic parts of the vector field gravitate in a different way. In the sub-Hubble regime, we recover the standard radiation-like behaviour of the energy density. However, in the super-Hubble regime, the behaviour is completely different to the Diff case, thus opening up a wide range of possibilities for cosmological model building. On the one hand, very much as in the scalar case, the different type of evolution of the homogeneous vector fields makes these theories a useful tool for the construction of models for the dark or the inflationary sectors. On the other hand, for certain $f(g)$, the magnetic energy density dilutes more slowly with the expansion due to the breaking of conformal invariance, thus effectively amplifying the magnetic fields compared to the standard Diff evolution. This type of effect allows us to obtain sizeable primaeval intergalactic magnetic fields excited in a minimal inflationary sector, which for certain values of a power-law $f(g)$ fulfil current observational constraints on IGMFs.

A Notation and conventions

- We use units in which $\hbar = c = k_B = 1$. Most unit conversions and values of constants in different units have been borrowed from the resourceful Appendix A in [KT90].

- We define Planck's mass as $M_P = G^{-1/2} = 1.2211 \times 10^{19}$ GeV, with G Newton's gravitational constant.

- "Standard Model", written in capital letters, refers to the Standard Model of particle physics. The word "Universe", written with capital U, refers to our particular Universe, whereas "universe" implies a general realisation.

- The natural logarithm is denoted log.

- Greek letters run over space-time indices $\mu, \nu, \cdots = 0, 1, 2, 3$, while Latin letters run over spatial indices $i, j, \cdots = 1, 2, 3$. Latin letters $a, b, \ldots$ are used in the context of a *vierbein* only and refer to flat indices. Spatial vectors are denoted in bold, so that $\mathbf{v}$ is the spatial part of v, whose components are v_i or v^i depending on its definition. Unit spatial vectors are denoted with a hat $\hat{\mathbf{v}} = \mathbf{v}/|\mathbf{v}|$.

- We use the mostly-minus signature $\eta_{\mu\nu} = \text{diag}(+, -, -, -)$. Geometry-related objects follow the definitions of [MTW73] and are listed in Appendix C.

- We define $\epsilon_{0123} = +1$ as the totally antisymmetric symbol. $\varepsilon_{\mu\nu\rho\sigma} = \sqrt{g}\epsilon_{\mu\nu\rho\sigma}$ is the Levi-Civita pseudotensor, with $g = \left|\det g_{\mu\nu}\right|$.

- Partial derivatives are denoted ∂ or with a colon ,. Covariant derivatives are denoted ∇ or with a semicolon ;. Further covariant derivatives specific to a spin connection are detailed in Appendix D.

- Derivatives with respect to cosmological time t are denoted with an overdot $\dot{a}$. Derivatives with respect to other time coordinates are indicated with a prime a'. Derivatives of a function with respect to its argument are also denoted with a prime, such as in $V'(\phi)$.

- Symmetrisation is defined with the symmetry factor

$$T_{(\mu\nu)} = \frac{1}{2}(T_{\mu\nu} + T_{\nu\mu}), \quad T_{[\mu\nu]} = \frac{1}{2}(T_{\mu\nu} - T_{\nu\mu}). \tag{A.1}$$

- The convention for Fourier transforms is

$$\tilde{f}(k) = \int \frac{\mathrm{d}x}{\sqrt{2\pi}} f(x) e^{-ikx}, \quad f(x) = \int \frac{\mathrm{d}k}{\sqrt{2\pi}} \tilde{f}(k) e^{ikx}, \tag{A.2}$$

  and in most cases, we will drop the tilde.

- An integral definition of the one-dimensional Dirac delta is

$$\delta(x) = \int \frac{\mathrm{d}k}{(2\pi)^3} e^{ikx}. \tag{A.3}$$

List of acronyms

ΛCDM	Lambda-cold dark matter
BBN	Big Bang nucleosynthesis
BH	black hole
CDM	cold dark matter
CMB	cosmic microwave background
Diff	diffeomorphism
DM	dark matter
DR	dark radiation
EW	electroweak
GR	general relativity
GW	gravitational wave
HDM	hot dark matter
IGMF	intergalactic magnetic field
LLI	local Lorentz invariance
LPI	local position invariance
MD	matter-dominated
MHD	magneto-hydrodynamics
NFW	Navarro-Frenk-White
NS	neutron star
PTA	pulsar timing array
QCD	quantum chromodynamics
RD	radiation-dominated
RH	reheating
RW	Robertson-Walker
SM	standard model
SNIa	type Ia supernova
TDiff	transverse diffeomorphism

TT	transverse-traceless
ULVF	ultralight vector field
UV	ultraviolet
WEP	weak equivalence principle
WKB	Wentzel–Kramers–Brillouin

B Special functions

Most formulae in this Appendix are borrowed from [AS65].

B.1 Bessel Functions

Bessel functions of first kind $J_\nu(x)$ and of second kind $Y_\nu(x)$ of order ν are two families of functions that solve Bessel's equation

$$x^2\frac{\mathrm{d}^2y}{\mathrm{d}x^2}+x\frac{\mathrm{d}y}{\mathrm{d}x}+(x^2-\nu^2)y=0. \tag{B.1}$$

Recurrence relations

$$J_{\nu-1}(x)+J_{\nu+1}(x)=\frac{2\nu}{x}J_\nu(x), \tag{B.2}$$

$$J_{\nu-1}(x)-J_{\nu+1}(x)=2J'_\nu(x), \tag{B.3}$$

also valid for Y_ν.

Asymptotic forms at $|x|\to 0$ and fixed ν

$$J_\nu(x)\sim\left(\frac{z}{2}\right)^\nu\Gamma(\nu+1)\quad(\nu\neq-1,-2,\dots), \tag{B.4}$$

$$Y_\nu(x)\sim-\frac{\Gamma(\nu)}{\pi}\left(\frac{2}{z}\right)^\nu,\quad(\mathrm{Re}\,\nu>0), \tag{B.5}$$

$$Y_0(x)\sim\frac{2}{\pi}\log z, \tag{B.6}$$

Asymptotic forms at $|x|\to\infty$ for $|\arg x|<\pi$

$$J_\nu(x)\sim\sqrt{\frac{2}{\pi x}}\cos\left(x-\frac{\nu\pi}{2}-\frac{\pi}{4}\right), \tag{B.7}$$

$$Y_\nu(x)\sim\sqrt{\frac{2}{\pi x}}\sin\left(x-\frac{\nu\pi}{2}-\frac{\pi}{4}\right). \tag{B.8}$$

The *spherical* Bessel functions $j_\ell(x)$, $y_\ell(x)$ are defined

$$j_\ell(x)=\sqrt{\frac{\pi}{2x}}J_{\ell+\frac{1}{2}}(x),\quad y_\ell(x)=\sqrt{\frac{\pi}{2x}}Y_{\ell+\frac{1}{2}}(x) \tag{B.9}$$

and solve the spherical Bessel equation

$$x^2\frac{\mathrm{d}^2y}{\mathrm{d}x^2}+2x\frac{\mathrm{d}y}{\mathrm{d}x}+(x^2-\ell(\ell+1))y=0. \tag{B.10}$$

First occurrences

$$j_0(x)=\frac{\sin x}{x}, \tag{B.11a}$$

$$y_0(x)=-\frac{\cos x}{x}, \tag{B.11b}$$

$$j_1(x)=\frac{\sin x}{x^2}-\frac{\cos x}{x}, \tag{B.11c}$$

$$y_1(x)=-\frac{\cos x}{x^2}-\frac{\sin x}{x} \tag{B.11d}$$

B.2 Jacobi elliptic functions

Jacobi elliptic functions are a set of twelve elliptic functions. Let m be a real parameter and φ the amplitude, we define the integral

$$u=\int_0^{\varphi}\frac{\mathrm{d}\theta}{\sqrt{1-m\sin^2\theta}}. \tag{B.12}$$

The copolar trio of elliptic functions are defined in terms of this integral as

$$\mathrm{sn}(u;m)=\sin\varphi, \tag{B.13}$$

$$\mathrm{cn}(u;m)=\cos\varphi, \tag{B.14}$$

$$\mathrm{dn}(u;m)=\sqrt{1-m\sin^2\varphi}, \tag{B.15}$$

sometimes called the elliptic sine, elliptic cosine and delta amplitude, respectively.

They obey the following relations

$$\mathrm{sn}^2(u;m)+\mathrm{cn}^2(u;m)=1, \tag{B.16}$$

$$\mathrm{dn}^2(u;m)=1-m\mathrm{sn}^2(u;m). \tag{B.17}$$

If u is a real variable, the functions sn, cn and dn are periodic with period $4K(m)$, $4K(m)$ and $2K(m)$ respectively, with

$$K(m)=\int_0^{\pi/2}\frac{\mathrm{d}\theta}{\sqrt{1-m\sin^2\theta}} \tag{B.18}$$

the elliptic integral of first kind.

Their derivatives are

$$\frac{\mathrm{d}}{\mathrm{d}u}\mathrm{sn}(u;m)=\mathrm{cn}(u;m)\mathrm{dn}(u;m), \tag{B.19}$$

$$\frac{\mathrm{d}}{\mathrm{d}u}\mathrm{sn}(u;m)=-\mathrm{sn}(u;m)\mathrm{dn}(u;m), \tag{B.20}$$

$$\frac{\mathrm{d}}{\mathrm{d}u}\mathrm{sn}(u;m)=-m\mathrm{sn}(u;m)\mathrm{cn}(u;m). \tag{B.21}$$

B.3 Legendre polynomials

Legendre polynomials $P_n(x)$ are a set of complete and orthogonal polynomials that are a solution to the differential equation

$$(1-x^2)P_n''(x) - 2xP_n'(x) + n(n+1)P_n(x) = 0. \tag{B.22}$$

Generating Rodrigues' formula

$$P_n(x) = \frac{1}{2^n n!}\frac{\mathrm{d}^n}{\mathrm{d}x^n}(x^2-1)^n. \tag{B.23}$$

First occurrences

$$P_0(x) = 1, \tag{B.24}$$

$$P_1(x) = x, \tag{B.25}$$

$$P_2(x) = \frac{1}{2}(3x^2-1). \tag{B.26}$$

They are normalised with respect to the norm $L^2[-1,1]$

$$\int_{-1}^{1} \mathrm{d}x\, P_m(x)P_n(x) = \frac{2}{2n+1}\delta_{mn}. \tag{B.27}$$

C Metric formulae

In this Appendix, we present the definitions and conventions regarding General Relativity used throughout this thesis, which mostly follow [MTW73]. Let $g_{\mu\nu}$ be the spacetime metric tensor. We often give it in terms of the line element $\mathrm{d}s^2$, which reads

$$\mathrm{d}s^2 = g_{\mu\nu}\,\mathrm{d}x^\mu\,\mathrm{d}x^\nu, \tag{C.1}$$

where x^μ are the coordinates.

We use the mostly-minus metric signature, so the flat (Minkowski) metric is

$$\eta_{\mu\nu} = \mathrm{diag}(+,-,-,-). \tag{C.2}$$

We define g as the absolute value of the metric tensor determinant

$$g = |\det(g_{\mu\nu})|. \tag{C.3}$$

The Christoffel symbols are

$$\Gamma^\lambda_{\mu\nu} = \frac{1}{2}g^{\lambda\rho}(\partial_\mu g_{\nu\rho} + \partial_\nu g_{\mu\rho} - \partial_\rho g_{\mu\nu}), \tag{C.4}$$

and the covariant derivative of covariant and contravariant vectors can be written as

$$\nabla_\mu V_\nu = \partial_\mu V_\nu - \Gamma^\lambda_{\mu\nu} V_\lambda, \tag{C.5a}$$

$$\nabla_\mu V^\nu = \partial_\mu V^\nu + \Gamma^\nu_{\mu\lambda} V^\lambda. \tag{C.5b}$$

Some useful identities [Wei72] involving contractions of the Christoffel symbols

$$\Gamma^\lambda_{\lambda\mu} = \frac{1}{\sqrt{g}}\partial_\mu\sqrt{g} \tag{C.6}$$

and covariant derivatives

$$\nabla_\mu V^\mu = \frac{1}{\sqrt{g}}\partial_\mu(\sqrt{g}V^\mu), \tag{C.7}$$

$$\nabla_\mu T^{\mu\nu} = \frac{1}{\sqrt{g}}\partial_\mu(\sqrt{g}T^{\mu\nu}) \quad (T^{\mu\nu}\text{ antisymmetric}). \tag{C.8}$$

The Riemann tensor is defined

$$R^\mu{}_{\nu\rho\sigma} = \partial_\rho\Gamma^\mu_{\nu\sigma} - \partial_\sigma\Gamma^\mu_{\nu\rho} + \Gamma^\mu_{\lambda\rho}\Gamma^\lambda_{\nu\sigma} - \Gamma^\mu_{\lambda\sigma}\Gamma^\lambda_{\nu\rho}, \tag{C.9}$$

and from its contraction, the Ricci tensor and Ricci scalar

$$R_{\mu\nu} = R^{\lambda}{}_{\mu\lambda\nu}, \tag{C.10}$$

$$R = g^{\mu\nu}R_{\mu\nu}. \tag{C.11}$$

The Weyl tensor is defined as the trace-free part of the Riemann tensor

$$C^{\mu\nu}{}_{\rho\sigma} = R^{\mu\nu}{}_{\rho\sigma} - 2\delta^{[\mu}{}_{[\rho}R^{\nu]}{}_{\sigma]} + \frac{1}{3}\delta^{[\mu}{}_{[\rho}\delta^{\nu]}{}_{\sigma]}R, \tag{C.12}$$

whereas its electric and magnetic parts are defined with respect to a unit timelike vector field u^μ, which typically is the fluid four-velocity, as [Goo89; HV90]

$$E_{\mu\nu} = C_{\mu\rho\nu\sigma}u^\rho u^\sigma, \tag{C.13a}$$

$$B_{\mu\nu} = \frac{1}{2}\varepsilon_{\mu\rho}{}^{\alpha\beta}C_{\alpha\beta\nu\sigma}u^\rho u^\sigma. \tag{C.13b}$$

C.1 Robertson-Walker metric

- **Robertson-Walker in cosmological time t and curvature k.** The line element

$$\mathrm{d}s^2 = \mathrm{d}t^2 - a^2(t)\left[\frac{\mathrm{d}r^2}{1-kr^2} + r^2(\mathrm{d}\theta^2 + \sin^2\theta\mathrm{d}\phi^2)\right]. \tag{C.14}$$

  Non-zero Christoffel symbols

$$\Gamma^i_{0j} = \frac{\dot{a}}{a}\delta^i{}_j, \tag{C.15a}$$

$$\Gamma^0_{ij} = \frac{\dot{a}}{a}g_{ij}, \tag{C.15b}$$

$$\Gamma^i_{jk} = \frac{1}{2}g^{il}(g_{lj,k} + g_{lk,j} - g_{jk,l}). \tag{C.15c}$$

  Ricci tensor

$$R_{00} = -3\frac{\ddot{a}}{a}, \tag{C.16a}$$

$$R_{ij} = -\left(\frac{\ddot{a}}{a} + 2\frac{\dot{a}^2}{a^2} + 2\frac{k}{a^2}\right)g_{ij}, \tag{C.16b}$$

  and Ricci scalar

$$R = -6\left(\frac{\ddot{a}}{a} + \frac{\dot{a}^2}{a^2} + \frac{k}{a^2}\right). \tag{C.17}$$

- **Flat Robertson-Walker in conformal time η.** The line element is

$$\mathrm{d}s^2 = a^2(\eta)(\mathrm{d}\eta^2 - \mathrm{d}\mathbf{x}^2). \tag{C.18}$$

Christoffel symbols

$$\Gamma^0_{00} = \frac{a'}{a}, \tag{C.19a}$$

$$\Gamma^i_{j0} = \frac{a'}{a}\delta^i{}_j, \tag{C.19b}$$

$$\Gamma^0_{ij} = \frac{a'}{a}\delta_{ij}. \tag{C.19c}$$

Einstein tensor

$$G^0{}_0 = 3\frac{a'^2}{a^4}, \tag{C.20a}$$

$$G^i{}_j = \left(2\frac{a''}{a^3} - \frac{a'^2}{a^4}\right)\delta^i{}_j. \tag{C.20b}$$

Including scalar perturbations in the longitudinal gauge Φ, Ψ and tensor perturbations h_{ij}

$$\mathrm{d}s^2 = a^2(\eta)\left[(1+2\Phi)\,\mathrm{d}\eta^2 - ((1-2\Psi)\delta_{ij} - h_{ij})\,\mathrm{d}x^i\,\mathrm{d}x^j\right], \tag{C.21}$$

the components of Einstein's tensor are

$$\delta G^0{}_0 = \frac{2}{a^2}\left[-3\mathcal{H}^2\Phi - 3\mathcal{H}\Psi' + \nabla^2\Psi\right], \tag{C.22a}$$

$$\delta G^0{}_i = \frac{2}{a^2}(\Psi' + \mathcal{H}\Phi), \tag{C.22b}$$

$$\delta G^i{}_j = -\frac{2}{a^2}\left(\left[\Psi'' + 2\mathcal{H}\Psi' + \mathcal{H}\Phi' + (2\mathcal{H}' + \mathcal{H}^2)\Phi + \frac{1}{2}\nabla^2(\Phi - \Psi)\right]\delta^i{}_j - \frac{1}{2}(\Phi - \Psi)_{,ij}\right) - \frac{1}{2a^2}(h''_{ij} + 2\mathcal{H}h'_{ij} - \nabla^2 h_{ij}). \tag{C.22c}$$

- **Flat Robertson-Walker in generic time τ**, with scale factor $a(\tau)$ and lapse function $b(\tau)$. The line element is

$$\mathrm{d}s^2 = b^2(\tau)\mathrm{d}\tau^2 - a^2(\tau)\mathrm{d}\mathbf{x}^2. \tag{C.23}$$

Christoffel symbols

$$\Gamma^0_{00} = \frac{b'}{b}, \tag{C.24a}$$

$$\Gamma^i_{j0} = \frac{a'}{a}\delta^i_j, \tag{C.24b}$$

$$\Gamma^0_{ij} = \frac{aa'}{b^2}\delta_{ij}. \tag{C.24c}$$

Einstein tensor

$$G^0{}_0 = 3\frac{a'^2}{a^2b^2}, \tag{C.25a}$$

$$G^i{}_j = \frac{1}{b^2}\left(2\frac{a''}{a} + \frac{a'^2}{a^2} - 2\frac{a'}{a}\frac{b'}{b}\right)\delta^i{}_j. \tag{C.25b}$$

D Fermions in curved spacetime

In this Appendix, we introduce the formalism necessary to deal with fermions in curved spacetime, which is used in Sec. 7.2.1. It is convenient to introduce the *vierbein* e^{μ}_{a} [Nak03], which allows us to use a non-coordinate basis $\{\hat{e}_a\} = \{e^{\mu}_{a}\partial_\mu\}$ defined so that it is orthogonal with respect to the spacetime metric $g_{\mu\nu}$, i.e.

$$e^{\mu}_{a}e^{\nu}_{b}g_{\mu\nu} = \eta_{ab}, \qquad g_{\mu\nu} = e^{a}_{\mu}e^{b}_{\nu}\eta_{ab}, \tag{D.1}$$

with $\eta_{ab} = \mathrm{diag}(+,-,-,-)$ the flat metric and e^{a}_{μ} the inverse of the vierbein (with respect to both types of indices)

$$e^{\mu}_{a}e^{a}_{\nu} = \delta^{\mu}_{\nu}, \qquad e^{\mu}_{a}e^{b}_{\mu} = \delta^{b}_{a}. \tag{D.2}$$

where we use Latin indices a, b for local Lorentz tensors and Greek indices $\mu, \nu, \ldots$ for generally covariant tensors. Let $\{\gamma^a\}$ be the Dirac matrices in flat spacetime, which satisfy the anticommutation relations $\{\gamma^a, \gamma^b\} = 2\eta^{ab}$. We can generalise these matrices to curved spacetime by defining $\gamma^\mu = e^{\mu}_{a}\gamma^a$, which can be found to satisfy

$$\{\gamma^\mu, \gamma^\nu\} = 2g^{\mu\nu}. \tag{D.3}$$

The adjoint of any gamma matrix can be compactly written as

$$(\gamma^\mu)^\dagger = \gamma^0\gamma^\mu\gamma^0, \tag{D.4}$$

where these $\gamma^0 = \gamma^a\big|_{a=0}$ are the flat ones.

The full covariant derivative of a spinor field, including the gauge connection term, can be written

$$D_\mu\Psi = \partial_\mu\Psi + \Gamma_\mu\Psi + iqA_\mu\Psi, \tag{D.5}$$

where Γ_μ is the spin connection [Dob+97; Nak03; Sha22], which implements the (spin connection) covariant derivative $\mathfrak{D}$ for objects which are defined on the Lorentz frame (those with flat indices)

$$\mathfrak{D}_\mu\Psi = \partial_\mu\Psi + \Gamma_\mu\Psi. \tag{D.6}$$

The specific form of the spin connection can be found by imposing the proper transformation laws under a local Lorentz transformation, which is

$$\Gamma_\mu = -\frac{i}{2}\Gamma^{a}{}_{\mu}{}^{b}\Sigma_{ab}, \tag{D.7}$$

where $\Sigma_{ab} = \frac{i}{4}[\gamma_a, \gamma_b]$ is the spinor representation of the generators of the Lorentz transformations. The adjoint of the spin connection is

$$\Gamma_\mu^\dagger = \frac{1}{8}\Gamma^a{}_\mu{}^b[\gamma_a, \gamma_b]^\dagger = -\gamma^0\Gamma_\mu\gamma^0, \tag{D.8}$$

where these γ^0 are the flat index ones.

The connection with flat indices is defined by

$$\nabla_a \hat{e}_b = \Gamma^c{}_{ab}\hat{e}_c, \tag{D.9}$$

and it relates to the connection with curved indices as follows

$$\Gamma^c{}_{ab} = e^c_\nu e^\mu_a \nabla_\mu e^\nu_b = e^c_\nu e^\mu_a(\partial_\mu e^\nu_b + e^\lambda_b \Gamma^\nu_{\mu\lambda}). \tag{D.10}$$

If we choose the connection to be metric and torsion-free, so $\Gamma^\nu_{\mu\lambda}$ are the Christoffel symbols, then it can also be shown that metricity imposes $\Gamma_{abc} = -\Gamma_{cba}$.

Let us note that it is possible to define a covariant derivative which acts in a covariant way both with respect to curved spacetime (as ∇ does) and to the Lorentz frame (as $\mathfrak{D}$ does), which we denote $\mathscr{D}$. This naturally involves the connections both with curved and flat indices. For instance, it acts on the vierbein as

$$\mathscr{D}_\nu e^\mu_b = e^a_\nu \partial_a e^\mu_b + \Gamma^\mu_{\lambda\nu} e^\lambda_b - \Gamma^c{}_{\nu b} e^\mu_c, \tag{D.11}$$

which can be shown to vanish $\mathscr{D}_\nu e^\mu_b = \mathscr{D}_\nu e^b_\mu = 0$ due to metricity of the connections.

Finally, let us compute the commutator of the connection with the curved gamma

$$[\gamma^\mu, \Gamma_\mu] = \frac{1}{8} e^\mu_c \Gamma^a{}_\mu{}^b \left[\gamma^c, [\gamma_a, \gamma_b]\right]. \tag{D.12}$$

By expanding the commutator, applying the Chisholm identity to the three-gamma products

$$\gamma^a\gamma^b\gamma^c = \eta^{ab}\gamma^c + \eta^{bc}\gamma^a - \eta^{ac}\gamma^b + i\epsilon^{abcd}\gamma^d\gamma^5, \tag{D.13}$$

where $\gamma^5 = i\gamma^0\gamma^1\gamma^2\gamma^3$, and performing some Dirac algebra, one can arrive at the following compact expression

$$[\gamma^\mu, \Gamma_\mu] = -\Gamma^a{}_{cb}\eta^{cb}\gamma_a = \nabla_\mu\gamma^\mu, \tag{D.14}$$

E TDiff-invariant Lorentz force

In this Appendix, we examine a different derivation of Lorentz force law to that presented in Sec. 7.2.1. In the following derivation, we mostly follow that on [IZ12, pp. 13–14].

In the Diff case, the current of a charged point particle with charge q following a trajectory $z^\mu(s)$, where s is the length of arc parameter, can be written as

$$j^\mu(\mathbf{x},\tau) = q\int \mathrm{d}s\, u^\mu \frac{\delta^{(4)}[x-z(s)]}{\sqrt{g}}, \tag{E.1}$$

where $u^\mu = \mathrm{d}z^\mu/\mathrm{d}s$ is the four-velocity and we have weighed the Dirac delta to make it a scalar. The total action in a Diff-invariant theory, including the mass action, would read

$$S = -\int \mathrm{d}^4x\,\sqrt{g}\left(\frac{1}{4}F_{\mu\nu}F^{\mu\nu} + j^\mu A_\mu\right) - m\int \mathrm{d}s\,. \tag{E.2}$$

In turn, the mass action for a point-like particle of mass m can be written as the four-velocity coupled to a mass current. Since the four-velocity is a unit vector $u_\mu u^\mu = 1$, one can write

$$\int \mathrm{d}s = \int \mathrm{d}s\, u_\mu u^\mu = \int \mathrm{d}^4x\,\sqrt{g}u_\mu \int \mathrm{d}s\, u^\mu \frac{\delta^{(4)}[x-z(s)]}{\sqrt{g}}, \tag{E.3}$$

so the action (E.2) can be written as

$$S = -\int \mathrm{d}^4x\,\sqrt{g}\left(\frac{1}{4}F_{\mu\nu}F^{\mu\nu} + j^\mu A_\mu + j^\mu_m u_\mu\right), \tag{E.4}$$

with the mass current

$$j^\mu_m = m\int \mathrm{d}s\, u^\mu \frac{\delta^{(4)}[x-z(s)]}{\sqrt{g}}. \tag{E.5}$$

From (E.4), we can translate this action into a TDiff-invariant action for a charged massive particle subject to an electromagnetic field, just by replacing $\sqrt{g}$ by $f(g)$, namely

$$S = -\int \mathrm{d}^4x\, f(g)\left(\frac{1}{4}F_{\mu\nu}F^{\mu\nu} + j^\mu A_\mu + j^\mu_m u_\mu\right). \tag{E.6}$$

In order to study the Lorentz force for this TDiff-invariant setup, we can consider the electromagnetic field to be external, ignoring possible backreaction, so the potential $A_\mu(x)$ is external and fixed and we can ignore the electromagnetic part of the action.

The rest of the action, after integrating the deltas out and changing the integration measure to coordinate time $\mathrm{d}\tau$, can be written as

$$S = -\int \mathrm{d}\tau \, \frac{f(g)}{\sqrt{g}} \left(q v^\mu A_\mu + m \frac{\mathrm{d}s}{\mathrm{d}\tau} \right), \tag{E.7}$$

where $v^\mu = \frac{\mathrm{d}z^\mu}{\mathrm{d}\tau} = (1, \mathbf{v})$ is the coordinate four-velocity, and $\frac{\mathrm{d}s}{\mathrm{d}\tau} = \sqrt{g_{\mu\nu} v^\mu v^\nu}$.

Variations of this action along the trajectory δz^α yield the following

$$\begin{aligned} \delta S = -\int \mathrm{d}\tau \, \frac{f(g)}{\sqrt{g}} \delta z^\alpha \Bigg[& q v^\mu \partial_\alpha A_\mu - q \frac{\sqrt{g}}{f(g)} \frac{\mathrm{d}}{\mathrm{d}\tau} \left(\frac{f(g)}{\sqrt{g}} A_\alpha \right) + \frac{m}{2} \frac{v^\mu v^\nu \partial_\alpha g_{\mu\nu}}{\sqrt{g_{\mu\nu} v^\mu v^\nu}} \\ & - m \frac{\sqrt{g}}{f(g)} \frac{\mathrm{d}}{\mathrm{d}\tau} \left(\frac{f(g)}{\sqrt{g}} \frac{g_{\alpha\beta} v^\beta}{\sqrt{g_{\mu\nu} v^\mu v^\nu}} \right) + \partial_\alpha \left(\frac{f(g)}{\sqrt{g}} \right) \left(v^\mu A_\mu + m \frac{\mathrm{d}s}{\mathrm{d}\tau} \right) \Bigg]. \end{aligned} \tag{E.8}$$

This effect described by Lorentz's force law is local, in the sense that variations of the spacetime along the trajectory can be neglected, so only the leading order in the adiabatic expansion needs to be considered, i.e. terms with metric derivatives can be neglected compared to terms with derivatives of the vector field. At leading order in the adiabatic expansion, this yields the equation of motion

$$m \, g_{\alpha\mu} \frac{\mathrm{d}u^\mu}{\mathrm{d}\tau} = q \left(v^\mu \partial_\alpha A_\mu - \frac{\mathrm{d}A_\alpha}{\mathrm{d}\tau} \right), \tag{E.9}$$

which, as we could expect, does not depend on the TDiff function $f(g)$. The four-velocity, at leading adiabatic order, can be written in a way that reminds of the Lorentz factor

$$u^\mu = \frac{\mathrm{d}z^\mu}{\mathrm{d}s} = \frac{\mathrm{d}z^\mu/\mathrm{d}\tau}{\mathrm{d}s/\mathrm{d}\tau} = \frac{v^\mu}{\sqrt{1-\mathbf{v}^2}}, \tag{E.10}$$

while the total derivative of the vector field can be expanded as

$$\frac{\mathrm{d}A_\alpha}{\mathrm{d}\tau} = \frac{\partial A_\alpha}{\partial \tau} + v^j \frac{\partial A_\alpha}{\partial x^j} = v^\mu \partial_\mu A_\alpha, \tag{E.11}$$

which allows us to write the equation of motion in a compact manner

$$m \frac{\mathrm{d}u^\alpha}{\mathrm{d}s} = q \, u_\mu F^{\alpha\mu}. \tag{E.12}$$

This expression is equivalent to (7.71).

Setting $\alpha = i$, one finds the following equation of motion for the RW background

$$\frac{\mathrm{d}}{\mathrm{d}\tau} \frac{m v^i}{\sqrt{1-\mathbf{v}^2}} = \frac{q}{a^2} (\partial_0 A_i - \partial_i A_0 + v^j \partial_j A_i - v^j \partial_i A_j). \tag{E.13}$$

After applying some vector identities and identifying the electric and magnetic fields (7.80), this equation can be rewritten as

$$\frac{\mathrm{d}}{\mathrm{d}\tau} \frac{m \mathbf{v}}{\sqrt{1-\mathbf{v}^2}} = \frac{q}{a^2} (\mathbf{E} + \mathbf{v} \times \mathbf{B}), \tag{E.14}$$

which is the Lorentz force law for a relativistic particle. On the other hand, if we set $\alpha = 0$, we can obtain the equation for the variation of energy

$$\frac{\mathrm{d}}{\mathrm{d}\tau}\frac{m}{\sqrt{1-\mathbf{v}^2}} = \frac{q}{b^2}\mathbf{v}\cdot\mathbf{E}. \tag{E.15}$$

References

[AAG18] H. Abedi, M. Ahmadvand, and S. S. Gousheh. "Electroweak Baryogenesis via Chiral Gravitational Waves". *Phys. Lett. B* 786 (2018). DOI: 10.1016/j.physletb.2018.07.065. arXiv: 1805.10645.

[Aas+15] J. Aasi et al. "Advanced LIGO". *Class. Quant. Grav.* 32 (2015). DOI: 10.1088/0264-9381/32/7/074001. arXiv: 1411.4547.

[Aba+16] K. N. Abazajian et al. "CMB-S4 Science Book, First Edition". 2016. DOI: 10.48550/arXiv.1610.02743. arXiv: 1610.02743.

[Abb+16] B. P. Abbott et al. "Observation of Gravitational Waves from a Binary Black Hole Merger". *Phys. Rev. Lett.* 116.6 (2016). DOI: 10.1103/PhysRevLett.116.061102. arXiv: 1602.03837.

[Abb+17a] B. P. Abbott et al. "GW170817: Observation of Gravitational Waves from a Binary Neutron Star Inspiral". *Phys. Rev. Lett.* 119.16 (2017). DOI: 10.1103/PhysRevLett.119.161101. arXiv: 1710.05832.

[Abb+17b] B. P. Abbott et al. "Gravitational Waves and Gamma-Rays from a Binary Neutron Star Merger: GW170817 and GRB 170817A". *Astrophys. J. Lett.* 848.2 (2017). DOI: 10.3847/2041-8213/aa920c. arXiv: 1710.05834.

[Abb+20] R. Abbott et al. "GW190814: Gravitational Waves from the Coalescence of a 23 Solar Mass Black Hole with a 2.6 Solar Mass Compact Object". *Astrophys. J. Lett.* 896.2 (2020). DOI: 10.3847/2041-8213/ab960f. arXiv: 2006.12611.

[Abb+21] R. Abbott et al. "Observation of Gravitational Waves from Two Neutron Star–Black Hole Coalescences". *Astrophys. J. Lett.* 915.1 (2021). DOI: 10.3847/2041-8213/ac082e. arXiv: 2106.15163.

[ABG48] R. A. Alpher, H. Bethe, and G. Gamow. "The Origin of Chemical Elements". *Phys. Rev.* 73 (1948). DOI: 10.1103/PhysRev.73.803.

[Abo+18] B. Abolfathi et al. "The Fourteenth Data Release of the Sloan Digital Sky Survey: First Spectroscopic Data from the Extended Baryon Oscillation Spectroscopic Survey and from the Second Phase of the Apache Point Observatory Galactic Evolution Experiment". *Astrophys. J. Suppl.* 235.2 (2018). DOI: 10.3847/1538-4365/aa9e8a. arXiv: 1707.09322.

[ÁC19] C. Álvarez-Luna and J. A. R. Cembranos. "Dark Photon Searches with Atomic Transitions". *JHEP* 07 (2019). DOI: 10.1007/JHEP07(2019)110. arXiv: 1812.08501.

[Ace+15] F. Acernese et al. “Advanced Virgo: A 2nd Generation Interferometric Gravitational Wave Detector”. *Class. Quantum Grav.* 32.2 (2015). DOI: 10.1088/0264-9381/32/2/024001. arXiv: 1408.3978.

[ACW07] L. Ackerman, S. M. Carroll, and M. B. Wise. “Imprints of a Primordial Preferred Direction on the Microwave Background”. *Phys. Rev. D* 75 (2007). DOI: 10.1103/PhysRevD.75.083502. arXiv: astro-ph/0701357.

[AdCM24] D. Alonso-López, J. de Cruz Pérez, and A. L. Maroto. “Unified Transverse Diffeomorphism Invariant Field Theory for the Dark Sector”. *Phys. Rev. D* 109.2 (2024). DOI: 10.1103/PhysRevD.109.023537.

[Ade+21] P. A. R. Ade et al. “Improved Constraints on Primordial Gravitational Waves Using Planck, WMAP, and BICEP/Keck Observations through the 2018 Observing Season”. *Phys. Rev. Lett.* 127.15 (2021). DOI: 10.1103/PhysRevLett.127.151301.

[AF07] E. Alvarez and A. F. Faedo. “Unimodular Cosmology and the Weight of Energy”. *Phys. Rev. D* 76 (2007). DOI: 10.1103/PhysRevD.76.064013. arXiv: hep-th/0702184.

[AFL08] E. Alvarez, A. F. Faedo, and J. J. Lopez-Villarejo. “Ultraviolet Behavior of Transverse Gravity”. *JHEP* 10 (2008). DOI: 10.1088/1126-6708/2008/10/023. arXiv: 0807.1293.

[AFL09] E. Alvarez, A. F. Faedo, and J. J. Lopez-Villarejo. “Transverse Gravity versus Observations”. *JCAP* 07 (2009). DOI: 10.1088/1475-7516/2009/07/002. arXiv: 0904.3298.

[Agh+20a] N. Aghanim et al. “Planck 2018 Results. I. Overview and the Cosmological Legacy of Planck”. *Astron. Astrophys.* 641 (2020). DOI: 10.1051/0004-6361/201833880.

[Agh+20b] N. Aghanim et al. “Planck 2018 Results. VI. Cosmological Parameters”. *Astron. Astrophys.* 641 (2020). DOI: 10.1051/0004-6361/201833910. arXiv: 1807.06209.

[Agr+20] P. Agrawal et al. “Relic Abundance of Dark Photon Dark Matter”. *Phys. Lett. B* 801 (2020). DOI: 10.1016/j.physletb.2019.135136. arXiv: 1810.07188.

[AHJ20] G. Alonso-Álvarez, T. Hugle, and J. Jaeckel. “Misalignment & Co.: (Pseudo-)scalar and vector dark matter with curvature couplings”. *JCAP* 02 (2020). DOI: 10.1088/1475-7516/2020/02/014. arXiv: 1905.09836.

[Akr+20] Y. Akrami et al. “Planck 2018 Results. X. Constraints on Inflation”. *Astron. Astrophys.* 641 (2020). DOI: 10.1051/0004-6361/201833887. arXiv: 1807.06211.

[Aku+19] T. Akutsu et al. “KAGRA: 2.5 Generation Interferometric Gravitational Wave Detector”. *Nat Astron* 3.1 (2019). DOI: 10.1038/s41550-018-0658-y. arXiv: 1811.08079.

[ALS18] P. Adshead, A. J. Long, and E. I. Sfakianakis. “Gravitational Leptogenesis, Reheating, and Models of Neutrino Mass”. *Phys. Rev. D* 97.4 (2018). DOI: 10.1103/PhysRevD.97.043511. arXiv: 1711.04800.

[Alv+06] E. Alvarez et al. “Transverse Fierz-Pauli Symmetry”. *Nucl. Phys. B* 756 (2006). DOI: 10.1016/j.nuclphysb.2006.08.003. arXiv: hep-th/0606019.

[AM05] S. Alexander and J. Martin. “Birefringent Gravitational Waves and the Consistency Check of Inflation”. *Phys. Rev. D* 71 (2005). DOI: 10.1103/PhysRevD.71.063526. arXiv: hep-th/0410230.

[Ama+17] P. Amaro-Seoane et al. “Laser Interferometer Space Antenna”. 2017. arXiv: 1702.00786.

[APS06] S. H.-S. Alexander, M. E. Peskin, and M. M. Sheikh-Jabbari. “Leptogenesis from Gravity Waves in Models of Inflation”. *Phys. Rev. Lett.* 96 (2006). DOI: 10.1103/PhysRevLett.96.081301. arXiv: hep-th/0403069.

[AR23] C. Altavista and J. Rey. “Induced Gravitational Waves and Baryon Asymmetry Fluctuations from Primordial Black Hole Formation”. 2023. arXiv: 2309.14993.

[Ari+12] P. Arias et al. “WISPy Cold Dark Matter”. *JCAP* 06 (2012). DOI: 10.1088/1475-7516/2012/06/013. arXiv: 1201.5902.

[Arm04] C. Armendariz-Picon. “Could Dark Energy Be Vector-Like?” *JCAP* 07 (2004). DOI: 10.1088/1475-7516/2004/07/007. arXiv: astro-ph/0405267.

[Arz+20] Z. Arzoumanian et al. “The NANOGrav 12.5-Year Data Set: Search For An Isotropic Stochastic Gravitational-Wave Background”. *Astrophys. J. Lett.* 905.2 (2020). DOI: 10.3847/2041-8213/abd401. arXiv: 2009.04496.

[AS65] M. Abramowitz and I. A. Stegun. *Handbook of Mathematical Functions with Formulas, Graphs, and Mathematical Tables*. New York City: Dover Publications, 1965. ISBN: 978-0-486-61272-0.

[Asa+99] T. Asaka et al. “Leptogenesis in Inflaton Decay”. *Phys. Lett. B* 464 (1999). DOI: 10.1016/S0370-2693(99)01020-5. arXiv: hep-ph/9906366.

[Aso+21] M. Asorey et al. “On the Vector Conformal Models in an Arbitrary Dimension”. *Eur. Phys. J. Plus* 136.10 (2021). DOI: 10.1140/epjp/s13360-021-02024-4. arXiv: 2107.13125.

[AW84] L. Alvarez-Gaume and E. Witten. “Gravitational Anomalies”. *Nucl. Phys. B* 234 (1984). Ed. by A. Salam and E. Sezgin. DOI: 10.1016/0550-3213(84)90066-X.

[Bar21] N. D. Barrie. "Gravitational Leptogenesis in Bounce Cosmology". *JCAP* 06 (2021). DOI: 10.1088/1475-7516/2021/06/049. arXiv: 2105.06624.

[Bas+19] M. Bastero-Gil et al. "Vector Dark Matter Production at the End of Inflation". *JCAP* 04 (2019). DOI: 10.1088/1475-7516/2019/04/015. arXiv: 1810.07208.

[BB17] J. S. Bullock and M. Boylan-Kolchin. "Small-Scale Challenges to the ΛCDM Paradigm". *Annu. Rev. Astron. Astrophys.* 55.1 (2017). DOI: 10.1146/annurev-astro-091916-055313. arXiv: 1707.04256.

[BB21] D. Bodeker and W. Buchmuller. "Baryogenesis from the Weak Scale to the Grand Unification Scale". *Rev. Mod. Phys.* 93.3 (2021). DOI: 10.1103/RevModPhys.93.035004. arXiv: 2009.07294.

[BBK11] M. Boylan-Kolchin, J. S. Bullock, and M. Kaplinghat. "Too Big to Fail? The Puzzling Darkness of Massive Milky Way Subhaloes". *Mon. Not. R. Astron. Soc.: Letters* 415.1 (2011). DOI: 10.1111/j.1745-3933.2011.01074.x. arXiv: 1103.0007.

[BCH20] M. A. Buen-Abad, R. T. Co, and K. Harigaya. "Common Origin of Warm Dark Matter and Dark Radiation". *JCAP* 12 (2020). DOI: 10.1088/1475-7516/2020/12/024. arXiv: 1911.13267.

[BD84] N. D. Birrell and P. C. W. Davies. *Quantum Fields in Curved Space*. Cambridge Monographs on Mathematical Physics. Cambridge, UK: Cambridge Univ. Press, 1984. ISBN: 978-0-521-27858-4.

[BDP05] W. Buchmuller, P. Di Bari, and M. Plumacher. "Leptogenesis for Pedestrians". *Annals Phys.* 315 (2005). DOI: 10.1016/j.aop.2004.02.003. arXiv: hep-ph/0401240.

[Ben+96] C. L. Bennett et al. "Four-Year COBE DMR Cosmic Microwave Background Observations: Maps and Basic Results". *Astrophys. J.* 464 (1996). DOI: 10.1086/310075.

[BFS97] J. D. Barrow, P. G. Ferreira, and J. Silk. "Constraints on a Primordial Magnetic Field". *Phys. Rev. Lett.* 78.19 (1997). DOI: 10.1103/PhysRevLett.78.3610. arXiv: astro-ph/9701063.

[BH07] C. G. Boehmer and T. Harko. "Dark Energy as a Massive Vector Field". *Eur. Phys. J. C* 50 (2007). DOI: 10.1140/epjc/s10052-007-0210-1. arXiv: gr-qc/0701029.

[BJ04] R. Banerjee and K. Jedamzik. "The Evolution of Cosmic Magnetic Fields: From the Very Early Universe, to Recombination, to the Present". *Phys. Rev. D* 70.12 (2004). DOI: 10.1103/PhysRevD.70.123003. arXiv: astro-ph/0410032.

[BLT11] D. Blas, J. Lesgourgues, and T. Tram. “The Cosmic Linear Anisotropy Solving System (CLASS) II: Approximation Schemes”. *JCAP* 07 (2011). DOI: 10.1088/1475-7516/2011/07/034. arXiv: 1104.2933.

[BM08] J. Beltran Jimenez and A. L. Maroto. “A Cosmic Vector for Dark Energy”. *Phys. Rev. D* 78 (2008). DOI: 10.1103/PhysRevD.78.063005. arXiv: 0801.1486.

[BM09] J. Beltran Jimenez and A. L. Maroto. “Cosmological Electromagnetic Fields and Dark Energy”. *JCAP* 03 (2009). DOI: 10.1088/1475-7516/2009/03/016. arXiv: 0811.0566.

[BM10] J. Beltran Jimenez and A. L. Maroto. “The Electromagnetic Dark Sector”. *Phys. Lett. B* 686 (2010). DOI: 10.1016/j.physletb.2010.02.038. arXiv: 0903.4672.

[BM24] A. G. Bello-Morales and A. L. Maroto. “Cosmology in Gravity Models with Broken Diffeomorphisms”. *Phys. Rev. D* 109.4 (2024). DOI: 10.1103/PhysRevD.109.043506. arXiv: 2308.00635.

[Bog+92] N. W. Boggess et al. “The COBE Mission: Its Design and Performance Two Years after Launch”. *Astrophys. J.* 397 (1992). DOI: 10.1086/171797.

[Bro+22] D. Brout et al. “The Pantheon+ Analysis: Cosmological Constraints”. *Astrophys. J.* 938.2 (2022). DOI: 10.3847/1538-4357/ac8e04. arXiv: 2202.04077.

[BSZ11] D. Blas, M. Shaposhnikov, and D. Zenhausern. “Scale-Invariant Alternatives to General Relativity”. *Phys. Rev. D* 84.4 (2011). DOI: 10.1103/PhysRevD.84.044001. arXiv: 1104.1392.

[CD18] R. R. Caldwell and C. Devulder. “Axion Gauge Field Inflation and Gravitational Leptogenesis: A Lower Bound on B Modes from the Matter-Antimatter Asymmetry of the Universe”. *Phys. Rev. D* 97.2 (2018). DOI: 10.1103/PhysRevD.97.023532. arXiv: 1706.03765.

[CDF19] G. Cusin, R. Durrer, and P. G. Ferreira. “Polarization of a Stochastic Gravitational Wave Background through Diffusion by Massive Structures”. *Phys. Rev. D* 99.2 (2019). DOI: 10.1103/PhysRevD.99.023534. arXiv: 1807.10620.

[CDS10] C. Caprini, R. Durrer, and X. Siemens. “Detection of Gravitational Waves from the QCD Phase Transition with Pulsar Timing Arrays”. *Phys. Rev. D* 82.6 (2010). DOI: 10.1103/PhysRevD.82.063511.

[Cem+12] J. Cembranos et al. “Isotropy Theorem for Cosmological Vector Fields”. *Phys. Rev. D* 86 (2012). DOI: 10.1103/PhysRevD.86.021301. arXiv: 1203.6221.

[Cem+18] J. Cembranos et al. “Constraints on Anharmonic Corrections of Fuzzy Dark Matter”. *JHEP* 08 (2018). DOI: 10.1007/JHEP08(2018)073. arXiv: 1805.08112.

[CG15] S. Clesse and J. García-Bellido. “Massive Primordial Black Holes from Hybrid Inflation as Dark Matter and the Seeds of Galaxies”. *Phys. Rev. D* 92.2 (2015). DOI: 10.1103/PhysRevD.92.023524. arXiv: 1501.07565.

[CGG22] R. Carballo-Rubio, L. J. Garay, and G. García-Moreno. “Unimodular Gravity vs General Relativity: A Status Report”. *Class. Quant. Grav.* 39.24 (2022). DOI: 10.1088/1361-6382/aca386. arXiv: 2207.08499.

[CKN93] A. G. Cohen, D. B. Kaplan, and A. E. Nelson. “Progress in Electroweak Baryogenesis”. *Annu. Rev. Nucl. Part. Sci.* 43.1 (1993). DOI: 10.1146/annurev.ns.43.120193.000331. arXiv: hep-ph/9302210.

[CL95] P. Coles and F. Lucchin. *Cosmology: The Origin and Evolution of Cosmic Structure*. Wiley, 1995. ISBN: 978-0-471-95473-6.

[CM13] J. P. Conlon and M. C. D. Marsh. “The Cosmophenomenology of Axionic Dark Radiation”. *JHEP* 10 (2013). DOI: 10.1007/JHEP10(2013)214. arXiv: 1304.1804.

[CMN13] J. A. R. Cembranos, A. L. Maroto, and S. J. Núñez Jareño. “Isotropy Theorem for Cosmological Yang-Mills Theories”. *Phys. Rev. D* 87.4 (2013). DOI: 10.1103/PhysRevD.87.043523. arXiv: 1212.3201.

[CMN14] J. A. R. Cembranos, A. L. Maroto, and S. J. Núñez Jareño. “Isotropy Theorem for Arbitrary-Spin Cosmological Fields”. *JCAP* 03 (2014). DOI: 10.1088/1475-7516/2014/03/042. arXiv: 1311.1402.

[CMN17] J. A. R. Cembranos, A. L. Maroto, and S. J. Núñez Jareño. “Perturbations of Ultralight Vector Field Dark Matter”. *JHEP* 02 (2017). DOI: 10.1007/JHEP02(2017)064. arXiv: 1611.03793.

[CMO22] R. T. Co, Y. Mambrini, and K. A. Olive. “Inflationary Gravitational Leptogenesis”. *Phys. Rev. D* 106.7 (2022). DOI: 10.1103/PhysRevD.106.075006. arXiv: 2205.01689.

[CMP19] S. Chabanier, M. Millea, and N. Palanque-Delabrouille. “Matter Power Spectrum: From Lyα Forest to CMB Scales”. *Mon. Not. R. Astron. Soc.* 489.2 (2019). DOI: 10.1093/mnras/stz2310. arXiv: 1905.08103.

[Co+19] R. T. Co et al. “Dark Photon Dark Matter Produced by Axion Oscillations”. *Phys. Rev. D* 99.7 (2019). DOI: 10.1103/PhysRevD.99.075002. arXiv: 1810.07196.

[Der+11] C. D. Dermer et al. “Time Delay of Cascade Radiation for TeV Blazars and the Measurement of the Intergalactic Magnetic Field”. *Astrophys. J.* 733.2 (2011). DOI: 10.1088/2041-8205/733/2/L21. arXiv: 1011.6660.

[DHN19] J. A. Dror, K. Harigaya, and V. Narayan. “Parametric Resonance Production of Ultralight Vector Dark Matter”. *Phys. Rev. D* 99.3 (2019). DOI: 10.1103/PhysRevD.99.035036. arXiv: 1810.07195.

[Di +21] E. Di Valentino et al. “In the Realm of the Hubble Tension – a Review of Solutions”. *Class. Quantum Grav.* 38.15 (2021). DOI: 10.1088/1361-6382/ac086d. arXiv: 2103.01183.

[DN13] R. Durrer and A. Neronov. “Cosmological Magnetic Fields: Their Generation, Evolution and Observation”. *Astron Astrophys Rev* 21.1 (2013). DOI: 10.1007/s00159-013-0062-7. arXiv: 1303.7121.

[Dob+97] A. Dobado et al. *Effective Lagrangians for the Standard Model*. Heidelberg: Springer Berlin, 1997. ISBN: 978-3-540-62570-4.

[Dod03] S. Dodelson. *Modern Cosmology*. Amsterdam: Academic Press, 2003. ISBN: 978-0-12-219141-1.

[Dom+20] V. Domcke et al. “Measuring the Net Circular Polarization of the Stochastic Gravitational Wave Background with Interferometers”. *JCAP* 05 (2020). DOI: 10.1088/1475-7516/2020/05/028. arXiv: 1910.08052.

[dRio+20] A. del Rio et al. “Spontaneous Creation of Circularly Polarized Photons in Chiral Astrophysical Systems”. *Phys. Rev. Lett.* 124.21 (2020). DOI: 10.1103/PhysRevLett.124.211301. arXiv: 2002.01593.

[Drl+15] A. Drlica-Wagner et al. “Eight Ultra-faint Galaxy Candidates Discovered in Year Two of the Dark Energy Survey”. *Astron. J.* 813 (2015). DOI: 10.1088/0004-637X/813/2/109.

[DS78] S. Dimopoulos and L. Susskind. “Baryon Number of the Universe”. *Phys. Rev. D* 18.12 (1978). DOI: 10.1103/PhysRevD.18.4500.

[Ein18] A. Einstein. “Über Gravitationswellen”. *Sitzungsber. Preuss. Akad. Wiss. Berlin (Math. Phys.)* 1918 (1918).

[Ein19] A. Einstein. “Spielen Gravitationsfelder Im Aufbau Der Materiellen Elementarteilchen Eine Wesentliche Rolle?” *Sitzungsber. Preuss. Akad. Wiss. Berlin (Math. Phys.)* 1919 (1919).

[EZ18] J. M. Ezquiaga and M. Zumalacárregui. “Dark Energy in Light of Multi-Messenger Gravitational-Wave Astronomy”. *Front. Astron. Space Sci.* 5 (2018). DOI: 10.3389/fspas.2018.00044. arXiv: 1807.09241.

[Fie+20] B. D. Fields et al. “Big-Bang Nucleosynthesis After Planck”. *J. Cosmol. Astropart. Phys.* 2020.03 (2020). DOI: 10.1088/1475-7516/2020/03/010. arXiv: 1912.01132.

[Fie11] B. D. Fields. “The Primordial Lithium Problem”. *Annu. Rev. Nucl. Part. Sci.* 61.1 (2011). DOI: 10.1146/annurev-nucl-102010-130445. arXiv: 1203.3551.

[Fin+00] F. Finkel et al. “The Lame Equation in Parametric Resonance after Inflation”. *Phys. Rev. D* 62 (2000). DOI: 10.1103/PhysRevD.62.103515. arXiv: hep-ph/0006117.

[Fix+96] D. J. Fixsen et al. “The Cosmic Microwave Background Spectrum from the Full COBE FIRAS Data Set”. *Astrophys. J.* 473 (1996). DOI: 10.1086/178173.

[Fix09] D. J. Fixsen. “The Temperature of the Cosmic Microwave Background”. *Astrophys. J.* 707.2 (2009). DOI: 10.1088/0004-637X/707/2/916. arXiv: 0911.1955.

[For89] L. H. Ford. “INFLATION DRIVEN BY A VECTOR FIELD”. *Phys. Rev. D* 40 (1989). DOI: 10.1103/PhysRevD.40.967.

[FS93] G. R. Farrar and M. E. Shaposhnikov. “Baryon Asymmetry of the Universe in the Minimal Standard Model”. *Phys. Rev. Lett.* 70 (1993). DOI: 10.1103/PhysRevLett.70.2833.

[FT19] D. G. Figueroa and E. H. Tanin. “Ability of LIGO and LISA to Probe the Equation of State of the Early Universe”. *JCAP* 08 (2019). DOI: 10.1088/1475-7516/2019/08/011. arXiv: 1905.11960.

[FY86] M. Fukugita and T. Yanagida. “Baryogenesis without Grand Unification”. *Phys. Lett. B* 174 (1986). DOI: 10.1016/0370-2693(86)91126-3.

[Gam46] G. Gamow. “Expanding Universe and the Origin of Elements”. *Phys. Rev.* 70.7-8 (1946). DOI: 10.1103/PhysRev.70.572.2.

[GM17] G. Gubitosi and J. Magueijo. “Correlation between Opposite-Helicity Gravitons: Imprints on Gravity-Wave and Microwave Backgrounds”. *Phys. Rev. D* 95.2 (2017). DOI: 10.1103/PhysRevD.95.023520. arXiv: 1610.05702.

[GMR16] P. W. Graham, J. Mardon, and S. Rajendran. “Vector Dark Matter from Inflationary Fluctuations”. *Phys. Rev. D* 93.10 (2016). DOI: 10.1103/PhysRevD.93.103520. arXiv: 1504.02102.

[Goo89] S. W. Goode. “Analysis of Spatially Inhomogeneous Perturbations of the FRW Cosmologies”. *Phys. Rev. D* 39 (1989). DOI: 10.1103/PhysRevD.39.2882.

[Gut81] A. H. Guth. “The Inflationary Universe: A Possible Solution to the Horizon and Flatness Problems”. *Phys. Rev. D* 23 (1981). Ed. by L.-Z. Fang and R. Ruffini. DOI: 10.1103/PhysRevD.23.347.

[Has12] J. Hasenkamp. “Dark Radiation from the Axino Solution of the Gravitino Problem”. *Phys. Lett. B* 707 (2012). DOI: 10.1016/j.physletb.2011.12.017. arXiv: 1107.4319.

[Haz+19] M. Hazumi et al. “LiteBIRD: A Satellite for the Studies of B-mode Polarization and Inflation from Cosmic Background Radiation Detection”. *J. Low Temp. Phys.* 194.5-6 (2019). DOI: 10.1007/s10909-019-02150-5.

[Hub29] E. Hubble. “A Relation between Distance and Radial Velocity among Extra-Galactic Nebulae”. *Proceedings of the National Academy of Science* 15 (1929). DOI: 10.1073/pnas.15.3.168.

[Hui+17] L. Hui et al. “Ultralight Scalars as Cosmological Dark Matter”. *Phys. Rev. D* 95.4 (2017). DOI: 10.1103/PhysRevD.95.043541. arXiv: 1610.08297.

[Hui+18] H. Hui et al. “BICEP Array: A Multi-Frequency Degree-Scale CMB Polarimeter”. *Proc. SPIE Int. Soc. Opt. Eng.* 10708 (2018). Ed. by G. Z. Angeli and P. Dierickx. DOI: 10.1117/12.2311725. arXiv: 1808.00568.

[HV90] J.-c. Hwang and E. T. Vishniac. “Analyzing Cosmological Perturbations Using the Covariant Approach”. *Astrophys. J.* 353 (1990). DOI: 10.1086/168583.

[Ich+07] K. Ichikawa et al. “Increasing Effective Number of Neutrinos by Decaying Particles”. *JCAP* 05 (2007). DOI: 10.1088/1475-7516/2007/05/008. arXiv: hep-ph/0703034.

[IZ12] C. Itzykson and J. Zuber. *Quantum Field Theory*. Dover Books on Physics. Dover Publications, 2012. ISBN: 978-0-486-13469-7.

[JMM24a] D. Jaramillo-Garrido, A. L. Maroto, and P. Martín-Moruno. “Symmetry Restoration for TDiff Scalar Fields”. 2024. arXiv: 2402.17422.

[JMM24b] D. Jaramillo-Garrido, A. L. Maroto, and P. Martín-Moruno. “TDiff in the Dark: Gravity with a Scalar Field Invariant under Transverse Diffeomorphisms”. *JHEP* 03 (2024). DOI: 10.1007/JHEP03(2024)084. arXiv: 2307.14861.

[JMN12] R. Jinno, T. Moroi, and K. Nakayama. “Probing Dark Radiation with Inflationary Gravitational Waves”. *Phys. Rev. D* 86 (2012). DOI: 10.1103/PhysRevD.86.123502. arXiv: 1208.0184.

[Kam+20] K. Kamada et al. “Gravitational Leptogenesis with Kination and Gravitational Reheating”. *JCAP* 01 (2020). DOI: 10.1088/1475-7516/2020/01/016. arXiv: 1911.02657.

[KGR05] T. Kahniashvili, G. Gogoberidze, and B. Ratra. “Polarized Cosmological Gravitational Waves from Primordial Helical Turbulence”. *Phys. Rev. Lett.* 95 (2005). DOI: 10.1103/PhysRevLett.95.151301. arXiv: astro-ph/0505628.

[KK16] M. Kamionkowski and E. D. Kovetz. “The Quest for B Modes from Inflationary Gravitational Waves”. *Ann. Rev. Astron. Astrophys.* 54 (2016). DOI: 10.1146/annurev-astro-081915-023433. arXiv: 1510.06042.

[KK19] S. Kawai and J. Kim. “Gauss–Bonnet Chern–Simons Gravitational Wave Leptogenesis”. *Phys. Lett. B* 789 (2019). DOI: 10.1016/j.physletb.2018.12.019. arXiv: 1702.07689.

[Kro94] P. P. Kronberg. “Extragalactic Magnetic Fields”. *Rept. Prog. Phys.* 57 (1994). DOI: 10.1088/0034-4885/57/4/001.

[KRS85] V. A. Kuzmin, V. A. Rubakov, and M. E. Shaposhnikov. “On the Anomalous Electroweak Baryon Number Nonconservation in the Early Universe”. *Phys. Lett. B* 155 (1985). DOI: 10.1016/0370-2693(85)91028-7.

[KS16] R. Kato and J. Soda. “Probing Circular Polarization in Stochastic Gravitational Wave Background with Pulsar Timing Arrays”. *Phys. Rev. D* 93.6 (2016). DOI: 10.1103/PhysRevD.93.062003. arXiv: 1512.09139.

[KT90] E. W. Kolb and M. S. Turner. *The Early Universe*. Vol. 69. Addison-Wesley Publishing Company, 1990. ISBN: 978-0-201-62674-2.

[Las+16] P. D. Lasky et al. “Gravitational-Wave Cosmology across 29 Decades in Frequency”. *Phys. Rev. X* 6.1 (2016). DOI: 10.1103/PhysRevX.6.011035.

[Lem27] G. Lemaître. “Un Univers Homogène de Masse Constante et de Rayon Croissant Rendant Compte de La Vitesse Radiale Des Nébuleuses Extra-Galactiques”. *Annales de la Société Scientifique de Bruxelles* 47 (1927).

[Lin83] A. D. Linde. “Chaotic Inflation”. *Phys. Lett. B* 129.3 (1983). DOI: 10.1016/0370-2693(83)90837-7.

[LL00] A. R. Liddle and D. H. Lyth. *Cosmological Inflation and Large Scale Structure*. Cambridge University Press, 2000. ISBN: 978-1-139-17518-0.

[LL92] D. H. Lyth and A. R. Liddle. “COBE, Gravitational Waves, Inflation and Extended Inflation”. *Phys. Lett. B* 291.4 (1992). DOI: 10.1016/0370-2693(92)91393-N. arXiv: astro-ph/9208007.

[LP12] H. S. Leavitt and E. C. Pickering. “Periods of 25 Variable Stars in the Small Magellanic Cloud.” *Harvard College Observatory Circular* 173 (1912).

[LQR05] D. H. Lyth, C. Quimbay, and Y. Rodriguez. “Leptogenesis and Tensor Polarisation from a Gravitational Chern-Simons Term”. *JHEP* 03 (2005). DOI: 10.1088/1126-6708/2005/03/016. arXiv: hep-th/0501153.

[LU18] D. López Nacir and F. R. Urban. “Vector Fuzzy Dark Matter, Fifth Forces, and Binary Pulsars”. *JCAP* 10 (2018). DOI: 10.1088/1475-7516/2018/10/044. arXiv: 1807.10491.

[Luo+16] J. Luo et al. “TianQin: A Space-Borne Gravitational Wave Detector”. *Class. Quantum Grav.* 33.3 (2016). DOI: 10.1088/0264-9381/33/3/035010. arXiv: 1512.02076.

[LWK99] A. Lue, L.-M. Wang, and M. Kamionkowski. “Cosmological Signature of New Parity Violating Interactions”. *Phys. Rev. Lett.* 83 (1999). DOI: 10.1103/PhysRevLett.83.1506. arXiv: astro-ph/9812088.

[Mag07] M. Maggiore. *Gravitational Waves. Vol. 1: Theory and Experiments*. Oxford Master Series in Physics. Oxford University Press, 2007. ISBN: 978-0-19-857074-5.

[Man+21] J. Manley et al. “Searching for Vector Dark Matter with an Optomechanical Accelerometer”. *Phys. Rev. Lett.* 126.6 (2021). DOI: 10.1103/PhysRevLett.126.061301. arXiv: 2007.04899.

[Mar16] D. J. E. Marsh. “Axion Cosmology”. *Phys. Rept.* 643 (2016). DOI: 10.1016/j.physrep.2016.06.005. arXiv: 1510.07633.

[Mar23] A. L. Maroto. “TDiff Invariant Field Theories for Cosmology”. 2023. arXiv: 2301.05713.

[MC81] V. F. Mukhanov and G. V. Chibisov. “Quantum Fluctuations and a Nonsingular Universe”. *JETP Lett.* 33 (1981).

[MCB15] C. J. Moore, R. H. Cole, and C. P. L. Berry. “Gravitational-Wave Sensitivity Curves”. *Class. Quant. Grav.* 32.1 (2015). DOI: 10.1088/0264-9381/32/1/015014.

[MFB92] V. F. Mukhanov, H. A. Feldman, and R. H. Brandenberger. “Theory of Cosmological Perturbations”. *Physics Reports* 215.5 (1992). DOI: 10.1016/0370-1573(92)90044-Z.

[MNS18] A. Maleknejad, M. Noorbala, and M. M. Sheikh-Jabbari. “Leptogenesis in Inflationary Models with Non-Abelian Gauge Fields”. *Gen. Rel. Grav.* 50.9 (2018). DOI: 10.1007/s10714-018-2435-8. arXiv: 1208.2807.

[MRdB01] S. McGaugh, V. Rubin, and E. de Blok. “High-Resolution Rotation Curves of Low Surface Brightness Galaxies: Data”. *The Astronomical Journal* 122.5 (2001). DOI: 10.1086/323448. arXiv: astro-ph/0107326.

[MSS13] A. Maleknejad, M. M. Sheikh-Jabbari, and J. Soda. “Gauge Fields and Inflation”. *Phys. Rept.* 528 (2013). DOI: 10.1016/j.physrep.2013.03.003. arXiv: 1212.2921.

[MTW73] C. W. Misner, K. S. Thorne, and J. A. Wheeler. *Gravitation*. San Francisco: W. H. Freeman, 1973. ISBN: 978-0-7167-0344-0.

[Muk05] V. Mukhanov. *Physical Foundations of Cosmology*. Oxford: Cambridge University Press, 2005. ISBN: 978-0-521-56398-7.

[MWC08] S. Mashchenko, J. Wadsley, and H. M. P. Couchman. “Stellar Feedback in Dwarf Galaxy Formation”. *Science* 319.5860 (2008). DOI: 10.1126/science.1148666. arXiv: 0711.4803.

[Nak03] M. Nakahara. *Geometry, Topology and Physics*. CRC Press, 2003. ISBN: 978-0-7503-0606-5.

[Nav+10] J. F. Navarro et al. "The Diversity and Similarity of Simulated Cold Dark Matter Haloes". *Mon. Not. R. Astron. Soc.* 402 (2010). DOI: 10.1111/j.1365-2966.2009.15878.x.

[NFW97] J. F. Navarro, C. S. Frenk, and S. D. M. White. "A Universal Density Profile from Hierarchical Clustering". *Astrophys. J.* 490.2 (1997). DOI: 10.1086/304888. arXiv: astro-ph/9611107.

[NIS20] K. Nomura, A. Ito, and J. Soda. "Pulsar Timing Residual Induced by Ultralight Vector Dark Matter". *Eur. Phys. J. C* 80.5 (2020). DOI: 10.1140/epjc/s10052-020-7990-y. arXiv: 1912.10210.

[NNW20] Y. Nakai, R. Namba, and Z. Wang. "Light Dark Photon Dark Matter from Inflation". *JHEP* 12 (2020). DOI: 10.1007/JHEP12(2020)170. arXiv: 2004.10743.

[NS11] A. E. Nelson and J. Scholtz. "Dark Light, Dark Matter and the Misalignment Mechanism". *Phys. Rev. D* 84 (2011). DOI: 10.1103/PhysRevD.84.103501. arXiv: 1105.2812.

[NV10] A. Neronov and I. Vovk. "Evidence for Strong Extragalactic Magnetic Fields from Fermi Observations of TeV Blazars". *Science* 328.5974 (2010). DOI: 10.1126/science.1184192. arXiv: 1006.3504.

[OK23] M. A. Oancea and A. Kumar. "Semiclassical Analysis of Dirac Fields on Curved Spacetime". *Phys. Rev. D* 107.4 (2023). DOI: 10.1103/PhysRevD.107.044029. arXiv: 2212.04414.

[Par55] E. N. Parker. "Hydromagnetic Dynamo Models." *Astrophys. J.* 122 (1955). DOI: 10.1086/146087.

[Per+99] S. Perlmutter et al. "Measurements of Ω and Λ from 42 High Redshift Supernovae". *Astrophys. J.* 517 (1999). DOI: 10.1086/307221.

[PF11] D. Paoletti and F. Finelli. "CMB Constraints on a Stochastic Background of Primordial Magnetic Fields". *Phys. Rev. D* 83.12 (2011). DOI: 10.1103/PhysRevD.83.123533. arXiv: 1005.0148.

[Pfe02] M. J. Pfenning. "Quantum Inequalities for the Electromagnetic Field". *Phys. Rev. D* 65 (2002). DOI: 10.1103/PhysRevD.65.024009. arXiv: gr-qc/0107075.

[Pir06] Yu. F. Pirogov. "General Covariance Violation and the Gravitational Dark Matter. I. Scalar Graviton". *Phys. Atom. Nucl.* 69 (2006). DOI: 10.1134/S1063778806080102.

[PP17] A. Papageorgiou and M. Peloso. "Gravitational Leptogenesis in Natural Inflation". *JCAP* 12 (2017). DOI: 10.1088/1475-7516/2017/12/007. arXiv: 1708.08007.

[PU04] A. Pilaftsis and T. E. J. Underwood. “Resonant Leptogenesis”. *Nucl. Phys. B* 692 (2004). DOI: 10.1016/j.nuclphysb.2004.05.029. arXiv: hep-ph/0309342.

[PW65] A. A. Penzias and R. W. Wilson. “A Measurement of Excess Antenna Temperature at 4080 Mc/s.” *Astrophys. J.* 142 (1965). DOI: 10.1086/148307.

[Rei+10] B. A. Reid et al. “Cosmological Constraints from the Clustering of the Sloan Digital Sky Survey DR7 Luminous Red Galaxies”. *Mon. Not. R. Astron. Soc.* 404.1 (2010). DOI: 10.1111/j.1365-2966.2010.16276.x.

[RFT80] V. C. Rubin, W. K. Ford Jr., and N. Thonnard. “Rotational Properties of 21 SC Galaxies with a Large Range of Luminosities and Radii, from NGC 4605 (R=4kpc) to UGC 2885 (R=122kpc).” *Astrophys. J.* 238 (1980). DOI: 10.1086/158003.

[Rie+19] A. G. Riess et al. “Large Magellanic Cloud Cepheid Standards Provide a 1% Foundation for the Determination of the Hubble Constant and Stronger Evidence for Physics beyond ΛCDM”. *Astrophys. J.* 876.1 (2019). DOI: 10.3847/1538-4357/ab1422. arXiv: 1903.07603.

[Rie+22] A. G. Riess et al. “A Comprehensive Measurement of the Local Value of the Hubble Constant with 1 Km/s/Mpc Uncertainty from the Hubble Space Telescope and the SH0ES Team”. *Astrophys. J. Lett.* 934.1 (2022). DOI: 10.3847/2041-8213/ac5c5b. arXiv: 2112.04510.

[Rie+98] A. G. Riess et al. “Observational Evidence from Supernovae for an Accelerating Universe and a Cosmological Constant”. *Astron. J.* 116 (1998). DOI: 10.1086/300499.

[Rub14] V. A. Rubakov. “The Null Energy Condition and Its Violation”. *Phys.-Usp.* 57.2 (2014). DOI: 10.3367/UFNe.0184.201402b.0137. arXiv: 1401.4024.

[Sak67] A. D. Sakharov. “Violation of CP Invariance, C Asymmetry, and Baryon Asymmetry of the Universe”. *Pisma Zh. Eksp. Teor. Fiz.* 5 (1967). DOI: 10.1070/PU1991v034n05ABEH002497.

[SCB14] H.-Y. Schive, T. Chiueh, and T. Broadhurst. “Cosmic Structure as the Quantum Interference of a Coherent Dark Wave”. *Nature Phys.* 10 (2014). DOI: 10.1038/nphys2996. arXiv: 1406.6586.

[Sch+10] D. R. G. Schleicher et al. “Small-Scale Dynamo Action during the Formation of the First Stars and Galaxies. I. The Ideal MHD Limit”. *A&A* 522 (2010). DOI: 10.1051/0004-6361/201015184. arXiv: 1003.1135.

[SD01] J. Sommer-Larsen and A. Dolgov. “Formation of Disk Galaxies: Warm Dark Matter and the Angular Momentum Problem”. *Astrophys. J.* 551.2 (2001). DOI: 10.1086/320211. arXiv: astro-ph/9912166.

[Ses+04] A. Sesana et al. “Low-Frequency Gravitational Radiation from Coalescing Massive Black Hole Binaries in Hierarchical Cosmologies”. *Astrophys. J.* 611.2 (2004). DOI: 10.1086/422185.

[Sha22] I. L. Shapiro. “Covariant Derivative of Fermions and All That”. *Universe* 8.11 (2022). DOI: 10.3390/universe8110586. arXiv: 1611.02263.

[Sha64] I. I. Shapiro. “Fourth Test of General Relativity”. *Phys. Rev. Lett.* 13 (1964). DOI: 10.1103/PhysRevLett.13.789.

[SK22] G. Sato-Polito and M. Kamionkowski. “Pulsar-Timing Measurement of the Circular Polarization of the Stochastic Gravitational-Wave Background”. *Phys. Rev. D* 106.2 (2022). DOI: 10.1103/PhysRevD.106.023004. arXiv: 2111.05867.

[Sor11] L. Sorbo. “Parity Violation in the Cosmic Microwave Background from a Pseudoscalar Inflaton”. *JCAP* 06 (2011). DOI: 10.1088/1475-7516/2011/06/003. arXiv: 1101.1525.

[Spo93] B. Spokoiny. “Deflationary Universe Scenario”. *Phys. Lett. B* 315 (1993). DOI: 10.1016/0370-2693(93)90155-B. arXiv: gr-qc/9306008.

[Spr+08] V. Springel et al. “The Aquarius Project: The Subhaloes of Galactic Haloes”. *Mon. Not. R. Astron. Soc.* 391 (2008). DOI: 10.1111/j.1365-2966.2008.14066.x.

[SS00] D. N. Spergel and P. J. Steinhardt. “Observational Evidence for Self-Interacting Cold Dark Matter”. *Phys. Rev. Lett.* 84.17 (2000). DOI: 10.1103/PhysRevLett.84.3760. arXiv: astro-ph/9909386.

[SS84] I. A. Strukov and D. P. Skulachev. “Deep-Space Measurements of the Microwave Background Anisotropy - First Results of the Relikt Experiment”. *Soviet Astronomy Letters* 10 (1984).

[ST08] N. Seto and A. Taruya. “Polarization Analysis of Gravitational-Wave Backgrounds from the Correlation Signals of Ground-Based Interferometers: Measuring a Circular-Polarization Mode”. *Phys. Rev. D* 77 (2008). DOI: 10.1103/PhysRevD.77.103001. arXiv: 0801.4185.

[Sta80] A. A. Starobinsky. “A New Type of Isotropic Cosmological Models without Singularity”. *Phys. Lett. B* 91 (1980). DOI: 10.1016/0370-2693(80)90670-X.

[Str+92] I. A. Strukov et al. “Anisotropy of the Microwave Background Radiation”. *Soviet Astronomy Letters* 18 (1992).

[Sur+10] S. Sur et al. “The Generation of Strong Magnetic Fields during the Formation of the First Stars”. *Astrophys. J.* 721.2 (2010). DOI: 10.1088/2041-8205/721/2/L134. arXiv: 1008.3481.

[Suz+16] A. Suzuki et al. “The POLARBEAR-2 and the Simons Array Experiment”. *J. Low Temp. Phys.* 184.3-4 (2016). Ed. by P. Camus, A. Juillard, and A. Monfardini. DOI: 10.1007/s10909-015-1425-4. arXiv: 1512.07299.

[tHoo76] G. ’t Hooft. “Symmetry Breaking through Bell-Jackiw Anomalies”. *Phys. Rev. Lett.* 37.1 (1976). DOI: 10.1103/PhysRevLett.37.8.

[Tro+18] M. A. Troxel et al. “Dark Energy Survey Year 1 Results: Cosmological Constraints from Cosmic Shear”. *Phys. Rev. D* 98.4 (2018). DOI: 10.1103/PhysRevD.98.043528. arXiv: 1708.01538.

[TW88] M. S. Turner and L. M. Widrow. “Inflation Produced, Large Scale Magnetic Fields”. *Phys. Rev. D* 37 (1988). DOI: 10.1103/PhysRevD.37.2743.

[Unr89] W. G. Unruh. “A Unimodular Theory of Canonical Quantum Gravity”. *Phys. Rev. D* 40 (1989). DOI: 10.1103/PhysRevD.40.1048.

[Vac91] T. Vachaspati. “Magnetic Fields from Cosmological Phase Transitions”. *Phys. Lett. B* 265 (1991). DOI: 10.1016/0370-2693(91)90051-Q.

[Wei04] S. Weinberg. “Damping of Tensor Modes in Cosmology”. *Phys. Rev. D* 69 (2004). DOI: 10.1103/PhysRevD.69.023503. arXiv: astro-ph/0306304.

[Wei72] S. Weinberg. *Gravitation and Cosmology: Principles and Applications of the General Theory of Relativity*. Wiley, 1972. 696 pp. ISBN: 978-0-471-92567-5.

[WFH67] R. V. Wagoner, W. A. Fowler, and F. Hoyle. “On the Synthesis of Elements at Very High Temperatures”. *Astrophys. J.* 148 (1967). DOI: 10.1086/149126.

[Wil14] C. M. Will. “The Confrontation between General Relativity and Experiment”. *Living Rev. Rel.* 17 (2014). DOI: 10.12942/lrr-2014-4.

[WKS10] M.-a. Watanabe, S. Kanno, and J. Soda. “The Nature of Primordial Fluctuations from Anisotropic Inflation”. *Prog. Theor. Phys.* 123 (2010). DOI: 10.1143/PTP.123.1041. arXiv: 1003.0056.

[Wor+22] R. L. Workman et al. “Review of Particle Physics”. *PTEP* 2022 (2022). DOI: 10.1093/ptep/ptac097.